LECTURES ON MARINE ACOUSTICS

Lecture notes presented at the 1971 short course
in Marine Acoustics conducted by the
Texas A&M University Department of Oceanography
with partial support of the
National Sea Grant Program
Institutional Grant GH-101 to
Texas A&M University

Volume II - Part I

SELECTED ADVANCED TOPICS IN MARINE ACOUSTICS

Edited by

Jerald W. Caruthers

June 1971
Reprinted April 1973

Sea Grant Publication No. TAMU-SG-73-403

College Station, Texas

FOREWORD

The two volumes LECTURES ON MARINE ACOUSTICS represent compilations of lectures presented at the short course in Marine Acoustics held at the Department of Oceanography of Texas A&M University between June 28 and July 2, 1971. The short course was conducted under the auspices of the National Sea Grant Program of the National Oceanic and Atmospheric Administration, U.S. Department of Commerce, through Institutional Grant GH-101 made to Texas A&M University.

Volume I, *Fundamentals of Marine Acoustics,* is a set of lecture notes prepared for the course "Marine Acoustics" given by the Department of Oceanography on a regular basis. Volume II, *Selected Advanced Topics in Marine Acoustics,* is a compilation of lecture notes presented by invited lecturers. The special lectures that were presented at the course and compiled into Volume II were selected on the basis of their emphasis on the environmental aspect and their application to civil uses.

I am grateful to each author for making his paper ready for reproduction.

Jerald W. Caruthers

FOREWORD TO REVISED EDITION

A second short course in Marine Acoustics was presented at Texas A&M University between June 25 and 29, 1973. Revised editions of LECTURES ON MARINE ACOUSTICS, Volume I, *Fundamentals of Marine Acoustics* and Volume II, *Selected Advanced Topics in Marine Acoustics,* were published for the course. In addition a new set of notes, Volume II - Part 2, *Selected Advanced Topics in Marine Acoustics,* was compiled from the new lectures presented at that time.

Jerald W. Caruthers
June 1973

TABLE OF CONTENTS

OPENING ADDRESS

Dr. Richard A. Geyer
Head of the Department of Oceanography
Texas A&M University, College Station, Texas

A one-week course in marine acoustics is rather an ambitious undertaking because of the breadth and diversification of this subject and its many uses in solving a broad spectrum of problems. This diversity of application is evidenced in the wide variations in both academic training and professional experience and activities of the dozen participating lecturers divided equally in number between within and outside of the University. It is therefore not surprising that the participants enrolled are representative of a diversified field of activities and come from a variety of areas in government, industry and universities. These are also the reasons why a course in marine acoustics lends itself quite naturally to sponsorship by the Sea Grant Program of the National Science Foundation. One of its major objectives is the dissemination of scientific and technological information to the ultimate user.

The rationale for the phrase "marine acoustics" is quite similar to that comprising the basis for marine biology, marine chemistry, marine geology, marine geophysics and so forth. It can be defined as the application of the fundamentals of acoustics to the solution of problems in the marine environment. This is the reason for the stress on fundamentals in this course, as well as specific applications. It is also the reason for emphasis on physics and mathematics as well as peripheral supporting subjects, such as signal processing and telemetry for example.

All too frequently, many acousticians in attempting to solve problems in the ocean have a tendency to ignore many of the effects of the marine environment. The fundamental physical principles involved in sound propagation in the sea are quite similar to those of other media such as the atmosphere or the solid earth. For example, the sound channel phenomenon so important to the understanding of marine acoustics also has its well-developed counterpart in the atmosphere, as well as in the solid earth. Such basic physical laws as Snell's Law and Fermat's Principle are equally valid in these three fundamental media comprising our planet. However, the differences lie in the many broad environmental characteristics indigenous to each of these media. These require special study and understanding if the problems inherent in a particular medium

are to be solved successfully.

Marine acoustic problems are especially complicated in many instances by the biological factors of the environment. These factors apply particularly to such areas as scattering and volume reverberation as well as their effects on instruments placed in the hostile marine environment. These instruments are vital for obtaining information to solve problems in marine acoustics. Similarly, a knowledge of the geotechnical properties of marine sediments is critical to the solution of interface problems in both military and civil applications of this subject.

In this regard, environmental factors are conspicuous by their absence as terms in the traditional and important Sonar Equation, even though many times these terms can be the overriding considerations in determining sound propagation in the sea in both time and spatial relationships.

To the casual observer leaning on the rail of a ship underway the appearance of the water could give him the impression that it is a homogeneous medium. Unfortunately, to those who must solve acoustic problems in this medium, nothing could be further from the truth especially in studying sound propagation in the sea. All sonar equipment is environmentally limited in its performance regardless of its power output or sound source capabilities. It is amazing in the early days of sonar design and development how many design engineers felt that increased sound ranges could be accomplished merely by increasing the power output of the equipment. They either did not realize or overlooked the tremendous significance of Snell's Law in determining sound propagation paths. It must always be remembered that environmental factors change not only in space but continually with time.

Similarly, those physicists and geophysicists who brought the science of seismic prospecting for oil exploration on land to a sophisticated stage of development, in general, did not foresee the effect of the bubble pulse phenomenon as a source of spurious reflections on seismograms. In the early days of marine seismic surveys, the results of this effect were often believed to indicate reflecting horizons of gelogic origin in the stratigraphic section of the earth, rather than reflecting events caused by bubble pulse phenomena. Thus, although the same basic principles of seismic prospecting apply to marine as well as land geophysical surveys, the special effects of the ocean environment had to be understood before the geologic significance of marine geophysical surveys could be interpreted properly. By now, the literature of seismic prospecting contains many papers recognizing this phenomenon and describes ways to recognize and circumvent it. Similarly, in the literature of marine acoustics, as it applies to sound propagation for military purposes, the effects of the deep scattering layer are described in some detail. These are caused by a combination of the marine organisms themselves, as well as frequently by the effects of the gases in

their swimbladders; and are now well recognized as a significant factor to be considered in predicting sound ranges.

Progress in marine acoustics is sometimes hampered by what may be described as "mental inertia" on the part of certain practitioners to new opportunities for study made available by improved and more sophisticated instrumentation. A rather recent example may be found in the reluctance on the part of some to recognize the importance of microstructure in vertical sound speed profiles made in the ocean by velocimeters. Too often the evidence for microstructure obtained from these profiles is attributed to instrument error rather than to a naturally occurring phenomenon. This attitude is maintained even though the reproducibility is excellent on both the up and down traces recorded. If the values on the velocimeter do not agree at control points as computed from Nansen-cast data, then the velocimeter data is often assumed per se to be the one in error, and not the values computed from the Nansen cast. This is nothing new and has its counterpart historically in the eventual grudging acceptance on the part of the Nansen-cast proponents of the validity of microthermal structure appearing in bathythermograph traces. When this fine structure was first observed on the original B/T traces, the reaction by many was the same. Hopefully, before too long, history will repeat itself in the acceptance of the data obtained from reliable velocimeters.

It is to be hoped that the participants of this course will at its conclusion have a much more complete understanding of not only the basic physical and mathematical principles of marine acoustics but of the tremendous importance of the environmental factors indigenous to the ocean that must be fully considered and understood before acoustic problems in this medium can be solved successfully. It is also to be hoped that at the conclusion of this course the participants will be in a much better position to decide for themselves the degree of success to be expected in solving those specific problems in marine acoustics they may have to cope with in their professional activities. They will also have a better knowledge of the literature and its varied sources available to turn to in solving these problems. Finally, because of the broad academic and professional backgrounds of the participants enrolled in this course, it is hoped that especially during question and answer periods they will not be reticent in actively participating to the mutual benefit of all involved. Such interaction can only lead to cross fertilization of ideas. These will result in a broader understanding of the potentialities of this subject to the solution of problems in the ocean for the benefit of all.

ACOUSTIC TELEMETRY AND SIGNAL PROCESSING

Stephen Riter
Assistant Professor
Texas A&M University

ABSTRACT

In this section basic considerations in the design of practical acoustic telemetry and signal processing systems are developed. These considerations are then applied to three representative modulation techniques: amplitude modulation, pulse position modulation, and digital frequency shift keying. These modulation techniques when used in an underwater telemetry system are discussed. Finally this material is related to the general problem of acoustic signal processing.

INTRODUCTION

The major justification for studying underwater acoustics aside from pure scientific interest is that acoustics provides a useful and efficient tool for transmitting information through the ocean. In other sections you will discuss in detail how the medium degrades and corrupts an acoustic signal. In this section we will discuss how one goes about designing effective systems which can extract as much information as possible from these obscuring factors.

COMMUNICATIONS CHARACTERISTICS OF THE UNDERWATER ACOUSTIC CHANNEL

The underwater acoustic channel is a complex randomly time varying media whose exact mathematical description is currently the subject of much active research by scientists and engineers. From a communications theory point of view the effects of prime importance are attenuation, dispersion and fading, and the addition of background noise. All of these effects will be discussed in other sections, however, here we will review dispersion and fading since from a communications theory point of view these effects are the most difficult to deal with.

As an acoustic signal propagates through the water it encounters various inhomogenieties in the medium which cause it to be randomly scattered along the transmission path. In addition when the signals encounter the earth-water or air-water interface they are reflected.

The effect of the scattering along the path is a dispersion of the signal in time and frequency. Since the receiver observes a sum of signals from each of the scattered paths there is a dispersion in time due to the difference in path length between the shortest and longest path. Thus if there is a path length difference of T seconds the received replica of a sharp transmitted pulse would be smeared out in time and would appear to have a time length of T + t seconds, where t is the length of the transmitted pulse.

The frequency dispersion results from the random motion of the scatterers with respect to each other. On reflection from a scatterer a slight doppler frequency shift would be imparted to the energy along each acoustic path. Since the received signal is composed of the sum of the signals from each path there would be a continuous random doppler shift of the received signal. This would for example cause a single transmitted sine wave of frequency f_o to be received as a sum of sine waves, with some mean frequency $f_o + f_D$, where f_D is the mean doppler frequency shift. The width of the spectrum of the received waves, F, is usually called the frequency spread and is a function of the velocity spread of the scatterers.

It can be shown [1] that the above scattering model leads to a received signal with a Rayleigh distributed probability density function for its amplitude and a uniformly distributed phase. Because of this random variation in amplitude, usually referred to as amplitude fading, and the complete loss of phase information, modulation techniques which convey information by varying the amplitude or phase of a carrier; for example, conventional amplitude modulation, phase modulation or variations thereof, are clearly poor choices for use with acoustic signals.

It should be pointed out here that, whereas in most applications communication system performance is independent of signal shape and improves with an increase in transmitted power, in a dispersive medium the amount of dispersion is a function of the signal, and hence increasing the amount of transmitted power increases the amount of dispersion. Consequently building more powerful transmitters is an inappropriate method for combatting these effects. Instead one must be careful to pick signal shapes which have an immunity to this type of degradation.

FREQUENCY

In other sections it is shown that there is a decrease in background noise and an increase in attenuation with frequency. Clearly then some best or optimum frequency exists for a given range. If all other parameters except attenuation and background noise were non frequency dependent then a solution for the optimum frequency is easily obtained. The result [2] is plotted in Figure 1. This curve is based upon some gross simplifications which tend to highlight the lower frequencies over the higher frequencies. For example man-made noise is predominantly low frequency in nature as is most offshore biological noise. In addition attenuation in a multipath environment is not necessarily deleterious since it serves to damp out echoes which arrive at the receiver from other paths. The point of the discussion however is brought out if one calculates the transmitter power required to obtain a zero dB signal to noise power ratio in sea state six as a function of range if the optimum choice of frequency is made. If this is done it can be seen [3] that acoustic communications in the 10 - 50 KHz frequency band over moderate ranges is quite feasible.

MODULATION TECHNIQUES

There are essentially three useful techniques available for coding information onto an acoustic signal. They are amplitude modulation (AM), pulse position modulation (PPM), and frequency shift keying (FSK). Variations of these techniques are of course possible. These techniques are also descriptive of various acoustic measuring systems which are not necessarily classified as telemetry systems. For example devices which measure the time of return of an acoustic pulse are really PPM detectors, etc.

AM

Amplitude modulation means that one varies the amplitude of a sinusoidal carrier in accordance with a linear function of the message to be sent. In one type of AM if the message to be transmitted is m(t) then one drives an acoustic source with

$$(1 + m(t)) \sin \omega_o t$$

where $|m(t)| \leq 1$. It can be shown that m(t) can be easily recovered by a simple envelope detector. Furthermore if the signal to noise ratio at the detector is (S/N) then the signal to noise ratio out of the detector is also (S/N) provided that the input (S/N) is above some threshold value. Unforturnately since the transmitted waveform is subjected to amplitude fading this is in most circumstances a rather poor method for transmitting information.

PULSE POSITION MODULATION

A PPM System operates by transmitting a short τ second tone once every T seconds. The time of transmission is a linear function of the value of the signal to be sent. A block diagram of a possible transmitter configuration is shown in Figure 2. In this realization a comparator is used to observe a linear saw-tooth wave form and the input voltage. When both are equal the comparator changes state. This transition time will then be a linear function of the input voltage. The output of the comparator is differentiated and clipped to give the required PPM pulse train. The pulse train is then used to generate high powered sinusoidal pulses of length, τ. These are applied to an acoustic projector, which transforms the electrical signals into acoustic tones for propagation through the channel.

The receiver would consist of a hydrophone followed by another threshold detector. This detector generates a pulse whenever the received signal exceeds some fraction, typically one half of its expected peak value. This pulse is then used to regenerate a replica of the transmitted voltage by using it to sample another linear sawtooth.

Since the transmitted information is contained in the time location of the pulse this type of modulation can be made particularly insensitive to interference, background noise and random fading. The output is, however, severely degraded by reflections from the boundaries of the media since they can cause the generation of incorrectly located pulses by the receiver's threshold detector. The performance of such systems have been analyzed in [4] from which Figure 3 is taken. In this figure the expected value of output noise is plotted versus input signal to noise ratio (A^2/N) for a transmitted frequency of 18 KHz, with 2BT the time bandwidth product of the signal as a parameter. From the curves we see that if (A^2/N) is above some critical or threshold value then a relatively small value of output noise is generated. Since the bandwidth of a sharp pulse is usually approximated by twice its reciprocal length we see that as long as we stay to the right of the threshold point we can decrease the output noise by decreasing the pulse length or increasing T. (This amounts to increasing 2BT.) One pays for an increase in T by a decrease in the amount of data transmitted, and for a decrease in the pulse length with an increase in system bandwidth. Even if one were willing to tolerate these costs the above factors still could not be increased indefinitely since for increased values of 2BT, increased values of (A^2/N) are necessary to operate to the right of the threshold point.

$E\{n^2\}$ is a measure of the effect of the input noise on the receiver's estimate of the pulse location, and can be used to determine critical system parameters. As an example suppose that it is desired to use 10 milli-second pulses to transmit information at a range of 1000 yards to a depth of 100 yards, with a pulse repetition frequency of 4 Hz.

The carrier frequency is 18 KHz and the total noise spectral density is -30dB. Assume zero dB directivity and 50% efficiency. What is the minimum transmitter power that can be used? For this case

$$2BT = (2)\frac{2}{10(10)^{-3}}\left(\frac{1}{4}\right) = 100$$

From the curves of Figure 3 we see that this corresponds to a required (A^2/N) of

$$(A^2/N) \approx 1500 \approx 31.7 \text{ dB}$$

The path loss at this transmitter frequency can be shown to be about 61 dB. The 50% efficiency contributes an additional 3 dB for a total power loss of 64 dB. The required peak transmitter power, P_T, is

$$P_T = 20\log_{10}A$$

which is easily seen to be

$$P_T = 64 - 30 + 31.7 = 65.7 \text{ dB}$$

Such an approach can also be used to design measurement systems where the desired information is contained in the location in time of a pulse, for example a bottom profiling system or a depth indicator.

FREQUENCY SHIFT KEYING

If the information to be transmitted is discrete in nature the modulation technique used must be some one of the numerous discrete modulation methods. These include frequency shift keying, digital frequency modulation, phase shift keying, amplitude shift keying, and countless variations thereof. Here we limit ourselves to frequency shift keying (FSK); however the extension to other modulation schemes is straightforward.

An FSK system operates by transmitting a T second tone at one of two frequencies, f_1 or f_2 to represent a binary "1" or "0" respectively. The receiver consists of two bandlimiting filters centered at f_1 and f_2 with nonoverlapping passbands. These filters are followed by devices designed to measure the energy in the passband of each filter. Usually this is an integrate and dump detector followed by some type of decision device which generates a "1" or "0" at the end of each signalling interval depending upon which filter had the greatest output. This technique is known to be optimum for signals of this type at low signal-to-noise ratios. It can be shown that the average probability of an incorrect decision on an individual digit for such a system operating over a nonfading channel in the presence of noise of spectral density No is [4]

$$P(E) = \frac{1}{2}\exp(-ET/No) \qquad (1)$$

where E is the average received signal power. Eq. 1 is strictly true for noise with a uniform spectrum. The extension to the non-uniform spectrum observed in underwater systems has been carried out by the author however the differences obtained are not sufficient to warrant the extra effort required.

If such a scheme is used in the underwater channel, dispersion will cause a pulse of length T and bandwidth W=1/T to be received as a pulse of length T+L and bandwidth W+B, where L and B are the time spread and frequency spread of the media. Moreover the amplitude of the received signal will be subjected to Rayleigh type fading. In such a situation there is a significant probability that on an individual transmission the received energy at the transmitted frequency will be small and an error will be made. In this case it can be shown that

$$P(E) = \frac{1}{2 + (\bar{E}T/No)} \qquad (2)$$

where $\bar{E}$ is average power in the fading signal.

In Figure 4 we plot Eq. (1) and (2) versus $(\bar{E}T/No)$ and (ET/No). As can be seen the effect of the fading can be catastrophic.

The best way to lessen the chance of an error due to fading is to use a technique called diversity. The idea behind diversity is simple, although the realization of a diversity system might be involved. Since the fading phenomena is purely random in nature, sometimes being present and sometimes being absent, one can clearly decrease the chance of an error by transmitting the message over and over again in the hope that all transmissions will not be obliterated by deep fades. Likewise, we may transmit multiples of frequencies to signify a 1 or 0 since the probability of a majority of frequencies being eliminated by deep fades is considerably smaller than losing a single tone. Finally we may use a number of separate receivers since the presence of a fade is also a random function of the location of the receiver. The techniques mentioned are called time, frequency and space diversity, respectively. Since all three diversity techniques are really making use of the same property of the disturbance, its randomness in time, space or frequency, we see that the parameter of importance is the number of different received signals one obtains, L, and not the means of obtaining the signals.

In Figure 4 we also plot P[E] versus (ET/No) for the optimum choice of L.

ACOUSTIC SIGNAL PROCESSING

Although the topics of telemetry and signal processing are parallel in most of the communications sciences, in the field of underwater acoustics they have tended to take on different meanings. By signal processing the acoustician usually means techniques for enhancing the sonar returns from underwater targets, so that a decision can be made as to whether or not a signal is present. Unfortunately there are a rather forbidding

number of possible signal processing procedures, and the number seems to be continuing to grow exponentially with time. In this section it is not possible to discuss or even mention all of these. Instead we claim that all the best procedures can be thought of as correlation processes where one is continuously comparing the received signal with replicas of the returns one is looking for. In a sense it can be shown that all other good signal processing schemes are approximations in some way or other of this technique.

BIBLIOGRAPHY

1] J. M. Wozencraft and I. M. Jacobs, Principles of Communication Engineering, (Wiley, New York, 1965).

2] S. Riter, "Underwater Acoustic Telemetry", Paper No. 1174 Offshore Technology Conference, Houston, Texas, April 1970.

3] S. Riter, ob. cit.

4] S. Riter, P. Boatright, and M. T. Shay, "PPM Acoustic Communications", IEEE Trans. on Audio and Acoustics, June 1971.

5] J. M. Wozencraft, ob. cit.

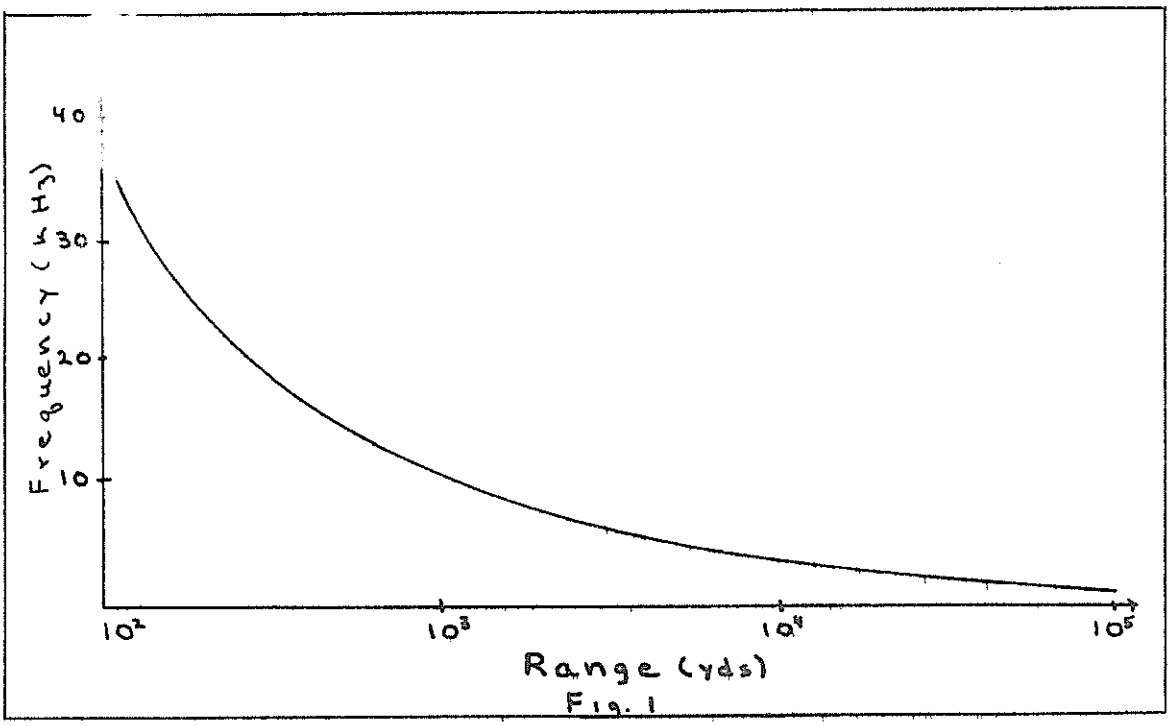
40
30
20
10
Frequency (kHz)
10^2
10^3
10^4
10^5
Range (yds)

Fig. 1

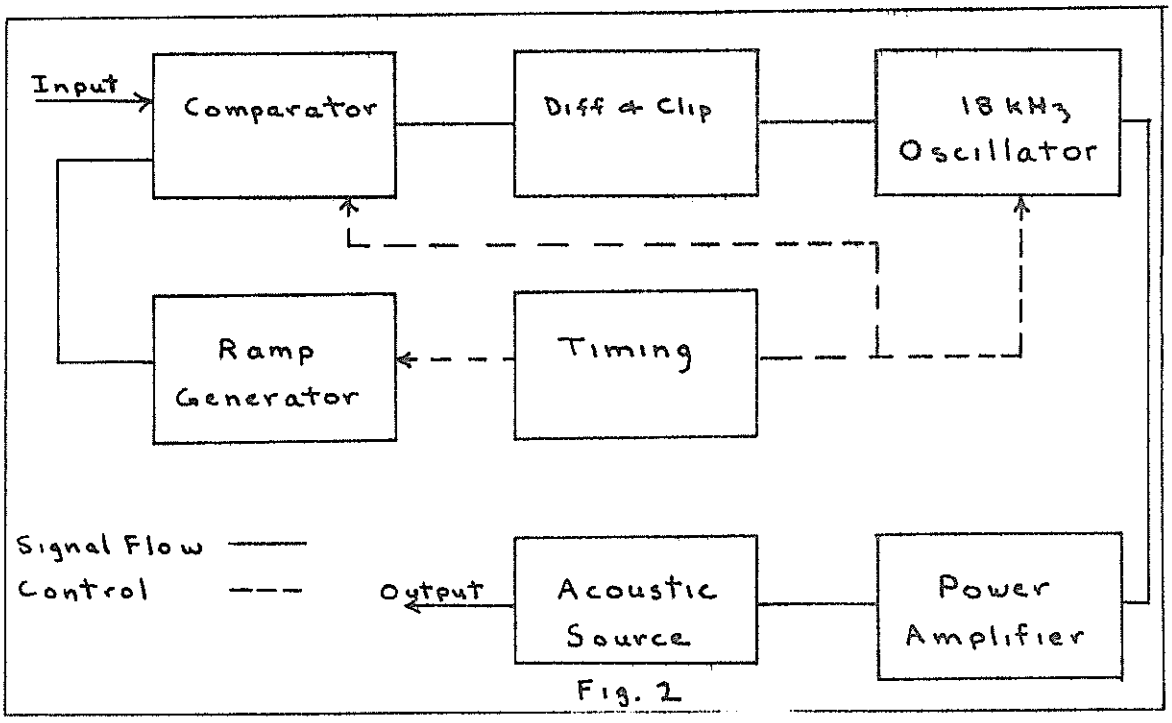
Input
Comparator
Diff & Clip
18 kHz Oscillator
Ramp Generator
Timing
Signal Flow
Control
Output
Acoustic Source
Power Amplifier

Fig. 2

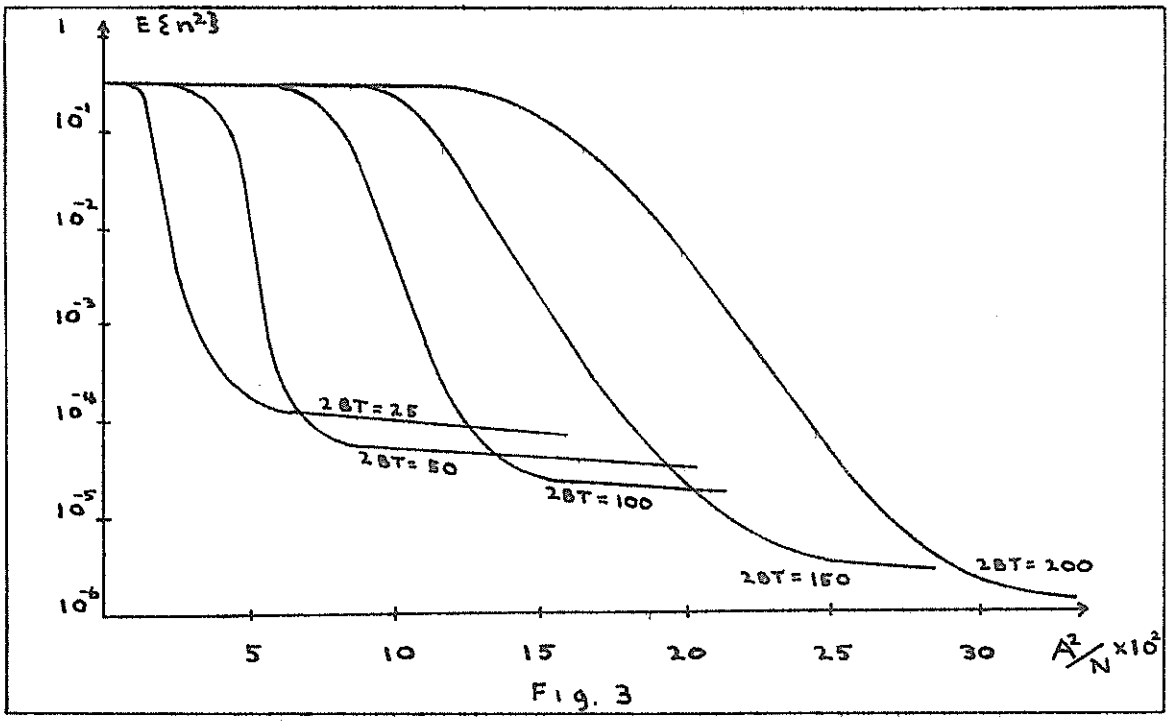
E{n²}
1
10⁻¹
10⁻²
10⁻³
10⁻⁴
10⁻⁵
10⁻⁶
2BT=25
2BT=50
2BT=100
2BT=150
2BT=200
5
10
15
20
25
30
A²/N x10²

Fig. 3

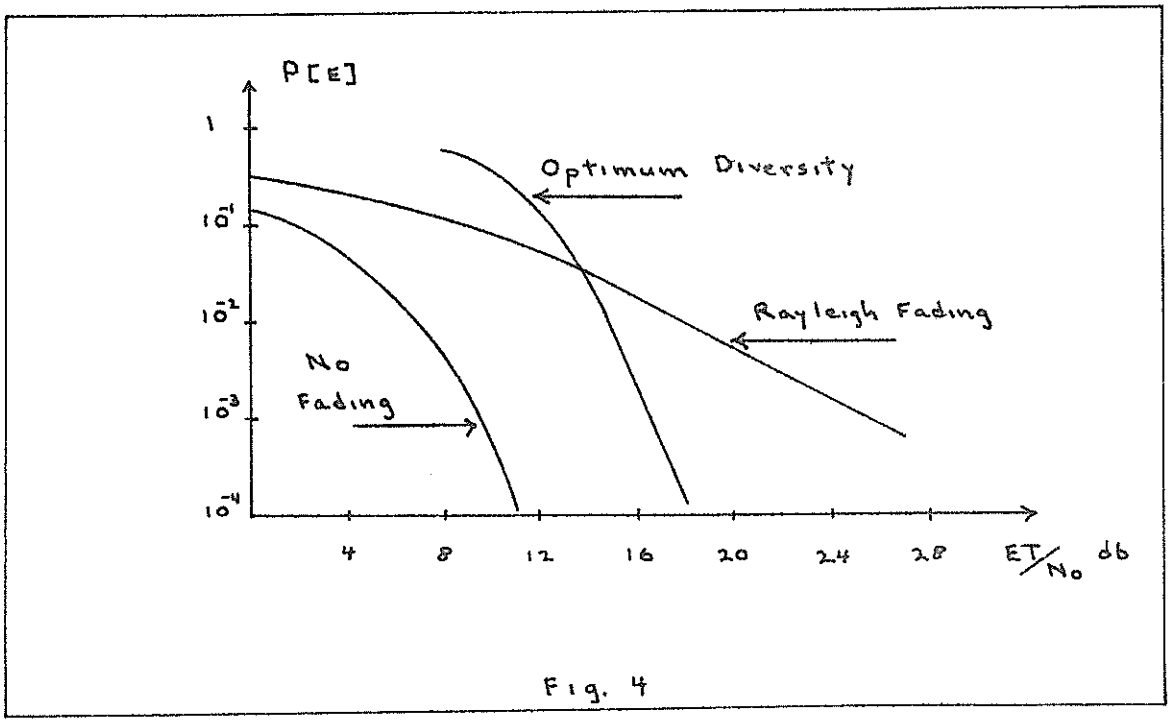
P[E]
1
10⁻¹
10⁻²
10⁻³
10⁻⁴
Optimum Diversity
Rayleigh Fading
No Fading
4
8
12
16
20
24
28
ET/No db

Fig. 4

WAVE THEORY:
SHALLOW WATER ACOUSTIC PROPAGATION

J. C. Novarini
Research Scientist
Hydrographic Office, Argentine Navy

INTRODUCTION

The propagation of sound in shallow water is a problem encountered for instance in coastal water and on the Continental Shelf for long range sound propagation. Distinction between shallow and deep water is quite arbitrary and there is no exact criterion of classification. Although in the geographical sense shallow water means depths less than 100 fathoms, in practice the distinction is based upon the dimensionless parameter hk, h being the water depth and k the horizontal wave number. When $hk < 10$ the case is considered a shallow water problem. However, it is to be noted that, for instance, with this criterion the high frequency case in relatively shallow water would be considered a deep water problem and this is not necessarily true since the sound will propagate mostly by successive reflections at the surface and the bottom (i.e., "channel effect") and this is far from the actual deep water propagation. Hence, following Urick,[1] we shall mean by shallow water propagation "propagation to distances at least several times the water depth, under conditions where both boundaries have an effect on transmission."

The actual problem of shallow water propagation is very complex since the boundaries are not well defined and are mostly of random nature. This, together with the fact that the boundaries are not plane parallel, makes it almost impossible to get a closed solution. In what follows a highly idealized problem will be solved, based mostly on the works of Brekhovskikh,[2] and Bradley and Hudimac.[3]

I. METHODS OF SOLUTION

Two approaches are used in the literature to solve the problem: the ray theory or "geometric acoustics," and the normal mode theory or "wave acoustics." Although they are not mutually exclusive,

one may have advantages over the other in specific cases.

As is known, in geometric acoustics, the paths of the rays are obtained through the Eikonal equation which is a solution to the Helmoltz equation for the high frequency case. The ray solution, although helpful in visualizing the phenomenon, only gives a picture of the ray path without regard to phase.

The wave acoustics solution is obtained, in general, by solving the Helmoltz equation through the separation of variables technique, and is particularly useful in the case where the acoustic wavelength is of the order of the water depth, the case in which the ray interpretation becomes meaningless. On the other hand, it can be shown that the curvature of a ray is related to the velocity gradient of the medium. For an isotropic medium the velocity gradient is zero and the ray is a straight line. Hence, if the boundaries of the region are recilinear and have well defined reflective properties, the method of images can be applied to obtain the solution, with the advantage that the solution can be either expressed as a sum of normal modes, or visualized as given the ray paths in the duct.

II. IMAGE THEORY

Let us consider first a plane parallel duct with boundaries at $z = 0$ and $z = h$, as illustrated in Fig. 1. The source is assumed to be a pulsating sphere of infinitesimal radius, situated at the point $z = z_0$, $r = 0$, and the receiver at z,r.

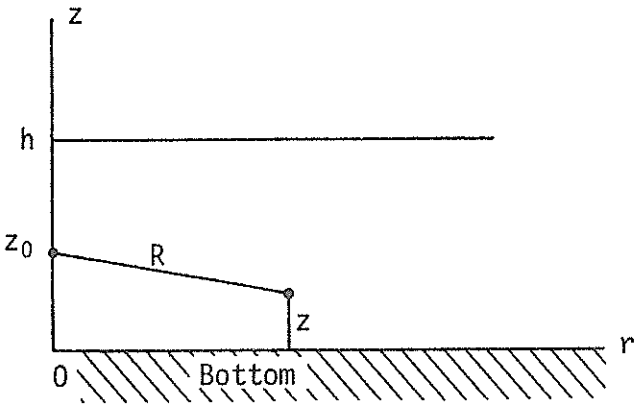

FIG. 1. Source and receiver

The medium will be assumed isotropic and homogeneous. The equation to be satisfied is the inhomogeneous Helmoltz equation

$$\nabla^2\psi + k^2\psi = \delta(r - r_0)\,\delta(z - z_0) \quad , \tag{1}$$

where ψ is the acoustic potential (for instance, the pressure) and δ is the Dirac's delta function whose properties are listed in Appendix A.

Since this is the shallow water problem the boundaries will be the air-water and the water-bottom interfaces, the former is a pressure release or free surface (i.e., zero acoustic pressure) and the latter is a rigid boundary (i.e., zero normal velocity). Hence, the boundary conditions will be

$$\psi = 0 \quad \text{at} \quad z = h \tag{2}$$

$$\frac{\partial\psi}{\partial z} = 0 \quad \text{at} \quad z = 0 \tag{2a}$$

and the reflection coefficient will be assumed $+1$ at the bottom (perfectly reflector and no phase change) and -1 at the sea surface (perfectly reflector, 180° phase change). We shall now use the image method to find the field at the receiver, or in other words, the field at an arbitrary point will be represented as the sum of the direct wave and waves radiated by a network of "image sources," which are obtained as a result of successive specular reflections of the source at the boundaries.

To the field of the source add the field of the image source as obtained by specular reflection at the lower boundary of the duct. Denoting the source by 01 and the image source obtained by reflection at the lower boundary by 03, the field will be

$$\psi = \psi_{0_1} + \psi_{0_3} = \frac{e^{ikR_{0_1}}}{R_{0_1}} + \frac{e^{ikR_{0_3}}}{R_{0_3}} \quad , \tag{3}$$

where $R_{0_1} = \sqrt{r^2 + (z - z_0)^2}$; $R_{0_3} = \sqrt{r^2 + (z + z_0)^2}$ are the distances from the source and image to the field point (z,r), respectively. Clearly, the expression for ψ given in (3) will satisfy the wave equation because each term satisfies it and will also satisfy the boundary condition at $z = 0$ since the system is symmetric with respect to that plane. But, it is also clear that (3) will not satisfy the boundary condition at $z = h$ since there is no symmetry. To overcome this problem another pair of image

sources, which are obtained by specular reflection of the two first sources at the upper boundary, can be added. Now the solution will satisfy the upper boundary condition, but no longer will it satisfy the lower boundary condition. However, another pair may be added to satisfy this condition and this process continued until an infinite network of image sources, lying on the z axis is obtained. Moreover, this series will converge and both boundary conditions will be satisfied. Recalling that there is a phase change in each reflection at the upper boundary, the total field at the field point can be written as

$$\psi = \sum_{\ell=0}^{\infty} (-1)^{\ell} \left[\frac{e^{ikR_{\ell_1}}}{R_{\ell_1}} + \frac{e^{ikR_{\ell_2}}}{R_{\ell_2}} + \frac{e^{ikR_{\ell_3}}}{R_{\ell_3}} + \frac{e^{ikR_{\ell_4}}}{R_{\ell_4}} \right] \qquad (4)$$

which satisfies the wave equation, the boundary condition and the singularity at the source; the last is provided by the term $\frac{e^{ikR_{0_1}}}{R_{0_1}}$.

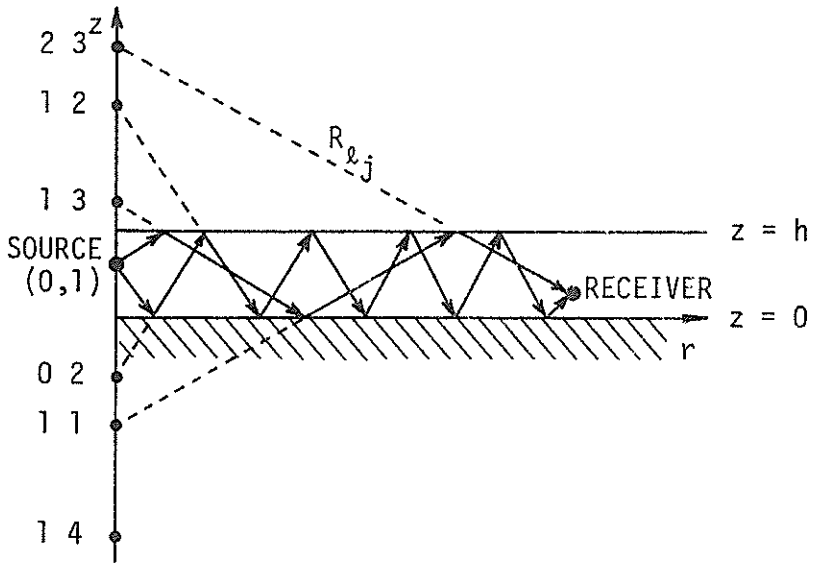

FIG. 2. Network of image for a shallow water duct

A few images of the network can be seen in Fig. 2. The distances R_{ℓ_j} are shown in Table I. It can be seen in Fig. 2 that there is a one-to-one correspondence between an image and a ray that represents a path of travel between source and receiver. The rays

provide the information on how the field propagates, and the summation of the images provides the phase and magnitude at the field point.

TABLE I. Distances to the image from the receiver

j	R_{ℓ_j}
1	$\sqrt{(z - z_0 - 2\ell h)^2 + r^2}$
2	$\sqrt{(z - z_0 + 2\ell h)^2 + r^2}$
3	$\sqrt{(z + z_0 - 2\ell h)^2 + r^2}$
4	$\sqrt{(z + z_0 + 2\ell h)^2 + r^2}$

III. NORMAL MODE SOLUTION

As mentioned before, another approach to the problem is given by the normal mode theory. The set of normal modes, each of which individually satisfy the wave equation, the boundary conditions, and propagates along the duct with its own velocity, will be obtained from the image solution. To do this, the integral representation of the field of a spherical wave in cylindrical coordinates must be used. The reason for this is that, while the field due to the image is spherical, the geometry of the problem has natural cylindrical symmetry. The integral representation of a spherical wave in cylindrical coordinates is[2]

$$\frac{e^{ikR}}{R} = -\frac{i}{2}\int_{-\infty}^{\infty} H_0^{(1)}\left(\sqrt{k^2 - \xi^2}\, r\right) e^{i\,\xi(z - z_0)}\, d\xi \quad , \qquad (5)$$

where $H_0^{(1)}$ is the Hankel function of first kind and $R = r^2 + (z - z_0)^2$.

Replacing R by R_ℓ , using (4), and writing $(-1)^\ell = e^{-i\pi\ell}$, the acoustic field will be

$$\psi = -\frac{i}{2}\sum_{\ell=-\infty}^{\infty} e^{-i\pi\ell}\int_{-\infty}^{\infty} H_0^{(1)}\left(\sqrt{k^2-\xi^2}\, r\right)\left\{e^{i\xi(z+z_0+2\ell h)} + e^{i\xi(z-z_0+2\ell h)}\right\}d\xi \quad , \tag{6}$$

but

$$e^{i\xi(z+z_0+2\ell h)} + e^{i\xi(z-z_0+2\ell h)} = e^{iz\ell h\xi}\, e^{i\xi z}\left\{e^{i\xi z_0} + e^{-i\xi z_0}\right\}$$

$$= 2\, e^{i2\ell h\xi}\, e^{i\xi z}\cos\xi z_0$$

then

$$\psi = -i\sum_{\ell=-\infty}^{\infty}\int_{-\infty}^{\infty} H_0^{(1)}\left(\sqrt{k^2-\xi^2}\, r\right)e^{-i\pi\ell}e^{i\xi z}\cos\xi z_0\, e^{i2\ell h\xi}d\xi \ . \tag{7}$$

At this point the Poisson formula,[4] which transforms one infinite series into another, must be used. The terms of the new series are obtained from the terms of the first one by a Fourier transformation, i.e.,

$$\sum_{\ell=-\infty}^{\infty} f(\tau) = \frac{1}{2\pi}\sum_{n=-\infty}^{\infty} F(n) \quad , \tag{8}$$

where

$$F(n) = \int_{-\infty}^{\infty} f(\tau)\, e^{-in\tau}\, d\tau \quad , \quad \tau = 2\pi\ell \ . \tag{8a}$$

Setting

$$f(2\pi\ell) = -i \int_{-\infty}^{\infty} H_0^{(1)} \left(\sqrt{k^2 - \xi^2}\, r\right) e^{-i\pi\ell} e^{i\xi z} \cos \xi z_0\, e^{i2\ell h\xi} d\xi \ ,$$

then using (8a)

$$F(n) = -i \int_{-\infty}^{\infty} H_0^{(1)} \left(\sqrt{k^2 - \xi^2}\, r\right) e^{i\xi z} \cos \xi z_0 \int_{-\infty}^{\infty} e^{-in\tau} e^{-\frac{i\tau}{2}} e^{i\frac{\tau h\xi}{\pi}} d\tau d\xi$$

$$= -i \int_{-\infty}^{\infty} H_0^{(1)} \left(\sqrt{k^2 - \xi^2}\, r\right) e^{i\xi z} \cos \xi z_0 \int_{-\infty}^{\infty} e^{i\tau\left[\frac{h\xi}{\pi} - (n + \frac{1}{2})\right]} d\tau d\xi \tag{9}$$

but from (6-A) and (5-A) it can be seen that

$$\int_{-\infty}^{\infty} e^{i\tau\left[\frac{h\xi}{\pi} - (n + \frac{1}{2})\right]} d\tau = \delta\left[\frac{h\xi}{\pi} - (n + \tfrac{1}{2})\right] = \frac{\pi}{h}\, \delta\left[\xi - (n + \tfrac{1}{2})\frac{\pi}{h}\right] . \tag{10}$$

Substituting (10) into (9), and using (3-A) equation (9) is easily integrated to give

$$F(n) = \frac{-2\pi^2 i}{h} H_0^{(1)}\left(\sqrt{k^2 - [n + \tfrac{1}{2})\tfrac{\pi}{h}]^2}\, r\right) \cos\left[\frac{(n + \frac{1}{2})\pi z}{h}\right] \cos\left[\frac{(n + \frac{1}{2})\pi z_0}{h}\right]$$

then, from (8)

$$\psi(r,z) = \frac{-2\pi i}{h} \sum_{n=0}^{\infty} H_0^{(1)}\left(\sqrt{k^2 - \left[\frac{(n + \frac{1}{2})\pi}{h}\right]^2}\, r\right) \tag{11}$$

$$X \quad \cos \frac{(n + \frac{1}{2})\pi z}{h} \cos \frac{(n + \frac{1}{2})\pi z_0}{h} \ , \tag{11}$$

with $k = \frac{2\pi}{\lambda}$; $0 \leq z \leq h$; $n = 0,1,2,\ldots,$

which is the acoustic field at any point (z,r) in the plane parallel duct expressed as a superposition of normal modes; n labels the different modes.

The z dependence of the amplitude of each mode is given by the factor $\cos[(n + 1/2)\pi z/h]$ and is shown in Fig. 3 for $n = 0,1,2$ and 3.

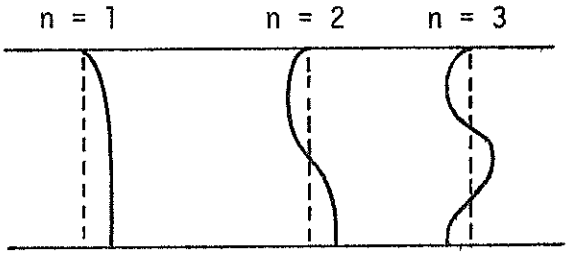

FIG. 3. Sound pressure versus depth for the first three modes

Defining a new parameter k_n by

$$k_n = \sqrt{k^2 - \left[\frac{(n + \frac{1}{2})\pi}{h}\right]^2} \quad , \tag{12}$$

it can be interpreted as the "wave number" of the nth normal mode, and so the nth normal mode will propagate along the duct with its own velocity c_n given by

$$c_n = \frac{\omega}{k_n} = \frac{c}{\sqrt{1 - \left[\frac{(n + \frac{1}{2})\lambda}{2h}\right]^2}} \tag{13}$$

with $\omega = kc$

Another useful interpretation is to think of k_n as

$$k_n = k \sin \theta_n \quad , \tag{14}$$

where from (12) and (14)

$$\theta_n = \cos^{-1}\left[\frac{(n + \frac{1}{2})\pi}{kh}\right] \quad . \tag{15}$$

θ_n represents then, the direction of propagation of a plane wave coming from a source image localized above or below the axes of the duct. That means that each mode can be interpreted as the superposition of two traveling waves with their fronts at definite angles of inclination θ_n, in different directions with respect to the vertical axes and in the same direction with respect to the horizontal axes. Fig. 4 shows this plane wave equivalence for the first mode.

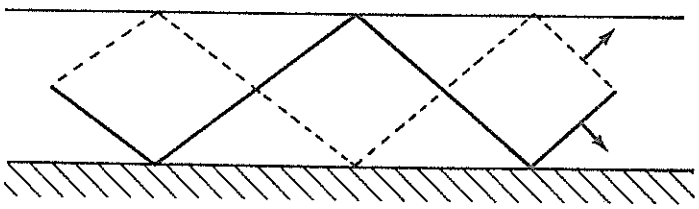

FIG. 4. Plane wave equivalent for the first mode

From (12) it is easily seen that normal modes can propagate in the duct without attenuation only if $kh > \pi/2$ or $h > \lambda/4$, the frequency belongs to this value of λ is

$$\omega_c = \frac{c\pi}{2h}$$

and is called "cut-off frequency." Waves with frequencies below ω_c will propagate in the duct with great attenuation. This can be seen from (12) since k_n becomes purely imaginary. The corresponding mode is called "evanescent mode."

Following Urick we can conclude that since the higher order image contribution die out rapidly because of their greater distances from the field point, only a few images are required and so the ray theory is more convenient for the case of short range

propagation. On the other hand, normal mode theory is more appropriate for long ranges because of the greater attenuation of the higher modes and so only a few modes are necessary to calculate the transmission.

IV. WEDGE SHAPED SHALLOW WATER DUCT

Obviously, the plane parallel duct with well defined reflective boundaries is only a poor first approximation since the actual case involves, in general, wedge shaped regions, bottoms, statistically rough boundaries, velocity gradients in the water layer, inhomogeneities in the medium, etc. Hence, in order to improve the first approximation to the actual case, the wedge shaped duct must be considered. For this case, the two approaches mentioned in the first section are usually employed to get a solution. Papers by Pierce[5] and Denham[6] attack the problem by using normal mode theory, while Kuznetsov[7] and Weston[8] use ray theory. Practical models and empirical theories have been developed by Macpherson and Daintith,[9] Marsh and Shulkin,[10] and Urick.[11] More recently, and considering simultaneously the two approaches, is the work by Bradley and Hudimac.[3] In what follows, a brief look at the wedge shaped case using image theory as presented by Bradley is shown

When the image process is applied to the wedge, the images appear on a circle with origin in the vertex of the wedge and radius equal to the distance source-vertex as shown in Fig. 5. For a wedge angle $\beta = \pi/n$, n integer, a finite number of images are required to completely satisfy the boundary conditions. But in the case where $\beta = \pi/a$, with a not an integer, the number of images required could be (not necessarily) infinite.

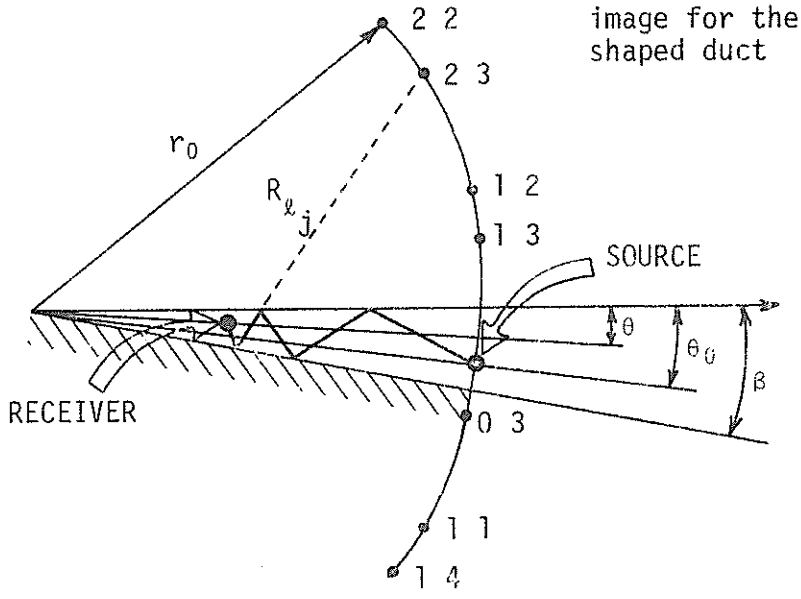

FIG. 5. Network of image for the wedge shaped duct

An important complication encountered in the wedge problem lies in the fact that the images on the circle are eventually going to appear on that part of the circle which represents the medium where the source is located and which, according to the conditions of the problem, can only contain the source. To overcome this problem, the theory of complex variables must be used. This is accomplished by introducing the concept of Riemann surface as a way of extending the θ coordinate. This extension allows for an infinite number of images. The images that appear on the Riemann surfaces (out of the principal plane) do not appear as observable images in the calculations of the field, but as imaginary images which will contribute to the so-called diffraction field to the total field. So, the acoustic field for a wedge shaped duct can be represented as

$$\psi = \sum_{\ell=-M}^{M} \left(\frac{e^{ikR_\ell}}{R_\ell}\right)_{\text{real}} + \sum_{|\ell|=M+1}^{\infty} \left(\frac{e^{ikR_\ell}}{R_\ell}\right)_{\text{imaginary}}$$

where $R_\ell^2 = r^2 + r_0^2 - 2\, r\, r_0 \cos(\theta \pm \theta_0 \pm 2\ell\beta) + (z - z_0)^2$.

M represents the number of images present in the principal plane of the extended Riemann surface. Hence it can be concluded that the acoustic field, as calculated from image theory, consists of two terms: one being a summation of real images and the other a sum of virtual images. The last one is the diffraction term contributing to the total field.

V. MODIFICATIONS TO THE SIMPLE THEORIES

The complications that arise in the actual case, mentioned in the last section, require further modifications to the first approximation already shown, to allow more realistic conditions on the surface, bottom, and water medium. The effect of attenuation in the bottom is considered in the papers by Eby, Williams, Ryan, and Zamkin;[12] Williams and Eby,[13] Kornhouser and Raney.[14] The effect of the surface roughness in shallow water propagation is considered by Clay,[15] and the problem of propagation of sound in a duct with inhomogeneities in the medium and at the boundaries has been considered by Lapin.[16]

APPENDIX A

Brief Review of the Dirac's Delta Function

In order to facilitate a variety of operations in mathematical physics, Dirac proposed the introduction of the so-called "Delta function" $\delta(x)$ which will be a representative of an infinitely sharply peaked function given symbolically by

$$\delta(x) = \begin{cases} 0 & (x \neq 0) \\ \infty & (x = 0) \end{cases} \tag{1-A}$$

but such that the integral of (x) is normalized to unit

$$\int_{-\infty}^{\infty} \delta(x)\, dx = 1 \quad . \tag{2-A}$$

A few properties are:

$$\int_{-\infty}^{\infty} f(x)\, \delta(x - a)\, dx = f(a) \tag{3-A}$$

for all continuous $f(x)$. In particular for $a = 0$

$$\int_{-\infty}^{\infty} f(x)\, \delta(x)\, dx = f(0) \quad . \tag{4-A}$$

$$\delta(ax) = \left(\frac{1}{|a|}\right)\delta(x) \quad , \qquad a \neq 0 \tag{5-A}$$

and a useful integral representation is given by

$$\delta(x) = \frac{1}{2\pi} \int_{-\infty}^{\infty} e^{ikx} dk \tag{6-A}$$

It is to be noted that (1-A) is not a proper statement and cannot be used to define a function, much less an integrable function. In fact the "Delta function" is not a function but a "functional" and has its theoretical support in the Theory of Distributions.

BIBLIOGRAPHY

1. R. T. Urick, Principles of Underwater Sound for Engineers, McGraw-Hill Book Co., Inc., New York, (1967).

2. L. M. Brekhovskikh, Waves in Layered Media, Academic Press, Inc., New York, (1960).

3. D. Bradley and A. A. Hudimac, "The Propagation of Sound in a Wedge Shaped Shallow Water Duct," Naval Ord. Lab. Rept. TR 235, (1970).

4. E. C. Titchmarsh, Introduction to the Theory of Fourier Integrals, New York, Oxford University Press, (1948).

5. A. D. Pierce, "Extension of the Method of Normal Modes to Sound Propagation in an Almost Stratified Medium," J. Acoust. Soc. Amer., 37, 19-27, (1965).

6. R. N. Denham, "Intensity Decay Laws for Sound Propagation in Shallow Water of Variable Depth," J. Acoust. Soc. Amer., 39, 1170-1173, (1966).

7. V. K. Kuznetsov, "A New Method for Solving the Problem of the Sound Field in a Fluid Wedge," Soviet Physics-Acoustics, 5, 171-176, (1959).

8. D. E. Weston, "Horizontal Refraction in a Three-Dimensional Medium of Variable Stratification," Proc. Phys. Soc., 78, 46-52, (1961).

9. T. D. MacPhersen and M. T. Daintith, "Practical Model of Shallow Water Acoustic Propagation," J. Acoust. Soc. Amer., 41, 850-854, (1967).

10. H. Marsh and M. Schulkin, "Shallow Water Transmission," J. Acoust. Soc. Amer., 34, 863-864, (1962).

11. R. T. Urick, "A Prediction Model for Shallow Water Sound Transmission," Naval Ord. Lab Rept. TR 67-12, (1967).

12. R. K. Eby et al., "Study of Acoustic Propagation in a Two-layered Model," J. Acoust. Soc. Amer., 32, 88-99, (1960).

13. A. O. Williams and R. K. Eby, "Acoustic Attenuation in a Liquid Layer Over a 'Slow' Viscoelastic Solid," J. Acoust. Soc. Amer., 34, 836-843, (1962).

14. E. T. Kornhauser and W. F. Raney, "Attenuation in Shallow Water Propagation Due to an Absorbing Bottom," J, Acoust, Soc. Am., 27, 689-692, (1955).

15. C. S. Clay, "Effect of a Slightly Irregular Boundary on the Coherence of Waveguide Propagation," J. Acoust. Soc. Amer., 36, 833, (1969).

16. A. D. Lapin, "Sound Propagation in Inhomogeneous Waveguides," Soviet Physics-Acoustics, 13, 198-200, (1967).

MARINE BIO-ACOUSTICS

Thomas J. Bright
Oceanography Department
Texas A&M University

I. Definition: Marine bio-acoustics may be defined as the study of sound in the sea where it results from or influences the behavior of marine organisms.

This definition excludes such things as echolocation of fish schools and deep scattering layer studies, but would include the effect of sonic booms upon behavior of aquatic organisms, or any inquiry into sound production or reception by marine animals.

II. Contribution of Marine Organisms to Ambient Sea Noise:

A. Under ideal conditions (sea dead calm, no vessels, no sound producing animals) the ambient noise pressure is about .18 to .20 dyne/cm^2. This corresponds to about -15 decibels (db), where 0 db corresponds to an acoustical pressure of 1 dyne/cm^2 (1 microbar), and is roughly comparable to a quiet night in country.

B. Average ambient sea noise is about 10 to 15 db and is due primarily to wave motion, current friction, and shipping (comparable to noise produced in a busy office).

C. Activity of marine animals can add 20 db or more to the average sea noise, often in a frequency range which can interfere with sonar gear, acoustic mines, and u. w. listening equipment (Figure 1). All major groups of marine animals (invertebrates, fishes, and mammals) contain marine representatives which are significant sound producing species.

III. Basic Terminology: The first step in characterizing a sound generally involves a subjective description in terms of other sounds more familiar to us. Marine bio-acoustical literature is, therefore,

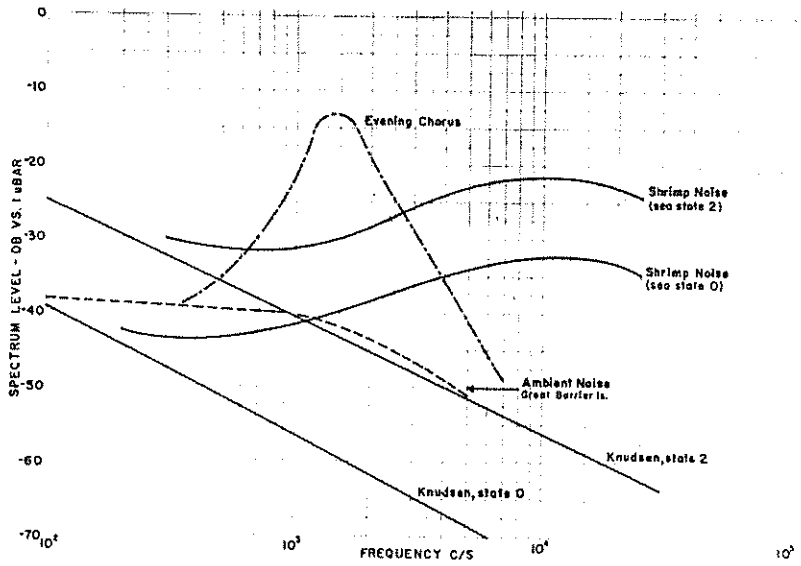

Figure 1. Spectrum level chart comparing New Zealand "evening chorus," attributed to the sea urchin Evechinus chloroticus, with typical snapping shrimp spectra as given by Knudsen. Prepared by R. I. Tait. (from Fish 1964)

full of references to sounds designated with onomatopoeias such as quack, squeak, squeal, moan, honk, etc. These are useful but, because very few, if any, other animals hear sounds exactly as we do, we must classify and analyze biological sounds in more objective terms if their behavioral meaning and significance to the organisms producing and perceiving them are to be determined.

A. Wave, Wave form, frequency and period as terms are generally used in standard physical sense.

frequency: use restricted to periodicity of sine waves and their derivatives.

rate: used to designate other periodicities of a higher order, e.g., pulse repetition rate.

basic signal:
elementary vibration:
elementary wave form:
— Sine wave that would exist as a continuous wave in the absence of the observed modulation

dominant frequency: refers to the frequency which has the

highest amplitude. In Marine bio-acoustics this is generally spread over a band of frequencies which may be 100 Hz wide, or more.

B. Pulse: a unitary homogeneous parcel of sound waves of finite duration. Such pulses when produced by animals are usually not singly detectable by the human ear and can be defined only through oscillographic or sound spectrum analysis.

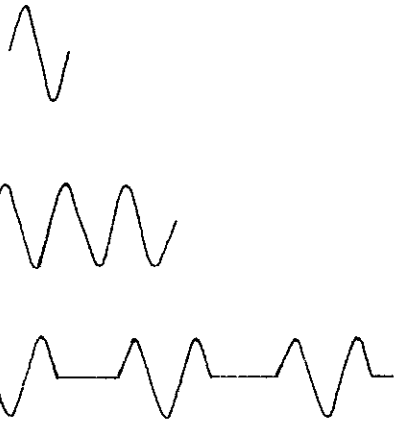

wave

wave train

pulse train

In reality, the basic sound produced by an animal and modulated into pulses is rarely a pure tone. More frequently it is a noise composed of a set of pure tones whose blending produces no regularity in the resultant wave form. When modulated temporally the end result is a series of noise pulses.

C. Click: a very short pulse separated by a much longer interval from its neighboring pulse.

Generally, these function in echolocation (dolphins, whales) and are composed of from 1 to 100 waves depending upon frequency. The higher frequency clicks tend to have more waves per pulse but are still of very short duration due to the short period of the wave.

D. Chirp: the shortest unitary rhythm-element that can readily be distinguished as such by the unaided human ear.

It may be composed of one or more pulses, or several pulse trains.

What would seem a chirp to human ear may be definable into a series of chirps (rhythm-pattern) by other animals. For example, the common 60 cycle hum that we associate with electronics is perceived by us as a sustained tone. The repetition rate is too high for the human ear to hear as a rhythm-pattern. Certain grasshoppers, however, hear the same sound as a series of discrete pulses occurring at a pulse repetition rate of 60 per second.

This is an important point to keep in mind when considering the significance of sounds as information vectors for different animals. The way we hear a sound may bear little resemblance to the manner in which it is perceived by other species. Thus it is difficult to judge the potentials of a sound for conveying information unless the auditory sensory capabilities of the animals under consideration are understood.

E. Ripple: a type of chirp which is perceived as a tremulous, throbbing or quavering tone. Basically of two types:

tremolo: a vibrating, beating or throbbing sound which may be amplitude modulated,

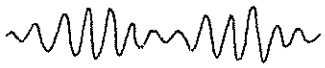

or pulse modulated,

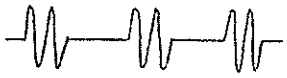

.

trill: a tremulous utterance of successive tones and, therefore, frequency modulated,

.

The pulse modulated tremolo appears to overlap somewhat the basic definition of a chirp insofar as the individual pulses are discernable by the human ear. This concept would seem to represent a borderline case where the pulse or pulse-train repetition rate is very close to that which can no longer be distinguished as a rhythm-pattern by the human ear.

F. First Order Sequence: a succession of chirps closely spaced in time and possibly combining to produce a specific sound unit. Example: staccato sound of squirrelfish.

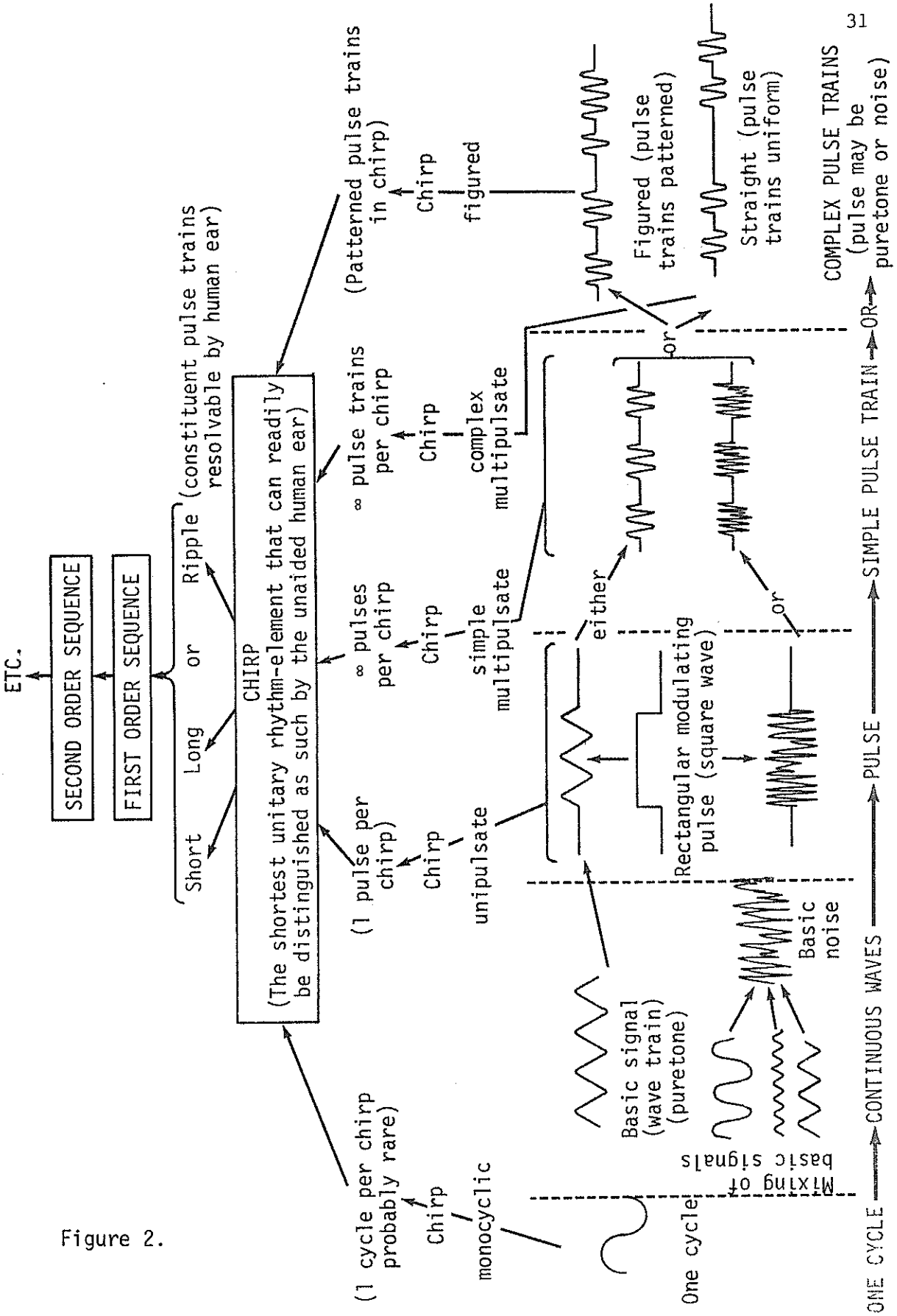
ETC.
SECOND ORDER SEQUENCE
FIRST ORDER SEQUENCE
Short
Long
or
Ripple
(constituent pulse trains resolvable by human ear)
CHIRP
(The shortest unitary rhythm-element that can readily be distinguished as such by the unaided human ear)
(1 cycle per chirp probably rare)
Chirp
monocyclic
(1 pulse per chirp)
Chirp
unipulsate
∞ pulses per chirp
Chirp
simple multipulsate
∞ pulse trains per chirp
Chirp
complex multipulsate
(Patterned pulse trains in chirp)
Chirp
figured
One cycle
Basic signal (wave train) (puretone)
Rectangular modulating pulse (square wave)
Basic noise
Mixing of basic signals
either
or
or
Figured (pulse trains patterned)
Straight (pulse trains uniform)
ONE CYCLE
CONTINUOUS WAVES
PULSE
SIMPLE PULSE TRAIN
OR
COMPLEX PULSE TRAINS
(pulse may be puretone or noise)

Figure 2.

G. Second Order Sequence: a succession of first order sequences.

Animal sounds can therefore, be viewed as a combination of a number of basic signals to form a basic sound, which is generally modulated through variation in amplitude or frequency into pulses, which are combined to form chirps, which in turn combine to form a rhythm-pattern.

Information may be transmitted through coding of the sound produced. This may be achieved through modulation of amplitude, dominant frequency, or temporal patterns of the pulses and chirps. For example, as shown in the following diagram, a series of chirps may be assembled in various ways temporally, much like a morse code. This type of patterning is thought to be significant in the case of fishes.

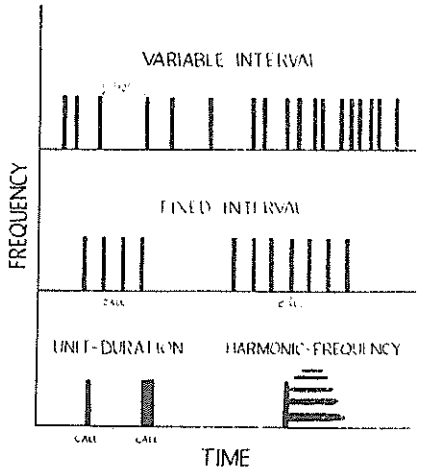

Figure 3. Diagrammatic representation of fish sounds (after Winn 1964).

Porpoises on the other hand appear to use frequency modulation rather extensively in their communicative efforts. During feeding scuffles, the Bottlenose Dolphin frequently emits sounds which, considering frequency in the vertical axis and time on the horizontal, could be contoured thusly,  . A single disturbed animal might emit  or  . The degree to which an animal can utilize the potential information capacity of a specific signal depends upon its hearing ability and the sophistication of the sensory apparatus associated with hearing. (To be discussed briefly later.)

All of the above applies basically to sounds classified as Purposeful animal sounds; those produced by the animal through the use of some specialized sound producing mechanism, and presumably for the purpose of communicating information to or influencing the behavior of other animals (various grunts and calls of fishes and porpoises).

On the other hand Adventitious sounds are produced by an animal incidentally during some activity, but not through the use of a specialized sound producing mechanism, and presumably not for any purpose of the animal producing it (feeding and swimming noises). Although these contribute to the ambient noise of an area and may provide information to certain species they are frequently so random and unstructured that it is difficult to refer them totally to the heirarchical classification of sounds described above.

IV. Visual Display of Animal Sounds

Two graphical means are commonly used to visually illustrate animal sounds. One is the familiar oscillogram giving information concerning amplitude integrated over all frequencies at any one instant (amplitude vs. time).

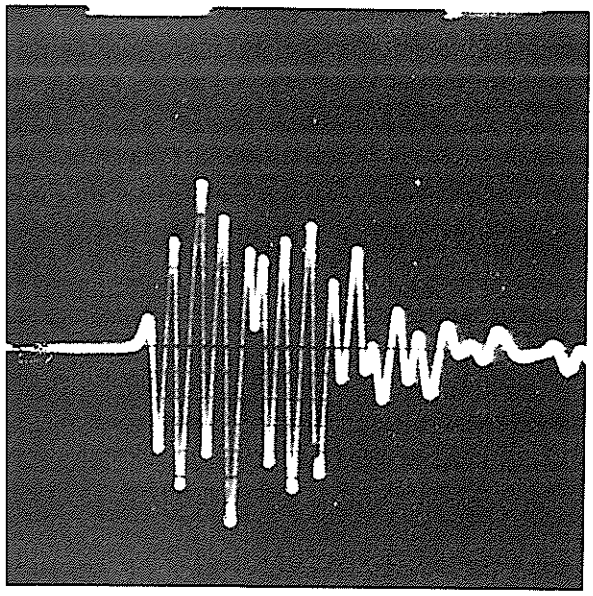

Figure 4. Oscillogram of single click produced by the barnacle Balanus balanoides in a Narragansett Marine Laboratory aquarium. Interval between timing marks is 1/240 sec. (from Fish 1964).

The other means employs sonograms produced by any of several sound spectrum analyzers (The Kay Electric Company Spectrum Analyzers are most popular). They provide an easily interpreted representation of sound structure in terms of frequency, amplitude, temporal, and harmonic structure. Basically, there are two types of sonograms. The standard sonogram depicts a sound in terms of frequency plotted on the vertical axis and time on the horizongal. Amplitude is roughly proportional to the darkness of the trace but a quantitative index of amplitude is not provided.

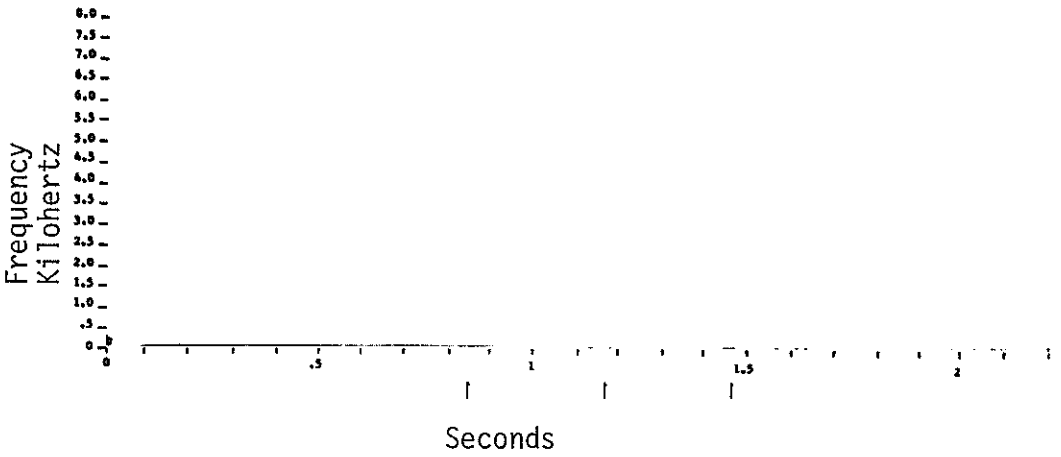

Figure 5. Standard sonogram of rasping sound of spiny lobster

The contour sonogram provides similar information but in addition the amplitude structure is contoured (in the Kay Vibralizer system at 6 db intervals over a dynamic range of 42 db).

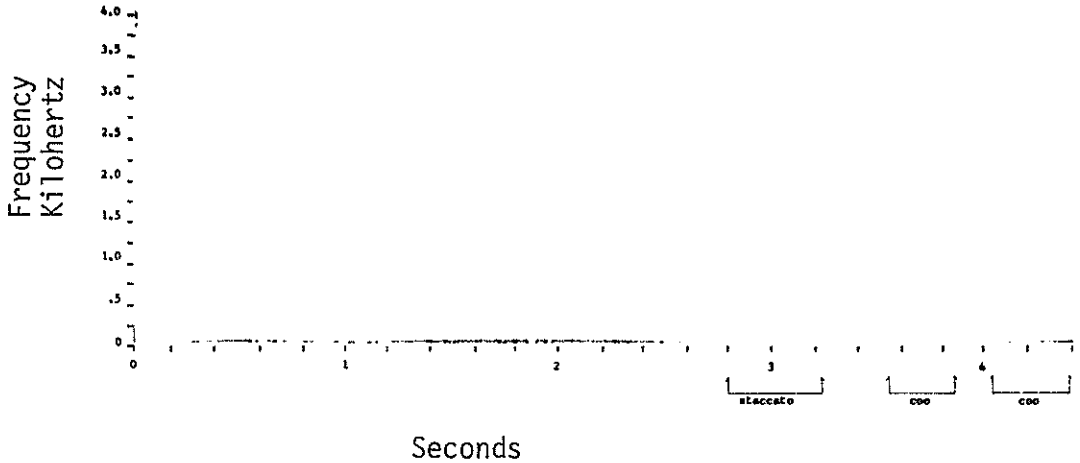

Figure 6. Contour sonogram of staccato and coo of the squirrelfish Holocentrus ascensionis

Unfortunately temporal resolution is obscured by the contouring so it is desirable to utilize both types of sonograms during analysis.

The time and frequency scales of sonograms are variable to suit the sounds being analyzed. One standard unit will analyze up to 16,000 Hz without modification. For higher frequency sounds a frequency translator may be used to increase the upper limit of analysis, or the recorded sound may be played at a slower than normal speed to bring the frequencies of the sound within the normal range of the analyzer.

These analyzers are much like the human ear in that, if pulses are produced at a rate so high that the analyzer cannot separate them, the pulse repetition rate will be added as a pure tone to the basic signal (pulse tone frequency). The resultant beat frequencies appear to be harmonics and the apparent harmonic interval is equivalent to the pulse repetition rate in cycles/second.

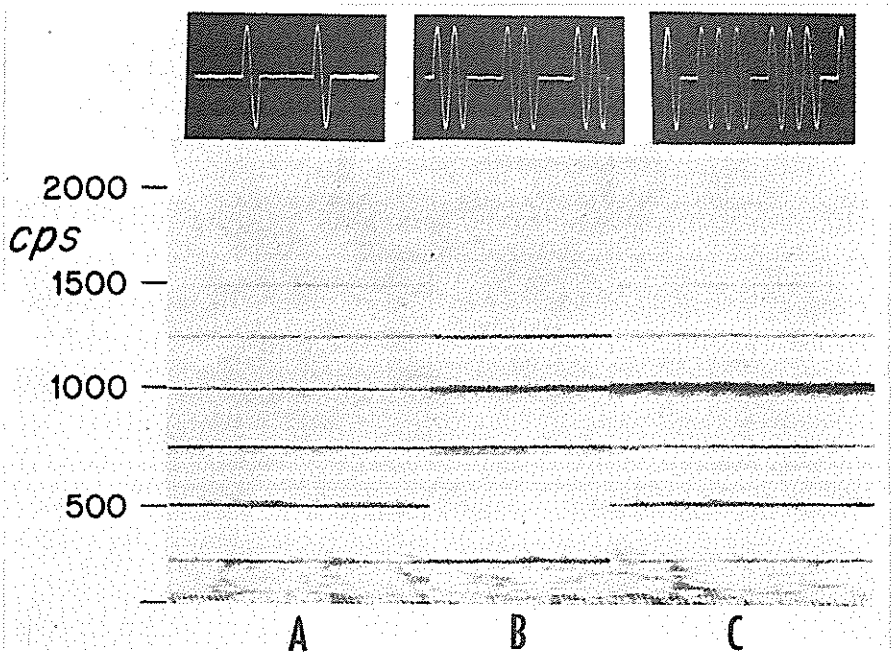

Figure 7. A is a 1000-Hz tone pulsed one cycle on and four cycles off; in B it is pulsed two cycles on and two cycles off, and in C it is pulsed three cycles on and one cycle off. The repetition rate of 250 pulses per second is the same for all three analyses. Note that the second harmonic of the repetition-rate is absent due to the symmetry of the pulses and pulse-intervals. The analyzing filter bandwidth is 20 Hz. (from Watkins 1967)

The trace representing the basic signal (1000 Hz in the above case) is usually darker (because most of the energy is expended at this frequency) if pulse duration is greater than the interval between pulses. If the duration of the pulse is equal to or less than the interval between pulses the darkness of the basic signal trace will be equal or less than the darkness of the traces representing the beat frequencies.

Fourier analysis computation can provide relative energy values for the pulse tone frequency (basic signal) and the
or "harmonics."

For example: for a 1000 Hz tone pulsed one cycle on and one cycle off, and assigning an energy value of one to the unpulsed tone, Fourier computations predict;

Frequency	Energy Value
500 (the fundamental of the pulse repetition rate)	0.178
1000 (second harmonic of prr, also the pulse-tone frequency)	0.250
1500 (3rd harmonic of prr)	0.064
2000 (4th)	0.000
2500 (5th)	0.004
3000 (6th)	0.000

These agree very well with spectral analysis of this type sound. Note the variability in energy content between beat frequencies. This is typical and varies greatly with the pulse repetition rate and length of pulses compared to interval between pulses.

Many supposed harmonic fish sounds show such a pattern of "enhanced" and "suppressed" harmonics.

The following sonogram shows the trace of a sound consisting of a pulse tone frequency of 1000 Hz where the pulse repetition rate is decreased in steps from about 500 cycles/sec. to about 10 cycles/sec. Note that as time progresses the harmonic bands converge (representing the decrease in pulse repetition rate) until they tend to fuse at the pulse tone frequency and show up toward the end of the sonogram as discrete pulses.

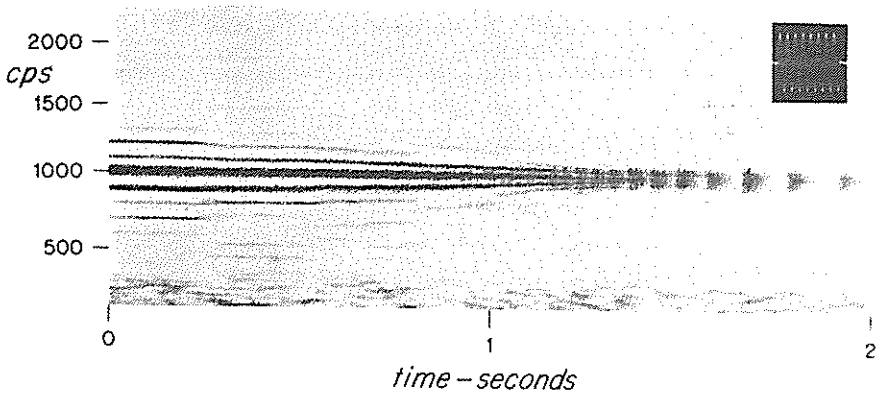

Figure 8. The interval between eight-cycle pulses at 1000 Hz is varied in two-cycle steps from two cycles to about 100 cycle (of the 1000 Hz). The pulse repetition rate may be read from the harmonic interval until the pulse becomes separated. The analyzing filter bandwidth is 20 Hz. (from Watkins 1967)

V. Sound Production and Sonic Mechanisms in Marine Invertebrates (Animals without backbones):

Sounds produced by invertebrates are most often snaps, clicks, or rasps, although some invertebrates may produce popping or sputtering sounds. The clicks, snaps, and rasps are usually white noise containing frequencies spanning the entire audible range, 20-20,000 Hz, and into the ultrasonic. These are usually stridulatory sounds, produced by contact of various hard parts during feeding or moving about, as well as through the action of special sound producing organs. The more important marine invertebrate sound producers belong to the Crustacean Arthropods, the Molluses, and possibly the Echinodermata (sea-urchins and relatives, see Figure 1).

A. Crustaceans

1. Snapping shrimp (Alpheidae) comprise one of the noisiest groups in the sea, and the most extensively studied. Their sounds are easily detected by a diver in the water. Descriptions of their sounds date back to 1795, and they were certainly known prior to that. During World War II, submarine

patrols complained that sizzling and crackling in shallow areas often masked all other water noise, and the sounds assumed immediate importance due to their interference with sonar signals.

The sounds are produced by large populations of small shrimps, and local background noise levels are correlated with population distribution. Knowledge of this, and of the biology and distribution patterns of the shrimps, allow prediction of the degree of interference to be expected in unmonitored areas. The combined snapping of a shrimp population in the vicinity of a coral reef can exceed 45 db in the 10-20 kHz range (see Fig. 1).

Snapping shrimp thrive in a global belt bounded approximately by 40°N and 40°S latitude (more specifically the 52°F winter surface isotherm), on coral, sponge, shell, or rock bottom, in depths less than 60 meters.

Individual snaps are short chirps with wideband frequencies extending to over 15 kHz. Our recordings in the Virgin Islands indicate apparent dominant frequencies at about 3 kHz and 5.5 kHz.

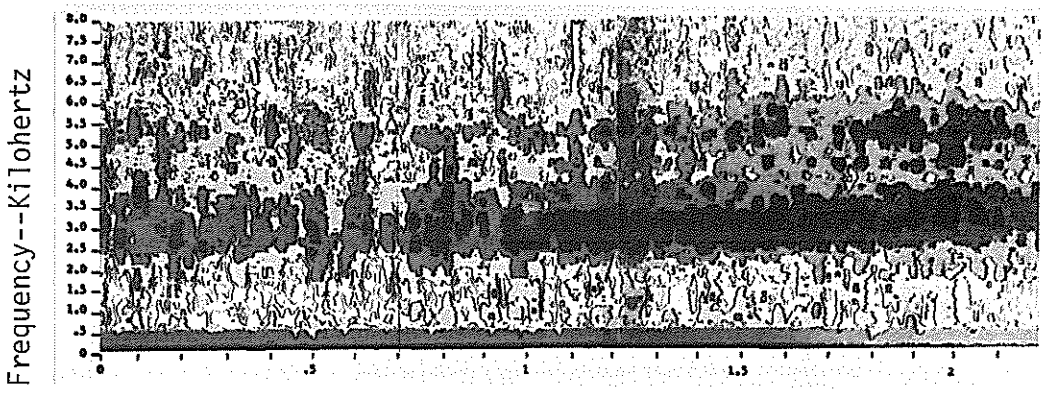

Figure 9. Snapping Shrimp noises

The mechanism of sound production in snapping shrimp is the larger of two chelipeds (claws). The dactyl (movable claw) is opened and may be held so by sucker-like discs on it and the chela (stationary claw). Tension placed upon the dactyl by adductor muscles closes the claw quickly and the glancing blow of the dactyl against the chela produces a snap-like sound (intensity often equal to that produced by snapping a large dry twig in two).

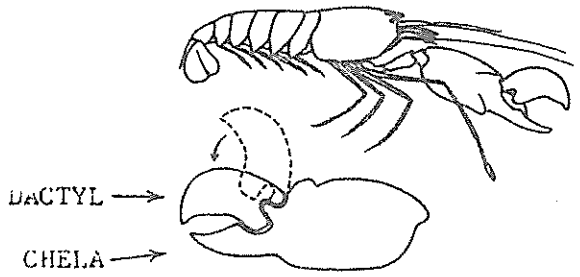

Figure 10. The snapping shrimp possesses an enlarged claw. The movable finger of this claw snaps sharply downward and produces a sound as it strikes the immovable "thumb." (after Dumortier, 1963) (from Tavolga, 1965)

Although snapping shrimp are the noisiest of the crustacea it is thought by some that the noise itself has no significance behaviorally, and is simply a by-product of another activity.

When the claw is closed quickly a tooth on the dactyl is forced quickly into a cavity in the chela resulting in an extremely intense squirt of water which can be directed at a predator or prey (offense or defense). A predator may thus be chased away or forbidden entrance to the burrow or cavity in which the shrimp lives. A potential meal on the other hand may be stunned by the intense stream of water (and possibly the loud snap) and therefore easily captured.

2. Spiny Lobster (Palinuridae)

Stridulatory sound production by spiny lobsters was mentioned by Athenaeus in the 3rd century A.D. The sounds produced are rasps and are known to any who have ever captured one of the creatures alive. The frequency and temporal structures are as shown in Figure 3 of the preceeding section. The sound producing mechanism is composed of a process on the inner face of the basal joint of the antenna. This process fits exactly over a longitudinal swelling along the side of the rostrum (snout). The swelling has minute teeth pointing forward. A striated membrane on the lower surface of the antennary process is drawn across the toothed rostral swelling, thereby producing a stridulatory vibration or rasp.

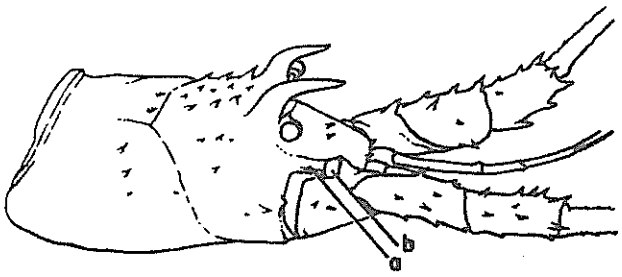

Figure 11. The spiny lobsters have a stridulatory organ at the base of the large antennae. A finely toothed orange ridge (a) is rubbed by a stiff membrane at the base of the antenna (b). The inside surface of the membrane is also serrated, and the rasping sound is produced when the base of the antenna is raised and the stridulatory membrane is stroked against the orange ridge. (after Moulton, 1957)(from Tavolga, 1965)

The significance of the rasp is not thoroughly understood, but the sound has been observed during fights between two individuals. Sound is usually produced during capture or disturbance and is accompanied by violent abdominal contractions, resulting in tail flips which propel the lobster backwards as it attempts to escape.

3. Additional known crustacean sound producers include certain barnacles (see Fig. 2), crabs, mantis shrimps, penaeid shrimps, and others.

B. Molluscs (clams, snails, squids, octopi, etc.)

1. Mussels (Mytilidae)

Whereas snapping shrimp produce localized intense noises in south temperate and tropical zones, similar background noises have been ascribed to the Mussel, Mytilus edulis, in New England coastal waters.

These bivalves (clams) attach to the substrate in large groups by means of a byssus composed of elastic threads which they continually secrete. Population concentrations occur from the Arctic to Cape Hatteras in estuaries where salinity is greater than 25.3% and where the substrate is hard enough (pilings, rocks, peat-like banks, etc).

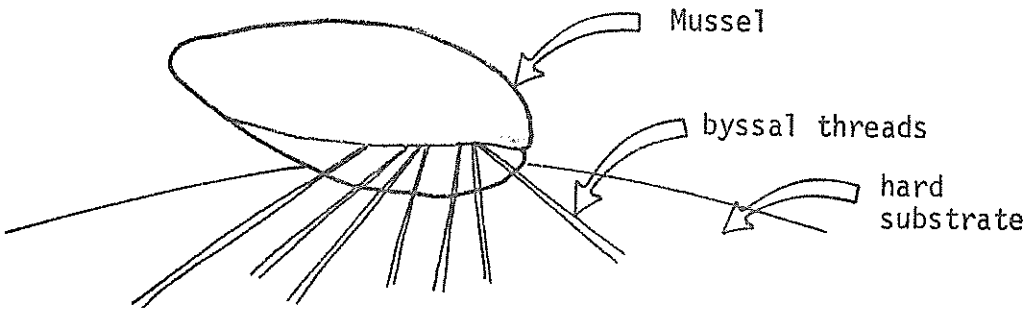

Figure 12. Mussel attached to substrate (after Fish 1964)

In an attempt to obtain a better position for feeding, and to prevent smothering by silt, members of a population move about by breaking or dislodging certain byssal threads, secreting new ones, or adding to old ones. They apply pressure to the threads by protruding and anchoring their muscular foot to the substrate and reorienting themselves, thereby stretching the threads. Stretching apparently causes a snapping noise to occur, as does dislodging or breakage. Snaps are of high amplitude with their greatest energy between 1 and 4 kHz.

Definite diurnal cycles of activity are indicated by variations in the rate of snapping in a mussel community. For example, 24 hr. monitoring periods indicate that snaps of 80-90 db reached a peak of 170/min at noon, fell to 28/min at 1900 hr. (sunset), and then rose rapidly again after 0630 hr. (sunrise).

The snapping and crackling of mussels is most persistent in Naragansett Bay in summertime when the water is warmer. This situation can be duplicated in the laboratory by raising the temperature from 10°C to 20°C. An increase in sound production is thus induced, indicating that the mussel activity rate is quite dependent upon temperature.

This also illustrates that certain sound production cycles are influenced by changes in environmental factors (light intensity, temperature, and others) on a daily and seasonal basis, and can therefore be used in some cases as indicators of such changes. It also indicates that bio-acoustical techniques can be employed to indicate behavioral phenomena not otherwise suspected in soniferous animals.

2. Other molluscs are known to produce less intense adventitious sounds. Various clams, including scallops, produce clicks when they close their valves. Squid produce popping noises with the expulsion of water through their propulsive siphon (analogous to the forced escape of air from a toy baloon).

VI. Sound Production and Sonic Mechanisms in Marine Fishes:

Fish and Mowbray recently published a book, "Sounds of Western North Atlantic Fishes," in which they describe sounds of 220 species of fishes from the Atlantic Coast of the U. S. and the Caribbean.

Considering the limited nature of investigations so far, and the fact that there are over 15,000 species of fish there is no way of knowing at the present time how many are capable of sound production. Some very vociferous forms have been known since antiquity (croakers of the family Sciaenidae). In some cases the fish choruses can be heard out of water by the unaided ear. Fishermen have also employed pipes or other stethoscope-like devices to locate concentrations of soniferous fishes.

A. Stridulatory mechanisms:

Fish sounds produced by stridulation of hard parts cover a frequency range of from below 100 Hz to above 8000 Hz. The predominant frequencies lie commonly in the 1000 to 4000 Hz range.

Some stridulations are modified due to the resonating qualities of the swim bladder, but others are not.

1. Swim bladder modulated stridulations:

One of the best examples of this type of sound production is exhibited by the grunts (family Pomadasyidae).

In these fishes opposing patches of teeth located in the pharynx are rubbed together by muscular action. The resulting scrape is modulated by the swim bladder, which acts as a resonator, into grunts, croaks, thumps, or knocks which range from 100-8000 Hz, but have predominant frequencies below 1000 Hz. The sounds are generally produced when the animal is disturbed or captured.

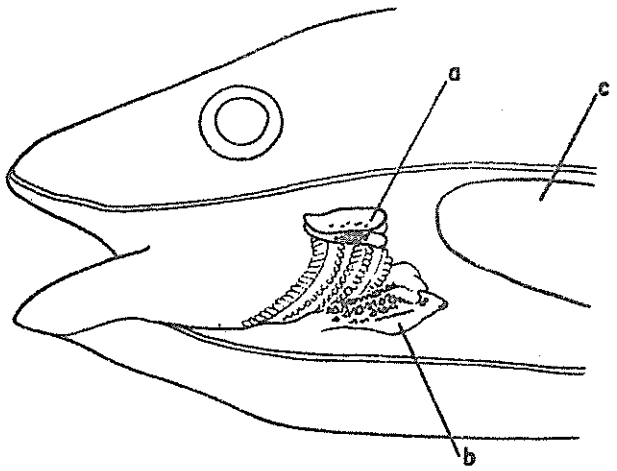

Figure 13. A dissection of the pharyngeal region of the grunt shows the location of the pharyngeal teeth that act as stidulatory organs in many species. The lower patch of denticles (b) is at the point of juncture of the gill arches and it is grated against the upper patch (a) during normal feeding or in sound production. The swim bladder (c), which is nearby, can act as a "resonator" to change the quality of the sound.
(from Tavolga 1965)

2. Unmodulated stridulation:

Feeding activities of fishes usually result in mechanical noises produced by the action of tooth against tooth or tooth against food.

These sounds possess predominant frequencies in the 1000 to 4000 Hz range and are usually described as rasps, scratches, clicks, or scrapes. For example: Parrotfishes (Scaridae) have beaklike teeth for scraping epifaunal organisms from reefs and rocks.

Some species produce stridulations through the rubbing of bone against bone, e.g., seahorse (Hippocampus), pipefish (Syngnathus).

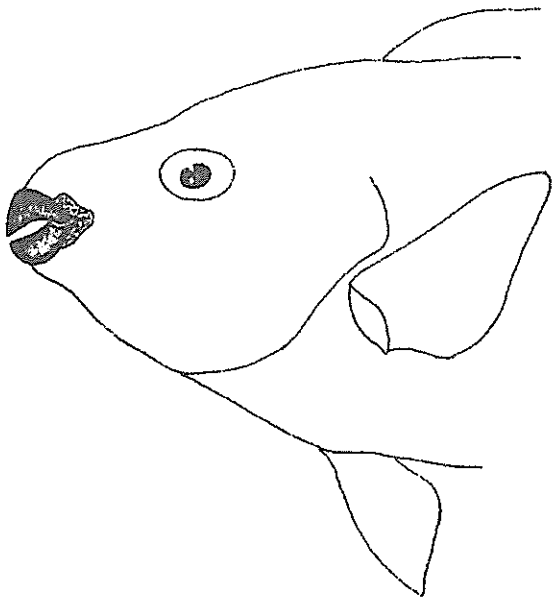

Figure 14. Parrotfish teeth used for scraping food from rock surfaces and reefs

B. Hydrodynamic and Swimming Sounds:

The movement of any object through water will create displacements and compressional waves. Many of these compressional waves, although generally below 500 Hz, and frequently subsonic, can be detected as sound by most hydrophones.

Such sounds can be produced in three ways by swimming fishes:

1. rhythmical effects of undulatory movements,
2. turbulence generated by flow noise (turbulences and concomitant pressure fluctuations produced by the motion of a body through water),
3. internally generated sounds due to friction between bones and muscles.

The most intense swimming noise occurs when a fish, or school of fish, turns rapidly or changes velocity.

Such a maneuver sounds like a low roar or a wooden mallet hitting the side of a boat underwater.

Additional examples:

1. The Blackbar Soldierfish, Myripristis jacobus, produces a fluttering during a momentarily violent chase to defend its territory against intruders.

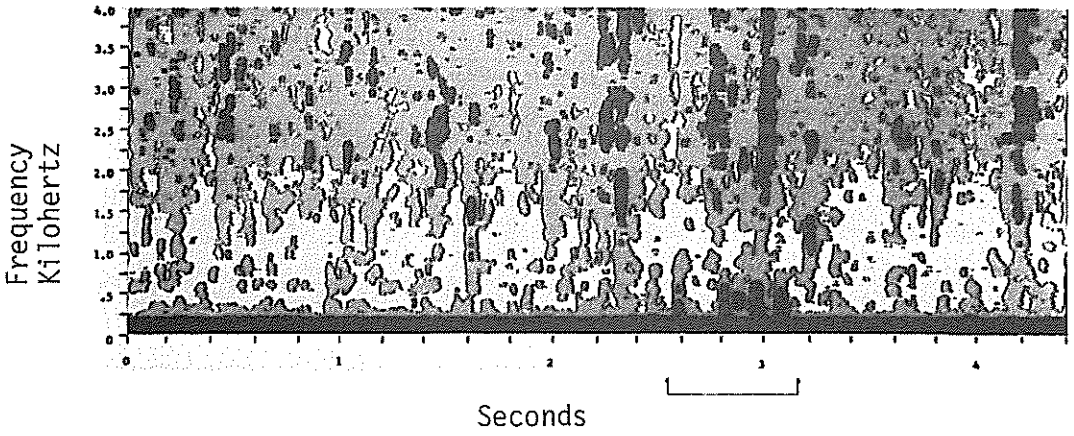

Figure 15. Flutter of Myripristis jacobus

2. The swimming sounds of the Graysby, during a lunge for prey, resemble those of a flock of birds rising.

3. A Trunkfish, which propels itself by skulling motions of its fins, can sometimes sound much like a moth fluttering in ones cupped hands.

C. Swim Bladder Mechanisms:

The function of the swimbladder in altering the quality of stridulatory sounds has already been mentioned. It also functions as the primary sound producing mechanism in numerous cases, and by several means.

1. Gas expulsion:

In Physostomous fishes (those whose swimbladders is connected to the esophagus through a tube) small bubbles are blown from the swim bladder into the esophagus and pharynx producing a series of pulses.

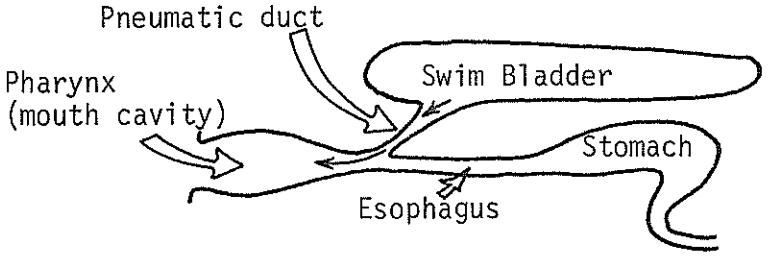

Figure 16. Pathway of bubbles during sound production by certain physostomous fishes

Such has been reported as the method of sound production in the Atlantic eel Anguilla.

2. Extrinsic Muscles:

The utilization of certain body wall muscles to vibrate the swimbladder is common. These muscles are usually contiguous to or attached to the swim bladder at some point.

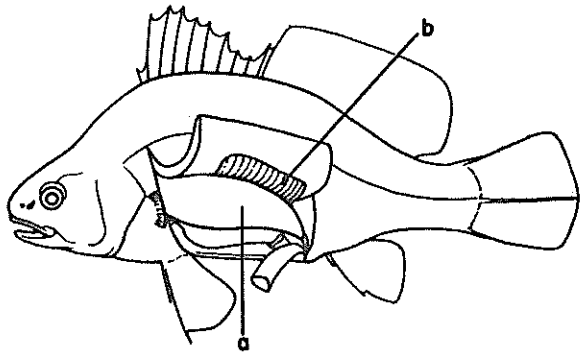

Figure 17. The drumfish possesses its sonic muscles in the lateral body wall, as shown in this dissection. The sonic muscles (b) vibrate against the swim bladder (a). (after Schneider and Hasler, 1960)(from Tavolga 1965)

Drumfish and Croakers (Sciaenidae) possess a pair of muscles in the lateral body wall adjacent to the swim bladder, and attached to the dorso-medial region of the bladder by a tendon.

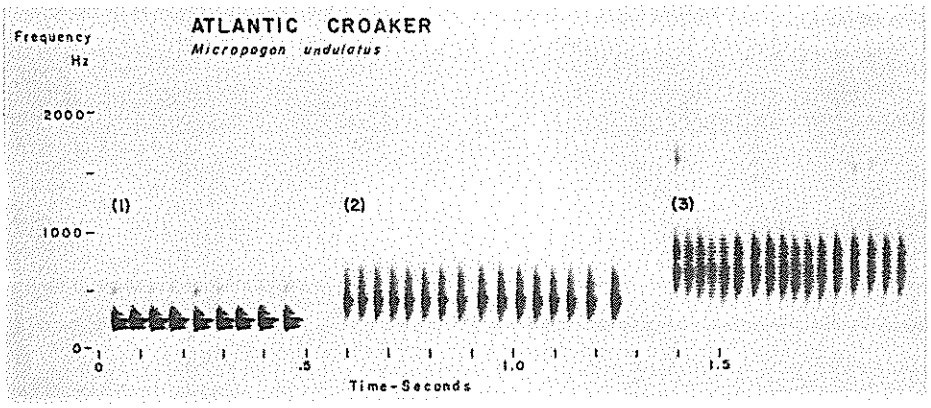

Figure 18. Sonogram of Croaker sounds (from Fish & Mowbray 1970)

The muscles act as constrictors exerting and releasing pressure on the bladder during cycles of contraction and relaxation. The vibrating of the muscles and the accompanying cyclical deformation of the swim bladder function to generate low frequency grunts and croaks.

Squirrelfishes are among the most soniferous of fishes. On coral reefs the chorus of squirrelfish sounds is second in significance only to snapping shrimp noises.

The squirrelfish mechanism involves two muscles, some ribs, and the swim bladder.

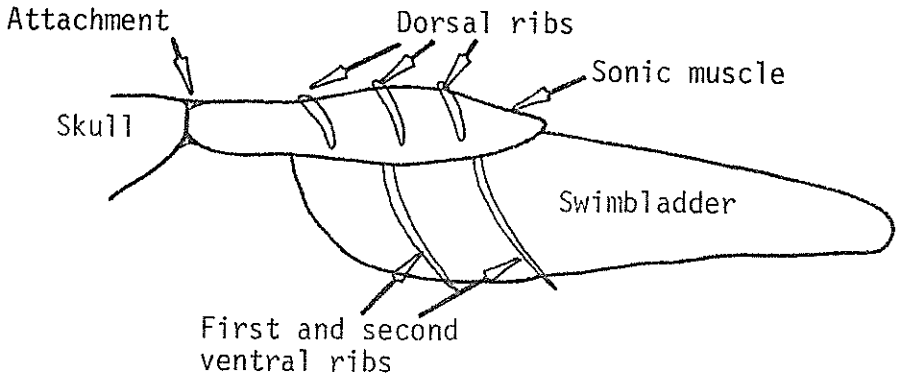

Figure 19. Sonic mechanism in the squirrelfish Holocentrus rufus. (after Winn & Marshall 1963)

The muscles, when twitching, pull the anterior lateral walls of the swim bladder forward and backward and in and out. The deformation of the bladder decreases posteriorly, but generates strong compressional waves and, therefore, sounds With this mechanism the fish produces either grunts or staccato calls.

See Figure 6 in the previous section, IV, on spectral analysis, for a sonogram of squirrelfish staccatos.

The biological significance of squirrelfish sounds is not thoroughly understood but during the day Holocentrus ascensionis maintains a specific territory. Grunts and very short staccatos seem associated with territorial defense. Aggressive encounters are usually accompanied by fin erection and a chase, possibly

nipping, and sometimes staccatos or grunts. It is not clear whether the chased, or chaser, or both produce the sounds.

For part of the night at least, H. ascensionis move out over the reef, apparently in search of food. Associated with this are apparent spontaneous staccato calls which, where the fishes are numerous, result in a chorus resembling the cooing of doves (Fig. 20).

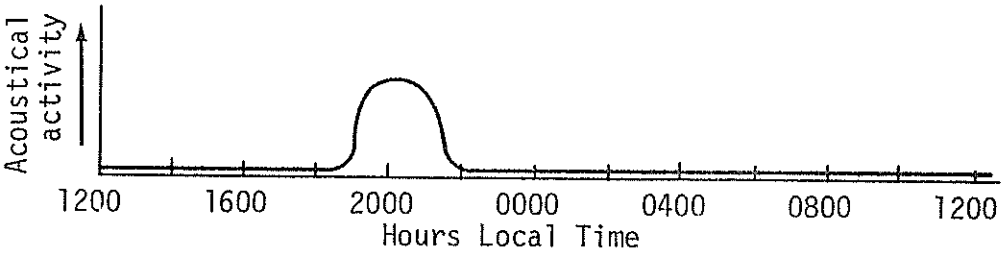

Figure 20. Diel cycle of acoustical activity in Holocentrus ascensionis. (Bright, unpublished)

It is interesting here to note the hearing capability of H. ascensionis in comparison to humans.

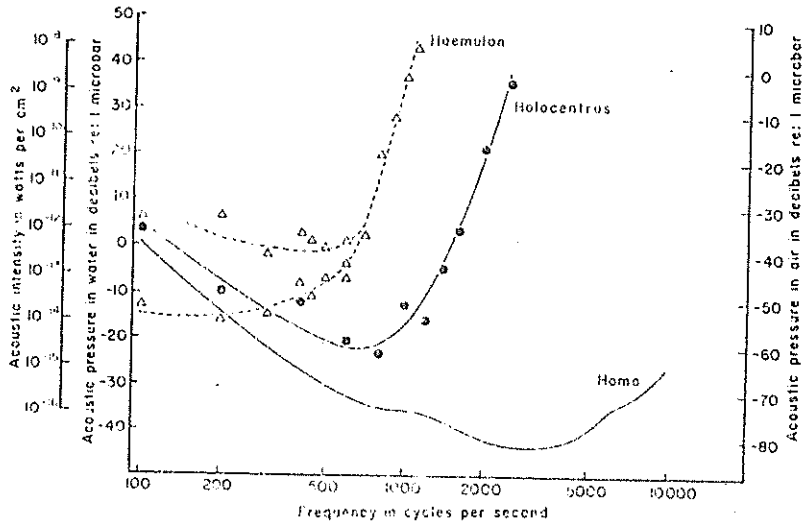

Figure 21. Composite graph showing comparisons of audiograms of the squirrelfish (Holocentrus ascensionis), the blue-striped grunt (Haemulon sciurus), and the human hearing curve according to Sivian and White (1933). All these curves are plotted against the extreme left-hand ordinate in terms of acoustic intensity (W/cm^2). The acoustic pressures in water are on the left ordinate and the equivalent acoustic pressures in air (against which the human audiogram is plotted) are on the right-hand ordinate. (Wodinsky and Tavolga 1964)

The threshold of hearing for H. ascensionis is lowest (hearing most sensitive) at about 500-1000 Hz. This is the range of frequencies wherein sonographs show the maximum expenditure of energy by this species in sound production. Thus the ear of the fish is, not unexpectedly, well suited to detect sounds produced by individuals of its own species.

The grunt, Haemulon scuirus, a stridulatory sound producer, shows maximum sensitivity in the region below 500 Hz. Sonographic analysis shows clearly that this is the region of maximum energy expenditure during sound production for this species.

D. Intrinsic Muscles:

Those sonic muscles completely attached to the swim bladder are referred to as intrinsic muscles. Under these conditions the swim bladder and attached muscles may actually be removed from the fish and stimulated electrically to produce sounds. Because of the intimate connection between bladder and muscles this system is probably the most efficient sound producing mechanism among the fishes. Certain Toadfishes (Batrachoididae), when disturbed, are capable of producing a sound which can be compared to a sledge hammer being struck against a rock underwater.

The Toadfish Opsanus tau also produces a unique harmonic boatwhistle-like sound.

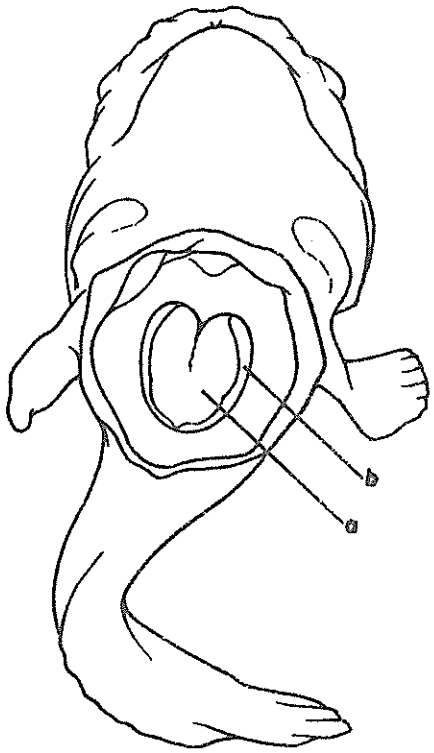

Figure 22. The toadfish possesses probably the most efficient sonic mechanism among the fishes. A dissection reveals the swim bladder (a) as a heart-shaped sac within the body cavity. Two heavy bands of muscle tissue (b) are attached to the sides of the bladder. (from Tavolga 1965)

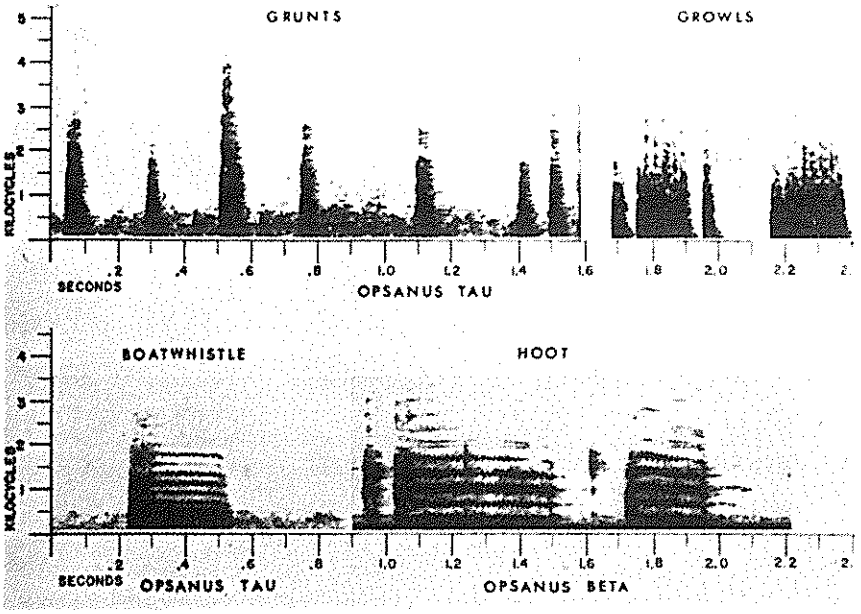

Figure 23. Sonograms of various toadfish sounds (from Winn 1964)

The boatwhistle sound, produced only by the male, is definitely associated with courting behavior. The male maintains spacing between himself and other males during the breeding season, and possibly attracts females, by emitting the sound. The depth of water in which the fish resides has a definite effect on the relative strength of certain toadfish sound harmonics. This is possibly related to the formation of standing waves at some frequencies at certain shallow depths. Similarly, when animals reside on hard as opposed to soft bottoms, a change in intensity of certain harmonics is noticed. These observations cast doubt upon the accuracy of observations made on fishes in captivity in small aquaria, at least where harmonic sounds are concerned.

We have experienced a great difference in the apparent relationship between frequency and energy expenditure between certain non-harmonic sounds made in the laboratory and in the field by the same species of fish.

E. An idea of the Biological Significance of Fish Sounds is given by the following table from Winn, 1964.

Table 1. Correlations between sounds and specific phases of behavior in some fishes

Behavior (*Non-reproductive*)	Sound and Species	References
Competitive Feeding	Suspected maximum number of sounds produced near midnight when feeding, croakers, Chesapeake Bay.	Dobrin, 1947
	Possibly *Epinephalus striatus*.	Moulton, 1958
	Aggressive behavior and sounds increased after feeding but not during the feeding of *Stenotomus chrysops*, *Prionotus carolinus* and others.	Fish, 1954; Brawn, 1961
Territorial Defense	Grunts against own species ,*Holocentrus rufus*.	Winn, Marshall and Hazlett, 1963
"Spontaneous" Sounds in Aggregation or School	Grunt sounds, of nocturnal schools, *Galeichthys felis*.	Tavolga, 1960
	Sob and yelp sounds at night when in small groups, *Bagre marinus*.	Tavolga, 1960
	Sounds of *Pygocentrus piraya*.	Meschkat, in Schneider, 1961.
	Sounds of *Therapon jarbua*.	Schneider, 1961
Confronted with New Stimulus Situations (e.g. Hand-held, Prodding, etc.)	Prodded grunt sounds of *Galeichthys felis*.	Tavolga, 1960
	Prodded grunt sounds of *Bagre marinus*.	Tavolga, 1960
	Prodded distress sounds and sounds when approached by another species of fish of *Micropterus boucei*.	Tavolga, 1960
	Grunts and growls of *Opsanus tau* and *Opsanus beta*.	Fish, 1954; Gray and Winn, 1961; Tavolga, 1960
	Warning staccato of *Holocentrus rufus* and *Holocentrus marianus* and different hand-held grunts.	Moulton, 1958; Winn, Marshall and Hazlett, 1963
	Warning sounds of *Epinephalus striatus*.	Moulton, 1958
	Aggressive defense sounds of *Gadus callarias*.	Brawn, 1961
	Other fishes.	Fish, 1952, 1954
Escaping	Grunts when escaping from attacks and grunts of another individual, *Porichthys notatus*.	Greene, 1924
	Escape sounds after aggressive encounter of codfish.	Brawn, 1961
Migration	Croaker migrations after reproduction.	Johnson, 1948
Exploring New Environment	Clicks of *Hippocampus hudsonius*.	Fish, 1953, 1954

Behavior (*Reproductive*)	Sound and Species	References
Spawning Migration	Many Sciaenidae.	Fish, 1954
Stationary Defense of Nest	Grunts and growls by male on nest against many objects but more toward other males, *Opsanus tau*.	Gray and Winn, 1961
	Grunts of *Porichthys notatus*.	Greene, 1924; Cohen and Winn, (in MS)
	Snoring sound of *Gobius jozo*.	Kinzer, 1961
Chasing	Isolated knocks of *Notropis analostanus*, probably males only.	Winn and Stout, 1960; Stout, 1963a, b
	Grunts by males of *Corvina nigra*.	Dijkgraaf, 1947
	Grunts of *Pomacentrus leucostictus*, possibly also non-reproductive territory.	Moulton, 1958
	Sounds in male to male encounters of *Gadus callarias*.	Brawn, 1961
Display Fighting	Rapid series of knocks of *Notropis analostanus*, probably males only.	Winn and Stout, 1960; Stout, 1963a, b
Courtship	Male sounds of *Bathygobius soporator*.	Tavolga, 1956, 1958b
	Male sounds of *Chasmodes bosquianus*.	Tavolga, 1958c
	Purring sounds, and occasional knocks of *Notropis analostanus*, probably only males.	Winn and Stout, 1960; Stout, 1963a, b
	Many sounds only at beginning of courtship, *Trichopsis vittatus*.	Marshall (work in progress)
	Some grunts produced by *Gadus callarias*.	Brawn, 1961
	Clicks of a pair of *Hippocampus hudsonius*.	Fish, 1953, 1954
Spawning	United pair of *Hippocampus hudsonius*.	Fish, 1954
"Spontaneous" Sounds by Male at Nest Site	*Opsanus tau* boatwhistle (possibly also *Opsanus beta*).	Fish, 1954; Gray and Winn, 1961; Tavolga, 1958c
	Probably staccato call of *Prionotus* spp.	Moulton, 1956
	Snoring sound of *Gobius jozo*.	Kinzer, 1961
Spontaneous Sounds of a Breeding Aggregation, Not Territorial	Male drumming of *Aplodinotus grunniens* seems to fit this category, in spawning aggregation.	Schneider and Hasler, 1960
	Possibly scratching sounds of a prespawning aggregation of female *Semotilus corporalis*.	Winn, unpublished

VII. Sound Production in Marine Mammals:

All marine mammal groups contain species which are known sound producers, and all but the order Carnivora, containing the Sea Otter Enhydra lutra, have representatives known to produce sounds underwater.

E.G. Seals (Pinnipeda)

Underwater barks
Bell-like underwater sounds of the walrus

Sea Cows (Sirena)

Squeaky and ragged underwater sounds

Porpoises and whales (Cetacea)

Extremely vociferous underwater

A. Cetacean sounds:

These are the subject of much inquiry and interest due to their potential to interfere with sonar, and also due to the echolocation abilities of certain cetaceans.

The frequency range of cetacean sounds is phenomenal, extending from below 20 Hz in some Mysticete (toothless) whales to well into the ultrasonic realm in the case of the Odontocete (toothed) whales and porpoises.

The behavioral significance of cetacean sounds is, again, poorly understood. The animals are extremely difficult to observe in the wild, being very mobile pelagic creatures. In captivity their behavior is undoubtedly quite unlike that in the natural habitat.

In general, we can say that cetacean sounds are either communicative (conveying information from one individual to another) or navigational (echolocation).

Almost nothing is known of the specific meanings of the typically low frequency (20-1000 Hz) Mysticete sounds. Some feel that the sonorous moans and screams of the Humpback Whale, Megaptera, as it migrates past Bermuda are manifestations of reproductive urges. There is good evidence that Odontocetes can vocally communicate information concerning their environment

to members of their herd. Some herds may even have their own individual dialects. Information is apparently transmitted largely through frequency modulation. See Section III for examples.

1. Echolocation

Tursiops truncatus, the Bottlenose Dolphin, has been studied quite extensively in an attempt to define its echolocation capabilities. The only types of signals clearly implicated in echolocation are creaking or clicking sound trains, frequently resembling a rusty hinge or a squeaking door noise lasting 2-10 sec. Such sounds, however, may be accompanied by other sounds of the communicative class.

Where vision is difficult or where a particularly interesting target is located the repetition rate of pulse emission may achieve 500 to 600 clicks per second, and what we perceive as squawks or barks may be the result of trains of clicks produced at rates up to 1200 per sec.

The clicks themselves are "white noise" probably extending up to 170 kHz but with the majority of energy expenditure below 30 kHz.

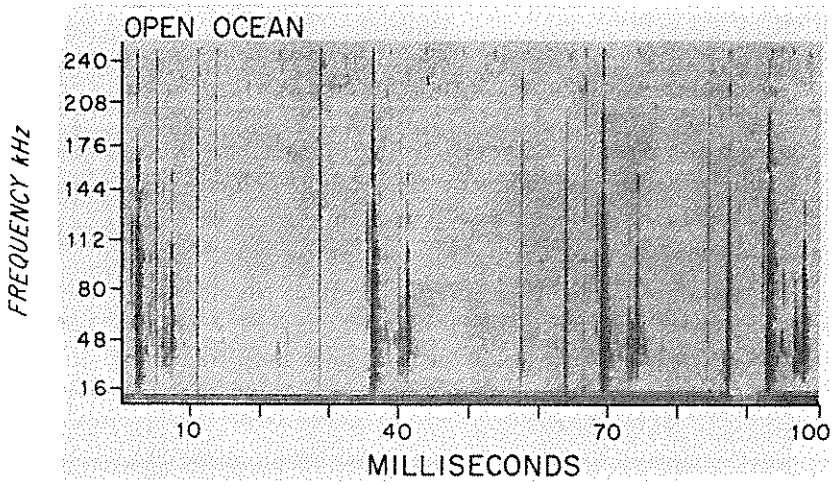

Figure 24. Echolocation clicks of the Porpoise Steno. (from Norris and Evans, 1967)

The hearing ability of Tursiops truncatus corresponds very well to this regime being most sensitive from 30-50 kHz.

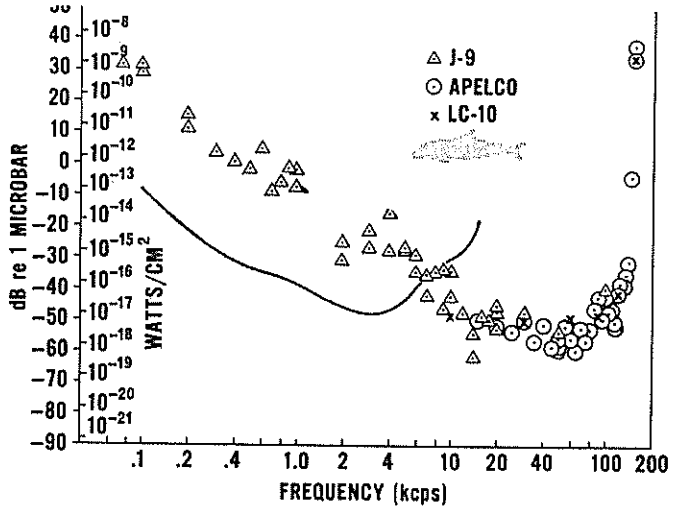

Figure 25. Audiogram of threshold values (Tursiops & Man). The triangles, circles, and crosses represent thresholds taken using the J-9, TM-8A and LC-10, respectively. The solid curve is the human audiogram of Sivian and White (1933) plotted against the ordinate in watts/cm^2. The other ordinate scale gives pressure level in dB (re 1 μbar) in water. This scale can be converted to dB (re 0.0002 dynes/cm^2) by adding 74 dB. The noise spectrum (not shown) for zero sea state (see Mellen (1952)) is about 40 dB (re 1 μbar) at 100 Hz decreasing with increasing frequency at the rate of approximately 5 dB per octave. (from Johnson 1962)

Clicks are produced underwater without release of air to the outside, apparently by the following mechanism.

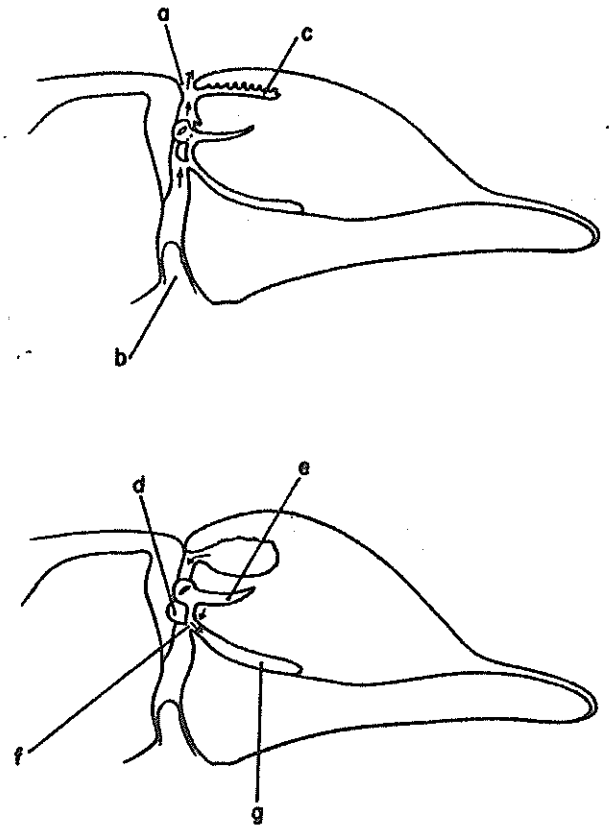

Figure 26. Sonic mechanisms in cetaceans. The series of two diagrams illustrate schematically the production of click sounds in the porpoise, as reconstructed by Norris (1964). In the upper figure, the blowhole (a) is open, as in a breathing cycle, and air can pass, during exhalation, from the larynx (b) through the nasal passages (arrows). When the blowhole closes, the upper vestibular sacs (c) become inflated. In the lower figure, the nasal plugs (d) block the nasal passage and pressure is exerted on the vestibular sacs. Air trickles past a small lip into the tubular sacs (e), inflating them. The click train is produced when air is forced through the narrow connecting sacs (f) into the lower premaxillary sacs (g). Recycling can occur by relaxation of the nasal plugs, which permits air to flow back into the vestibular sacs. (from Tavolga 1965)

Sounds are also produced by extruding air through the blowhole, and probably by forcing air through the larynx, although cetaceans have no vocal cords.

Echolocation sounds, however, apparently originate at the slits of the tubular sacs. These sounds, at least at 100 kHz, are highly directional and in some cases are only detected by a hydrophone when the dolphin's nose is pointed directly at it. How the directionality is achieved is not thoroughly understood but it is speculated that the manner in which the sound is reflected from the skull and adjacent structures plays a crucial role.

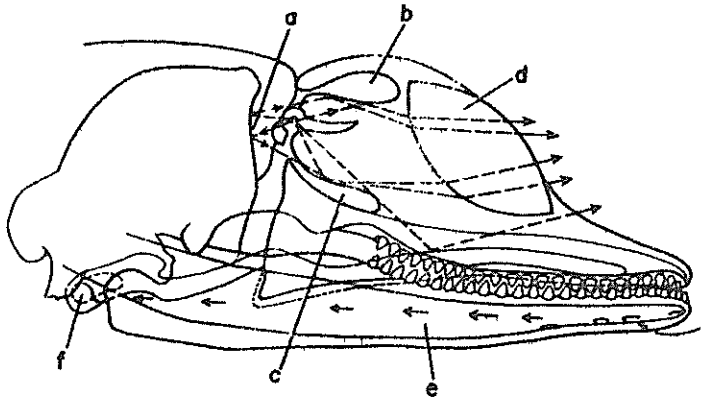

Figure 27. Diagram of a porpoise head with arrows to illustrate the possible sound pathways using the base of the tubular sacs as the point of sound source. Reflection can occur from the nasal surface of the skull (a), the vestibular (b) and premaxillary sacs (c), and the upper jaw which contains an air sac extension of the eustachian canal. All these reflected and direct sound paths are further focussed by the melon (d) whose fatty tissue acts as an acoustic lens. Sound reception, according to Norris (1964), can take place through the lower jaw (e) which is acoustically coupled to the dense bone surrounding the inner ear (f). (after Norris, 1964)(from Tavolga 1964)

The fatty melon is thought to be an acoustical lens, focusing the clicks into a narrow forward directed beam. The melon can be deformed by muscles adjacent to it.

Cup-shaped processes of the Maxillary (upper jaw) bones form a parabolic reflecting area behind the sound source but the bones on the left and right of the midline are not symmetrical. These asymmetries in the shapes of the bones are thought to result in a

modulation, by differentially resonating or damping certain portions of the total sound emission as it is reflected from the anterior surface of the cranium, which produces essentially 2 beams, one on left and one on the right, having slightly different acoustical properties.

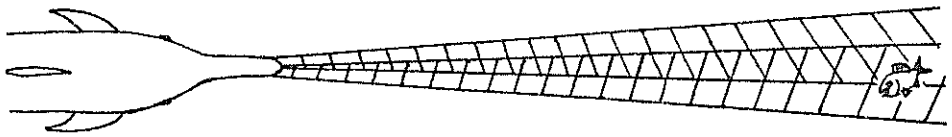

Figure 28. Hypothetical overlapping asymmetrical echolocation beams of Bottlenose Dolphin

Such bilateral variations in sound quality and pressure would be represented in returned echoes in relation to the position of the object being scanned.

Tursiops is known to produce a sound emission that is asymmetrical with regard to sound pressures on either side of its rostrum above the level of the lower jaw. It is likely that such asymmetry will be found to extend to frequency and harmonic composition as well.

Cetaceans ears are customarily acoustically isolated from the surrounding medium by being enclosed in a mass of mucous foam which, because of the gas bubbles it contains, prevents most of the sound from reaching the ear unless it enters through a specific sound transmission linkage.

In Tursiops, returning echolocation clicks apparently enter the receptor system at the forward tip of the lower jaw, through pores in the bone, and are transmitted to the region of the ear through a mass of fatty tissue. Thus reception as well as transmission seems to be directionally oriented in these forms (see Figure 26).

REFERENCES

The following papers and books were used extensively during preparation of these notes. Reference to them and the papers accompanying them where symposium volumes are concerned will provide a suitable entree into marine bio-acoustical literature for those who are interested.

1. Broughton, W. B. 1963. Method in Bio-Acoustical Terminology. In "Acoustical Behavior of Animals," R. G. Busnel, Ed., pp. 3-24, Elsevier, Amsterdam.

2. Dumortier, B. 1963. Morphology of Sound Emission Apparatus in Arthropoda. In "Acoustic Behavior of Animals," R. G. Busnel Ed., pp. 277-345, Elsevier, Amsterdam.

3. Evans, W. E. 1967. Vocalization Among Marine Mammals. In "Marine Bio-Acoustics, Volume 2," W. N. Tavolga, Ed., pp. 159-186.

4. Fish, Marie P. 1964. Biological Sources of Sustained Ambient Sea Noise. In "Marine Bio-Acoustics," W. N. Tavolga, Ed., pp. 175-194, Pergamon Press.

5. Fish, Marie P. and William H. Mowbray. 1970. Sounds of Western North Atlantic Fishes. 207 pp. Johns Hopkins.

6. Iversen, R. T. S., P. J. Perkins and R. D. Dionne. 1963. An Indication of Underwater Sound Production by Squid. Nature, Vol. 199, pp. 250-251.

7. Johnson, C. Scott. 1967. Sound Detection Thresholds in Marine Mammals. In "Marine Bio-Acoustics, Volume 2," W. N. Tavolga, Ed., pp. 247-260, Pergamon Press.

8. Norris, I. S. 1964. Some Problems of Echolocation in Cetaceans. In "Marine Bio-Acoustics," W. N. Tavolga, Ed., pp. 317-336, Pergamon Press.

9. Norris, K. S. and W. E. Evans. 1967. Directionality of Echolocation Clicks in the Rough Tooth Porpose, Steno Bredanensis (Lesson). In "Marine Bio-Acoustics, Volume 2," W. N. Tavolga, Ed., pp. 305-316, Pergamon Press.

10. Tavolga, William N. 1965. Review of Marine Bio-Acoustics, Technical Report: NAVTRADEVCEN 1212-1, U. S. Naval Training Device Center, Port Washington, N.Y., 100 pp.

11. Watkins, William A. 1967. The Harmonic Interval: Fact or Artifact in Spectral Analysis of Pulse Trains. In "Marine Bio-Acoustics, Volume 2," W. N. Tavolga, Ed., pp. 15-43, Pergamon Press.

12. Winn, Howard E. 1964. The Biological Significance of Fish Sounds. In "Marine Bio-Acoustics," W. N. Tavolga, Ed., pp. 213-231, Pergamon Press.

13. Winn, H. E. and J. A. Marshall. 1963. Sound Production Organ of the Squirrelfish Holocentrus rufus, Physiol. Zoöl. 36: pp. 34-44.

THE SONAR EQUATIONS

R. J. Urick
Research Physicist
Naval Ordnance Laboratory, Silver Spring, Md. 20910

1. Uses of the Equations

The sonar equations are a set of relationships among the basic factors of sonar. They

a. make possible performance predictions - or "Post"-dictions - for existing sonars

b. make possible the rational design of new sonars

c. form a convenient framework to tie together all the important effects occurring in underwater sound.

2. Examples

Examples of simple problems in prediction and design are

a. How far away can a diver, using a particular hand-held echo ranging set, detect the presence of a target such as a wreck on the ocean floor?

b. What modifications of the present design can be made - within practical limits - to achieve a specified longer detection range, or lower cost at the same range?

3. The Basic Equality

The equations rest on a certain basic equality. It is: when a certain system function is just achieved,

signal level = background masking level.

4. Meaning

The words in the basic equality may be stated to mean

signal = the desired portion of the acoustic field

level = the "intensity", or rate of acoustic power flow across a given unit area, expressed in db relative to that of a standard intensity.

background = the undesired portion of the acoustic field

masking = that portion of the background that masks or interfers with the signal.

5. Sonar Parameters

To proceed further, we must expand the basic equality in terms of quantities called the sonar parameters. These quantities, while not unique, have been established by sonar usage, and are related to the medium, the target or the equipment:

Parameters Defined by the Medium

Transmission Loss (TL)

Ambient Noise Level (NL)

Reverberation Level (RL)

Parameters Defined by the Target

Target Strength (TS) (for "active" sonars)

Target Source Level (SL) (for "passive" sonars)

Parameters Defined by the Equipment

Projector Source Level (SL)

Self-noise Level (NL)

Receiving Directivity Index (DI)

Detection Threshold (DT)

Note, in passing, that the same symbol is used some times for more than one parameter. This means that they are basically the same and occur in the same way in the equations. Note also that the above choice is arbitrary; other quantities might be used, such as sound velocity or scattering cross-section. The various parameters have been established by sonar usage; various symbols for the parameters appear in the literature. The parameters are all ratios of intensity or power, and are therefore expressible in decibels. Table 1 lists these ratios; Table 2 gives units and reference points.

6. Signal Level

With these definitions, the signal level on the left side of the basic equality is given by

$SL - 2(TL) + TS$ for active sonars*

$SL - TL$ for passive sonars.

7. Background Level

The background masking level is

$NL - DI + DT$ for noise backgrounds

$RL + DT$ for reverberation backgrounds (active sonars only)

8. Statement of the Equations

We have therefore one sonar equation for the passive case, namely:

$$SL - TL = NL - DI + DT$$

and two for the active case, depending on the kind of background:

$$SL - 2(TL) + TS = NL - DI + DT \quad \text{(noise)}^{**}$$

$$= RL + DT \quad \text{(reverberation)}^{**}$$

*Using a coincident sound source and receiving array both pointing toward target. This is the "Monostatic" case. For bistatic operation, using a separated source and receiver, the 2TL's are different and we would have $SL - TL_1 - TL_2 + TS$.

**The two DT's in these equations will, in general, be different.

TABLE 1

THE SONAR PARAMETERS, THEIR DEFINITIONS, AND MEASUREMENT LOCATIONS

Parameter	Symbol	Definition
Source Level	SL	10 log $\frac{\text{intensity of source}}{\text{reference intensity}}$*
Transmission Loss	TL	10 log $\frac{\text{signal intensity at 1 yard}}{\text{signal intensity at target or receiver}}$
Target Strength	TS	10 log $\frac{\text{echo intensity at 1 yd from target}}{\text{incident intensity}}$*
Noise Level	NL	10 log $\frac{\text{noise intensity}}{\text{reference intensity}}$*
(Receiving) Directivity Index	DI	10 log $\frac{\text{noise power generated by an equivalent non-directional hydrophone}}{\text{noise power generated by actual hydrophone}}$
Reverberation Level	RL	10 log $\frac{\text{reverberation power at hydrophone terminals}}{\text{power generated by signal of reference intensity}}$*
Detection Threshold	DT	10 log $\frac{\text{signal power to just perform a certain function}}{\text{noise power at hydrophone terminals}}$

*The reference intensity is that of a plane wave of rms pressure 1 dyne/cm^2.

TABLE 2

TERMINOLOGY OF VARIOUS COMBINATIONS OF THE SONAR PARAMETERS

Name	Parameters	Remarks
Echo Level	SL-2(TL)+TS	The intensity of the echo as measured in the water at the hydrophone
Noise Masking Level	NL-DI+DT	Another name for these two combinations is "minimum detectable echo level"
Reverberation Masking Level	RL+DT	
Echo Excess	SL-2(TL)+TS -(NL-DI+DT)	Detection just occurs, under the probability conditions implied in the term DT, when the echo excess is zero.
Performance Figure	SL-(NL-DI)	Difference between the source level and the noise level measured at the hydrophone terminals
Figure of Merit	SL-(NL-DI+DT)	Equals the maximum allowable one-way transmission loss in passive sonars, or the maximum allowable two-way loss for TS=0 in active sonars.

9. Significance of DT

The equality of the sonar equations means that when the equality occurs, a certain function is just being performed. This function may be detection (implied by the term (Detection Threshold) or, target acquisition (as by a diver making an acoustic sweep), or a mine actuation (as in an acoustic mine) or a successful classification. The word just implies certain probabilities. Both the function involved and the desired probabilities affect and determine the DT in the equations.

10. Special Names

For certain purposes, particular names have been given to different combinations of parameters. These are listed in Table 3. Of these the most popular is figure-of-merit. When the background is noise, the figure-of-merit lumps together all the equipment parameters against an arbitrary, specified target. Its magnitude is an indicator of the "merit" of the sonar, and is equal to the maximum tolerable TL for which the target can be detected with a detection probability (and a false alarm probability) implied by the value of DT used.

Another useful number is echo excess for active sonars or signal excess for passive sonars. It is the signal-to-background ratio expressed in db. It is zero when detection just occurs and the sonar equation is satisfied. It is a positive number of db at short ranges and a negative number at long ranges.

Generally speaking, in a design or prediction problem the engineer will make a plot of signal level and background level vs. range over all ranges of interest, as a key to what is occurring at ranges other than the one at which detection (or some other function) takes place.

11. Difficulty with Short Transients

The equations are written in terms of intensity. SL in particular is the intensity of the sound emitted by the source, averaged over a period of time. But over what period? For long-pulse sonars, there is no difficulty in specifying an averaging time; the time period is essentially that of the pulse itself. But what about short pulse sonars? In particular, how about explosive sound sources for which the intensity vs. time function is like Fig. 1a?

12. Waveform Distortion

An added problem for short transients is the time distortion introduced by 1) propagation in the medium and 2) the

TABLE 3

DEFINITIONS AND REFERENCE POINTS OF THE SONAR PARAMETERS

NAME	DEFINITION	UNITS	POINT OF REFERENCE
Source Level (of Projector or Target)	Intensity level of sound emitted by projector or target.	db above 1 dyne/cm^2 in a 1 cps band for a wideband source.	1 yd from "acoustic center" of source.
(Transmitting) D.I.	10 log $\frac{I}{I'}$, I = actual intensity on axis (when used as projector) I' = intensity of a nondirectional source of same power output.	db	any distant point along transducer axis.
Target Strength	Ratio of the reflected intensity from a target to the incident intensity.	db	1 yd from "acoustic center" of target.
Transmission Loss	Ratio of the intensity at unit distance from the source to the intensity at some distant point.	db	1 yd from source.
Noise Level (Ambient or Self Noise	Equivalent isotropic intensity.	db above 1 dyne/cm^2 in a 1 cps band.	at receiving transducer.
Reverberation Level (Scattering Strength)	Involves "scattering strength" of the reverberating area of volume defined similarly to target strength.	db	1 yd from reverberating area or volume (for Scattering (Strength).
Detection Threshold	Ratio of signal to background levels for a stated probability of performing some given function (detecting, homing, etc.)	db. Signal in receiver band, noise in 1 cps band.	Transducer electrical terminals.

finite size of the target in echo ranging. This distortion is sometimes so severe, as for explosive pulses, that the echo bears no similarity in waveform to the initial emitted waveform. Compare the echo of Fig. 1b with the waveform of Fig. 1a. Even more severe distortion occurs for explosive transmission down the deep ocean "Sofar" sound channel, wherein an explosion becomes a long drawn-out blob some 10 seconds long after propagating a thousand miles.

13. Conservation

To get around this difficulty, we appeal to energy considerations, noting that by whatever mechanisms this distortion takes place, the acoustic energy of the source, in the absence of absorptive processes, must be conserved. As an example, we may note that spherical spreading in a uniform, non-absorptive, unbounded medium is a result of conservation of energy, not of intensity.

14. Intensity and Energy Flux Density

In terms of the pressure-time function p(t) of a plane wave the average intensity over the interval 0 to T is

$$I = \frac{1}{T} \int_0^T \frac{p^2(t)}{\rho c} \, dt$$

The energy flux density of the wave is the total acoustic energy passing through a unit area, and is given by

$$E = \int_0^\infty \frac{p^2(t)}{\rho c} \, dt$$

This is finite for a transient p(t). If p(t) lasts only from time 0 to time T, then we have $E = I \cdot T$.

15. Echo Level for Energy

If we use energy flux density instead of intensity in the active sonar equation, the energy flux density level of the echo is, as before,

$$SL' - 2(TL') + TS'$$

where SL' is the energy flux density of the source as just defined, TL' is the transmission loss for energy flux density and is the same as the ordinary TL in the steady state long-pulse case, and TS' is a ratio of energy flux densities of the echo and the incident wave (all in db). On the right

hand side, NL is the intensity level of a continuous noise; we must multiply it by a time (by adding 10 log time in db) to convert it to energy density.

16. Echo Duration

The time to be used in this conversion is somewhat arbitrary but the duration of the echo suggests itself as being most reasonable. If this is called t_e, the right-hand side becomes

$$NL - DI + DT + 10 \log t_e$$

One carrying over 10 log t_e to the left side we obtain an equation of intensity instead of energy density

$$SL' - 10 \log t_e + 2(TL)' + TS' = NL - DI + DT$$

where TL' and TS' are intensity ratio (in db) appropriate for CW a long-pulse sonars, for which all propagation paths can be added up. We note here the appearance of a new intensity source level equivalent SL' - 10 log t_e (after converting to db) to divide the energy flux density of the source by the duration of the echo. For short pulses, the echo duration t_e becomes a sonar parameter in its own right.

17. Equivalent Source Level

If short flat topped pings of duration t_o are used for echo ranging, the energy density source level is

$$SL' = SL + 10 \log t_o$$

and the source level to be used in the sonar equations is

$$SL + 10 \log t_o/t_e$$

18. Signal Stretching

t_e is always longer than t_o. The medium and target stretch out the initial source pulse. This stretching is caused by multipath propagation (involving a spread of travel times) and by the extension in range of the target (ditto). For long-pulse sonars, t_e and t_o are nearly the same, but for short pulses, for which $t_e <> t_o$, the effective source level is less and must be taken into account in calculations.

19. A Compensation

The effect of signal stretching is not all band, however, because it increases the time available for signal integration

or processing, and improves DT. Hence there is here a partial but not total, compensation for the lower source level caused by signal stretching of short pulses.

$$DT = 10 \log d/2\tau$$

$$= 5 \log dw/\tau$$

20. Radar Analogies

Similar equations occur in radar, though in linear form and with different parameters. An example is given in Skolnik "Introduction to Radar Systems", McGraw-Hill, 1962, Eq. 201 as

$$R_{max} = \left[\frac{P_t G A_e \sigma}{(4\pi)^2 Smin}\right]^{1/4}$$

where R_{max} = maximum radar range, P_t = transmitted power, G = antenna gain, A_e = effective antenna aperture, σ = radar target cross-section, Smin = minimum detectable signal. If we convert to db by taking 10 times the logarithm of the various quantities and rearrange, we obtain

$$10 \log \frac{P_t \cdot G}{4\pi} + 10 \log \frac{\sigma}{4\pi} - 10 \log R_{max}^4 = 10 \log S_{min} - 10 \log A_e$$

The analogous sonar equation is

$$SL + TS - 2(TL) = (NL + DT) - DI$$

where the corresponding quantities are given in the same order. Note that, in radar, TL is usually taken as merely the loss due to spherical spreading, namely 20 log r; in sonar, TL is a complicated parameter involving the vast multitude of effects associated with sound propagation in the sea.

21. Noise and Reverberation Limitation

In active sonars, it is necessary to know whether the background is noise or reverberation. This requires a number of separate computations of echo level and reverberation level as a function of range, plus a comparison with the noise level, to determine whether the echoes will be noise limited or reverberation limited at different ranges. Once this is done and a plot is drawn, and if it is clear which

kind of limitation applies for the problem at hand, the appropriate form of the equation may be used with confidence. When large changes are made, the entire matter must be re-examined.

22. Using the Equations

In practical use, the appropriate form of the equations is solved for the particular parameter of interest. In design problems, this is usually one of the equipment parameters noted above. In prediction problems, the unknown is usually TL or one of the target parameters. Mixed situations often occur. Indeed, sonar design is a trial and error process involving all the various parameters that are not firmly specified in advance, and involving trade-offs between practical design and hoped-for performance.

23. Prediction Problem

A pinging long-pulse sonar of source level 130 db and receiving directivity index 10 db echo ranges against a target of target strength 15 db. In a noise background of spectrum level (1 Hz band) - 30 db, and with a DT of + 10 db, at what range can it just detect the target, if simple spherical spreading is assumed? Solving the active noise-limited equation for TL, we obtain

$$2(TL) = SL + TS - NL + DI - DT$$

On substituting the numbers,

$$\begin{aligned} 2(TL) &= 130 + 15 + 30 + 10 - 10 = 175 \text{ db} \\ TL &= 87\ 1/2 = 20 \log r \\ \log r &= 4.38 \\ r &= 24{,}000 \text{ yds} \end{aligned}$$

24. A Design Problem

Here the quantity of design interest is apt to be buried in one of the parameters. The first step is to identify which one of the parameters is the unknown, then solve for it, and extract the design quantity being sought. An example is the following: A fish-finding sonar is to be designed that will detect a school of fish of TS = 0 at a range of 1000 yds. Its source level is to be no more than 100 db and it must give an echo 10 db above the spectrum level of the background equal to -40 db. If it must use a line transducer operating at a frequency of 50 kHz, how long must the transducer be?

Here the unknown parameter is DI. Solving the noise equation for DI we have

$$DI = 2(TL) - SL - TS + NL + DT$$

Assuming spherical spreading with an absorption coefficient of 15 db/kyd, we find with r = 1000, $TL = 20 \log r + \alpha r \times 10^{-3} = 60 + 15 = 75$ db.

All the other quantities are stated above. Substituting we get

$$DI = 150 - 100 - 0 - 40 + 10 = 20 \text{ db}$$

For a line transducer of length L at wave length λ, the relation for DI is

$$DI = 10 \log \frac{2L}{\lambda}$$

Substituting DI = 20, = 1.2 inches at 50 kHz, we find L = 60 inches. If the engineer does not like this answer for any practical reason, he would at this point go back to the problem statement, make whatever changes he could get away with, and resolve the sonar equation.

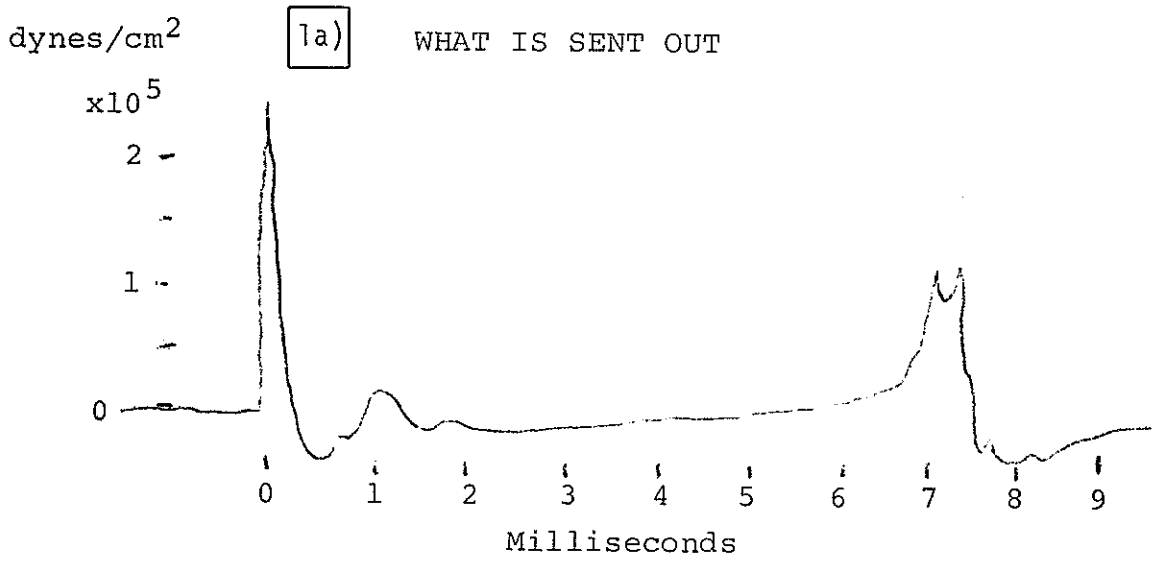

4 lbs TNT exploded at 4000 ft and recorded broadband at 300 ft

1b) WHAT IS RECEIVED

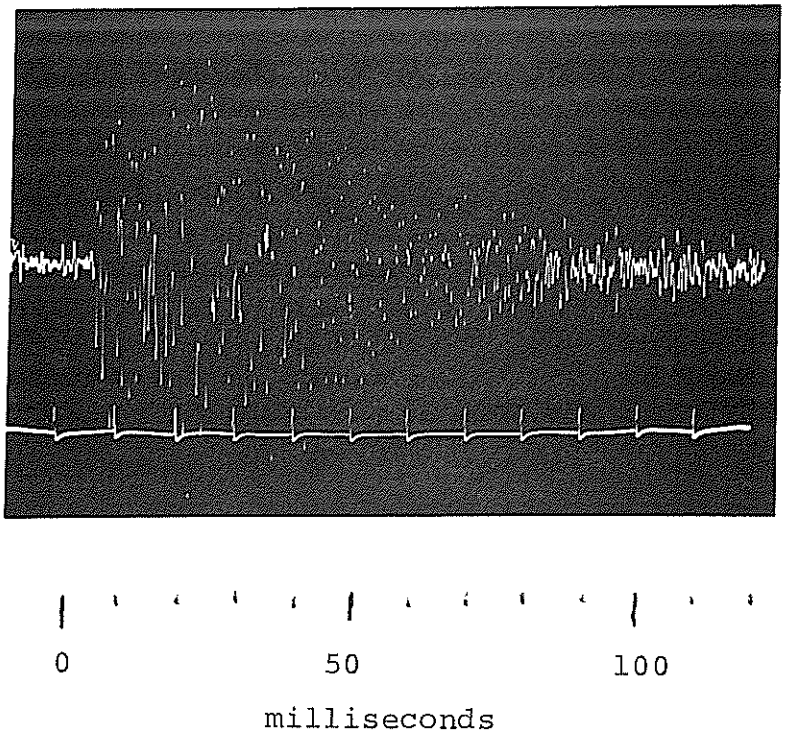

Submarine echo recorded 500-5000 Hz

Fig. 1

SOUND PROPAGATION IN THE SEA

R. J. Urick
Research Physicist
Naval Ordnance Laboratory, Silver Spring, Maryland

1. Physical Equations of Acoustics

The propagation of a disturbance in an elastic medium rests upon the wave equation. For a perfect non-viscous fluid, the wave equation for small disturbances can be obtained easily from four basic relationships of physics. These are;

Equation of Continuity

$$\frac{\partial s}{\partial t} = -\left(\frac{\partial u_x}{\partial x} + \frac{\partial u_y}{\partial y} + \frac{\partial u_z}{\partial z}\right) \tag{1}$$

$$s = \text{"condensation"} = \frac{\rho - \rho_o}{\rho_o}$$

$$u = \text{partial velocity}$$

Equation of State: $P_o = f(\rho, T)$, P_o = pressure, ρ = density, T = temperature. For small rapid changes (adiabatic)

$$p = ks \tag{2}$$

$$p = P - P_o, \quad P = \text{instantenous pressure}$$

$$k = \text{bulk modulus}$$

Equations of Motion

$$f_x = \rho_o \frac{\partial u_x}{\partial x} \text{ etc.} \tag{3}$$

$$f_x = \text{x component of force} \tag{3}$$

Equations of Force

$$f_x = \frac{-\partial p}{\partial x} \quad \text{etc.} \tag{4}$$

2. Wave Equations

On combining, differentiating, and adding the above, we obtain a single equation, called the wave equation relating the pressure to x, y, z, and t:

$$\frac{\partial^2 p}{\partial t^2} = \frac{k}{\rho_o}\left(\frac{\partial^2 p}{\partial x^2} + \frac{\partial^2 p}{\partial y^2} + \frac{\partial^2 p}{\partial z^2}\right)$$

The quantity k/ρ_o has the dimensions of $(\text{velocity})^{+2}$ and is abbreviated c^{+2}. Eighteenth century mathematicians knew that the wave equation in one dimension (i.e., for a plane wave) could be satisfied by functions of the form $p = f(x \pm ct)$. It follows that c is the propagation velocity of the pressure disturbance p.

3. Wave Theory

The wave equation can be solved by two different theoretical approaches: wave theory and ray theory. Both are frequently encountered in underwater sound. Wave theory seeks functional solutions of the wave equation that satisfy the boundary and source conditions. The most simple example is the one-dimensional equation

$$\frac{\partial^2 p}{\partial t^2} = c^2 \frac{\partial^2 p}{\partial y^2}$$

for a plane wave propagating parallel to the y axis. This has solutions of the form $p = (\sum_n A_n \sin k_n y + \sum_n B_n \cos k_n y) \sum_m e^{iw_m(t - m)}$ where the terms in parentheses are adjusted to fit the specified pressure conditions existing at boundaries such as the sea surface and bottom, and where the time terms are adjusted to fit what is radiated by the source. In practical problems the wave theory solution is often extremely complicated.

4. Ray Theory

This centers around the idea of wave fronts and rays normal to them. Wave fronts are surfaces of constant phase. They can be shown to satisfy the eikonal equation (eikon = Greek word for image)

$$\left(\frac{\partial W}{\partial x}\right)^2 + \left(\frac{\partial W}{\partial y}\right)^2 + \left(\frac{\partial W}{\partial z}\right)^2 = n^2(x,y,z)$$

where the surfaces $W(x,y,z)$ are wavefronts and $n = \frac{c_o}{c(x,y,z)}$ is the index of refraction. The eikonal equation is useful because (1) there is no time dependence and (2) it leads to a set of ordinary differential equations that in turn lead to Snell's Law and to the equations for the curvature of rays in terms of the gradient of the index of refraction n. These make ray diagrams possible. Ray diagrams give a pictorial and quantitative picture of the distribution of sound in the sea.

5. Comparison

Both theories have limitations. Wave theory gives a formally complete solution to a propagation problem, but one difficult to interpret and having grave mathematical difficulties for real boundary and medium conditions (ex. rough surface, actual velocity profiles). Ray theory gives answers that are clearly visualized and with boundary conditions that are easy to insert. It does not handle diffraction problems; it is independent of nature of the source of sound and is valid only under restricted conditions. These restrictions are equivalent to saying that the direction of a ray, the sound velocity, and the sound intensity do not change much in the distance of one wavelength. Wave theory is often applied to propagation in sound channels, especially at low frequencies; ray theory is appropriate for deep ocean propagation where the peculiar velocity structure ($c(x,y,z)$) of the sea can be readily taken into account.

6. Transmission Loss

The sonar parameter pertinent to propagation is transmission loss, defined as

$$TL = 10 \log \frac{I_1}{I_r}$$

where I_1 is the intensity at the reference distance (one yard) from the source, and I_r is the intensity at distant point.

7. The Free Field

The simplest propagation condition is that of the unbounded, uniform, absorption-free fluid. By conservation, the acoustic power ρ (or more properly the energy flux density) crossing any spherical surface surrounding the source is the same. Therefore the intensity I_1 at distance r_1 is related to the intensity I_2 at r_2 by

$$I_1 = \frac{\text{power}}{\text{area}} = \frac{P}{4\pi r_1^2} \; ; \quad I_2 = \frac{P}{4\pi r_2^2}$$

$$\therefore \quad \frac{I_1}{I_2} = \frac{r_2^2}{r_1^2}$$

$$TL = 10 \log \frac{I_1(r_1=1)}{I_2} = 10 \log \frac{r_2^2}{(1)^2} = 20 \log r_2 \text{ db}$$

This is called spherical or inverse-square spreading.

8. A Fortunate Happenstance

It often happens that for measured data spherical spreading is found to occur where it has no right to occur. It is often found in sound channels when the loss due to leakage counter balances the gain due to channeling. Spherical spreading is a ubiquitous occurrence that is often appealed to in practical problems when no more precise quantization of the propagation is possible. Yet, free-field spreading seldom truly exists for underwater sound. Much of what follows in this write-up deals with deviations from the free-field condition.

9. Absorption

The absorption of sound refers to the conversion of sound to heat. Spreading and scattering cause a loss of intensity by redistributing the sound in space; absorption is a true loss of sound energy. It manifests itself as a reduction in intensity in terms of a certain number of decibels per unit distance travelled, and is expressed as an attenuation coefficient α db per kiloyard. α varies strongly with temperature, frequency, and salinity. Examples of the magnitude of α for a salinity of 35 ppt are as follows:

	40°F	80°F
1 kHz	.07	Uncertain
10 kHz	1.0	0.4
100 kHz	35	35

At high frequencies, beyond 500 kHz, the viscosity of the sea water medium is the dominant cause of absorption. At lower frequencies, in the range 5-500 kHz, absorption is caused by an ionic relaxation process of the MgSo4 molecule--one of the minor dissolved salts in sea water--a process having a relaxation time of the order of 10 microseconds. At still lower frequencies, below 5 kHz, another process, of yet undetermined origin, becomes important. All told, because of these various processes, the absorption coefficient varies with frequency at a fixed temperature of 39°F in a remarkably complicated manner, as follows:

$$\alpha = \underset{(<5\ \text{kc})}{\frac{0.1\ f^2}{1 + f^2}} + \underset{(5\text{-}500\ \text{kc})}{\frac{40\ f^2}{4100 + f^2}} + \underset{(>500\ \text{kc})}{5 \times 10^{-4} f^2}$$

(Low Freq. Med. Freq. High Freq.)

where α is in db per kiloyard and f is in kHz. The three terms, in the order of frequency, correspond to the three processes mentioned above.

10. A Rule of Thumb

The combination of spherical spreading plus an attenuation due to absorption give the following expression for the transmission loss TL (from 1 yard) out to r yards:

$$TL = 20 \log r + \alpha r \times 10^{-3}$$

where α is in db per kiloyard. This expression applies strictly only for short ranges and high frequencies, but is also useful, as a working rule, for many other conditions, as mentioned in paragraph 8 above.

11. Velocity of Sound (properly, "Speed" of Sound)

The velocity of sound in sea water is the most precisely known of all underwater acoustic quantities. It has been determined by precise laboratory measurements with an uncertainty of only a few hundredths of one percent. It varies in a complicated way with temperature, salinity, and depth. Formulas and tables have been published by Wilson, Del Grosso and others. Generally speaking, the velocity of sound increases with increasing temperature, salinity, and depth. The increase of velocity with depth is important in isothermal water, such as in mixed layers and at great depths in deep water.

12. Velocity Profile in the Deep Sea

Sound velocity varies with depth in deep open water in a characteristic manner. At any particular spot in the sea, the velocity-depth function is called the velocity profile at that spot. Because the temperature largely determines the velocity, it is commonly determined from shipboard with a bathythermograph (BT) which gives a curve of temperature vs. depth. Complicated instruments suitable for use at sea to measure sound velocity directly--called velocimeters--may be bought from a number of manufacturers. Yet, no discrepancy between the velocity computed from the BT and that measured with a velocimeter in deep water appears to have ever been noted.

The deep sea may be divided into a number of layers having different characteristics. Near the surface down to depths of a few hundred feet occurs the surface layer that is subject to the near-surface influences of heating and cooling, evaporation and wind-mixing. Below the surface layer in mid and high latitudes is a layer of decreasing velocity called the seasonal thermocline having a temperature gradient that varies with the seasons. Below this layer, down to a depth of 3000-4000 feet in mid-latitudes, is the main thermocline in which occurs the main part of the decrease in temperature between the surface and the cold abyssal depths of the oceans. From here to the bottom occurs the deep isothermal layer where the water is essentially isothermal (near 39°F) and the velocity of sound increases with depth.

There is therefore a depth in the sea at which the velocity of sound is a minimum. This minimum forms the axis of the deep sound channel in which sound is constantly returned to the axis by refraction within the layers of the velocity profile having opposite gradients above and below. The sound channel axis in the North Atlantic and Pacific Oceans is deepest at latitudes near 30°N. It lies at a

slightly shallower depth near the equator, and rises to near the surface in high latitudes. A typical velocity profile is shown in Fig. 1.

13. Refraction

The practical importance of the velocity profile is that by using it ray diagrams can be drawn to show the regions of low sound intensity (shadow zones) and high intensity (convergence zones). More generally ray diagrams show how sound is distributed throughout the body of the sea. From computer-produced ray diagrams, accurate measurements can be made to give the intensity at moderate ranges away from shadow zones and caustics.

14. The Sea Surface

The surface of the sea exerts profound influences on underwater sound:

(1) It forms a mirror-like reflector (when not too rough) that creates interference regions of high and low intensity in the near sound field.

(2) It scatters sound incident on it, so as to redistribute sound in space and give rise to surface reverberation.

(3) It casts a shadow, forming a shadow zone, at shallow depths when a negative gradient extends up to the surface.

(4) It contributes to the background of ambient noise by a process not yet completely understood.

15. The Sea Bottom

The sea bottom also affects underwater sound in various ways:

(1) It is also a reflector of sound (through a much poorer one than the sea surface) and provides paths for reaching long ranges in deep water by the bottom reflection (bottom-bounce).

(2) It is a scatterer as well as a reflector, creating bottom reverberation.

(3) It casts a shadow in the positive sound velocity gradient near the deep sea bottom.

The reflectivity of the sea bottom is of great practical importance to present-day sonars. The reflection loss at the bottom is affected by the contour (roughness) of the bottom, the density and sound velocity of the bottom materials, and the layered structure of the bottom (since low frequency sounds penetrate it to considerable depths). The reflectivity of the ocean flow has been surveyed by the Marine Geophysical Survey of the USN Oceanographic Office, and survey work continues at the present time.

16. Sound Channels

Because of the peculiarities of most velocity profiles, together with the existence of the ocean boundaries, channels or ducts exist in the sea. A channel or duct may be said to occur whenever sound, in travelling horizontally outward from the source, is prevented from spreading vertically and becomes confined to some extent--by the boundaries of the channel. Various kinds of sound channels are found in the sea. Some are caused primarily by the boundaries, others by the presence of layers in the sound velocity profile containing a velocity minimum. In such layers, refraction causes sound to return repeatedly to the depth of minimum velocity. This depth is called the axis of the sound channel.

17. Transmission Loss in Channels

A simple model for transmission in sound channels leads to the following expression for the transmission loss (from 1 yard) to r yards:

$$TL = 10 \log r + 10 \log r_o + (\alpha + \alpha_L) r \times 10^{-3}$$

where r_o is the transition range separating the regions of spherical and cylindrical spreading and α_L is the leakage coefficient expressing the rate at which sound leaks out of the channel.

18. The Mixed Layer Channel

The windy temperate parts of the deep sea are characterized by the presence of a mixed layer just beneath the sea caused by turbulent wind-induced mixing. This mixing is often so thorough that the layer becomes isothermal to a few thousandths of a °C. The pressure effect (para. 11) causes the sound velocity in the mixed layer to increase down to the base of the layer. The axis of the mixed layer channel is therefore at the surface. The radio counterpart of this kind of channel is called a ground-based duct.

A mixed layer exists nearly all the time in the windy North Atlantic north of 40° latitude. In the tropics it is found less often and tends to disappear in the afternoon. The reduction in sonar ranges caused by this disappearance was called, long ago, the afternoon effect. The presence or absence of the layer is of great importance for surface ship hull-mounted sonars.

The mixed layer is a relatively poor sonar duct. It is leaky because of

(1) scattering out of the duct by the rough sea surface.

(2) diffusion out of the duct at its base.

(3) failure of low frequencies (long wavelengths) to be trapped.

(4) horizontal variability such as lateral changes in the duct and internal waves.

19. The Deep Ocean Channel

This is sometimes called the SOFAR channel because of its use in sound fixing ranging for aviation rescue. It is formed by the reversal in the velocity gradient, and a velocity minimum, between the main thermocline and the deep isothermal layer (para. 12). Because its thickness is measured in thousands of feet and, because it is not always bounded by the sea surface or bottom, it is an efficient (low-leakage) duct. A small explosive charge can be "heard" after travelling several thousand miles in the deep ocean channel.

It is characterized by severe transmission distortion due to multipath transmission. At a distance of one thousand miles the sound of an explosive charge detonated on the axis becomes a long,drawn-out blob,some 10 seconds long,having a characteristic signature consisting of a gradual smooth build-up to a climax, followed by a sudden termination. This signature is created by the existence of many transmission paths of differing travel time. The first sound to be received travels in long loops far from the axis; the last sound received travels down the channel axis.

An important feature of this channel is the presence within it of caustics and their adjacent convergence zones. For a deep source the pattern of the caustics is a characteristic one, consisting of the ray leaving the source plus pairs of caustics branching from this ray at its crests and troughs. A shallow hydrophone towed outward in range from a shallow source experiences a succession of zones 30-35 miles

apart and about 3 miles wide (in mid-latitudes), in which the intensity is 10 to 20 db higher than it would be in the free-field with absorption; this increase is called the convergence gain. The coherence of sound in the vertical is higher as well inside convergence zones than outside; the higher intensity and improved coherence make for better detection of long-range targets when they happen to lie in one of the convergence zones surrounding the source.

Another favorable path in the deep sound channel is the reliable acoustic path (RAP). This is a path, starting at the depth where the sound velocity is the same as at the surface (called the critical depth), and extending up to the surface. This ray path has the greatest range to a surface target and is "reliable" in that it is not influenced by surface and bottom effects.

In the Arctic, the axis of the deep sound channel lies at the sea surface, and propagation to long ranges takes place by a series of upward circular arcs. This, together with the fact that the Arctic is often ice covered, gives rise to some unique propagation phenomena in this part of the world.

20. Internal Channels

More locally, internal channels are found from time to time and place to place. These are of smaller thickness, of the order of a few hundred feet or so, and of small velocity contrast. They are often regular features of the velocity profile, as in the Gulf or Maine or between Long Island and Bermuda. They can be used by ship-towed sonars for detecting submarines and are avoided by submarines fearing detection. In the summer, the Mediterranean Sea has a strong internal channel with an axis at a depth near 300 feet.

21. Shallow Water Channels

By "shallow" is meant a water depth so small and a range so great that both the sea surface and sea bottom strongly influence the propagation. Practically, shallow water means the water of bays, harbors, and coasts out to the edge of the Continental Shelf; often a depth of 100 fathoms is understood as a rough working limit of "shallow" water. Of course, "shallow" water becomes acoustically "deep" at short enough ranges and short enough wavelengths.

When downward refraction exists in shallow water, the reflection loss at the bottom and the strength of the negative gradient are the two principal determinants of transmission loss in the channel. In the isothermal condition (upward refraction) the roughness of the sea surface becomes more important.

Both normal mode and ray theory (para. 3, 4) have been applied to the shallow-water problem, and a relatively vast theoretical literature exists. In both theories it is difficult to take care of the actual boundary conditions prevailing at the time and place where a particular transmission run may have been made. Analogously, our ability to predict the transmission to be expected at a given time and place is poor compared to our prediction ability for deep water transmission. Shallow water is subject to many kinds of variability, such as those caused by the tides and the seasons.

22. Low-Frequency Cutoff in Channels

Any sound channel has a lower frequency limit below which it ceases to be an effective duct and the leakage becomes high. This cut-off frequency may be thought of as the frequency corresponding to the longest wavelength that "fits" in the duct; this "fit" is determined by the velocity profile and the boundary conditions of the duct. In mode theory this wavelength is that of the first normal mode.

An expression for the cutoff frequency of a shallow water duct is

$$f_{co} = \frac{c_W}{4H} \left[1 - c_W^2/c_b^2\right]^{-1/2}$$

where H = water depth, c_W and c_b are the sound velocities in the water and in the bottom. For a high velocity bottom ($c_b \to \infty$), the cut-off wavelength is one fourth of the water depth. Some typical cut-off frequencies are the following:

Deep Ocean Channel	0-10 Hz
Mixed Layer Channel	100 Hz (400 ft. thick)
Mixed Layer Channel	1000 Hz (100 ft. thick)
Shallow Water Channel	30 Hz (sand bottom, 100 ft. depth)

23. Transmission Paths in the Deep Sea

In deep water there are a number of ways in which the sound emitted by a source can reach a receiver at a distance. These involve paths occurring in the various sound channels as well as reflections from the surface and bottom, and are referred to as propagation modes. A number of propagation modes (not the same as "normal modes") are drawn in Fig. 2. They show pictorially the complexity of sound propagation in the sea. Some of the paths shown are important at short ranges, others at long ranges. Often, more than one mode can occur and contribute to the sound field, depending upon source and receiver depths, range, frequency, and the conditions of the sea and its boundaries.

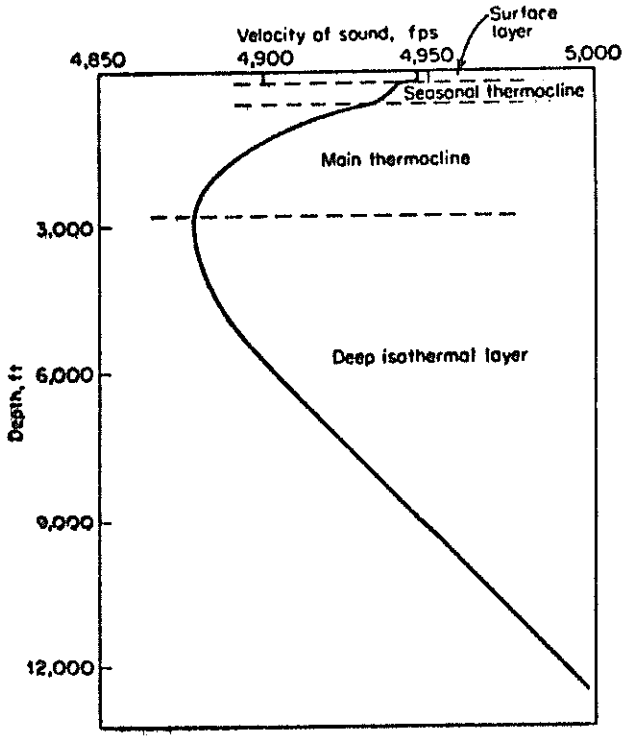

FIG. 1 TYPICAL DEEP OCEAN
VELOCITY PROFILE IN MID-LATITUDES

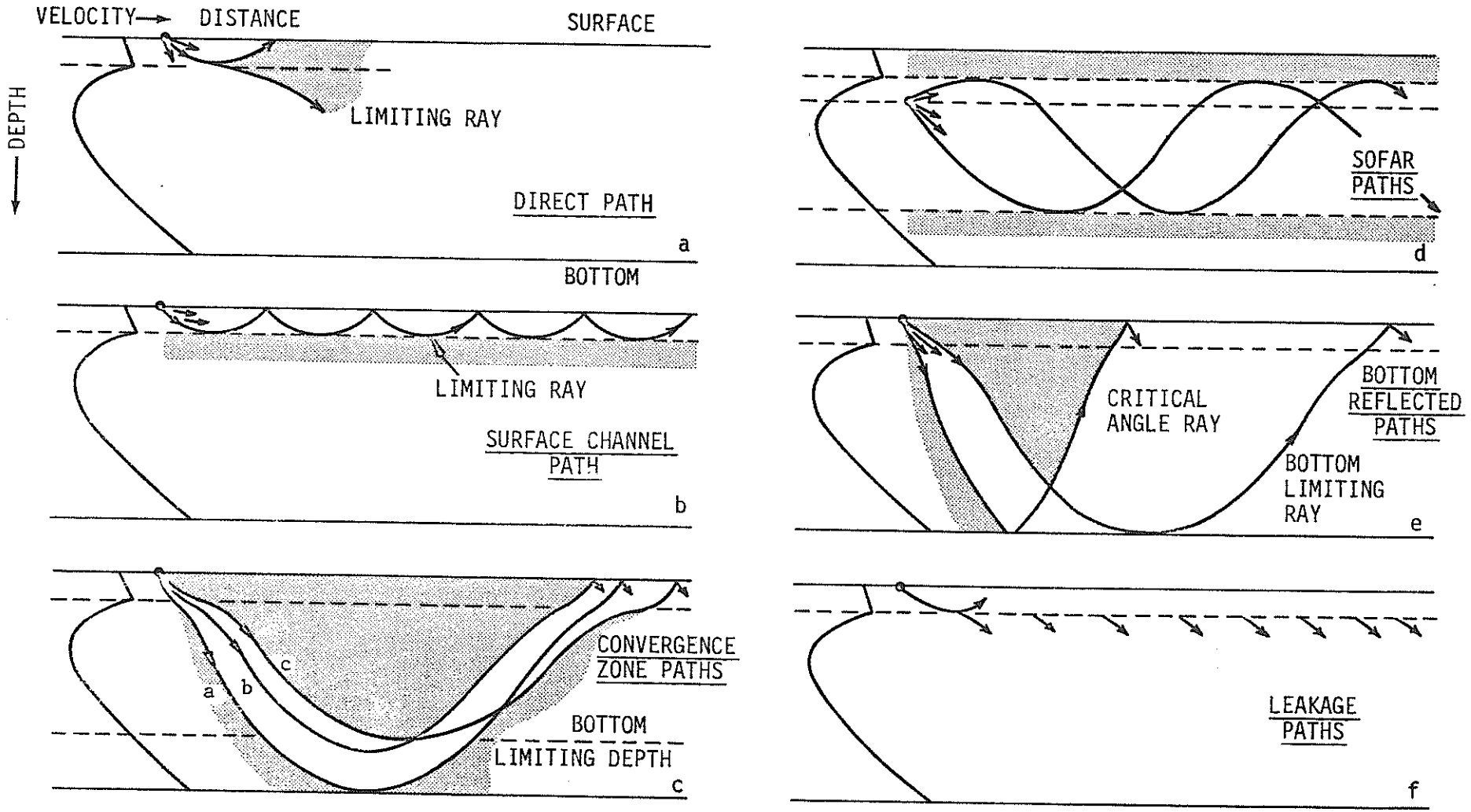

FIG. 2 RAY PATHS IN DEEP WATER

SCATTERING AND REVERBERATION

Claude W. Horton, Sr.
Professor of Physics and Geological Sciences
The University of Texas at Austin
and Applied Research Laboratories

INTRODUCTION

The acoustic waves emitted by a localized source of sound are scattered by objects located in the medium and by the interfaces and surfaces of the medium. If the receiving hydrophone is located near the source, the received signal is usually referred to as reverberation. The measurement of reverberation is relatively easy, and since the data are of considerable practical importance, the results of many experimental observations are available. In the experimental configuration that is second in order of difficulty, use is made of an omnidirectional source and receiver that are substantially separated in space. This arrangement is most useful for the study of scattering from surfaces and the results are commonly referred to as a measurement of forward scattering. There are very few measurements in the laboratory and even fewer measurements in the field in which a directional transducer is used to insonify a small volume or area of scatterers and the scattered energy is measured as a function of direction in space.

CHARACTERIZATION OF THE SOURCE

The measurements of reverberation and forward scattering can be divided into two basic categories according as the source is impulsive like an explosion or an air gun or a pulse of known wave form like a pulsed cw or an FM signal. Usually when an impulsive source is used, the received signal has a wide frequency spectrum which is divided into frequency bands, say an octave or a third-octave in width, which are recorded on separate channels. This procedure is of value when one wishes to study the effects of parameters such as wind speed, wave height, diurnal migration of scatterers, bottom type, and frequency. On the other hand if the statistical characteristics of the scattered field are desired, for example for the purpose of designing signal processors, it is much better to generate an acoustic signal of known wave form by electronic techniques.

In both of these methods it is necessary to know the source level with considerable accuracy (0.1 dB, say) in order to obtain absolute

values for the scattering strengths. This is illustrated below in Eq. (6). This problem is relatively easy to overcome if electronic signals of known wave form are used because the signal in the medium, even near the source, has an amplitude that does not exceed the linear behavior of the medium. Thus the source strength can be obtained readily by placing a calibrated hydrophone in the Fraunhofer zone of the transducer.

If the source is impulsive, the signal amplitude exceeds the linear response of the medium. Thus the minimum distance at which a monitoring hydrophone can be placed depends on the strength of the source and even for small charges this minimum distance is inconveniently large. Fortunately, the problem of source levels for the commonly used explosives has been studied rather extensively and tables and graphs are available which relate source strength to the weight of the explosive.[1]

The intensity of a source is commonly characterized as follows. Any source of finite size produces a diverging wave which at suitably large distances has a spherical wave front of the form

$$p(r,\theta,\varphi,t) = (p_o/r)F(\theta,\varphi)P(t-r/c) \quad , \qquad (1)$$

where $F(\theta,\varphi)$ characterizes the directionality of the source and $P(t)$ the wave form. The distance to the observation point from some point o in the vicinity of the transducer is r. The point o is often called the phase center of the transducer. The acoustic velocity of the medium is c and the strength of the source determines the constant p_o.

The function $F(\theta,\varphi)$ is normalized to have a maximum value of one on the acoustic axis of the transducer. Equation (1) can be used to calculate an intensity on the acoustic axis of the form I_s/r^2, where r is measured in yards. The resulting value I_s is customarily used as a measure of the strength of the source.

THE MODEL OF POINT SCATTERERS

The wave emitted by the source can be scattered by a variety of scatterers. Even a continuous interface such as the air-sea or the sea-bottom interfaces can be modeled with "point" scatterers such as facets or bosses. If the medium has discrete objects such as fish, air bubbles, or particulate matter scattered through a significant volume, the returned energy will be called volume reverberation. Similarly one speaks of surface and bottom reverberation.

Intermediate cases occur frequently. For example, the distribution of volume scatterers may be so localized in depth that they behave as a surface. Alternately, the distribution of air bubbles near the air-sea interface, although properly a surface effect, may be distributed through a layer so thick that the analysis for volume scatterers should be used.

The reverberation process may be analyzed at several levels of sophistication but only the most simple analysis will be presented here. A complicated structure may be assigned to each scatterer. Thus, the scattered wave may have a directional dependence; the scattering strength may depend on aspect; the structure of the scatterer may be frequency dependent so that the wave form is distorted; and the structure may be time dependent so that bivariate Fourier transforms must be used to describe the scattered wave form. Further, the scatterer may have a velocity so that Doppler shifts are introduced into the scattered waves. Nonetheless, many of the principal features of reverberation can be illustrated by a model of ideal point scatterers distributed at random over a surface or throughout a volume.

In this spirit let us suppress all variability except an amplitude factor a_k and a travel time delay $t_k (= 2r_k/c)$ for the k^{th} scatterer. Then, if the medium is homogeneous and isotropic, the returned signal from the transmitted pulse defined in Eq. (1) is

$$R(t) = p_o \sum_k (a_k/r_k^2) F(\theta_k, \varphi_k) P(t-2r_k/c) \quad , \qquad (2)$$

where $(r_k, \theta_k, \varphi_k)$ is the location of the k^{th} scatterer measured in a coordinate system with origin at the phase center of the transducer. The summation extends over all scatterers that are located in the part of the beam pattern common to the transducer and the hydrophone and in a spherical shell whose thickness is determined by the pulse length of the wave form $P(t)$.

Geometric illustrations of the domain of the summation are shown in Figs. 1, 2, and 3 for bottom reverberation. Figure 1 shows the area of summation when the source and receiver are omnidirectional and the scatterers are distributed on a plane surface a distance h from the transducer. If the transducer is directional and has axial symmetry about the acoustic axis, the area of scatterers over which the summation extends is all or part of an ellipse as shown in Fig. 2. Figure 2a shows the relevant area for a long pulse while Figs. 2b and 2c show the relevant areas for shorter pulses. The illustrations in Fig. 2 are for a large grazing angle. When the grazing angle, φ, is smaller than the half angle of the transducer pattern, as in Fig. 3, the shape of the insonified area changes drastically. Figures 2 and 3 are taken from a report by Muir et al.[2] that describes an interesting study of the Brazos River bottom. Some of the results of this study will be presented later in the talk.

A more realistic illustration of the geometry of surface reverberation is presented in Fig. 4. This figure is taken from the Ph.D. dissertation of Flemons.[3] Figures 6 and 7 show photographs from the air-water interface measured with this geometry.

Before proceeding to the discussion of Eq. (2), it might be helpful to show an experimental arrangement and some data. Reverberation measurements carried out at sea are important, but the inevitable motion of the transducer platform and the complexity of the medium make it difficult to use the measurements to check theoretical work. For this purpose it is desirable to mount the transducer on a relatively motionless platform or, even better, on the bottom as illustrated in Fig. 5. This figure illustrates an experiment performed by Dr. J. E. Blue[4] at a location 3 miles offshore in the Gulf of Mexico near Port Aransas, Texas, where the water depth is 50 feet. The projector and receiver were located 9 feet off the bottom and could be rotated in azimuth throughout 360 deg in steps of 12 deg. By depressing the acoustic axis 10 deg, backscattering could be measured for grazing angles between 6 deg and 16 deg. The results of this work are given in Blue's Ph.D. dissertation.[4]

Figure 6 shows a few photographs of surface reverberation for a wind driven surface. These measurements, which were made in Lake Travis, show the effect of pulse length. The three photographs on the left show the appearance of surface reverberation for a long cw pulse (110 cycles) while the photographs on the right correspond to 11 cycles of a cw pulse. In addition to the distinction between narrow-band and broad-band behavior these photographs show a second difference of interest. In the photographs on the left, the travel time is only four to nine times the acoustic pulse duration. In the photographs on the right this factor ranges from forty to ninety. It may be of interest to point out that the first burst of energy near a travel time of 4 milliseconds is associated with a minor lobe of the transducer pattern. This is illustrated in Fig. 4, which is a realistic drawing of the experimental geometry of these measurements.

Figure 7 shows three photographs of surface reverberation for a FM pulse of band width 9.6 kHz, center frequency 110 kHz, and pulse length 1.25 msec. All of the photographs in Figs. 6 and 7 show clearly the nonstationary character of reverberation.

Equation (2) defines a stochastic process that is a generalization of the shot effect analyzed by Rice.[5] It is customary in theoretical studies to assume that the scatterers are distributed in space in accordance with a Poisson distribution. That is, in the case of volume scattering, for example, it is assumed that if N is the average number of scatterers per unit volume and ΔV is a small volume element such that $N\Delta V \ll 1$, the probability of finding a scatterer in the volume ΔV is $N\Delta V$, and that this probability does not depend on the location of the scatterers outside the volume ΔV. It is also assumed in the usual analyses that multiple scattering processes can be neglected. Faure,[6] Ol'shevskii,[7] and Middleton[8,9] analyze Eq. (2) and calculate various and second order statistics of R(t).

Since R(t) is not a stationary process, time averages cannot be equated to ensemble averages. This point is highly significant and will

be returned to later. However, there is a large body of field measurements which are based on the assumption that time averaging over a short interval is a legitimate operation. The equipment used in reverberation studies normally has zero dc response so a time average over at least a few cycles of the lowest frequency in the reverberation will insure a time average $\overline{R(t)} = 0$. Short time averages of the square of R(t), $R^2(t)$, are commonly referred to as intensity and represented as a theoretical counterpart to the experimentally determined intensity.

For a correct theoretical analysis of Eq. (2) the reader is referred to the publications mentioned above.[6-9] However, instructive approximate formulas can be developed easily if one assumes that the location of each scatterer is fixed and assigns all of the variability to the amplitudes a_k. Let us assume that the a_k are all statistically independent of one another and that each a_k has the same probability density. In particular assume

$$\langle a_k \rangle = 0$$

$$\langle a_j a_k \rangle = a_o^2(r_k)\, \delta_{jk} \quad , \tag{3}$$

where δ_{jk} is the Kroneker delta. The functional dependence on r_k is introduced since it is common for volume scatterers to vary with depth and surface scatterers to vary with grazing angle. Further, the directivity pattern is idealized so that $F(\theta,\phi)$ is unity in the insonified region and zero outside. The variability of the a_k can be removed by forming the ensemble average. These restrictions give

$$\left\langle R^2(t) \right\rangle = p_o \sum_{k=1}^{N(r_k)} \left| a_o^2(r_k)/r_k^4 \right| P^2(t-2r_k/c) \quad . \tag{4}$$

The upper limit of the sum is written $N(r_k)$ to remind the reader that the number of scatterers contributing to the reverberation increases with time because the size of the volumes and areas insonified increases with time.

Equation (4) is simple but it provides a clear basis on which to demonstrate the importance of pulse length on the behavior of reverberation. If the pulse length in the medium is very short compared with r_k, the time integral needed for the time average can be approximated by treating the coefficient of $P^2(\cdot)$ constant and writing

$$\overline{\langle R^2(t)\rangle} = \langle \overline{R^2(t)} \rangle = p_o \overline{P^2(t)} \sum_{k=1}^{N(r_k)} \left| a_o^2(r_k)/r_k^4 \right| \quad . \tag{5}$$

Next the total number of scatterers can be expressed as the product of the number N per unit volume (or area) and the volume (or area) of the insonified region. We are thus lead to characterize the scatterers as having a strength $N\, a_o^2(r_k)$ per unit volume (or area). In fact this is the ad hoc assumption on the basis of which reverberation measurements are frequently analyzed.

On the other hand if the pulse length is significant in comparison with (say, 10% of) the travel time $2r_k/c$, Eq. (5) does not give an adequate approximation to the behavior of the time average. In this case it is not permissible to develop the statistical properties of reverberation from the simplified Eq. (5).

EXPERIMENTAL RESULTS

It was pointed out above that if the pulse duration is much shorter than the travel time, and if the model of a large number of statistically independent scatterers is valid, the intensity of the beam, expressed as a short-term time average, depends only on the geometry of the beam and the density and strength of the scatterers. In fact the scattering process can be defined adequately as a scattering strength in dB per unit area or unit volume, and can thereby be incorporated into the sonar range equation. For example, in surface reverberation one may write

$$L_R = L_i - 2H + S_B + A \quad , \tag{6}$$

where

L_R = reverberation level in dB relative to 1.0 μbar at the receiving hydrophone

L_i = source level at 1 yard

H = one-way total transmission loss

S_B = reverberation strength per unit area

$A = 10 \log_{10}$ (area insonified).

As an example of experimental values of S_B' for various bottom types, Fig. 8 is copied from a paper by McKinney and Anderson.[10] The reader is referred to their paper for the meanings of the symbols but the alphabetical symbols are ordered according to the particle size with A representing fine sandy mud and M representing sandy pebble gravel of

mean size 4.2 mm. Then data are repeated in a simplified form in Fig. 9.

Another example of experimental value of bottom scattering strength is shown in Fig. 10. These data were measured in the Brazos River near Brazoria, Texas, by Muir et al.[2] The acoustic pulses were 500 μsec in duration and consisted of a gated cw oscillator of frequency 85 kHz. The medium was fresh water of depth 13 feet. The stratification of the river bottom was somewhat complex but the uppermost 1 to 3 in. consisted of a fine "fluffy" mud whose mean particle size was 4 microns.

The reader is referred to a survey paper by Chapman[11] for a summary of this approach to scattering measurements and for a large number of graphs of scattering strengths for surface, bottom, and volume reverberation. This survey contains references up to 1967.

STATISTICS OF REVERBERATION

It is clear from the discussion above that reverberation is a nonstationary process. The immediate consequence of this fact is the conclusion that the experimenter must be very circumspect in performing and interpreting time averages. It is only in the last year or two that data processing systems have been designed so that adequate samples can be prepared and analyzed for the calculation of reverberation statistics as ensemble averages. Practical techniques of sampling narrow-band, high-frequency time series are described by Grace and Pitt.[12] As an example, suppose a sequence of reverberation records like those shown in Figs. 6 and 7 for a wind driven water surface is recorded. Each record is different but the sequence may constitute a finite set of samples from the same parent population. In this case one can sample the records in such a way that meaningful ensemble averages can be calculated.

Before proceeding with the analysis, the reverberation samples must be tested for independence and homogeneity in order to establish confidence that the samples are all from the same parent population. Two important and useful tests are the runs test which provides assurance that the samples are independent of each other, and the Kolmogorov-Smirnov test for homogeneity which gives assurance that each sample of reverberation has the same first order probability distribution.

Figure 11 shows a plot of these significance tests for a set of 150 samples of reverberation which pass both tests. In each case 5% of the values of the test statistic exceeds the theoretical limit associated with a value of 0.05 for the level of significance.

Not all data will pass these tests. Reverberation samples collected in a time interval of 20 minutes have shown internal evidence of a change in the water surface sufficiently great to change the statistics of the sample.

Figure 5 was a drawing of an installation used in the Gulf of Mexico to measure bottom reverberation in which 30 different reverberation samples were measured in 30 different directions from the transducer. It was hoped that these 30 samples would be independent and homogeneous, but they failed the tests. The scattering strength of the bottom showed a variation that depended on the angle between the sonar beam and the direction to the coast.

The most simple statistical parameter that one can visualize is the ensemble average $\langle (R(t_1) \rangle$ at a time t_1. Actually this quantity is difficult to measure because it is affected by the motion of the transducer, inhomogeneities in the medium, and small errors in the timing clock that is used to measure t_1. If these three sources of error combine to introduce a random error of the order of the period of the center frequency of $R(t)$, the experimental values of $\langle R(t_1) \rangle$ will be zero regardless of the nature of the scatterers.

However, one can show theoretically that in some cases $\langle R(t_1) \rangle$ can be different from zero. Bourianoff and Horton[13] have carried through a computer simulation of reverberation from a sea surface and showed that in the case analyzed, the ensemble average is different from zero and is itself a quasi-periodic function of t_1. The conditions that lead to a non-zero average are a short pulse length and a low amplitude relief of the surface.

The first order statistics of surface reverberation show that the first order probability density is gaussian. Blue[4] found, for example, that bottom reverberation of center frequency 80 kHz was gaussian to the 0.05 level of significance even when the reverberation came from an area of only 0.5 sq yd on the bottom. However, the presence of fixed large scatterers can produce significant non-zero values of the coefficient of excess. In keeping with this gaussian distribution it is regularly found that the first order probability density of the reverberation is Rayleigh distributed. An example of a histogram of experimental reverberation in the Brazos River is shown in Fig. 12.

When one turns to second order statistics of a noise process, the concern is with second order probability densities and with the covariance function. Again one may work with instantaneous samples or with samples from the envelope. Figure 13 shows a plot of the covariance function from the envelope of a suite of samples of bottom reverberation measured in the Brazos River. The curve does not go to zero since the envelope has a non-zero average. The solid curve is the theoretical curve computed for a narrow-band noise whose band width corresponds to the acoustic signals as modified by the transducer.

Bivariate probability distributions for the envelope of surface reverberation for both noise and cw signal have been plotted by Jourdain.[14] He also plots some data regarding the bivariate distribution of instantaneous samples of surface reverberation. These will be referred to later.

Although it is abundantly clear that reverberation is not a stationary process, it is tempting to search for some way of treating the data so as to introduce some order. The concept of a gaussian process is not limited to stationary processes since both the mean and the covariance function can be time dependent. Consider in this regard the centered gaussian process with the bivariate distribution such that the ensemble average of the square of the instantaneous value is a function of the time

$$\left\langle x^2(t) \right\rangle = \sigma^2 s(t) \tag{7}$$

where σ is a constant. If the covariance function is

$$\left\langle x(t_1)x(t_2) \right\rangle = \sigma^2 \rho \sqrt{s(t_1)s(t_2)} \tag{8}$$

with ρ a function of $(t_2-t_1)(|\rho| \leqq 1)$, then one can introduce a new gaussian process $y(t)$ defined by

$$y(t) = x(t)/\sqrt{s(t)} \quad . \tag{9}$$

and the resulting process is stationary.

Ol'shevskii[7] has used this idea to suggest that reverberation, although not a stationary process, can be reduced to stationarity by a similar change of variable. Thus he suggests normalizing the reverberation, $R(t)$, by dividing by the square root of the short term time average $\overline{R^2(t)}$. Jourdain[14] analyzes some reverberation samples and computes $\rho(t_2-t_1)$ for two different positions in the reverberation. He finds that ρ is the same and concludes that Ol'shevskii's suggestion is applicable to reverberation. However, the reverberation samples generated on a computer by Bourianoff and Horton[13] do not yield to this reduction. These two results need not be contradictory, however, for Jourdain worked with a transmitter pulse 90 cycles in duration while the pulse of Bourianoff and Horton was only 2 cycles.

If one has a nonstationary process $x(t)$, one can compute the covariance function

$$K(t_1,t_2) = \left\langle x(t_1)x(t_2) \right\rangle \tag{10}$$

without any assumptions about stationarity. If $x(t)$ is a narrow-band process of center frequency ω_0, $K(t_1,t_2)$ will oscillate with frequency ω_0 so it would be better to plot the envelope of $K(t_1,t_2)$. We can now define a new concept called local stationarity. Silverman[15] suggested the definition that the process is locally stationary if $K(\cdot)$ may be factored in the form

$$K(t_1,t_2) = K_1\left(\frac{t_1+t_2}{2}\right)K_2(t_2-t_1) \quad .$$

On the other hand Middleton has suggested that K_1 be replaced by $K_1(t_1)$. In either case the envelope of $K(t)$ has the form of a long, sharp ridge located on the line $t_1=t_2$. The height of the ridge on this line, that is the function $K_1[(t_1-t_2/2]$, is a graph of the instantaneous intensity of the process. $K_2(t_2-t_1)$ gives a slice across the ridge and shows the correlation function of the individual pulse shape $P(t)$ (see Eq. (1)) out of which the process is formed.

Dr. Plemons[3] has analyzed his reverberation data in this manner and has plotted graphs of $K(t_1,t_2)$ and also of the two-dimensional Fourier transform of this quantity. The plots of the two-dimensional covariance and of its Fourier transform provide the best method of presenting non-stationary time series so that one can analyze and interpret them. Dr. Plemons will publish his data in the near future.

FORWARD SCATTERING

In the case of forward scattering there is a striking difference in behavior according as the surface is smooth or rough. The critical parameter is not simply the root-mean-square roughness, F_o, of the surface but rather a factor $R = kF_o(\sin \phi_R + \sin \phi_S)$ where ϕ_R and ϕ_S are the grazing angles of the rays to the receiver and to the source, respectively. R is often referred to as the Rayleigh parameter and it is useful in that it enables one to codify measurements on different surfaces. When this parameter is small, the surface reflects the incident wave in the specular direction with a small loss of amplitude representing the energy scattered in the other directions. This wave is called the coherent reflection although there is a small shift in phase associated with the small fluctuation in amplitude. Consequently, the behavior of scattering in the specular direction is often portrayed as fluctuations in the amplitude and phase in the coherent signal arriving at the receiver.

Figure 14 shows how the percentage fluctuation in the amplitude varies with the Rayleigh parameter for three different surfaces. Although these measurements were made in a laboratory by Melton and Horton,[16] measurements on sea surfaces by Gulin and Malyshev[17] and Brown[18] show similar behavior. Figure 15 shows the percentage fluctuations in the phase measured in a laboratory model.

The loss of amplitude suffered by a coherent wave on being scattered from a slightly rough surface can be expressed in dB as in Fig. 16. This figure shows the experimental and theoretical calculations reported by Horton and Melton.[19] The theoretical values were computed with the aid of the Helmholtz integral mentioned in the next section.

The manner in which the amplitude decreases as the Rayleigh parameter increases can be measured for various frequencies and grazing angles. If the probability density of the relief of the scattering surface is known, this experimentally measured dependence can be used to determine F_o, the root-mean-square relief of the bottom. This type of calculation has been carried out by Clay[20] for a set of acoustic measurements in the Hatteras Abyssal Plain (33°N, 71°W). He concluded that the roughness of the plain is less than 0.4 m.

THE WAVE THEORY MODEL OF REVERBERATION

The present discussion of reverberation has been restricted to the point scattering model because it is easily visualized, it has been analyzed extensively in the literature, and it provides good suggestions for methods of processing the experimental data. Further, it provides a realistic model of the volume reverberation where the scatterers are isolated objects. The major drawback to the model is that there is no way to relate the properties of the point scatterers to the shape and statistics of the sea surface or sea bottom. This difficulty can be avoided by using some of the integral theorems[21] of wave propagation and integrating over the scattering surface. This approach was pioneered by Brekhovski, Isacovich, and Eckart. An up-to-date historical survey has been prepared by Horton[22] and presented at the 80th meeting of the Acoustical Society of America held in Houston, November 3-6, 1971. The major drawback to this method is that the analytic calculating can be carried through only for surfaces of small Rayleigh numbers.

THE LITERATURE

The reader who wishes to pursue the theory of point scatterers should read the papers by Faure,[6] Ol'shevskii,[7] and Middleton[8,9] in this order. The best survey of the use of integral theorems in scattering problems is the book by Beckmann and Spizzichino.[23] Later references can be found in the survey by Horton.[22] The most useful introductions to the experimental work are provided by Fortuin[24] and Chapman.[11]

ACKNOWLEDGEMENTS

I am indebted to my friends and colleagues at the Applied Research Laboratories for their permission to use the illustrations in the text. In particular I wish to thank Dr. T. G. Muir for permission to use Figs. 2, 3, 10, 12, and 13, Dr. T. D. Plemons for permission to use Figs. 4, 6, 7, and 11, Dr. J. E. Blue for permission to use Fig. 5, and Dr. C. M. McKinney for permission to use Figs. 8 and 9.

REFERENCES

1 R. J. Urick, "Handy Curves for Finding the Source Level of an Explosive Charge Fired at a Depth in the Sea," J. Acoust. Soc. Am. 49, 935-936 (1971).

2 T. G. Muir, Jr., et al., "A Geoacoustic Survey of the Brazos River. Part I: Environmental Studies, Part II: Ultrasonic Attenuation Studies, Part III: Reverberation Studies," DRL-A-294, Defense Research Laboratory, The University of Texas at Austin (April 1968).

3 T. D. Plemons, "Spectra, Covariance Functions, and Associated Statistics of Underwater Acoustic Scattering from Lake Surfaces," Ph.D. dissertation, The University of Texas at Austin (June 1971).

4 J. E. Blue, "Signal Detection in Inhomogeneous Reverberation," Ph.D. dissertation, The University of Texas at Austin (June 1971).

5 S. O. Rice, "Mathematical Analysis of Random Noise," Bell System Tech. J. 23, 184-294 (1944).

6 P. Faure, "Theoretical Model of Reverberation Noise," J. Acoust. Soc. Am. 36, 259-266 (1964).

7 V. V. Ol'shevskii, Characteristics of Sea Reverberation (Consultants Bureau, New York, 1967).

8 D. Middleton, "A Statistical Theory of Reverberation and Similar First-Order Scattered Fields. Part I. Waveforms and the General Process," IEEE Trans. on Information Theory IT-13, 372-392 (1967).

9 D. Middleton, "A Statistical Theory of Reverberation and Similar First-Order Scattered Fields. Part II. Moments Spectra, and Special Distributions," IEEE Trans. on Information Theory IT-13, 393-414 (1967).

10 C. M. McKinney and C. D. Anderson, "Measurements of Backscattering of Sound from the Ocean Bottom," J. Acoust. Soc. Am. 36, 158-163 (1964).

11 R. P. Chapman, "Sound Scattering in the Ocean," Chap. 9 in V. M. Albers, Underwater Acoustics Vol. 2 (Plenum Press, New York, 1967).

REFERENCES (Cont'd)

12 O. D. Grace and S. P. Pitt, "Sampling and Interpolation of Bandlimited Signals by Quadrature Methods," J. Acoust. Soc. Am. 48, 1311-1318 (1970).

13 G. I. Bourianoff and C. W. Horton, Sr., "Ensemble and Time Averages of Reverberation from a Sea Surface: A Computer Study," J. Acoust. Soc. Am. 49, 237-245 (1971).

14 J. Y. Jourdain, "Proprietes Statistiques Monodimensionelles et Bidimensionelles des Echos de Reverberation. Application à la Reverberation de Surface pour Deux Types d'Emission," in Colloque National sur le Traitement du Signal et ses Applications (Groupe d'Etude du Traitement du Signal, Université Marine Nationale) Vol. 2, pp. 737-784. A Colloquium held in Nice, France, 5-10 May 1969.

15 R. A. Silverman, "Locally Stationary Random Processes," IRE Trans. on Information Theory IT-3, 182-187 (1957).

16 D. R. Melton and C. W. Horton, Sr., "Importance of the Fresnel Correction in Scattering from a Rough Surface. I. Phase and Amplitude Fluctuations," J. Acoust. Soc. Am. 47, 290-298 (1970).

17 E. P. Gulin and K. I. Malyshev, "Statistical Characteristics of Sound Signals Reflected from the Undulating Sea Surface," Sov. Phys.-Acoust. 8, 228-234 (1963).

18 M. V. Brown, "Intensity Fluctuations in Reflections from the Ocean Surface," J. Acoust. Soc. Am. 46, 196-204 (1969).

19 C. W. Horton, Sr., and D. R. Melton, "Importance of the Fresnel Correction in Scattering from a Rough Surface. II. Scattering Coefficient," J. Acoust. Soc. Am. 47, 299-303 (1970).

20 C. S. Clay, "Coherent Reflection of Sound from the Ocean Bottom," J. Geophys. Res. 71, 2037-2046 (1966).

21 See specifically the Helmholtz and Kirchhoff theorems discussed in B. B. Baker and E. T. Copson, The Mathematical Theory of Huygen's Principle (Clarendon Press, Oxford, 1953), 2nd ed.

22 C. W. Horton, Sr., "A Review of Reverberation, Scattering, and Echo Structure," ARL-TR-70-42, Applied Research Laboratories, The University of Texas at Austin (December 1970).

REFERENCES (Cont'd)

23 P. Beckmann and A. Spizzichino, The Scattering of Electromagnetic Waves from Rough Surfaces (The MacMillan Co., New York, 1963).

24 Leonard Fortuin, "Survey of Literature on Reflection and Scattering of Sound Waves at the Sea Surface," J. Acoust. Soc. Am. 47, 1209-1228 (1970).

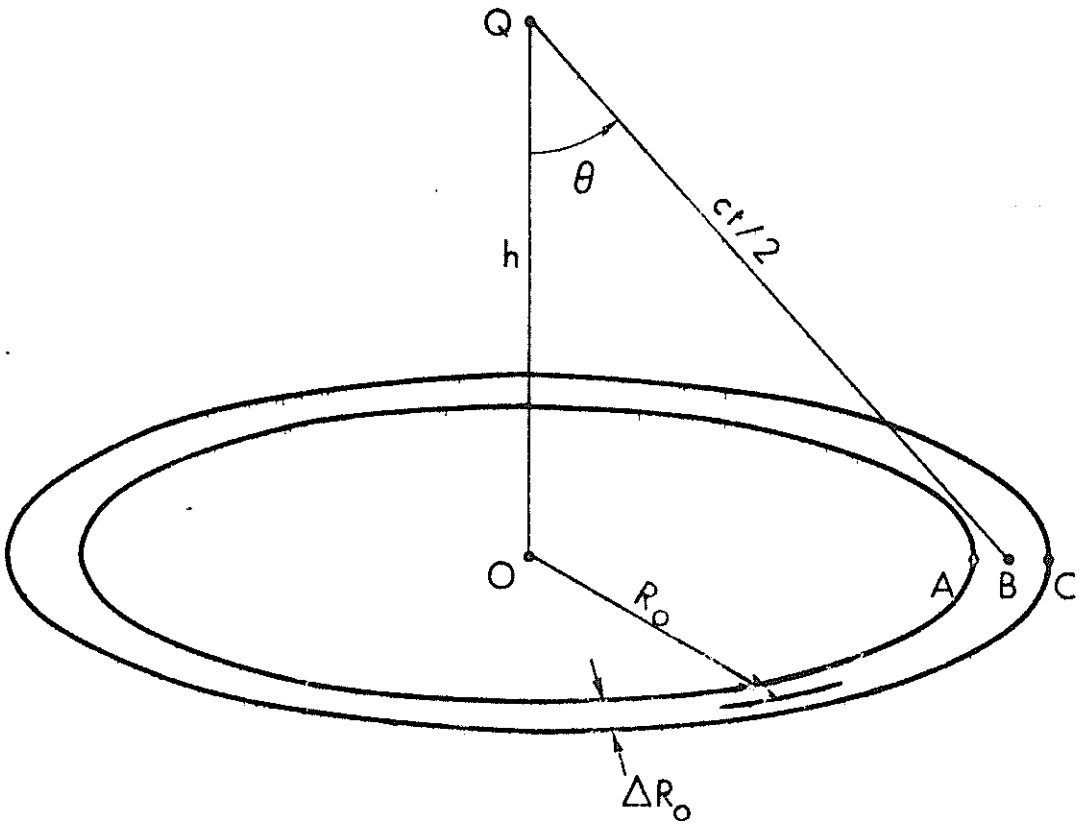

FIGURE 1
THE GEOMETRY OF REVERBERATION

D - 1 - UT
DWG AS-66-961
C W H - R F O
9 - 21 - 66

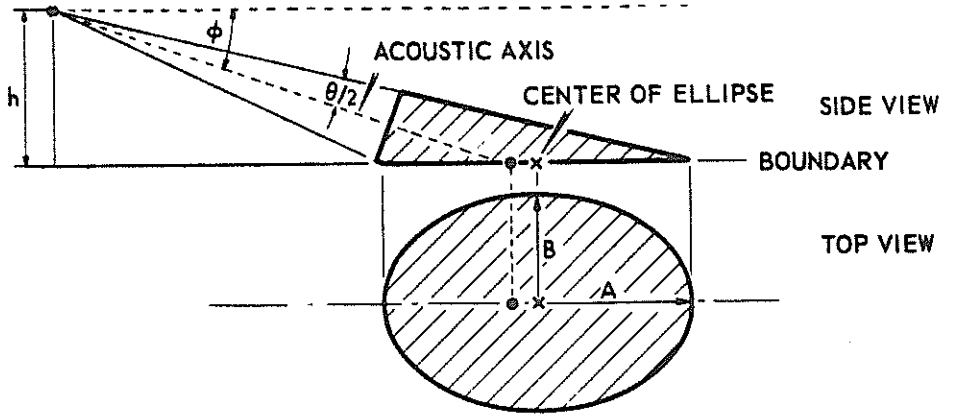

(a) LONG PULSELENGTHS

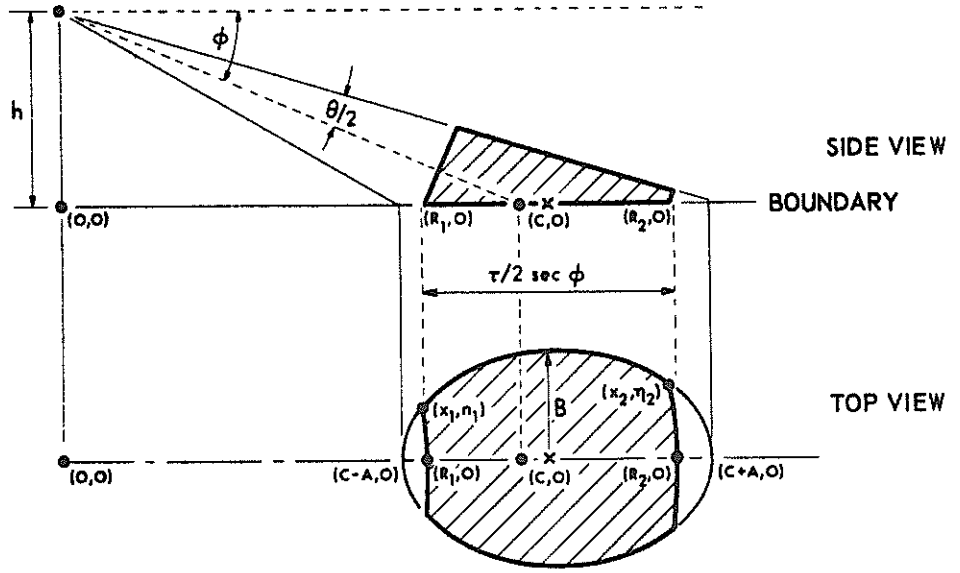

(b) SHORT PULSELENGTHS

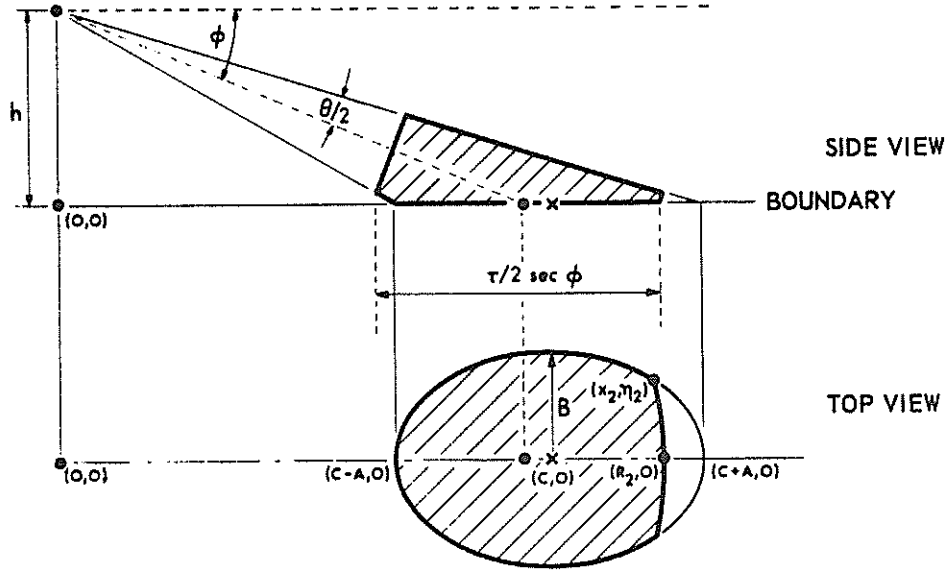

(c) INTERMEDIATE PULSELENGTHS

DRL - UT
AS-68-143
TGM - RFO
2 - 21 - 68

FIGURE 2
GEOMETRY OF THE REVERBERATION EXPERIMENT
CASE I - LARGE GRAZING ANGLES

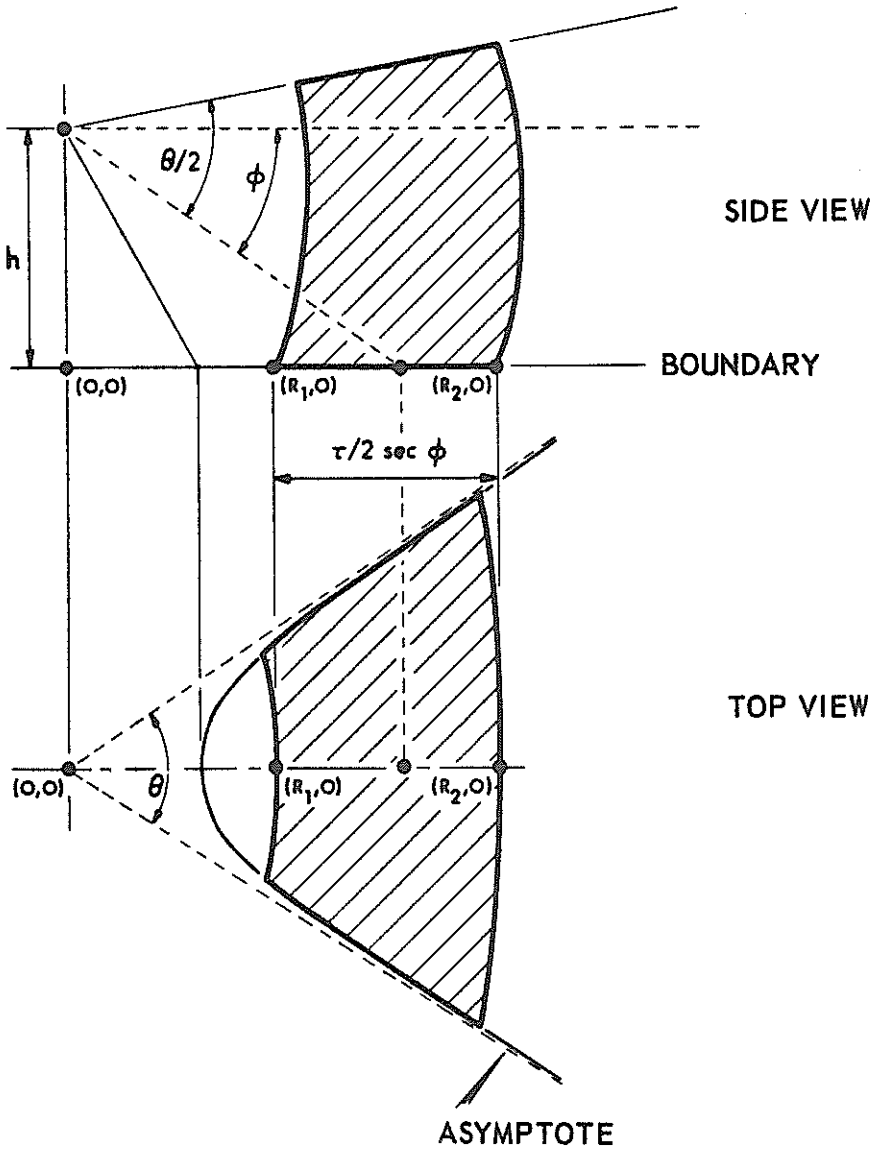

FIGURE 3
GEOMETRY OF THE REVERBERATION EXPERIMENT
CASE III – SMALL GRAZING ANGLES

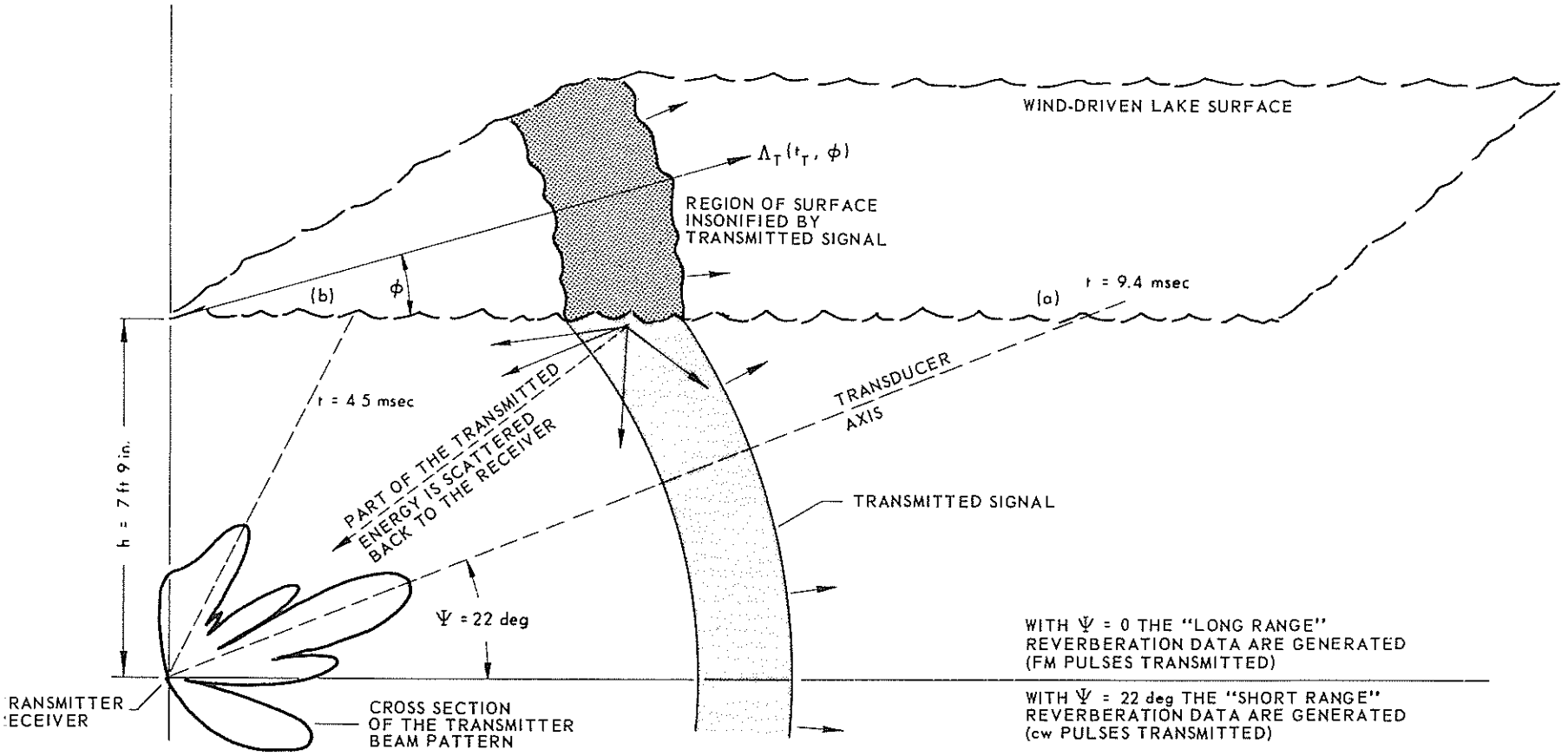

FIGURE 4
GEOMETRY OF THE SCATTERING EXPERIMENT
ON THE LAKE SURFACE

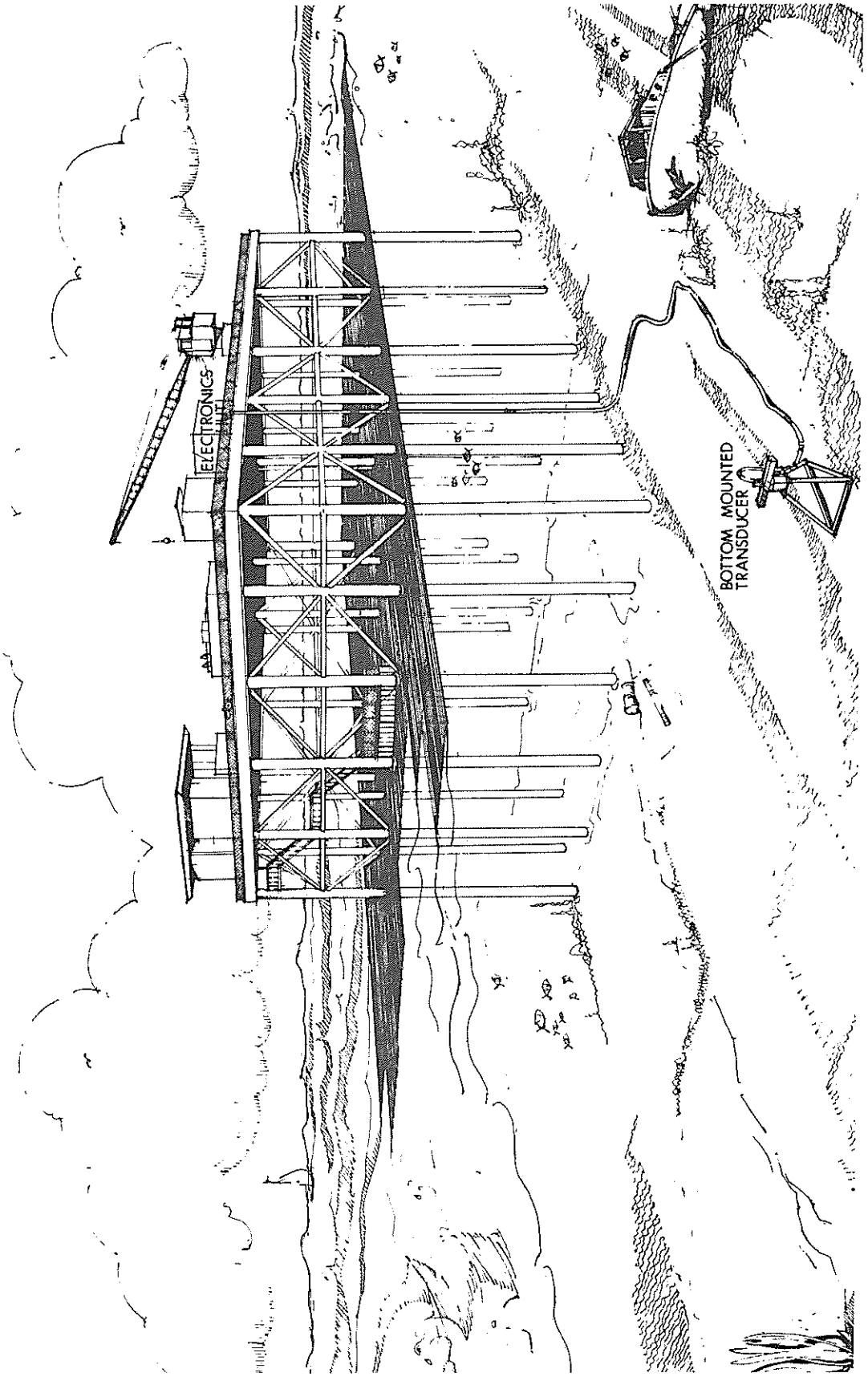

FIGURE 5
GULF OIL PLATFORM REVERBERATION SITE

ARL - UT
AS - 71 - 329
JEB - DR
3 - 24 - 71

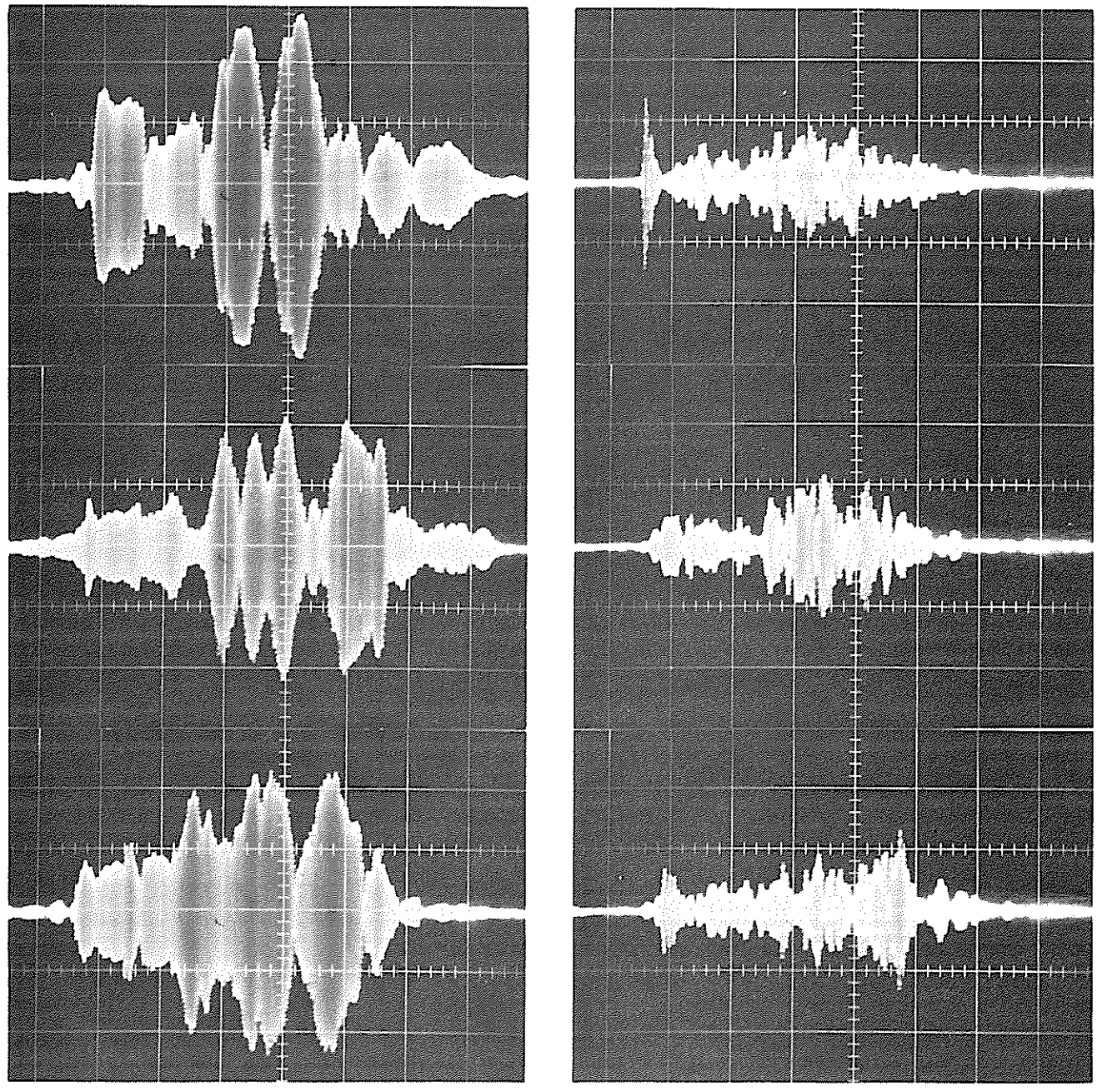

FIGURE 6
CONSECUTIVE REVERBERATION RETURNS FROM THE SURFACE PRODUCED BY TRANSMITTING PULSED cw SIGNALS HAVING TIME DURATIONS OF 1.0 msec AND 0.1 msec

DEPTH OF TRANSMITTER AND RECEIVER: 7 ft 9 in. (SEE Fig. 1)
GRAZING ANGLE (Ψ) OF ACOUSTIC AXIS: 22 deg
FREQUENCY OF cw PULSE: 110 kHz

ARL - UT
AS-71-58
TDP - RFO
2 - 5 - 71

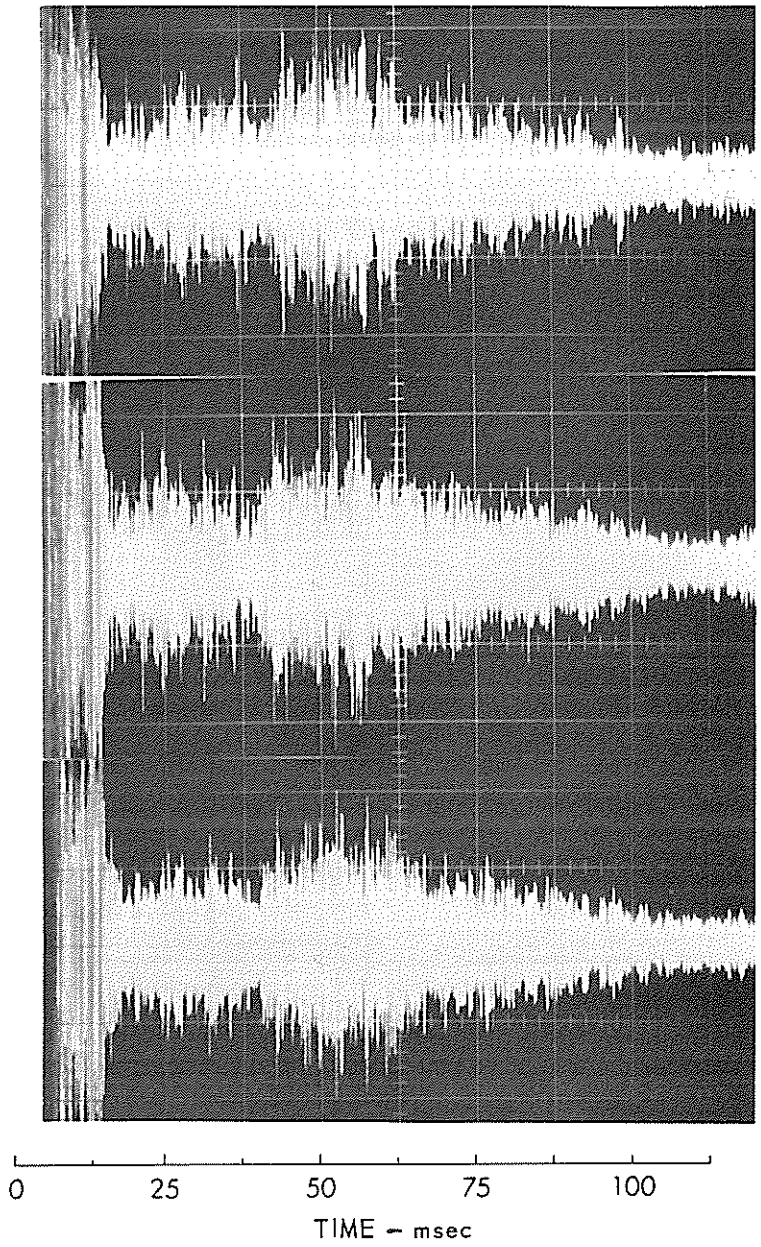

FIGURE 7

RANDOM REVERBERATION RETURNS FROM THE SURFACE, GENERATED BY FM TRANSMITTED SIGNALS OF DURATION 1.25 msec, BANDWIDTH 9.6 kHz, AND CENTER FREQUENCY 110 kHz

TRANSMITTER AND RECEIVER DEPTH: 8.0 ft
GRAZING ANGLE: 0 deg
(SEE Fig. 2–1)

ARL - UT
AS-71-59
TDP - RFC
2 - 5 - 71

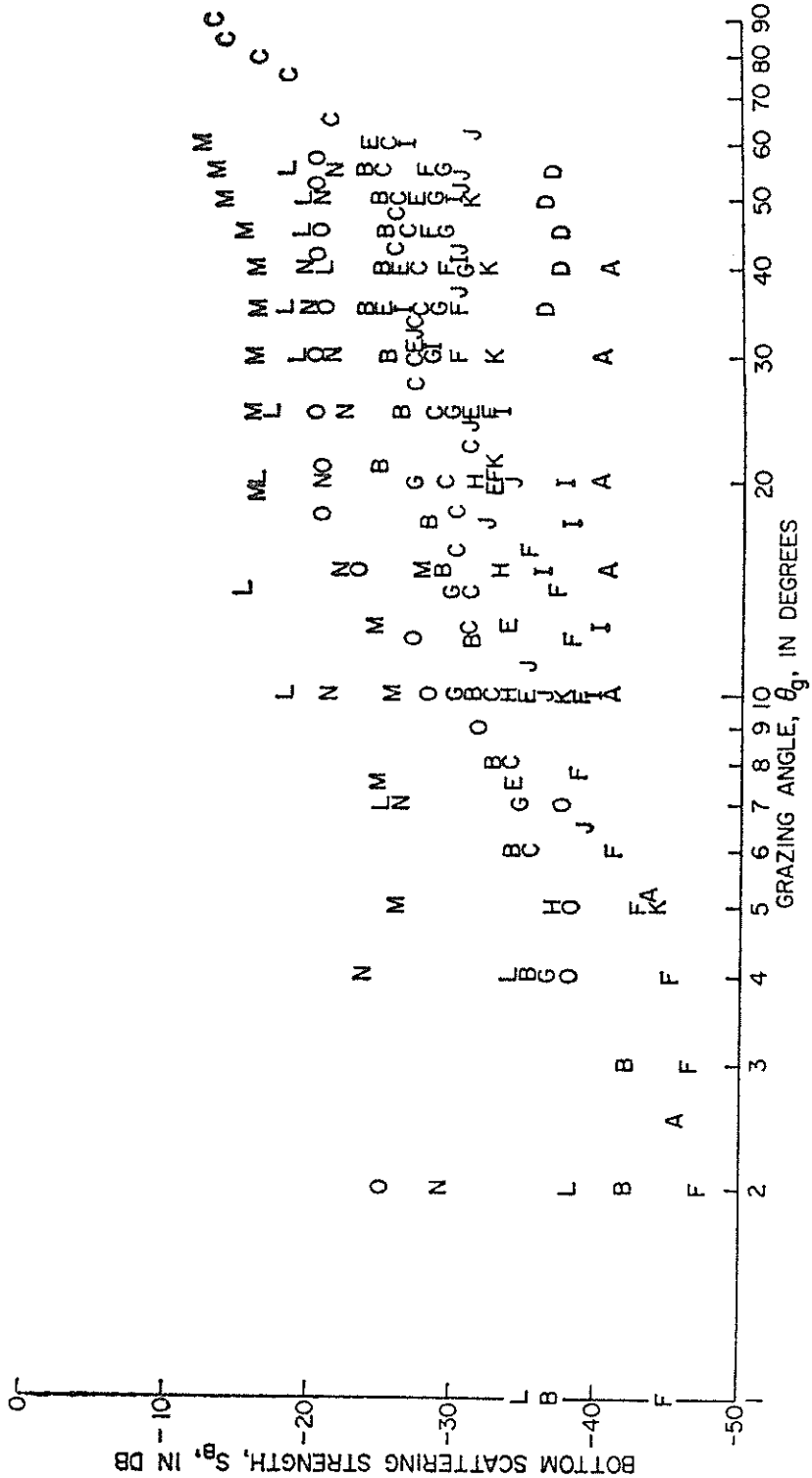

FIGURE 8

Bottom backstrength S_B as a function of grazing angle θ_g for a frequency of 100 kc/sec. Symbols are the same as given in Table I.

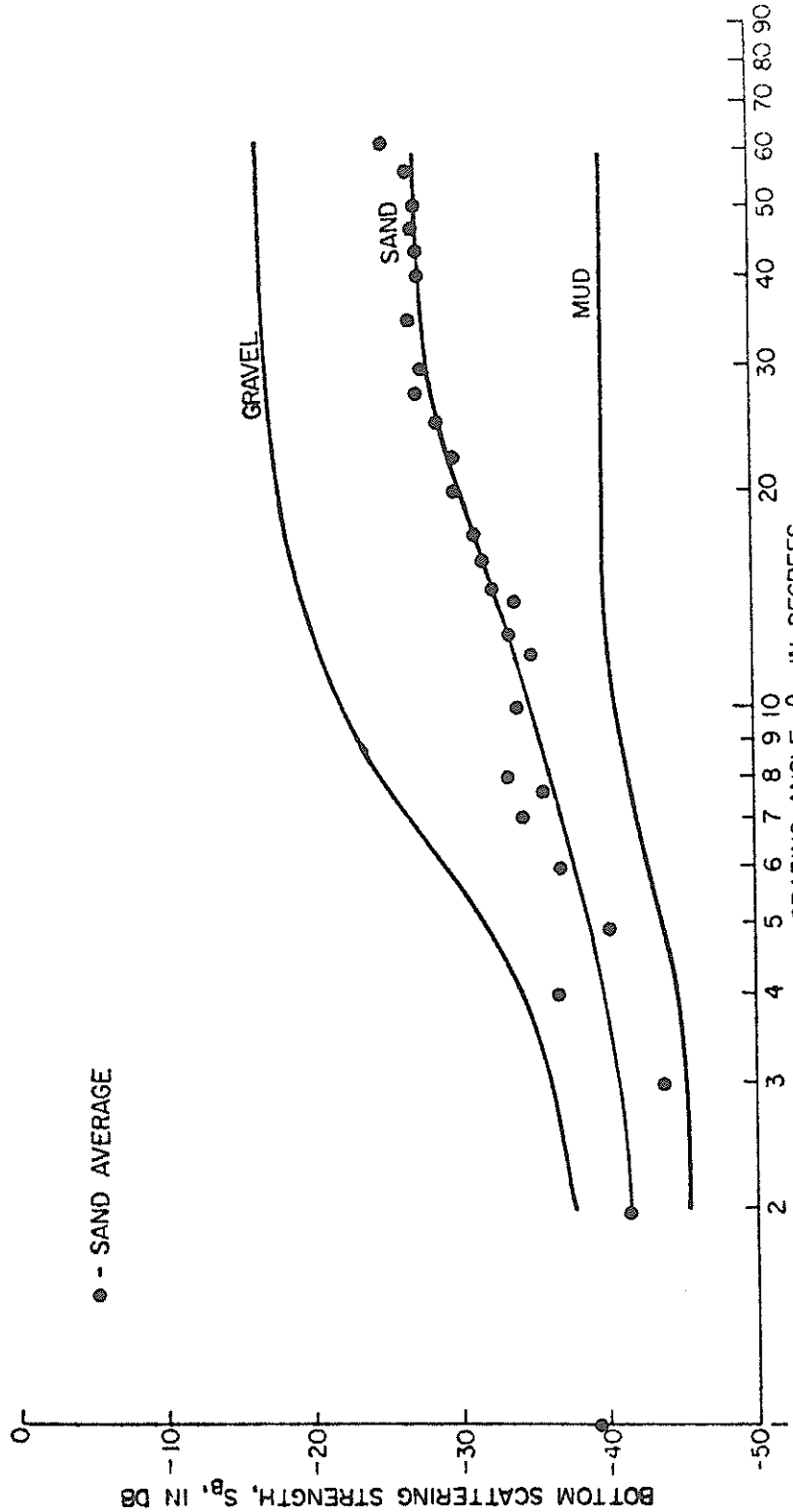

FIGURE 9
Average curves for bottom-backscattering strength S_B as a function of grazing angle θ_g.

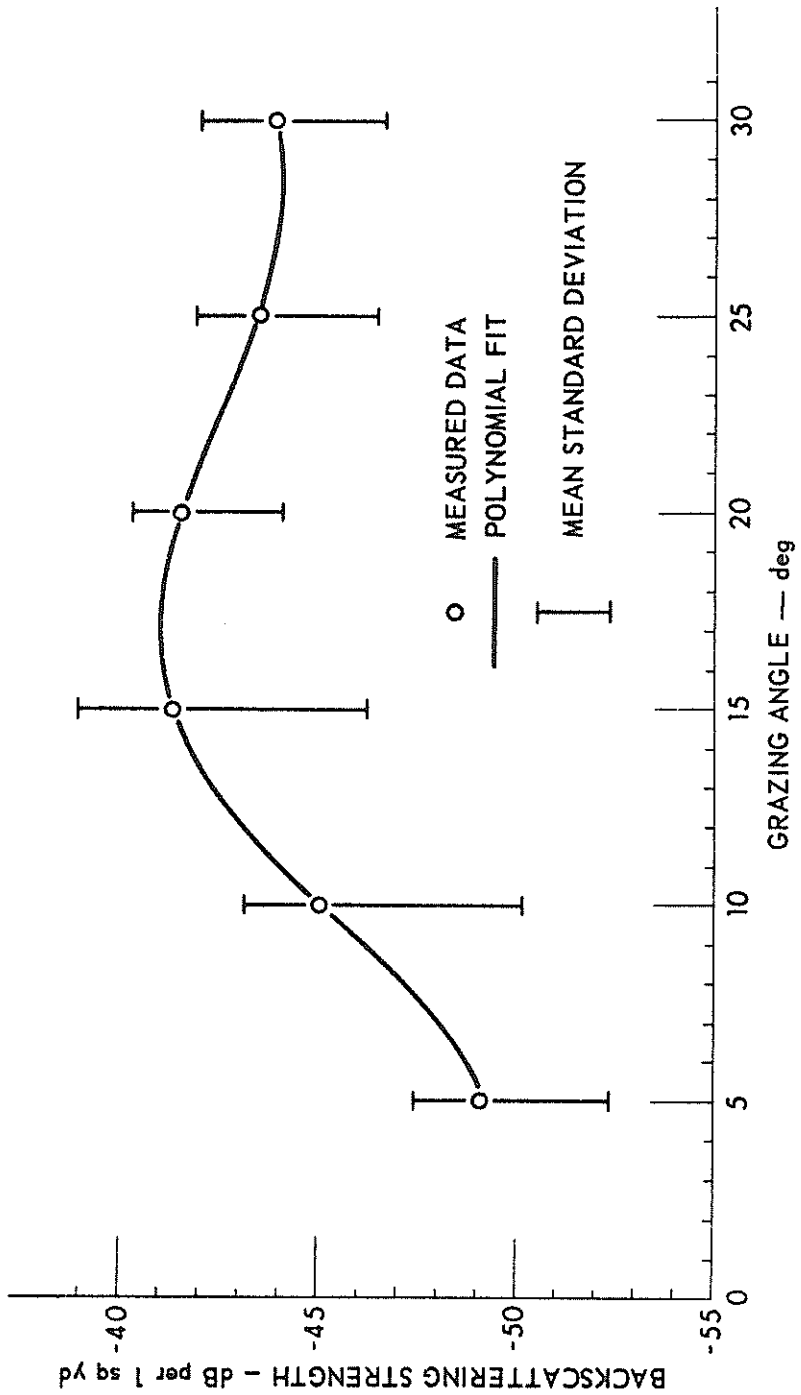

FIGURE 10
85 kHz BOTTOM BACKSCATTERING STRENGTH vs GRAZING ANGLE
BRAZOS RIVER NEAR BRAZORIA, SITE THREE, 13 SEPTEMBER 1967

DRL - UT
AS-68-146
TGM - RFO
2 - 21 - 68

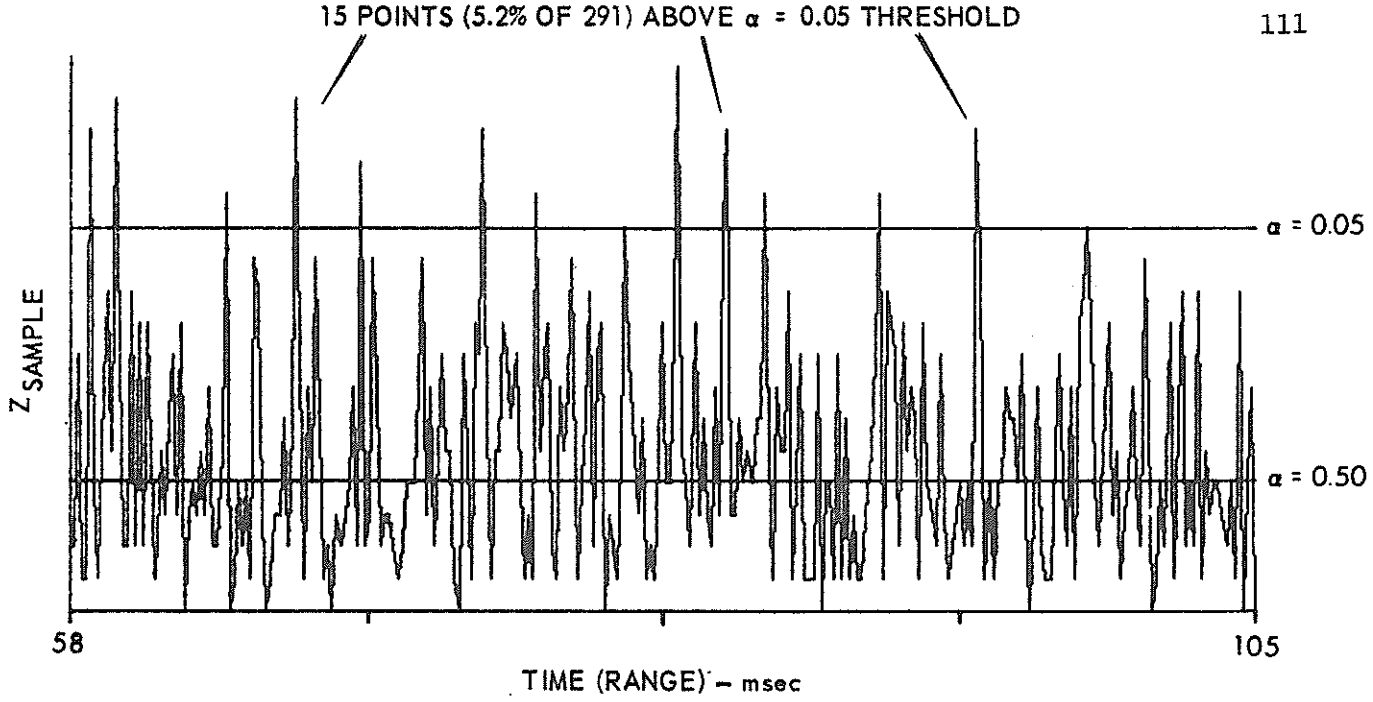

(a) ONE SAMPLE RUNS TEST FOR SAMPLE INDEPENDENCE
(ENSEMBLE SIZE = 150)

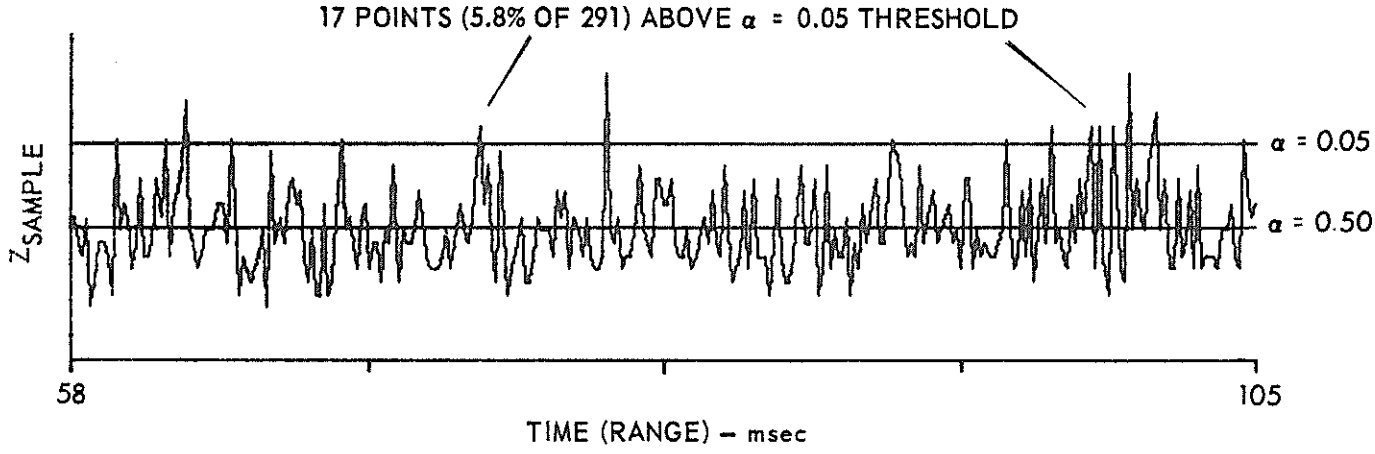

(b) KOLMOGOROV-SMIRNOV TEST FOR HOMOGENEITY
(1st 75 MEMBERS OF EACH ENSEMBLE COMPARED WITH 2nd 75 MEMBERS)

FIGURE 11
TESTS FOR INDEPENDENCE AND HOMOGENEITY
OF LONG RANGE FM REVERBERATION

THE TIME INTERVAL (58, 105) msec CONTAINS
291 INDEPENDENT CROSS SECTIONS (DATA ENSEMBLES)
T = 1.25 msec W = 9.6 kHz f_0 = 110 kHz
LINEAR FM "CHIRP" TRANSMITTED SIGNAL

ARL - UT
AS-71-297
TDP - RFO
3 - 18 - 71

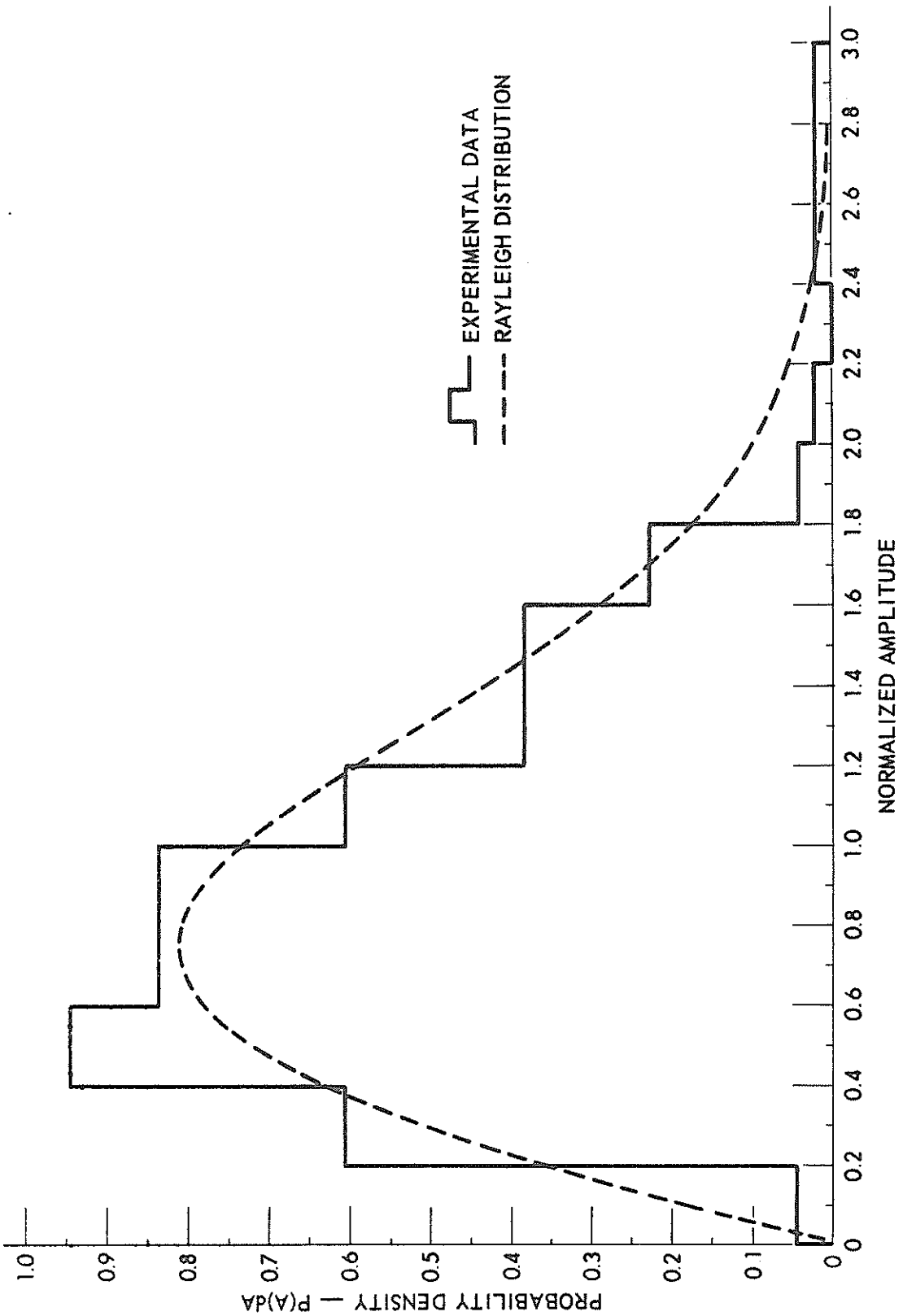

FIGURE 12
FIRST ORDER STATISTICS
BRAZOS RIVER BOTTOM REVERBERATION DISTRIBUTION DENSITY

DRL - UT
AS-68-147
TGM - RFO
2 - 22 - 68

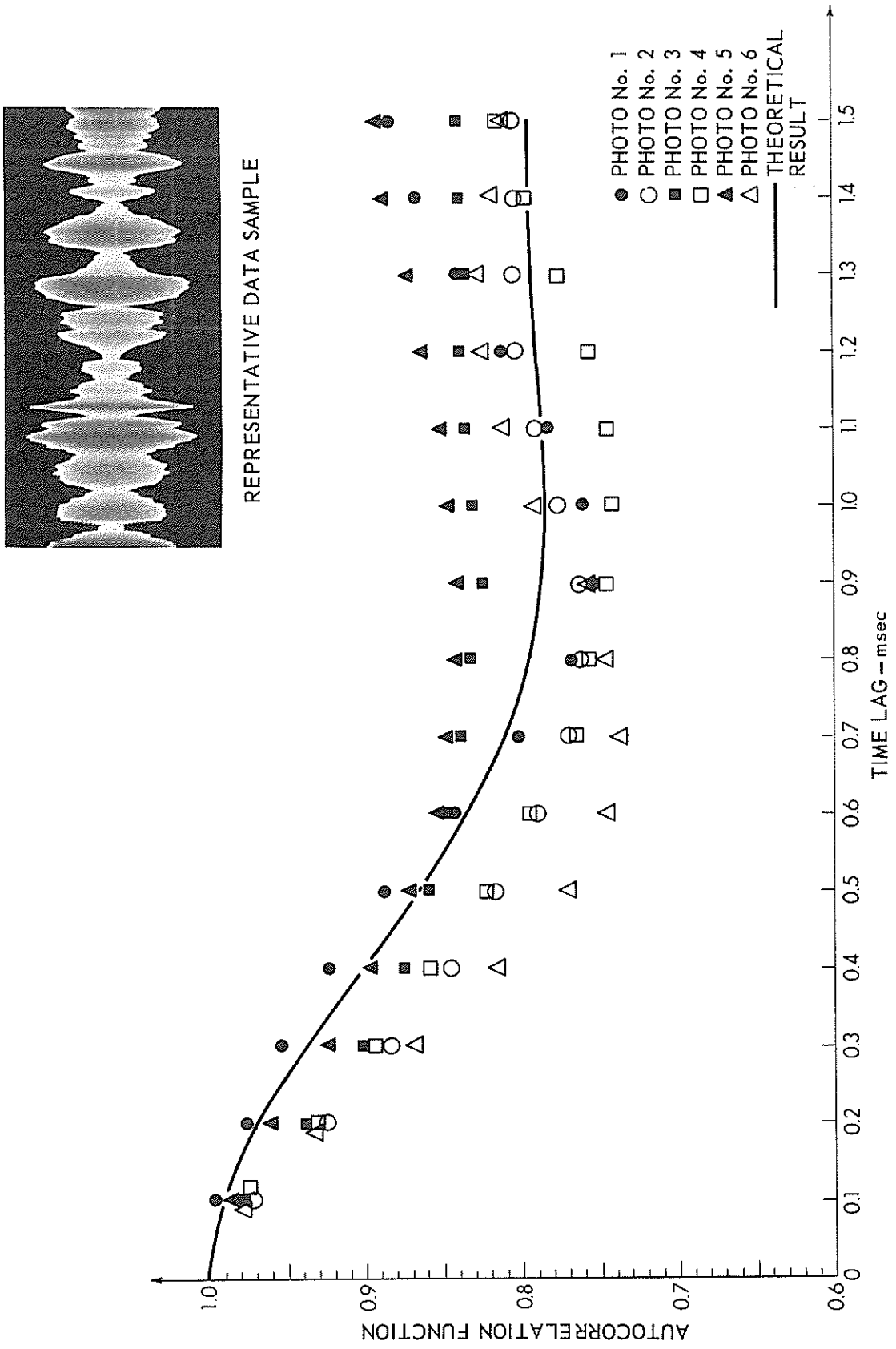

FIGURE 13
AUTOCORRELATION OF REVERBERATION ENVELOPE

DRL - UT
AS-68-432
TGM - BJB
3 - 28 - 68

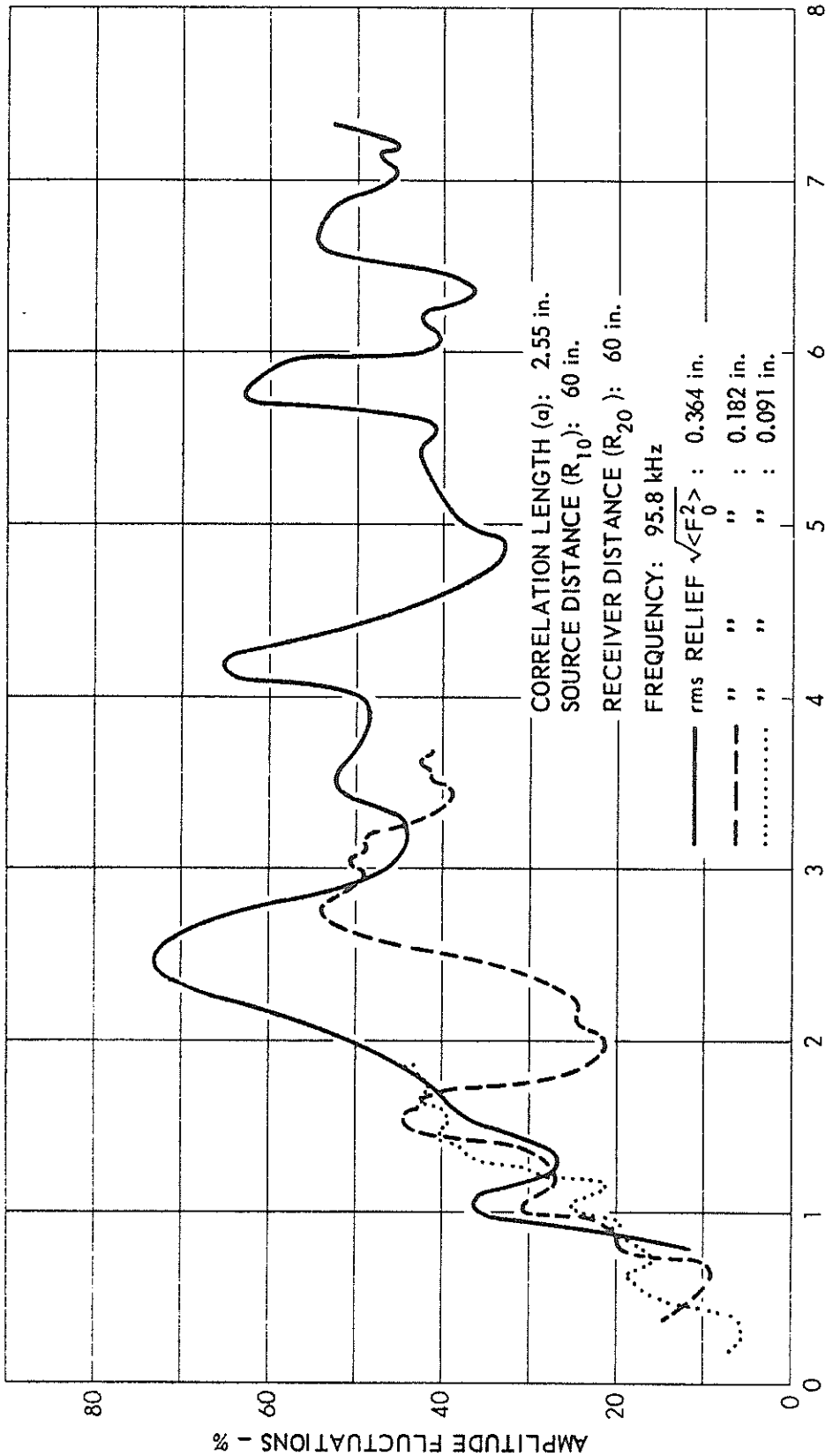

FIGURE 14
AMPLITUDE FLUCTUATIONS IN THE SPECULAR DIRECTION
PRESSURE RELEASE RANDOM SURFACE

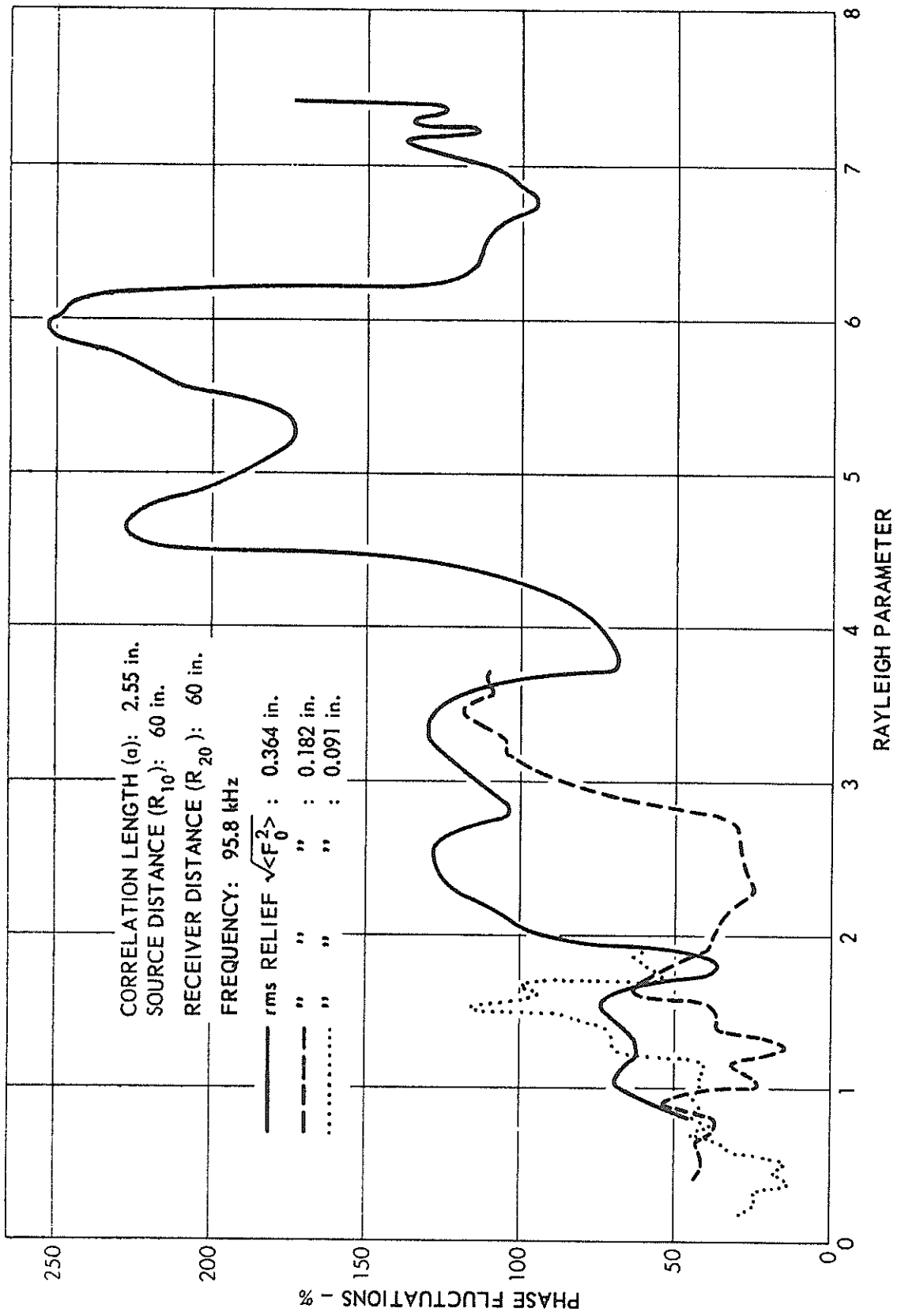

FIGURE 15
PHASE FLUCTUATIONS
IN THE SPECULAR DIRECTION
PRESSURE RELEASE RANDOM SURFACE

DRL - UT
AS-68-1142
DRM - RFO
9 - 17 - 68

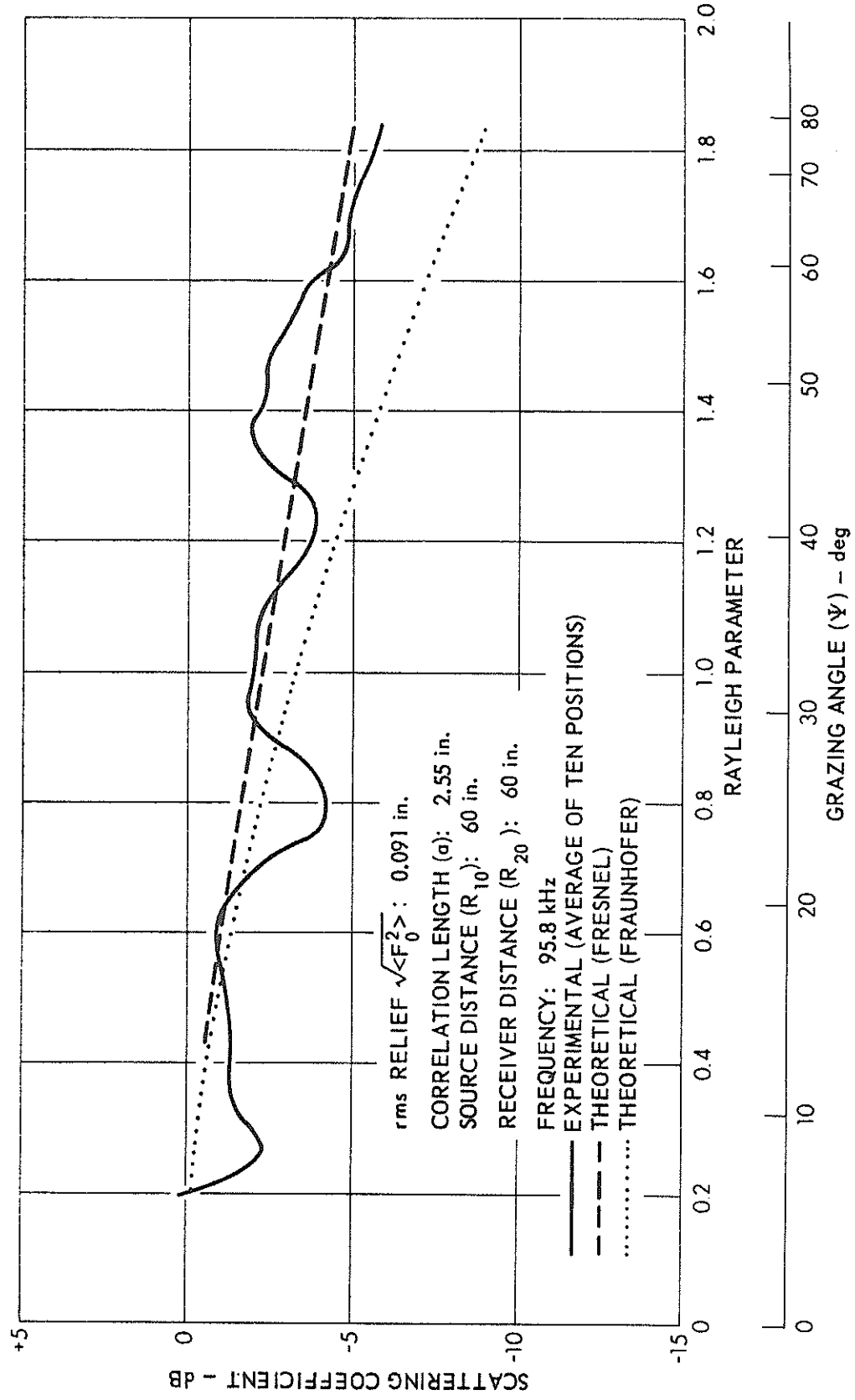

FIGURE 16
SCATTERING COEFFICIENT
IN THE SPECULAR DIRECTION
PRESSURE RELEASE RANDOM SURFACE

DRL - UT
AS-68-1135
DRM - RFO
9 - 13 - 68

SEISMIC REFLECTION AND REFRACTION:
TRAVEL TIME ANALYSIS

Davis A. Fahlquist
Associate Professor, Departments of Geophysics and Oceanography
Texas A&M University

INTRODUCTION

Acoustic methods provide a powerful technique for the study and mapping of sediment and crustal structure lying beneath the sea floor. Such studies utilize a wide range of energy sources: explosives, arc discharges, air and gas guns, vibroseis, and piezoelectric transducers. The energy levels and spectral characteristics vary widely for the various sources; the effective depth of penetration of the acoustic signals may vary from a few meters (e.g., 12 kh and 3-1/2 kh transducers) to many kilometers (e.g., explosives). Analysis based on ray theory and travel times along ray paths is useful in interpretation of seismic reflection and refraction experiments using these various sources.

Analysis of the travel time graphs obtained in seismic reflection and refraction experiments are based on ray calculations. Previous speakers have discussed the eikonal approximation to the wave equation; its limitations, and the subsequent solution in terms of wave surfaces and rays. The limitations of ray theory are not a serious disadvantage in the interpretation of seismic reflection and refraction profiles.

In contrast with the propagation of compressional waves only in fluids, the transmission of seismic energy through solids may include the propagation of shear waves as well. The speed of propagation of these two types of waves are given by

$$\alpha = \sqrt{\frac{\lambda + 2\mu}{\rho}} \qquad \text{P wave}$$

$$\beta = \sqrt{\frac{\mu}{\rho}} \qquad \text{S wave} \tag{1}$$

where μ, λ are constants describing the elastic behavior of a homogeneous

isotropic medium.

In wide angle reflection profiling and in refraction profiling conversion of P→S and S→P can occur at boundaries in the medium where the speed and/or the acoustic impedance change. For the purposes of this discussion we shall be concerned only in the P wave paths.

Snell's Law governing propagation along ray paths in the medium states

$$\frac{\sin i_1}{C_1} = \frac{\sin i_2}{C_2} = \ldots\ldots = \frac{\sin i_n}{C_n} = p \qquad (2)$$

where p = ray constant; C_i = speed in i^{th} layer.

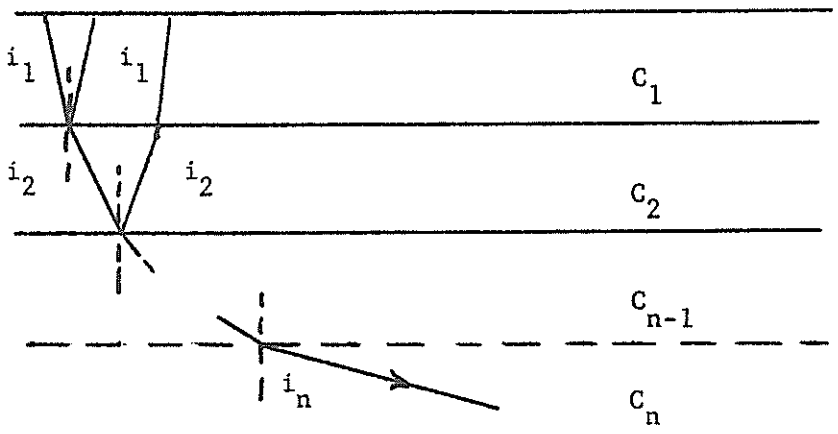

Fig. 1

Snell's Law thus describes the refraction occuring along the ray path as the energy passes through layers of varying speeds (Fig. 1). For reflection at an interface, the law simply states that the angles of incidence and reflection are equal.

The concept of apparent wave speed along a horizontal interface is also useful in the interpretation of reflection and refraction data. Consider a plane wave propagating upward at an angle i toward the sea surface at a speed C_0 (Fig. 2).

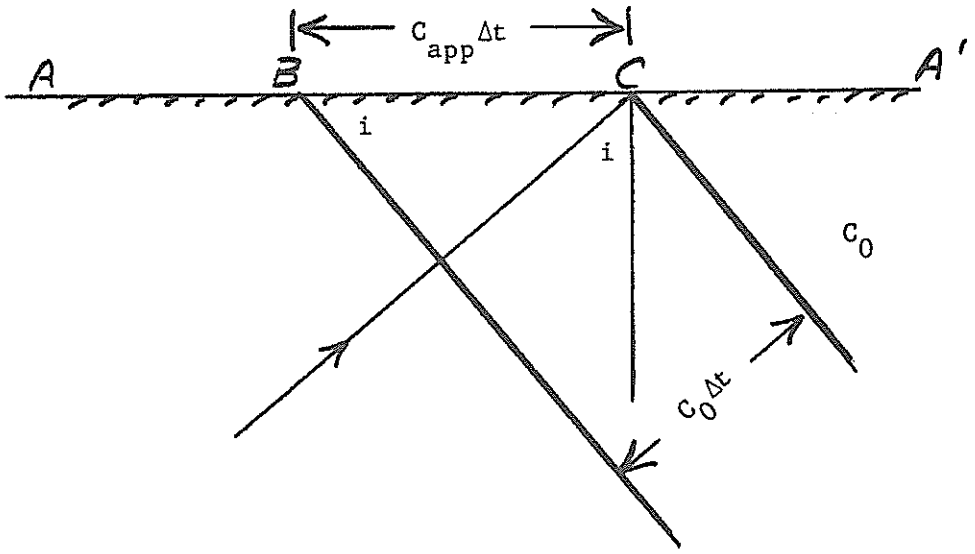

Fig. 2

The wave front advances from position 1 to position 2 in a time Δt; the distance of advance along the ray path is $C_0\Delta t$. However, detectors placed at B and C in the surface would measure a speed, C_{app}, where $C_{app} > C_0$. The apparent velocity along the surface is given by

$$\sin i = \frac{C_0\Delta t}{C_{app}\Delta t} \tag{2}$$

$$\text{or } C_{app} = \frac{C_0}{\sin i}$$

Only in the limit where $i \rightarrow 90^o$ will $C_{app} \rightarrow C_0$.

I. TRAVEL TIME: REFLECTED WAVES

1. Reflection from a single horizontal layer

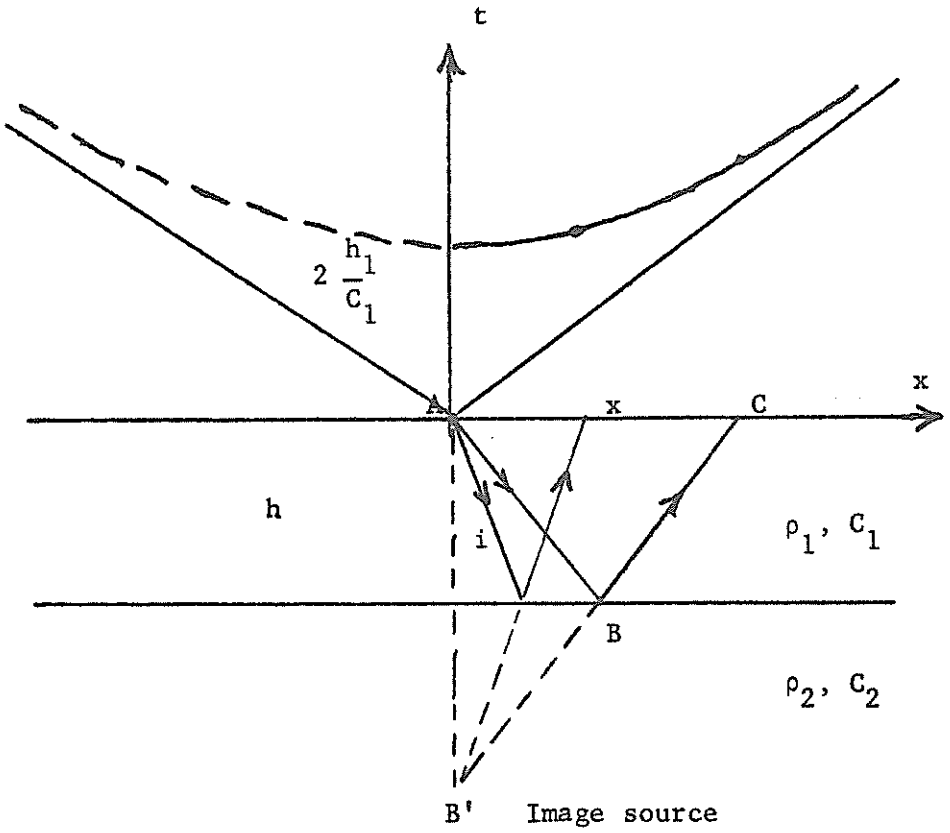

Fig. 3

Consider first the travel time associated with a reflected wave traveling through a homogeneous isotropic layer of thickness h and reflected back to the surface along path $\overline{AB}$ and $\overline{BC}$ (Fig. 3). The travel time will be given by

$$t = \frac{\overline{AB} + \overline{BC}}{C_1} = \left[\frac{x^2 + 4h^2}{C_1^2} \right]^{1/2} \tag{4}$$

The equation is a hyperbola with an intercept on the t axis at $x = 0$ of $t = \frac{2h}{C_1}$. As the range, x, increases the travel time t also increases ; the curve is symmetric about the t axis. In seismic profiling experiments in deep water the source and detector are treated as if both were located at point $A(x = 0)$ and the reflection path over a flat bottom is vertical . In wide angle reflection experiments the source and detector/or detectors are no longer held fixed relative to each other but are allowed to separate.

The slope of the travel time curve is given by

$$\frac{dt}{dx} = \frac{x}{C_1} \left[x^2 + 4h^2 \right]^{-1/2} \tag{5}$$

and the angle of emergence of the ray is given by

$$\sin i = \frac{x}{(x^2+4h^2)^{1/2}} = C_1 \frac{dt}{dx} \tag{6}$$

As x becomes very large the time difference between the reflection arrival and the direct arrival ($t = x/C_1$) will approach zero, and the inverse slope of the reflection curve will be the speed, C_1, of the medium.

2. Determination of speed from reflection profiles

The determination of true depth to a reflecting horizon is dependent on a knowledge of the speed of propagation of the wave through the layer. The speed may be determined from wide angle reflection profiles and/or refraction profiles. In the case of reflection from a single layer we note that Equat. 4 can be written as

$$t^2 = \frac{x^2+4h^2}{C_1^2} \tag{7}$$

If we let $t^2 = T$ and $x^2 = X$ this becomes

$$T = \frac{X}{C_1^2} + \frac{4h^2}{C_1^2} \tag{8}$$

A graph of T versus $X(t^2 - x^2)$ is linear, the inverse slope yielding the square of the speed, C_1, and the intercept at $X = 0$ yielding a measure of the thickness, h.

II. TRAVEL TIME: REFRACTED WAVES

1. Refraction from a single horizontal layer

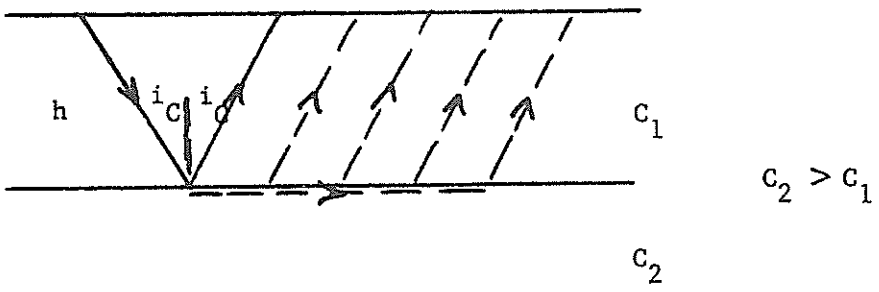

Fig. 4

Consider a single homogeneous isotropic layer with speed C_1 overlying a half space of speed C_2 (Fig. 4). For a ray path originating in the upper medium and incident on the boundary we have

$$\frac{\sin i_1}{C_1} = \frac{\sin i_2}{C_2} = p \tag{9a}$$

For an angle of incidence i, such that $i_2 = 90^\circ$ we have

$$\sin i_1 = \frac{C_1}{C_2}$$

$$i_1 = \sin^{-1} \frac{C_1}{C_2} = i_C \tag{9b}$$

and the ray path in the lower medium is directed along the boundary; when this condition occurs i_1 is called the critical angle for refraction. Ray theory fails to predict the transmission of energy back to the surface of the upper medium along ray paths emerging at the critical angle, i_C (dashed lines in Fig. 4). However, a Huygen wave front diagram (Fig. 5) will allow us to visualize how a secondary wave front is generated at the boundary and propagates back to the surface.

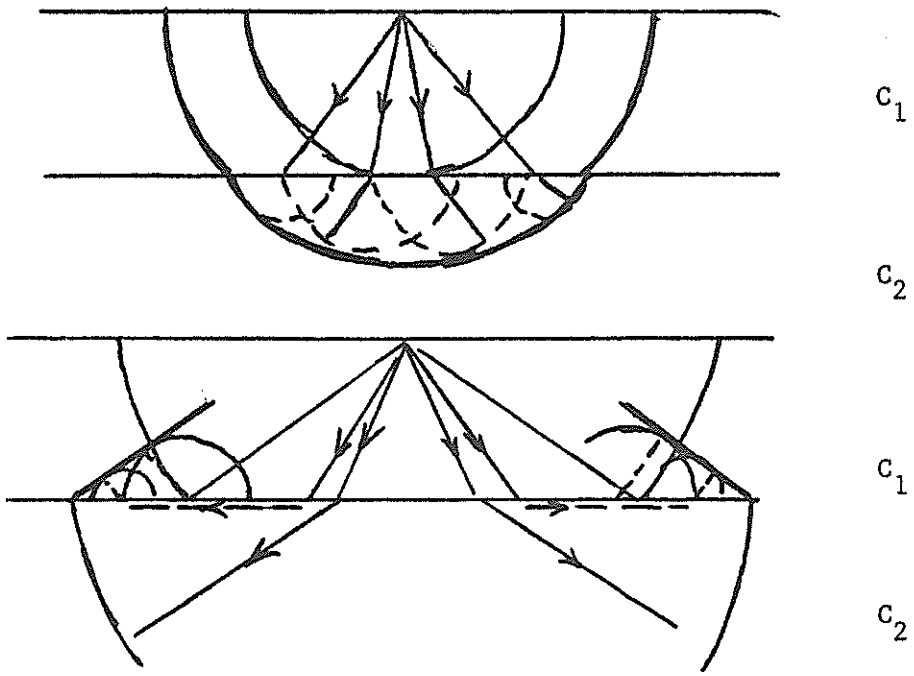

Fig. 5

The refracted wave in the lower medium moves outward with speed C_2. Since $C_2 > C_1$ the wave fronts in the upper and lower medium will be discontinuous at the boundary. As the wave in the lower medium gradually moves outward disturbing the interface, secondary wavelets are emitted into the upper medium. These wavelets coalesce to form a conical wave front moving upward toward the surface at the critical angle, i_c.

For the single layer, the apparent velocity measured along the surface will be

$$C_{app} = \frac{C_1}{\sin i_c} = \frac{C_1}{\frac{C_1}{C_2}} = C_2 \tag{10}$$

The apparent velocity measured along the surface is the speed, C_2, of the lower medium. The travel time equation for the refracted arrival is given by

$$t = \frac{\overline{AB} + \overline{CD}}{C_1} + \frac{\overline{BC}}{C_2}$$

$$= \frac{x}{C_2} + \frac{2h_1 \cos i_c}{C_1} \tag{11}$$

$$\text{where } \cos i_c = \left[1 - \left(\frac{C_1}{C_2}\right)^2\right]^{1/2}$$

The equation for the travel time is a straight line whose inverse slope yields the speed of the lower media. The thickness, h_1, of the layer may be determined from the intercept at $x = 0$.

$$t(0) = \frac{2h_1}{C_1} \cos i_c \tag{12}$$

Measurement of travel times from a shot point to detectors along the surface thus permit a determination of the speed of propagation in the lower media as well as the thickness of the first layer.

Extension of this technique to a sequence of horizontal layers ($C_n > C_{n-1}$) is straight forward. (See, for example, Officer, C. B.)[1]. The travel time graph for a multi-layer system is shown schematically in Fig. 6 and the travel time equations are given below.

$$t_1 = x/C_1$$

$$t_2 = x/C_2 + \frac{2h_1}{C_1} \cos i_{12}$$

$$t_3 = x/C_3 + \frac{2h_1}{C_1} \cos i_{13} + \frac{2h_2}{C_2} \cos i_{23} \qquad (13a)$$

$$t_k = \frac{x}{C_k} + \sum_{n=1}^{k-1} \frac{2h_n}{C_n} \cos i_{nk}$$

and $$\frac{\sin i_{nk}}{C_n} = \frac{1}{C_k} \quad n = 1, 2, \ldots, k-1 \qquad (13b)$$

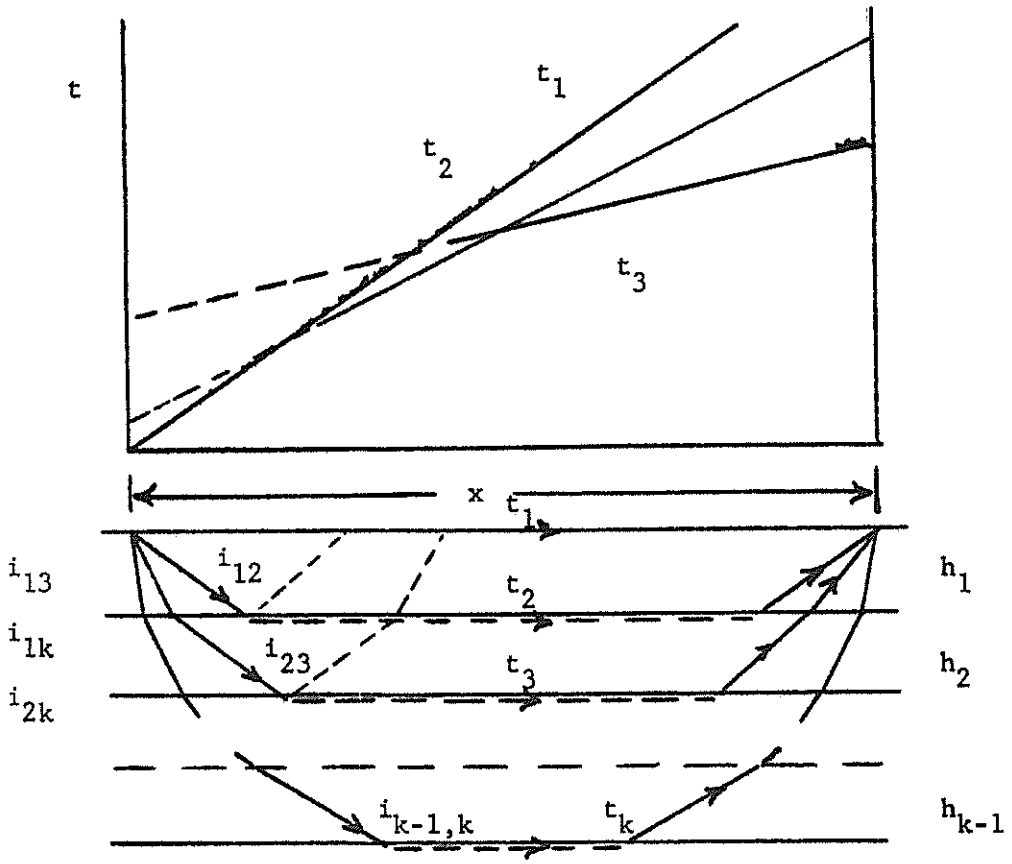

Fig. 6

III. REFLECTION AND REFRACTION FROM DIPPING LAYERS

1. Reflection

Analysis of reflection and refraction data can be extended to the case of dipping layers. Fig. 7 illustrates the geometry and travel time graph associated with a single dipping interface.

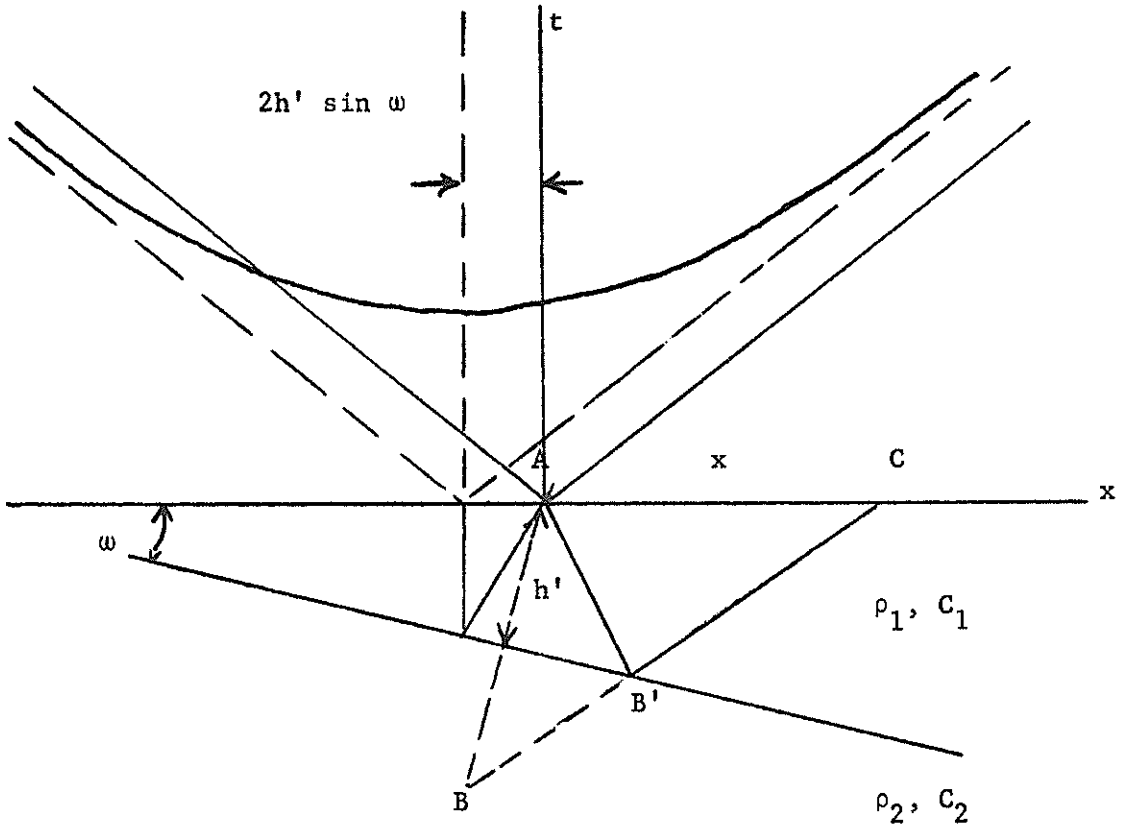

Fig. 7

A detailed analysis of reflections from a dipping interface has been given by Slotnik.[2] The reflection travel time is given by

$$t = \frac{\left[(x + 2h' \sin \omega)^2 + (2h' \cos \omega)^2 \right]^{1/2}}{C_1} \qquad (14a)$$

$$\text{or } C_1^2 t^2 = x^2 + 4xh' \sin \omega + 4h'^2 \qquad (14b)$$

If, in Equation a we make the substitution $X = x + 2h' \sin \omega$, the travel time equation becomes

$$C_1^2 t^2 = X^2 + 4h' \cos^2 \omega \qquad (14c)$$

Again, as in the case of a horizontal layer the travel time equation is a hyperbola with an axis of symmetry at $x = -2h' \sin \omega$. For $x = -2h' \sin \omega$ we have $X = 0$ and $t = \frac{2h' \cos \omega}{C_1}$.

2. Refraction

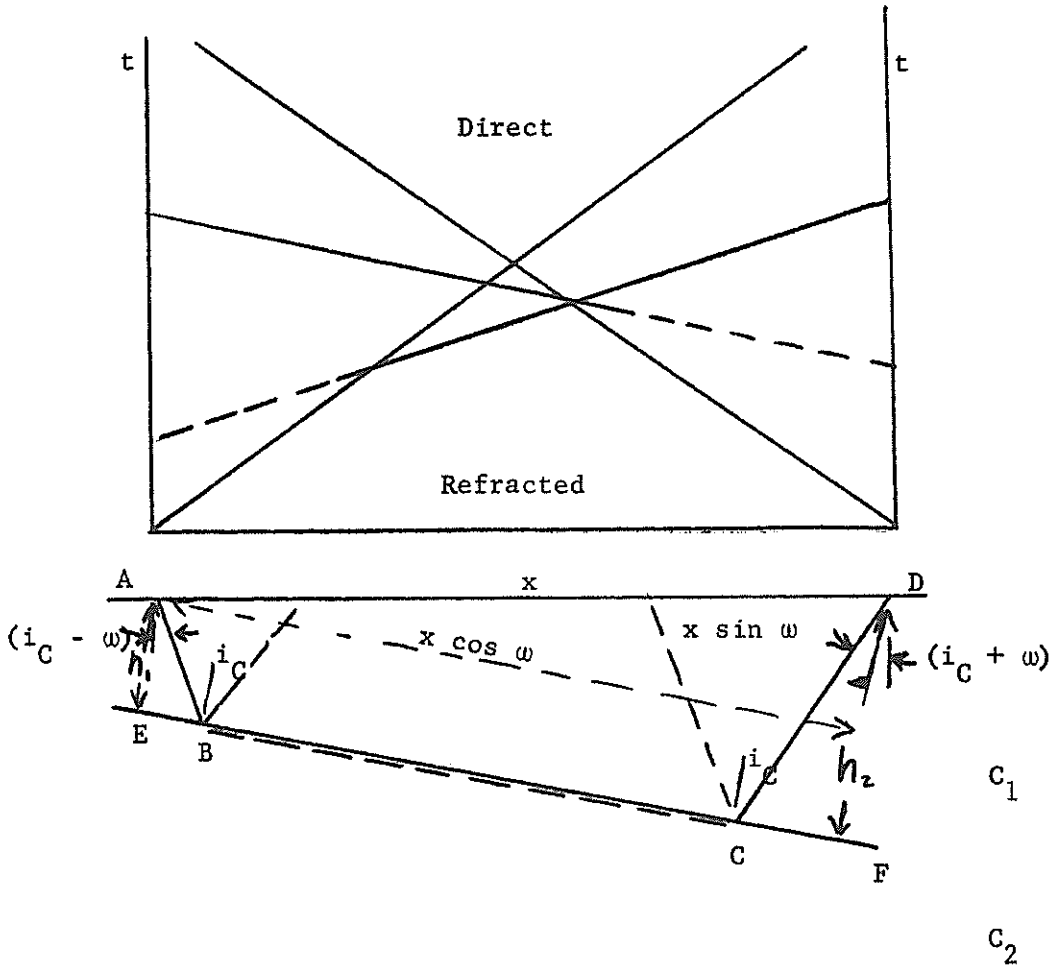

Fig 8.

In Section II-1 it was shown that the apparent velocity measured from the travel time graph for a single horizontal layer was equal to the speed, C_2, in the lower medium. Referring now to Fig. 8 we see that the apparent velocity measured on the surface for a wave front traveling from C D is different from that of a wave front traveling from B A. In particular we may write

$$\sin (i_C + \omega) = \frac{C_1}{C_{app}\ \overline{CD}} \tag{15a}$$

$$\sin (i_C - \omega) = \frac{C_1}{C_{app}\ \overline{BA}} \tag{15b}$$

$$\text{and } \sin i_C = C_1/C_2 \tag{15c}$$

Equations 15 a, b may be solved simultaneously for the critical angle, i_C, and the angle of dip, ω.

$$i_C = 1/2 \left[\sin^{-1} \frac{C_1}{C_{app}\ \overline{CD}} + \sin^{-1} \frac{C_1}{C_{app}\ \overline{BA}} \right] \tag{16a}$$

$$\omega = 1/2 \left[\sin^{-1} \frac{C_1}{C_{app}\ \overline{CD}} - \sin^{-1} \frac{C_1}{C_{app}\ \overline{BA}} \right] \tag{16b}$$

Once i_C is known the velocity of the lower medium, C_2, may be determined directly from the critical angle relationship. The apparent velocities used in Eq. 16 a, b are obtained directly from the travel time graph; the speed obtained for the wave traveling along $\overline{CD}$ is called the downdip velocity, that along $\overline{BA}$ the updip velocity.

The travel times for a given distance, x, will not be the same except for the end points of the profile, i.e., the reverse points. The travel time equations may be obtained with the help of a simple geometric construction (Fig. 8).

$$\begin{aligned} t_{downdip} &= \frac{\overline{AB} + \overline{CD}}{C_1} + \frac{\overline{BC}}{C_2} \\ &= \frac{\overline{AB} + \overline{DC}}{C_1} + \frac{\overline{EF} - \overline{EB} - \overline{CF}}{C_2} \\ &= \frac{(2h_1 + x \sin \omega)}{C_1 \cos i_C} + \frac{x \cos \omega - (2h_1 + x \sin \omega) \tan i_C}{C_2} \end{aligned} \tag{17}$$

This equation reduces to

$$t_{downdip} = \frac{2h_1 \cos i_C}{C_1} + \frac{x}{C_1} \sin (i_C + \omega) \qquad (18a)$$

The corresponding equation for the updip travel time is

$$t_{updip} = \frac{2h_2 \cos i_C}{C_1} + \frac{x}{C_1} \sin (i_C - \omega) \qquad (18b)$$

3. Multiple layers

The ray path analysis outlined in the previous sections can be directly extended to multi-layer media, either horizontally stratified or dipping. Elementary discussions of the reflection problem may be found in Stotnik.[2] The multi-layer refraction problem is discussed by Ewing, et.al[2] and presented also by Officer[1] and Steinhart and Meyer.[4] Further discussions on refraction analysis have been edited by Musgrave.[5]

BIBLIOGRAPHY

[1]C. B. Officer, Introduction to the Theory of Sound Transmission, McGraw Hill (1958).

[2]M. M. Slotnick, Lessons in Seismic Computing, Society of Explora-Geophysics (1959).

[3]M. Ewing, G. P. Woollard, and A. C. Vine, B. G. S. A., 50, 257-296 (1939).

[4]J. Steinhart and R. P. Meyer, Explosion Studies of Continental Structure, Carnegie Institution of Washington Publication 622 (1961).

[5]A. W. Musgrave, Seismic Refraction Prospecting, Society of Exploration Geophysics (1967).

TWENTY YEARS IN UNDERWATER ACOUSTICS: GENERATION AND RECEPTION

T. F. Hueter
Vice President and General Manager
Honeywell Inc., Marine Systems Center

Looking back at the accomplishments—and also at the struggles—of the past two decades in the underwater acoustic transducer field will help us to understand the possibilities and limitations of the present state of the art, and to get a feeling for the rate at which further progress might take place.

Many of the innovations currently being made or planned in sonar were being "seeded" at MIT, Harvard, Brown, or Cal Tech in the early 1950's, and, if one adds an additional five to eight years of development for production prior to introduction of fleet equipment that is fully tested and evaluated, it all totals up to a gestation period of a quarter of a century. In terms of R&D dollars, tours of duty, administrations, fiscal policies, and shipbuilding cycles, this amounts to a good deal of change. It is thus apparent that much depends on the wisdom and foresight of those who are called upon to prognosticate and show the way.

In looking back, then, we are searching for a milestone...or a time capsule...which might have recorded the state of affairs and the expectations of the acoustic physicists and engineers around 1950. In 1950, the members of the Panel on Underwater Acoustics of the National Research Council (NRC) stated their view of basic problems and challenges in underwater acoustic generation and reception.

Many possible transduction mechanisms, ranging from solid state to chemical and mechanical, were recommended in 1950 for more systematic research. Two that showed early signs of pregnancy *did* survive these 20 years as strong contributors to new engineering solutions: namely, ferroelectric ceramics (Howatt, Jaffee, Mason, in the late forties) and hydroacoustics (Bouyoucos Thesis, June 1951; Patent April 1954). By contrast, we now view the very strong recommendations of the NRC report for a broad-based research program in cavitation phenomena as less visionary; actual sonar performance has benefited little from much of this work. The modern approach is to sidestep, rather than to overcome, the cavitation limitation of seawater.

With regard to our ability to meet specifications, here is a typical statement in the 1950 report that would raise an eyebrow in 1971:

> ...transducer performance can usually be calculated reasonably well. In most cases, we can build transducers which perform within a few dB of theory, at least if some trial and error is allowed.

It has taken some pretty dedicated people at the Navy's transducer laboratories—notably NUC, San Diego—and also in industry, to overcome this cavalier attitude toward design prediction and production tolerance, and I will relate some of their results later.

Many of the developments that did take place, and the problems that were solved, during the past 20 years in the area of underwater acoustics generation and reception seem to have been set in motion by several challenges presented to transducer scientists and engineers from outside their own disciple. Figure 1 shows some of these causative relationships. For example, new insights into the various modes of propagation of sound in the ocean supported by extensive field work have pointed strongly to the possibility of acoustic echo-ranging to much larger distances than ever before thought possible. In order to do this, however, sound frequencies of increasingly larger wavelengths were shown to be necessary, and a demand for efficient low-frequency transducer elements of substantial power output developed. Much new transducer technology was brought into being through the research activities surrounding Project Artemis then under way at Columbia University.

From a closer analysis of propagation paths of the type shown in Figure 2, it also appeared advantageous to move sound sources and receivers to locations at greater depth, particularly as the interest in bottom-mounted acoustic installations developed. Indeed, the past two decades have been an era of technological mastery of the deep ocean. Using new materials and processes, much work has been accomplished in solving problems of pressure integrity and leak prevention, mooring and recovery of deep sea packages, power storage, and cable technology.

Another significant challenge to the transducer people resulted from the advances in sonar systems engineering through the influence of such disciplines as information theory and digital data processing. Although the transducer continues to be essentially an analog device, it has increasingly been called upon to interface into electronic systems based on digital technology.

During the past two decades, many precepts of information theory found useful in radar during World War II have had a great impact on sonar. The significance of the time bandwidth product for the processing of complex underwater signals led to increasing pressure on transducer designers to provide not only for flat receiving response, but also for broad transmitting response. Also, the concept of an acoustic receiving array as a correlator, formulated in 1952 by Faran and Hills at Harvard, presented the sonar systems engineers with entirely new beamforming possibilities.

It was now possible to trade spatial and temporal characteristics of an array; for example, one could provide for sharper beams by using bandwidth rather than by increasing array size. Figure 3 summarizes some of the payoff obtained from applying the precepts of information theory to transducer design—a point that, strangely, was missed in the 1950 NRC report.

More bandwidth automatically meant higher coupling coefficients, which put a premium on research related to ferroelectric crystals and ceramics. Much new fundamental work was going on in this area in the late forties and early fifties—particularly at MIT under Hans Mueller and Von Hippel. This was translated quite rapidly into applications engineering—and later, production engineering—initially at such places as Brush-Clevite, Gulton Industries, and the Bell Telephone Laboratories, followed by several others during the past ten years.

A considerable art in designing, fabricating, and testing ferroelectric ceramic transducers has come into being during the past two decades. The perfection of the material properties involved a good deal of molecular engineering in which additives were introduced to keep electrical and mechanical losses low, procedures for electroding and polarizing were established, and casting, pressing, and aging techniques were developed. The result of all this work is summarized in Tables I and II, which show some of the salient features of the more commonly used titanates and zirconates. We note that substantial increases in effective coupling coefficients and power-handling capacity (low loss factor) have been achieved through proper blending of ingredients.

Many of these new piezoelectric materials are now readily available on a commercial basis, with outstanding success in some areas. They have generally proved more cost-effective than crystals (ADP) and magnetostrictive materials, while providing wider margins in power and sensitivity. Only in some special applications where ruggedness and shock resistance are at a premium are magnetostrictive transducers still considered superior. One such application will be discussed later.

During the past 20 years, rapid advances in solid-state physics have revolutionized electronics engineering: the transistor was born and applied and eventually transformed into microcircuitry. Digital computers became sufficiently compact and reliable to find their way through the hatches of submarines into the control rooms of destroyers.

As digital processors and memories made possible the rapid digestion, correlation, and classification of data from larger volumes of ocean, new concepts in the spatial manipulation of acoustic signals developed. Although arrays of transducer elements have been used for some time, the beamforming possibilities by modern sonar theory also presented new challenges to transducer designers in the area of array design to meet new surveillance demands.

As a result of this work, greatly improved arrays with lower side lobes and provisions for beam steering over wide angular sectors have come into use. At the same time, we learned to improve the element sensitivity, to suppress structure-borne noise, and to reduce flow noise. All this had to be accomplished over a wider range of hydrostatic pressures and covering increasingly wider frequency bands. Thus, much design flexibility was achieved throughout the past 20 years, aided by progress in the theory of multiplicative and additive arrays. As Figure 4 shows, we are now able to work with a wide variety of array configurations, backed in most cases by good theory, which lend themselves to towing, conformal mounting on hulls, beam steering from end fire to broadside, and to sidelooking sonar and synthetic-aperture types of applications, borrowed from the radar world.

A much-used type of array is the searchlight transducer. One version, using a large number of small elements that are suitably phased and packaged for deep-submergence applications, is shown in Figure 5. But, even when a design is based on well known principles, there are still cases where theory bogs down for mathematical reasons because of the necessity of working with complex boundary conditions or finite frequency bands or non-ideal dome structures.

For example, the quest for larger power and lower frequency, as in Columbia University's Project Artemis, led to the construction of large assemblies of active elements, with dimensions of several wavelengths. These pursuits have confronted us with new and initially quite disturbing phenomena of element interactions occasionally causing large variations in the complex radiation impedance, as seen by the individual array elements. Here, additional theoretical effort became necessary to deal with a practical problem which was not anticipated. It should be noted, however, that we find an inkling of this type of problem earlier in the 1950 National Research Council report:

> No adequate theoretical treatment (nor adequate empiricism for that matter) is available for radiators which have dimensions comparable with one wavelength and which are set in baffles other than an infinite rigid plane. This now causes difficulty, particularly in the design of large arrays, for low-frequency listening.

The real problem occurred in the early 1960's with two active low-frequency arrays built for the ARTEMIS and the LORAD programs. Both arrays demonstrated local hot spots where the effective element impedance assumed negative radiation resistance values which were traced to mutual impedance terms that, until this time, had been ignored by most array designers.

However, the significance of some earlier work was soon recognized by Pritchard, who in 1960, wrote in the *Journal of the Acoustical Society of America*:

> The first calculation of mutual acoustic reactance appears to be that of Karnovskii (1941), who evaluated the complex mutual impedance for pulsating spheres of radius small relative to a wavelength. Recently (1956), this same writer extended his calculations, in the case of mutual resistance only, to a more general spherical radiator of arbitrary size and order. Resistive and reactive components of the mutual impedance between two circular pistons were calculated by S. J. Klapman (1940) using a direct integration procedure.

Out of this work, the concept of velocity control was developed by a group of transducer research people working under John Hickman at NUC, San Diego–"velocity control" being an electronic means of protecting the individual transducer element against extreme local impedance variations while at the same time reducing these variations by proper choice of piston size and element spacing.

One of the first, very large low-frequency arrays developed by Frank Massa for long-range propagation research is shown in Figure 6. The dipole-type transducer element used in this array was introduced by John Chervenak of the Naval Research Laboratory. A rigid, box-shaped outer shell resonates with a spring-mounted, internal mass, using variable reluctance-type magnetic excitation. After the introduction of appropriate measures for velocity control, this array was used successfully during the past six years for propagation experiments conducted from its mother ship, the *Mission Capistrano*. As can be imagined, for an array that is 50 feet high, 35 feet wide, and weighs 150 tons, the requirement of suspending it on 1500 feet of cable—of generating, transmitting, and impedance-matching close to one million watts of power to it—and of keeping the mother ship on station during the course of experiment—are formidable requirements indeed. At this scale, problems of power storage and conversion loom very large. Here, we can still agree with a pragmatic statement made in the 1950 NRC report, which called for study of the economy of energy storage in batteries, springs, compressed air, and other such devices, including evaluation of energy–weight ratios and energy–volume ratios.

Another use of these large, low-frequency planar arrays that has gone through several concept-formulation stages in recent years would incorporate such arrays into the hull or the keel of a large surface ship, with one array on each side, as shown in Figure 7. Quoting from an article by I. Cook, which appears in the June 1969 *Naval Engineers Journal*:

> ...from a sonar standpoint, it is desirable to have a wedge—maybe ten degree total angle—and to have the arrays tilted to the vertical for bottom bounce utilization perhaps 20 degrees. Such a combination in an appendage faired to the hull of the ship will be a rather large proportion of the underwater wetted surface. There has been talk of a conformal array, where the transducer array surface would conform to the shape of the underwater hull, so that an appendage is not required, but this introduces so much complexity not only in the physics of the transducers but in other aspects, like beamforming of a non-symmetrical surface, that it has been deferred until planar array technology experience has been acquired.

Innovative efforts such as this have required extensive computer modeling of the radiation characteristics, and baffle properties for such arrays. They represent a severe test for our current understanding of acoustic array properties, and the realization of such fully-integrated arrays is one of the major challenges of the future. The utility of such arrays depends on the feasibility for steering beams from broadside to end-fire without loss of radiation efficiency and pattern integrity, and also on the ability of compensating for the ship's motion. This is no small task because, with large steering angles, the near-field becomes increasingly non-uniform with large pressure and velocity fluctuations conducive to cavitation, placing excessive demands on velocity control. Also, the phase relationships necessary for low side-lobe beams are difficult to maintain over wide frequency bands.

The current approach for surface-ship sonar as used by our new generation of destroyers is depicted in Figure 8. The bubble-shaped bow dome contains a cylindrical array, of the type shown in Figure 9, whose axial symmetry renders beamsteering fairly simple, compared with the situation just described.

Again quoting from the June 1969 article by I. Cook:

> Beamforming is much less complex in a cylindrical array, for no matter in which direction the beam is formed in azimuth, the symmetry of the transducer favorably allows identical electronic equipment for the phasing and time delays necessary to form the beam. Even for depression angles, the same is true. This is not the case for a planar array where for each and every direction in space, whether in azimuth, or in depression angles, a new combination of electronic equipment is required.

The ideal shape for broadest array coverage, uniform in all directions, is spherical. The loading characteristics of sets of pistons located on such a surface were shown to be reasonably uniform by C. Sherman as early as 1955. These predictions were later confirmed experimentally with the help of scale models. The use of such modeling, both on the computer and by size reduction of actual arrays (Figure 10), has become common practice in recent years after some disappointments with designs based on theory alone. Full-scale spherical arrays have been developed for submarine applications by the Submarine Signal Division of Raytheon in cooperation with the Underwater Sound Laboratory in New London. As of today, they represent a state of the art that is well understood and highly successful for both active echo-ranging and passive listening. This impressive spherical transducer assembly shown in Figure 11 has a diameter of 15 feet and well over a thousand active radiators. It is integrated into the bow of the submarine by an acoustically transparent dome that provides minimum beam distortion—a considerable acoustic achievement in itself.

Smaller submarines, such as the *STAR III* shown in Figure 12, have used reflector-type arrays as a suitable compromise in producing directivity at wavelengths too large to be handled by a hull-mounted conventional array.

The paraboloid array shown produces an 18-degree beam at a frequency of 4 kHz. Reflectors of many shapes and forms have been studied during the past ten years by McKinney and co-workers at the University of Texas, particularly for high-frequency, high-resolution sonar applications.

The most innovative approach to reflector design was originated by W. Toulis, who investigated the acoustic properties of air-filled thin-walled metal tubes of elliptical cross-section, as obtained by squashing. Open frameworks of such squashed tubes are the acoustical analog to the open wire nets used as radar reflectors. A large-scale installation built according to Toulis' design principles by North American Rockwell for a fixed-bottom installation is shown in Figure 13. It is being used by the University of Miami for measurements of phase stability across the Gulf Stream at frequencies near 500 Hz.

Compliant-tube structures of this kind have been used in several applications requiring low ρc, such as reflectors and acoustic Lunenburg lenses, and as filling material for pressure release cavities. One such application is in the 400-Hz line array shown in Figure 14. Each element is a barrel-staved arrangement of ceramic bender bars, to be described later, with a

compliant tube core within the barrel for pressure relief. The use of compliant tubes for pressure relief is limited to about 2000-foot water depth, because of the intrinsic relationship between collapse strength, and the compliance of tubes of elliptical cross-section.

The large-scale propagation experiments of Project Artemis and LORAD have demonstrated the advantages of deep acoustic installations that would be either bottom-mounted or suspended from suitable support structures. This did generate a good deal of motivation toward solving or circumventing the pressure release requirement with which all unidirectional piston radiators are faced. While good acoustic coupling to the medium must be provided at the piston's front face, a high degree of decoupling from the medium, the mounting structure, or housing, is desired at the back end of the piston and all its moving parts.

Table III lists common pressure-release materials that provide suitable solutions for such decoupling: corprene, stacks of onionskin paper, and, more recently, syntactic foams—all substances of some type of cellular structure with low characteristic acoustic impedance. Most of these, with the exception of the last two on the table, progressively lose their dynamic compliance under prolonged exposure to high hydrostatic pressure.

One way around this difficulty presents itself, particularly at low frequencies, through the use of free-flooded cavities, as embodied in magnetostrictive scrolls and ceramic rings. The art of magnetostrictive scroll—arrays was perfected during the late fifties and early sixties by Leon Camp at Bendix. Figure 15 shows a set of such rings, without windings, built of annealed 0.01 inch-thick nickel 204 alloy strip, wound into scrolls four inches thick and consolidated with an epoxy adhesive. The power capacity of this particular array is 100 kW, radiated omnidirectionally in the horizontal plane, which corresponds to about 52 watts per pound of nickel.

The operating frequency of such structures is obtained simply by dividing the sound velocity of the flooding medium by the mean ring diameter, which gives 1.5 kHz for a three-foot-diameter ring.

For linear operation, magnetostrictive devices require a biasing field or a direct current, which is one of the disadvantages that must be traded off against the obvious advantages of ruggedness, low-impedance characteristics, and little need for encapsulation. On the other hand, ceramic rings are lighter than the scroll assemblies shown, and they do not require an external d-c bias, having been permanently polarized during manufacture. Initially, such rings were centrifugally cast in one piece, radially polarized, and driven in the k_{31} mode from longitudinally affixed striped electrodes. Many failures in the field led to the requirement for increasing both the mechanical strength and electroacoustic performance of ceramic ring transducers. Shown in Figure 16 is greatly improved design for the *BRASS III* transducer, developed and fabricated by the General Electric Company for the Underwater Sound Laboratory in New London.

The segmented construction allows use of k_{33} coupling, which is 20 percent higher than k_{31}, and the fiber glass wrapping provides a mechanical bias that protects the ceramic

against fractures at the peak amplitudes resulting from driving fields of 6 to 8 volts per millisecond.

During the past decade, a considerable amount of new technology (tangential drive, low loss material, mechanical bias) has been applied to deep-operating sources such as these, which generate at source levels in the 120 to 130 dB range, at frequencies between 0.5 to 5 kHz.

Whereas magnetostrictive transducers of the large ring or scroll type shown here have a definite place in the low-frequency deep-immersion area of application, they have lost the race to the ferroelectric, permanently-polarized ceramics for all those applications where single-ended piston radiators are appropriate.

Most multi-element sonar arrays, such as the cylindrical and spherical configurations shown earlier, use the longitudinal-vibrator-type element composed of a radiating front end of light weight and a heavy back mass, with a spring composed of active ceramic rings or discs in the middle, as shown in Figure 17. Twenty years ago, the active spring of this so-called tonpilz transducer design consisted of stacks of Rochelle salt, ADP, or nickel laminations. To date, these designs have been replaced by ceramic structures that are cheaper to fabricate and assemble and provide higher electromechanical coupling, acoustic bandwidth, and power-handling capability.

This transition from nearly perfect crystals to artificially compounded ceramics has not been without problems. A good deal of new ceramic technology from the mixing of the powders to the baking, electroding, and polarizing of the piece parts had to be developed, together with suitable quality control procedures and test instrumentation. But, ceramics continued to exhibit one serious shortcoming: namely, their inability to support much tensile stress, which led to fracture at power levels that were mandatory for active sonar applications. If the vibrations could be maintained under a mechanical bias, as in precompression of the ceramic stack, high power loads could be sustained without the stress cycle ever becoming tensile.

Simple as this sounds, it took an invention to enable us to visualize the right solution and to put it into practice: the inventor was Harry Miller—then at Clevite, now at USL— and the time of the invention was 1954. He applied his invention in the form of a tie rod through the center of the longitudinal vibrator assembly, as shown in Figure 18.

The central stress rod acts as a spring that is soft compared with the ceramic stack itself, but which still provides a large d-c force. The relative softness of the spring preserves both coupling coefficient and bandwidth of the transducers, whether in the form of the tie rod for stacks, or of fiber glass wrapping for rings. The latter technique was introduced into transducer design several years later. Today, the use of mechanical bias is universal in acoustic power generation in the range from 100 Hz to 100 kHz.

In order to be able to better predict both element and array performance, new equivalent circuits and distributed parameter math models were developed that take account

of structural details—such as tie rods, cement joints, and mounting losses—–that were neglected by the earlier lumped mass-spring approaches. In this area, much groundwork was laid by the U. S. Navy's transducer laboratories, both in San Diego and in New London. Here, Ed Carson and Gordon Martin improved the predictability of longitudinal vibrator design, and Ralph Woollett further clarified the role of the electromechanical coupling coefficient as a key design parameter.

Some of the difficulties encountered by the transducer designers derived from insufficient knowledge of the material characteristics (rubber, paper, cement) or of the influence of manufacturing tolerances on array performance, and from the inability to measure certain acoustic parameters with sufficient accuracy. The complexity of manufacturing tolerance analysis for multi-element arrays is depicted in schematic form in Figure 19. In spite of much progress in the use of math-model predictions and production-tolerance analysis, there are still serious gaps between calculated and actual transducer-array performance. They relate to theoretical inadequacies that remain in the area of radiation loading (boundary conditions), structural coupling effects, and loss mechanisms.

Therefore, in many real situations that warrant some kind of tolerance analysis but in which one is confronted with too many independent parameters, the only practical way is to set up production on a go/no-go basis. Subsequent evaluation of the over-all system performance in a well-instrumented underwater test environment is still the best way to determine whether the system will fly. This brings to mind another statement from the 1950 NRC report: "It should be emphasized that our ability to approach theoretical limits of performance is based on considerable empiricism, and several false starts may be necessary."

Although this advice has not always been heeded during the recent era of paper cost-effectiveness studies, test instrumentation has progressed tremendously in recent years. The needs of the sonar engineer have been reinforced by a surge in audio-engineering and testing technology, and by the exacting measurement techniques developed for noise control. As a result, much automated recording and data-reduction capability and improved displays are now available to the developers and manufacturers of sonar transducer test instrumentation. Figure 20 summarizes some of the more significant advances in acoustic calibration equipments and test ranges made during the past two decades. The use of optical holography in analyzing the complex vibrational patterns of radiators is demonstrated in Figure 21, where the pattern change caused by 10 percent detuning is shown for the same piston.

With the availability of excellent test facilities, both at land-locked test sites and at the various open-sea test ranges, a certain amount of empiricism in transducer design will continue to be beneficial to innovation in this area. In fact, the math-modeling way of life that has become *de rigueur* with some Navy laboratories has been considered a bit of a deterrent by imaginative acousticians who try to introduce unorthodox approaches to transduction. Likewise, to some potential users the inability to fit a new mechanism with high performance claims into available modeling software schemes has also been a deterrent.

Figure 22 lists some unusual transduction techniques, most of which have had initial rough going in winning acceptance. They have been classified into two types. The first takes advantage of special modes of vibration of structures suitable for modular array configuration; the other class uses some form of fluid dynamic or hydromechanical energy conversion. Because of the direct coupling of hydraulically, chemically, or electrically-stored energy to the fluid medium (rather than through a special transducer material), the controlled release of such energy at megawatt levels has seen much refinement in the past two decades. Also included in this listing are such explosive sources as shaped charges and electric sparks, which have found considerable application in seismic profiling.

The scope of this paper does not permit a detailed discussion of all mechanizations of the concepts shown in Figure 22, but a few examples will be cited from each category:

Structural Modes

Whereas in the mass-spring resonators discussed before, the radiating member is designed to be as stiff as possible, it can be of advantage—particularly at low frequencies—to couple the mechanical spring directly to the medium. This will save considerable weight while retaining adequate radiation characteristics, as in the simple tuning fork. One successful use of structural resonance for low-frequency sound generation is the Honeywell bender bar transducer shown in Figure 23. Flexing-bar resonators may be clamped or hinged at either end of the bar. Hinged bars are used in pairs for dynamic balance, allowing for lighter weight and better radiation loading.

These bars are made of two layers of ceramic, each layer being composed of many individually electroded segments. Bar lengths from 10 cm to 1 m have been used. Precompression rods are used to keep the composite ceramic assembly from tensile fracture at high vibration amplitudes. The central volume of the barrel-staved multibar transducer, shown earlier in Figure 14, is filled with compliant tubes for pressure relief.

Another flexural transducer, derived by W. J. Toulis from his work with compliant tubes, has found application in the type of underwater projector which was depicted in Figure 13. It consists of an outer shell, formed from circular or elliptical arches of aluminum or steel excited into flexural resonance by a central ceramic stack similar to those used in conventional longitudinal vibrators. Again, as in the bender bar, the mass of the vibrating system is distributed, rather than lumped, and is contained in the unavoidable mass of the spring structure. This of course increases the power-to-weight ratio of these types of transducers. In the flextensional design by North American Rockwell, shown in Figure 24, the shell serves as housing for protection and isolation of the high voltages applied to the ceramic stack.

In addition to first-order bar modes and shell modes, there is the possibility of using higher order ring modes for compact line transducers. These are capable of some directionality in reception or transmission: by proper phasing of multi-electroded ring sections, cardioid beam patterns may be formed in four quadrants. A multimode transducer of the type originated by S. Ehrlich of Raytheon is shown in Figure 25.

Fluidic Drive

Underwater whistles, jets, and water-hammer devices have long been items of study and speculation. Systematic efforts to harness the energy available in hydraulic accumulators by controlled conversion into modulated fluid flow have finally resulted in some transducer types that are both practical and reliable. Figure 26 shows a hydroacoustic valve amplifier developed by John Bouyoucos. A conventional ceramic vibrator is used to excite oscillations of a mechanical valve spool that is coupled to it by a liquid spring. High-pressure hydraulic flow is switched by the spool valve to force a flexural disc radiator into high amplitude oscillations. The coupling of the three resonator systems is such that adequate energy transfer and phase continuity are provided over a relative bandwidth of 20 percent. A hydroacoustic, two-piston source built by General Dynamics according to these principles is shown in Figure 27.

Modules of this type may be stacked up to form line or planar arrays for greater directionality. In such systems, energy storage is provided by pneumatic accumulators that are trickle-charged from low-power pumps capable of deep submersion (Figure 28). Although only prototype installations are in existence today, it appears that the more conventional transduction devices will see some competition from both structural-mode transducers and hydroacoustic sources as these new mechanisms become sufficiently well understood during the next decade.

Having thus reviewed some of the progress made and difficulties encountered in underwater sound transmission and reception since 1950, one should conclude with a prognosis of things that might be ahead. With less research and development spending, and a more pragmatic approach to life, these changes will most likely be more in the nature of gradual improvements in theory, in materials, and in efficiency. The greatest impact on underwater sound reception and generation will result from the full adaptation of digital technology into the processing and interpretation of acoustic signals, of ever-increasing bandwidth, with full use of all the potential inherent in modern computers. Thus, software will assume its place alongside hardware, and standardization and interchangeability of equipment will come about.

The variability of sonar propagation conditions in the ocean will ultimately set the limits on the acoustic detection performance that can be achieved. Systematic propagation research slanted toward specific surveillance-system needs will continue to be worthwhile. Particularly long-term observations over fixed propagation paths in extreme ocean environments will have to be undertaken, leading to new challenges in transducer design and signal processing.

TABLE I. BARIUM TITANATE CERAMICS

% $BaTiO_3$	ADDITIVES	% ADD.	FIRST USED	DIELECTRIC CONSTANT	PLANAR COUPLING	LOSS TANGENT 2 KV/CM	CHARACTERISTIC FEATURES
100%	NONE	0%	1946	1900	-.36	.050	HIGH DIELECTRIC, TEMPERATURE VARIATIONS, TIME VARIATIONS, DRIVE LIMITATIONS
95%	CALCIUM TITANATE	5%	1950	1200	-.33	.040	IMPROVED STABILITY
95%	CALCIUM TITANATE COBALT	5% .3%	1951	1000	-.32	.032	REDUCED LOSSES
80%	LEAD TITANATE CALCIUM TITANATE	12% 8%	1954	400	-.19	.022	FILTER APPLICATIONS
95%	CALCIUM TITANATE COBALT	5% .75%	1960	1300	-.30	.012	HIGHEST DRIVE CAPABILITIES OF ALL BARIUM TITANATES

TABLE II. LEAD-ZIRCONATE TITANATE CERAMICS

CERAMIC TYPE	FIRST USED	DIELECTRIC CONSTANT	PLANAR COUPLING	LOSS TANGENT AT 2KV/CM	CHARACTERISTIC FEATURES
PZT-4	1955	1300	-.52	.019	HIGH COUPLING, BEST FOR PROJECTOR APPLICATION, TIME VARIATIONS MORE THAN BARIUM TITANATE, SILVER ADHESION CAN BE A PROBLEM
PZT-5A	1958	1700	-.60	.114	HYDROPHONE APPLICATIONS, SENSITIVE TO PRESSURE CYCLES
PZT-5H	1958	3400	-.65	.114	HIGHEST DIELECTRIC CONSTANT AND COUPLING OF ALL TITANATES, GOOD TIME STABILITY
PZT-8	1964	1000	-.50	.006	HIGHEST DRIVE CAPABILITIES OF ALL CERAMICS, STABLE WITH TIME, TEMPERATURE, AND PRESSURE

TABLE III. PASSIVE TRANSDUCER MATERIALS

MATERIAL	USED AS DECOUPLER	USED AS REFLECTOR	MAXIMUM USEFUL DEPTH
AIR		✔	50 FEET
AIRCELL RUBBER		✔	50 FEET
CORPRENE	✔	✔	200 FEET
BELLEVILLE SPRING	✔		1200 FEET
ONIONSKIN PAPER	✔		1500 FEET
COMPLIANT TUBES		✔	2500 FEET
MIN-K 2000	✔	✔	10,000 FEET (PLUS)
SONITE	✔	✔	10,000 FEET (PLUS)

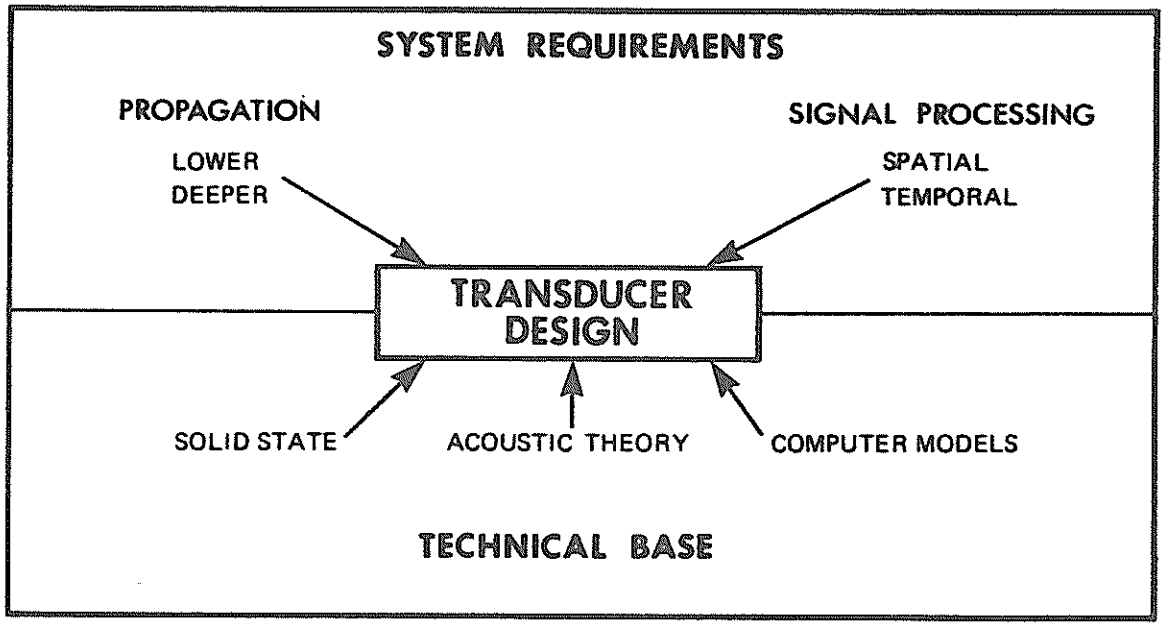

Figure 1. Causative Relationships in Transducer Design

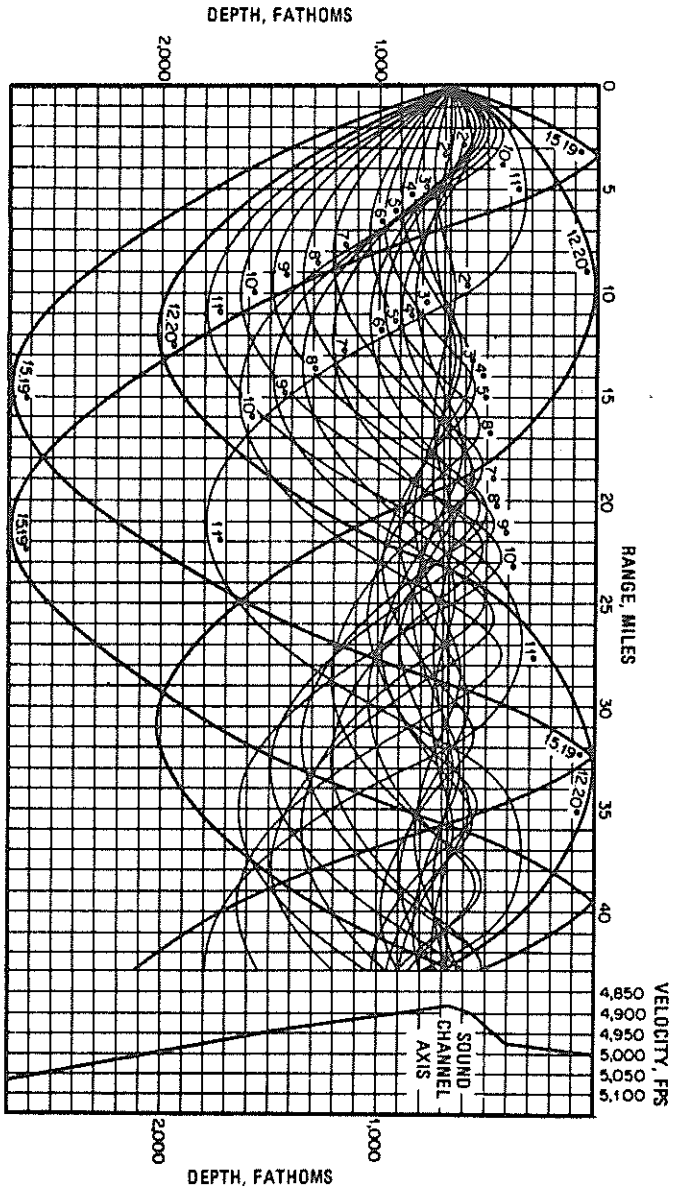

Figure 2. Deep Sound Channel Propagation [From M. Ewing & J. L. Worzel, "Long-Range Sound Transmission," *Geol. Soc. Am. Mem.* 27, 1948]

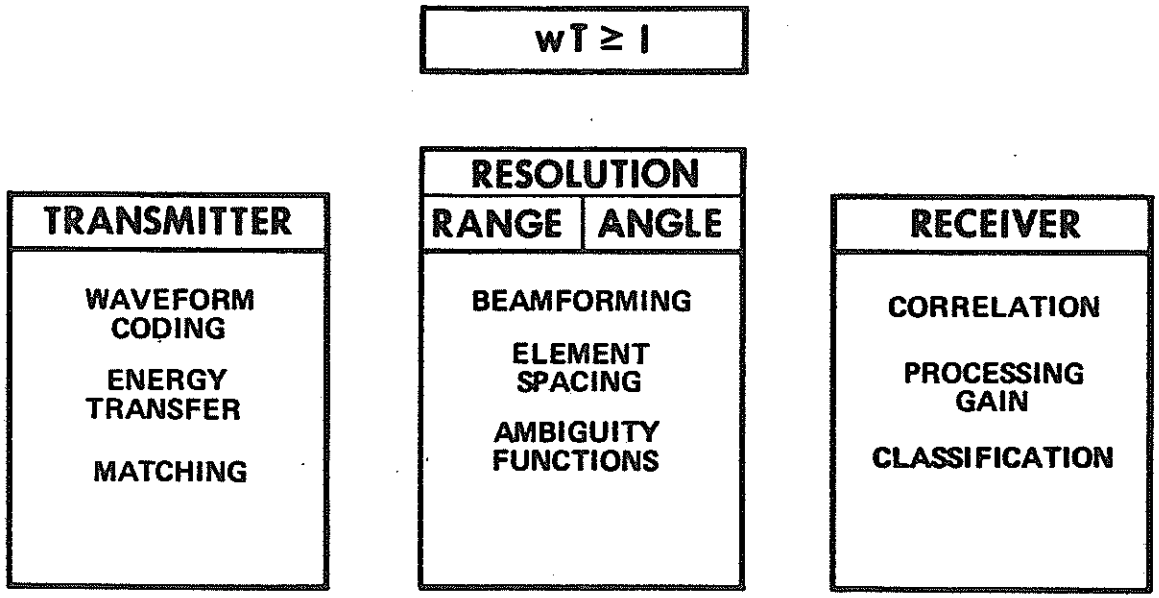

Figure 3. Design Areas Affected By the Time-Bandwidth Product Concept of Information Theory

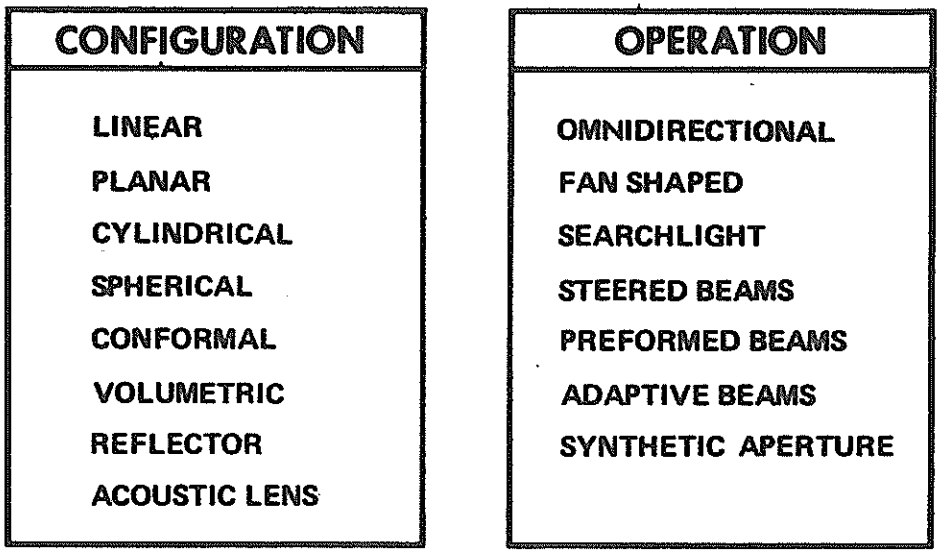

Figure 4. Underwater Acoustic Arrays

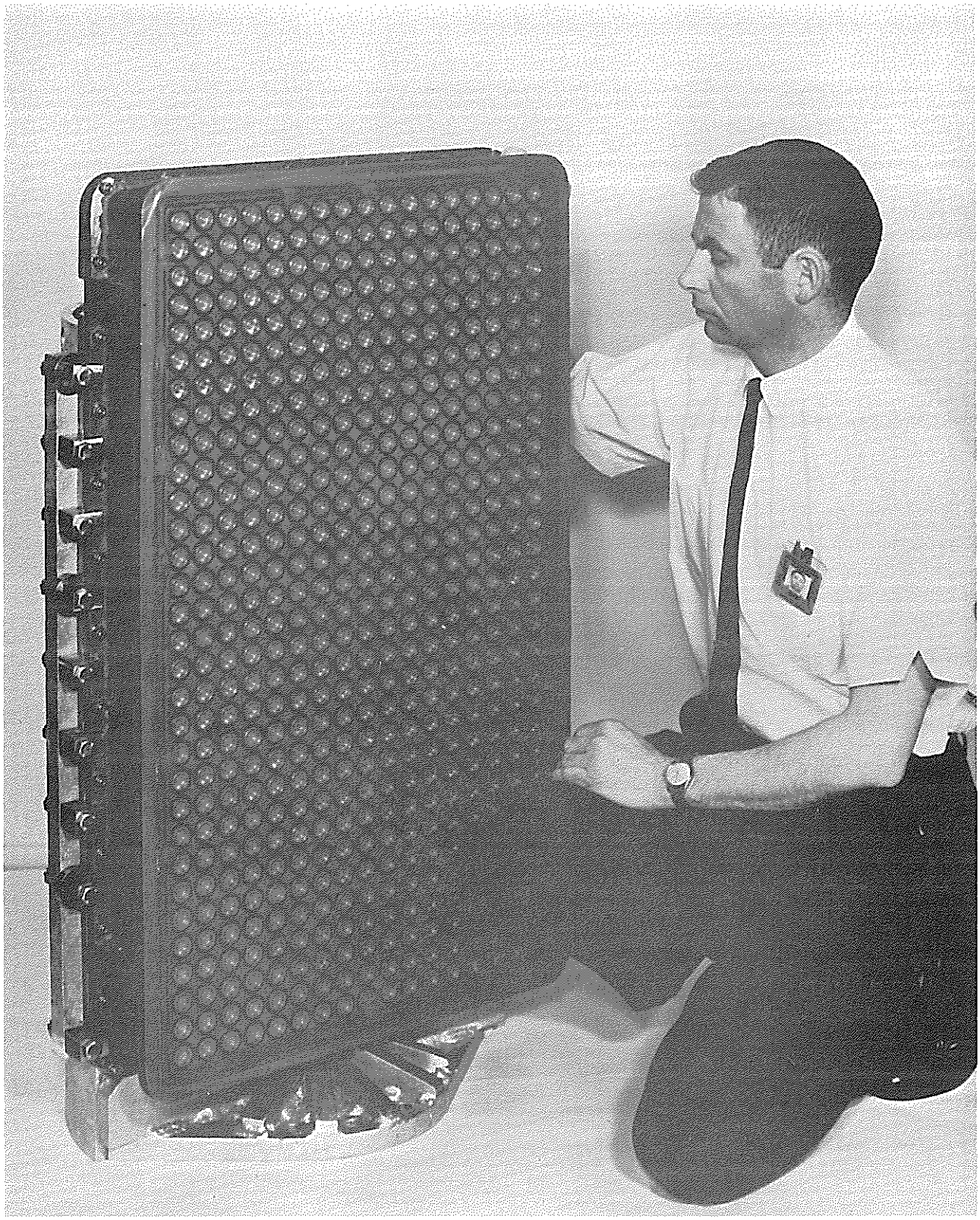

Figure 5. Dolphin Array (Honeywell)

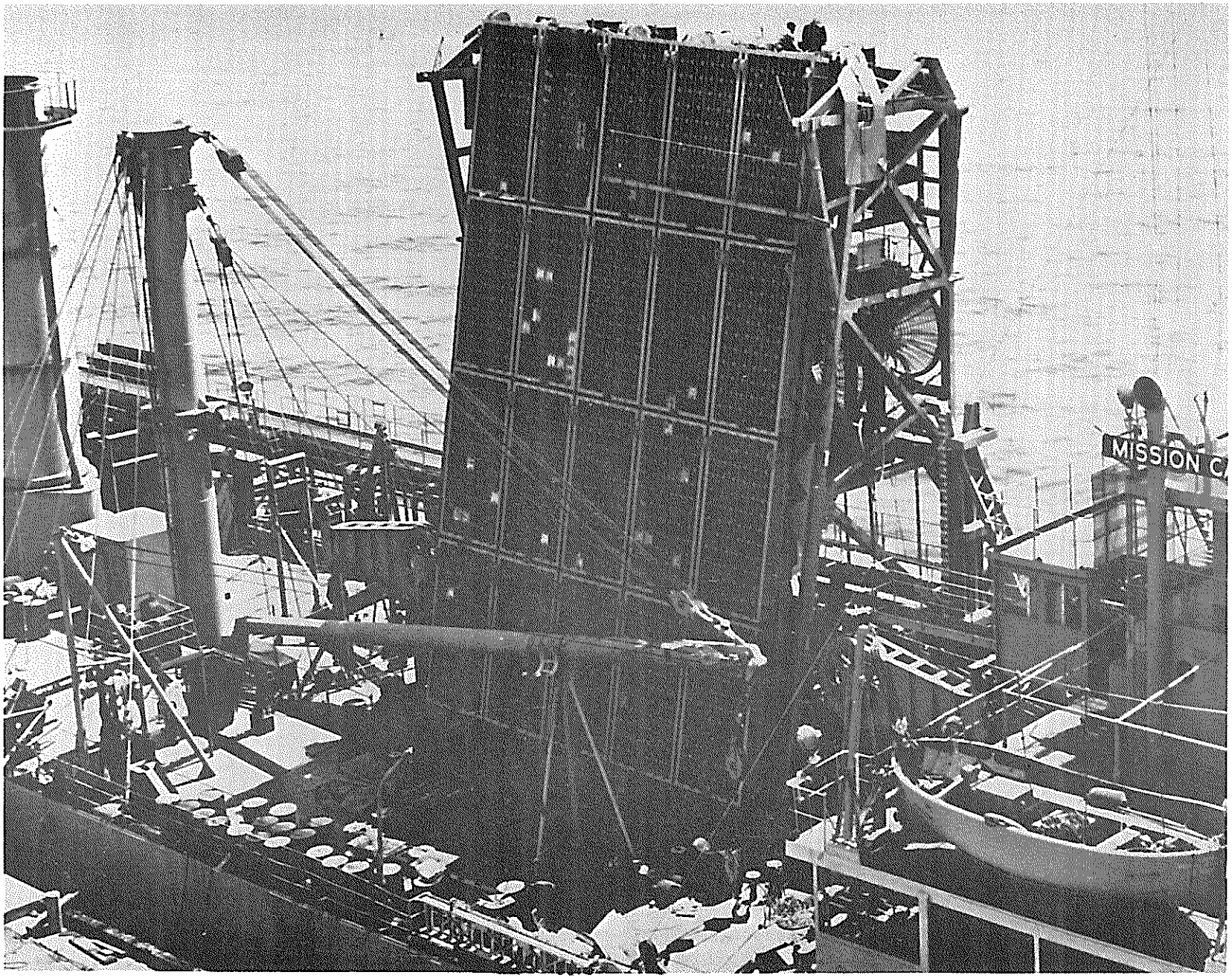

Figure 6. TR11C Array (Massa)

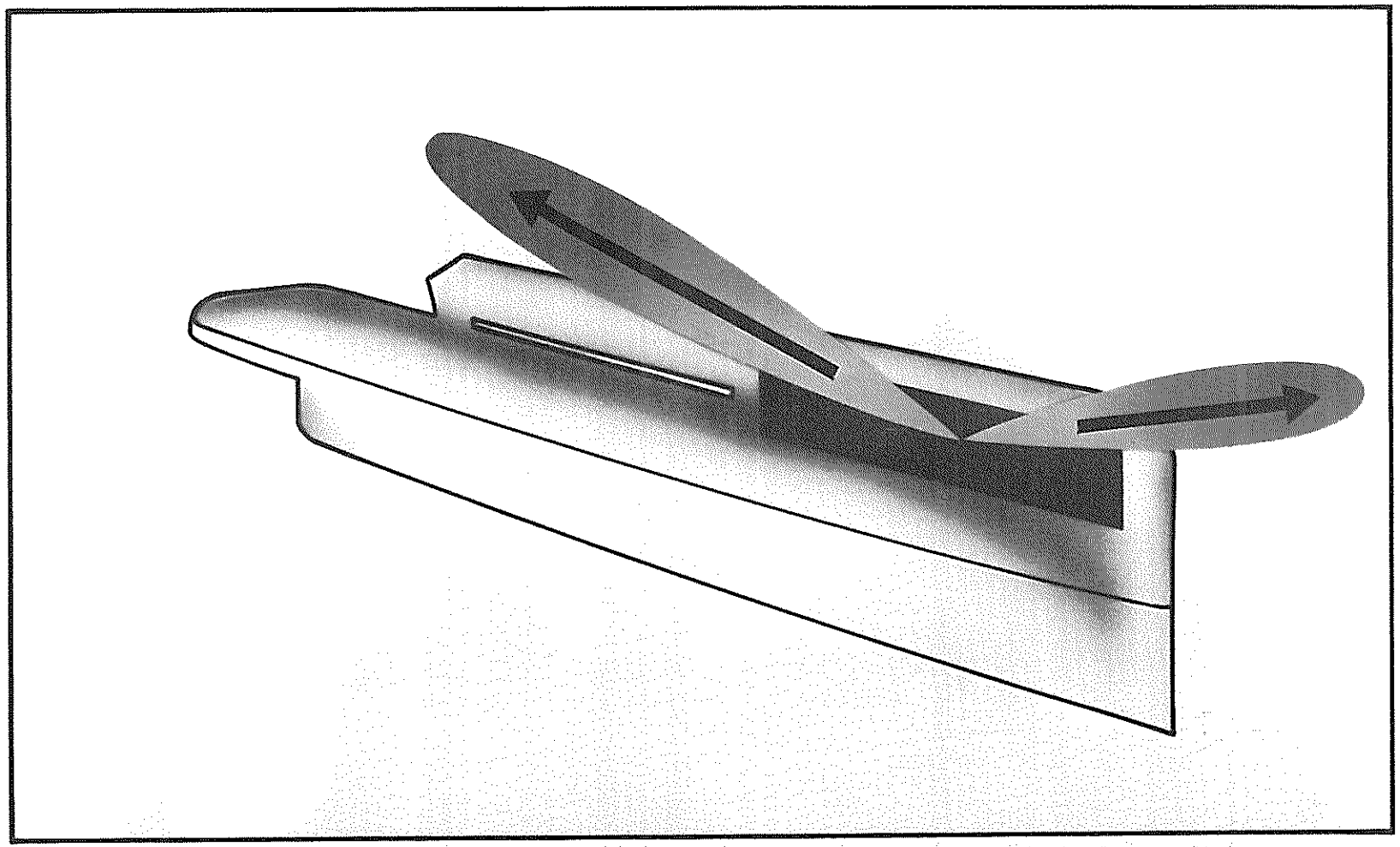

Figure 7. Planar Array Concept

Figure 8. New Generation of Destroyers Using Bow-Mounted Sonar

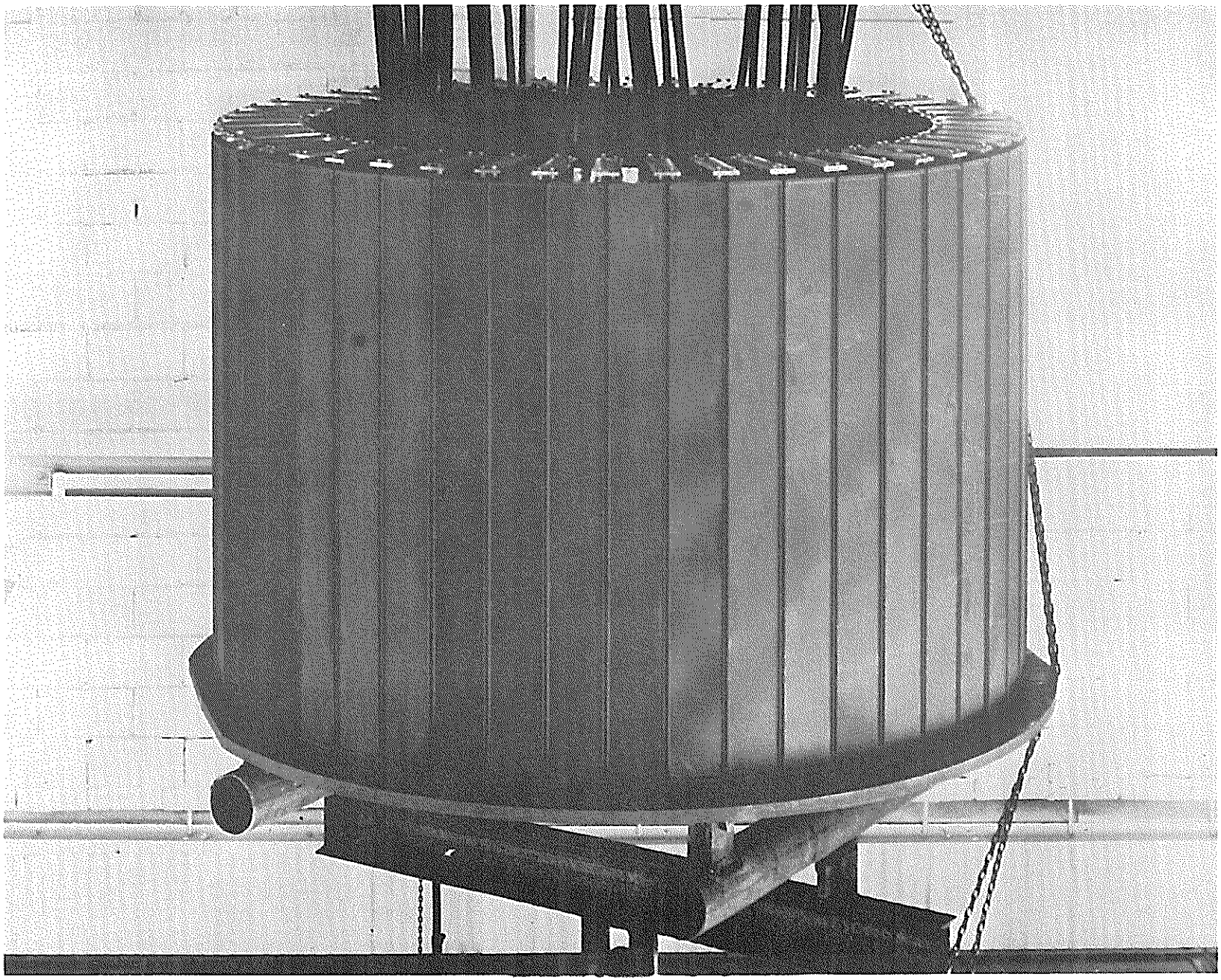

Figure 9. Cylindrical Sonar Array (Bendix)

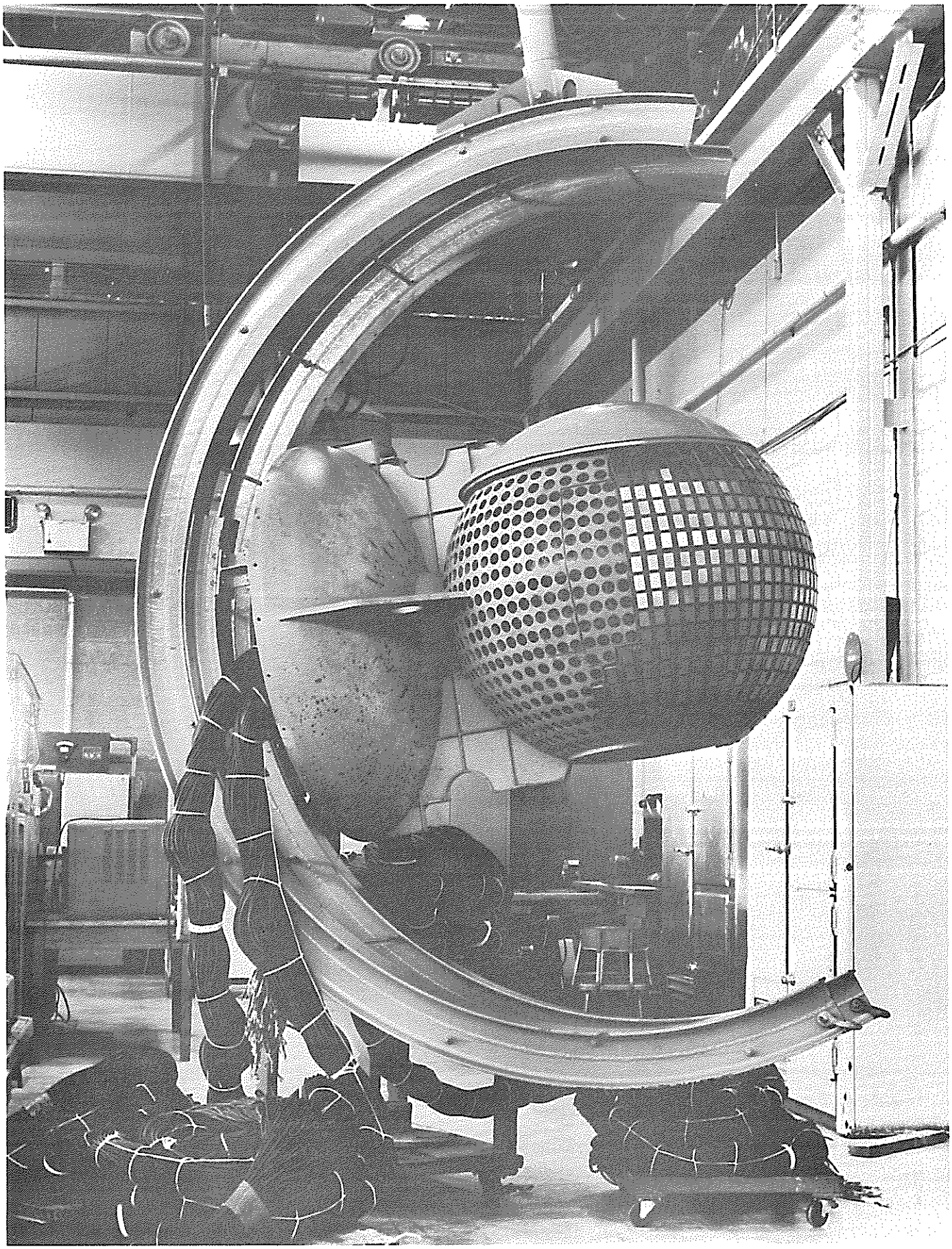

Figure 10. Spherical Array Scale Model (Raytheon)

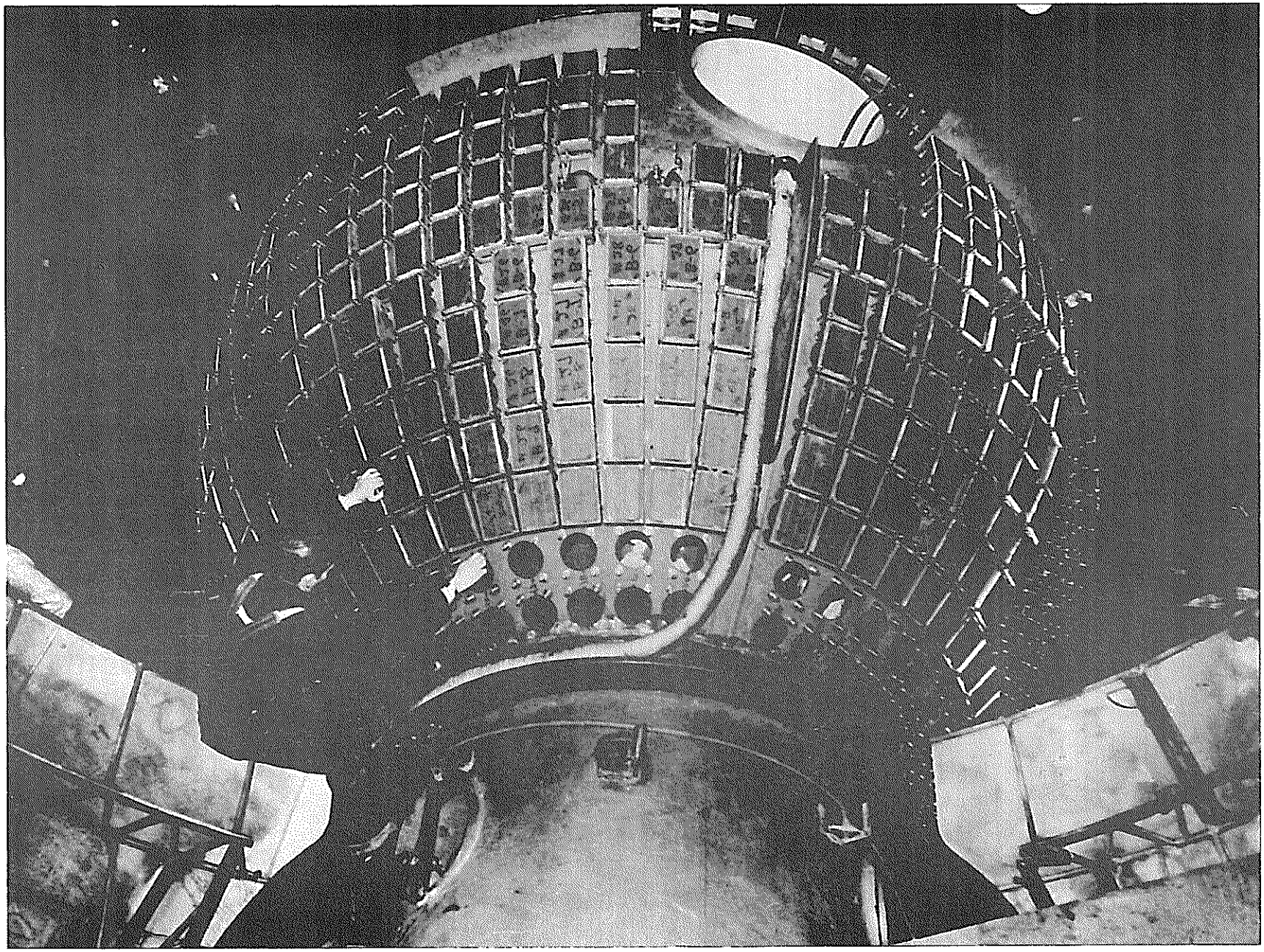

Figure 11. AN/BQS-6 Transducer Array (Raytheon)

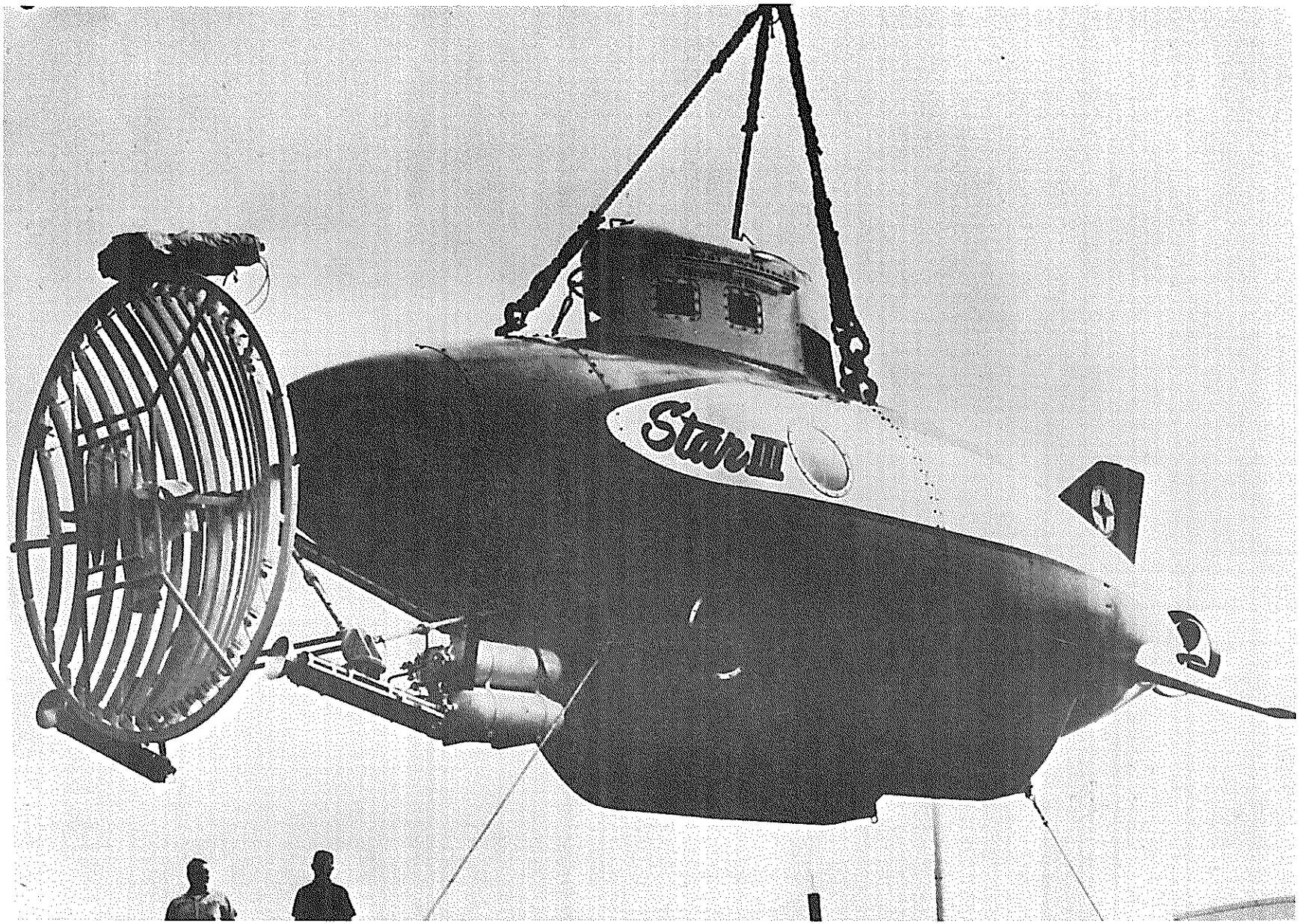

Figure 12. Star III with 400-Hz Source (North American Rockwell)

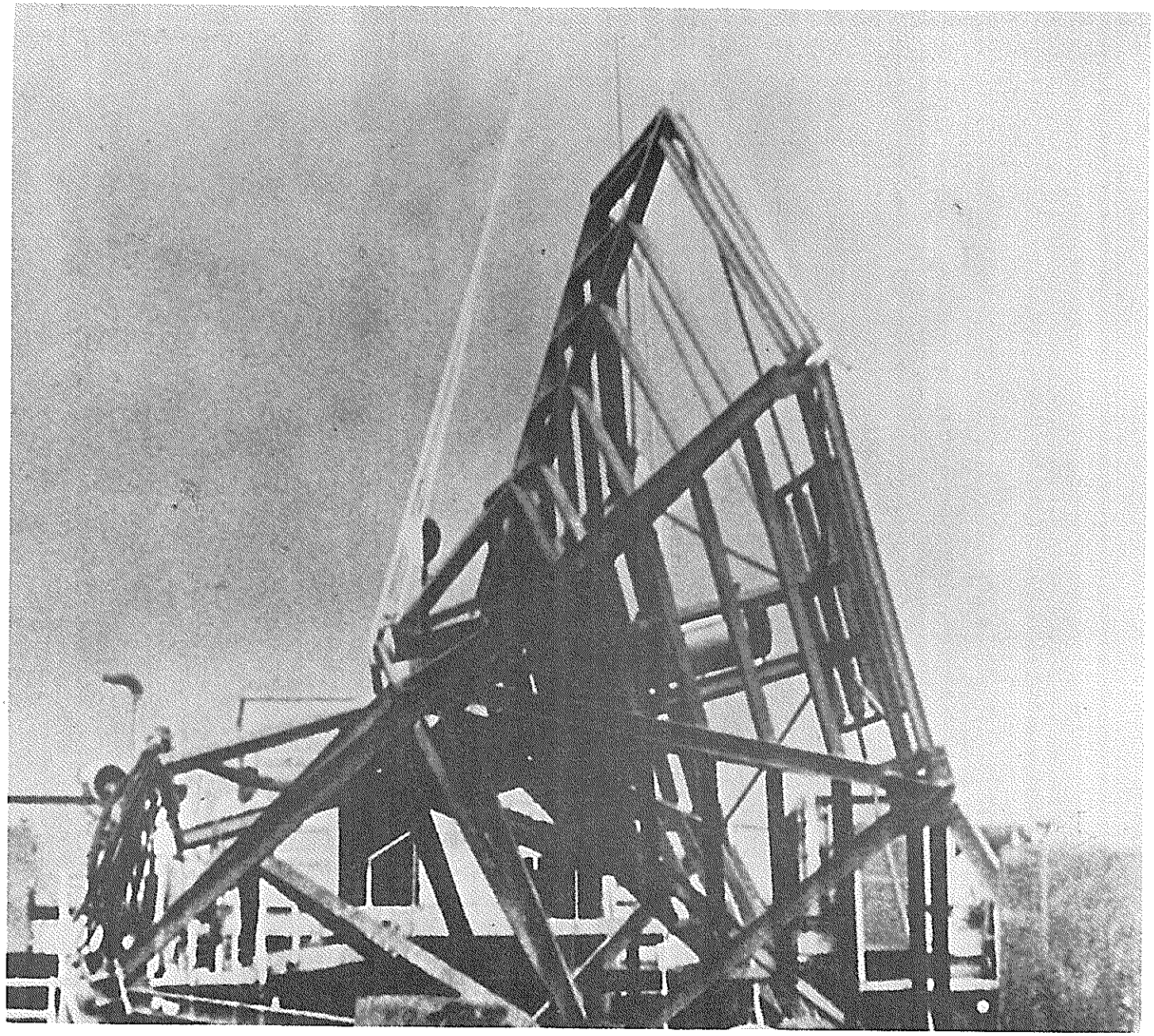

Figure 13. Parabolic Reflector Assembly (North American Rockwell)

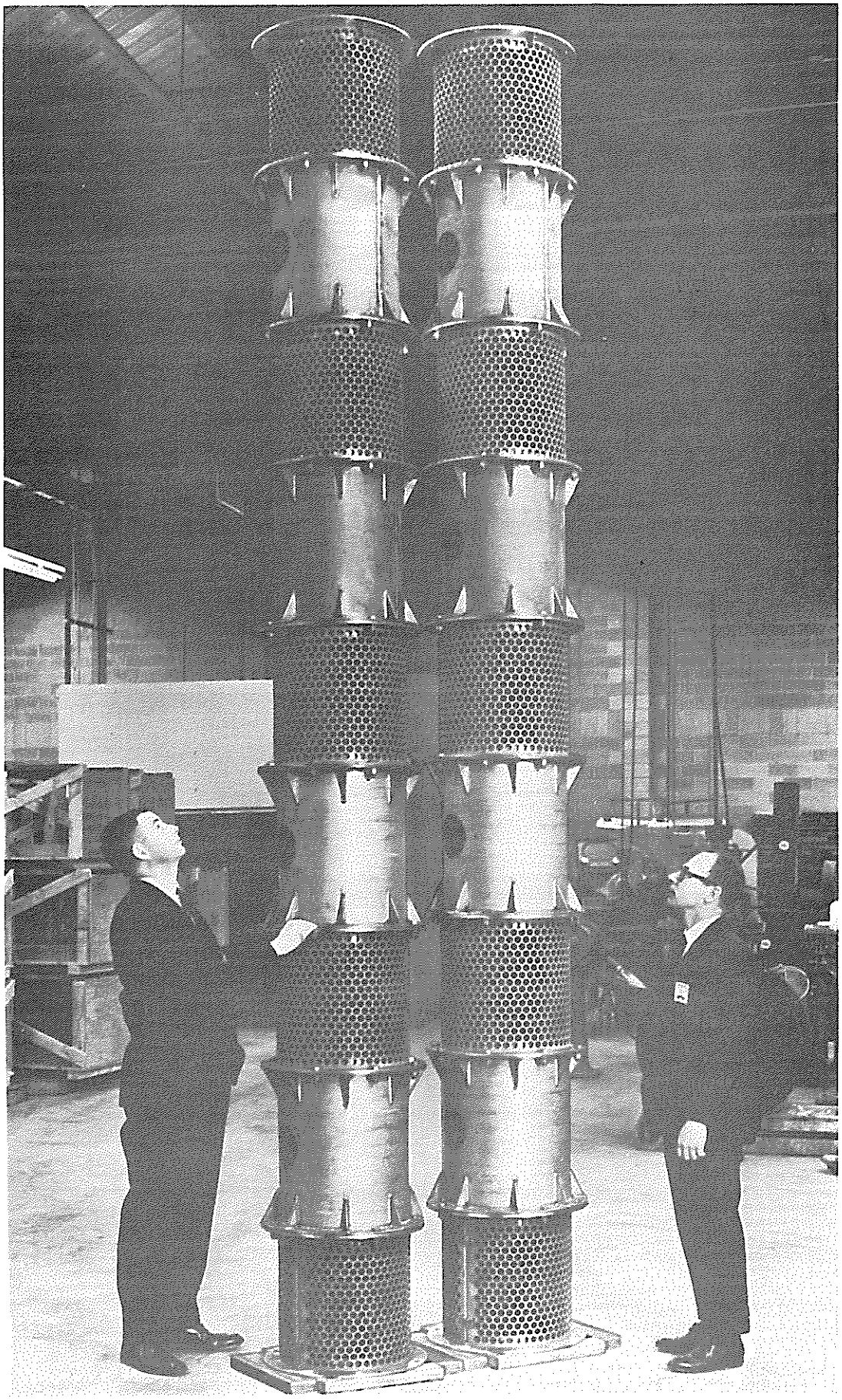

Figure 14. 400-Hz Line Array (Honeywell)

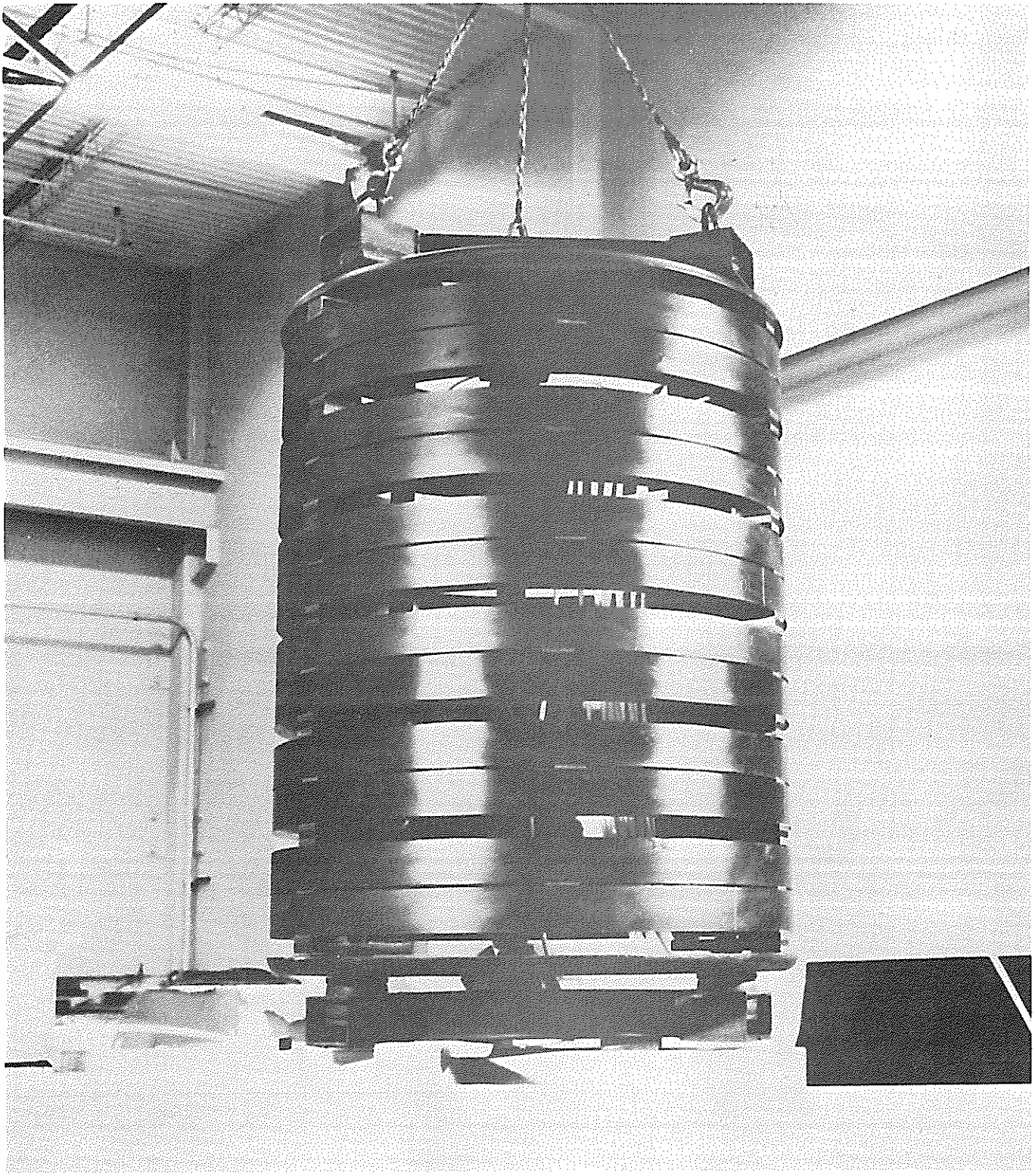

Figure 15. Scroll Assembly (Bendix)

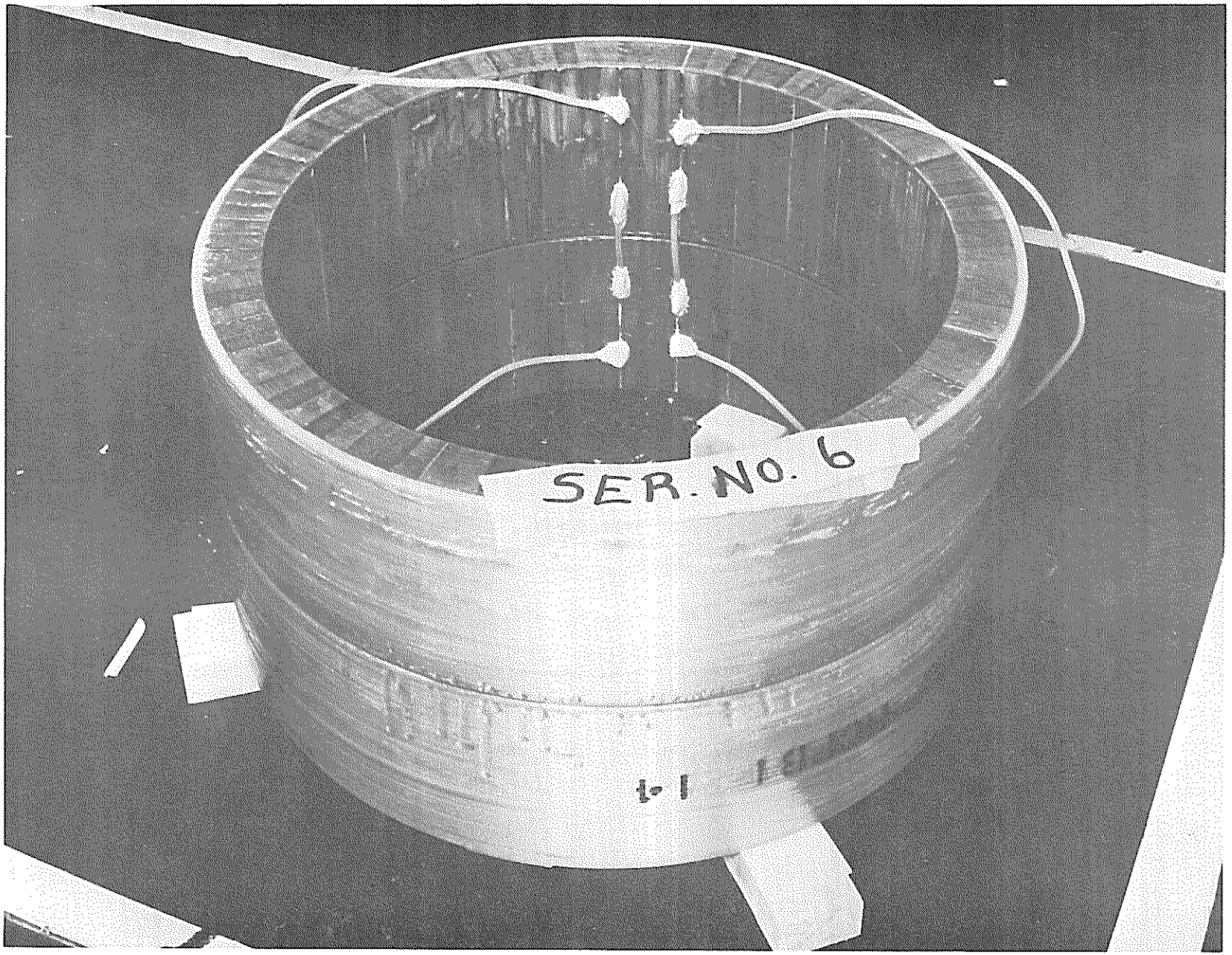

Figure 16. Brass III Ring (GE)

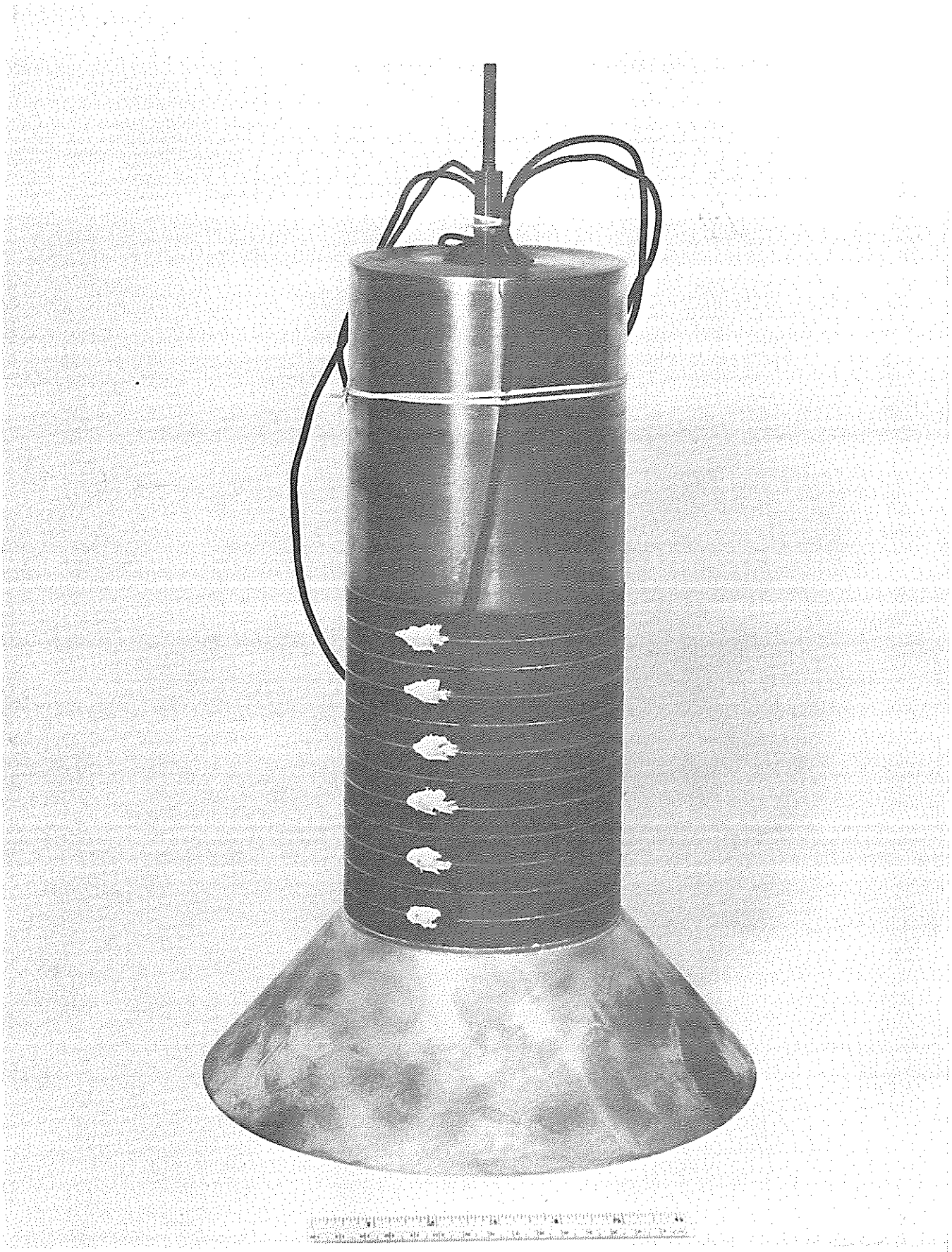

Figure 17. Ceramic Ring Stack (Honeywell)

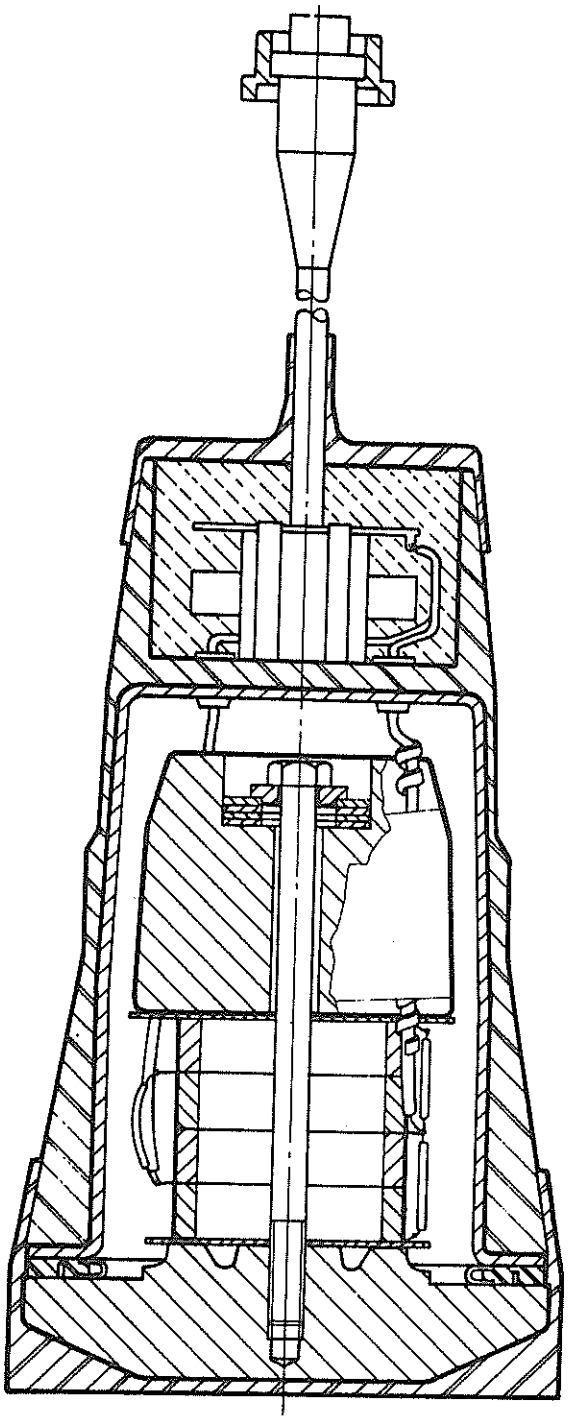

Figure 18. Longitudinal Vibrator (Massa)

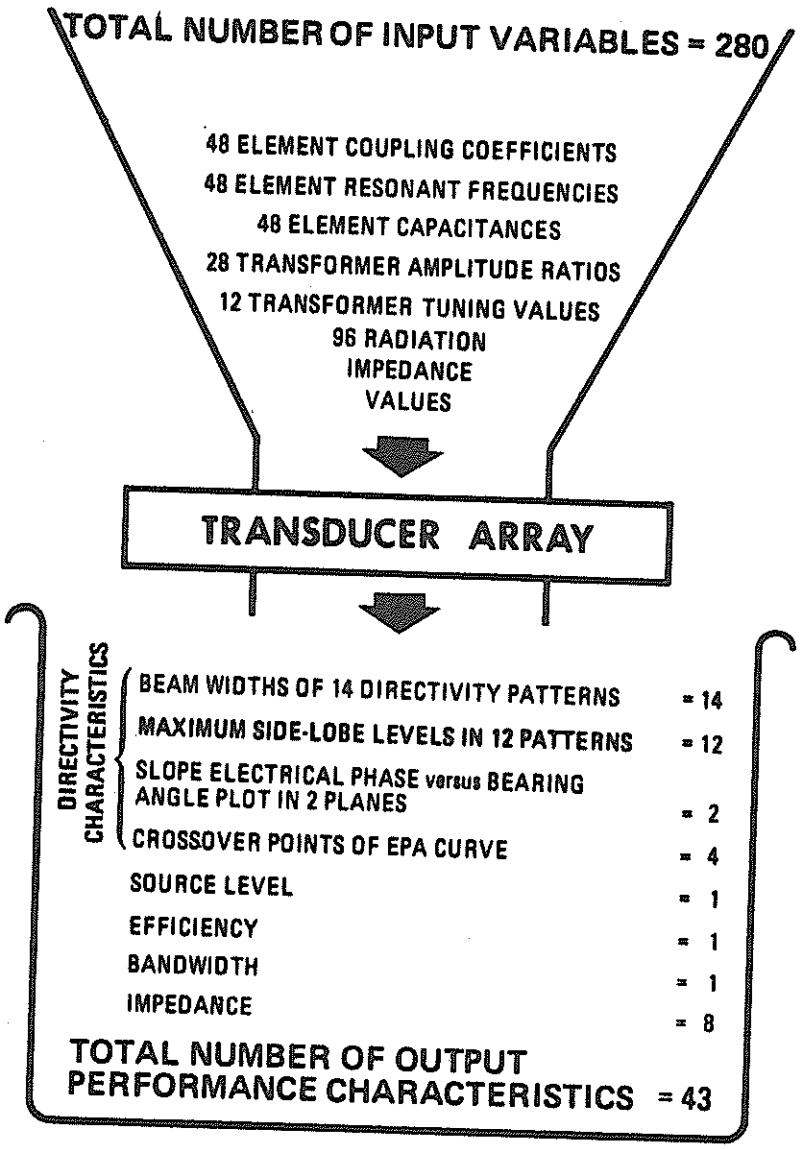

Figure 19. Complexity of Manufacturing Tolerance Analysis for Multi-Element Arrays

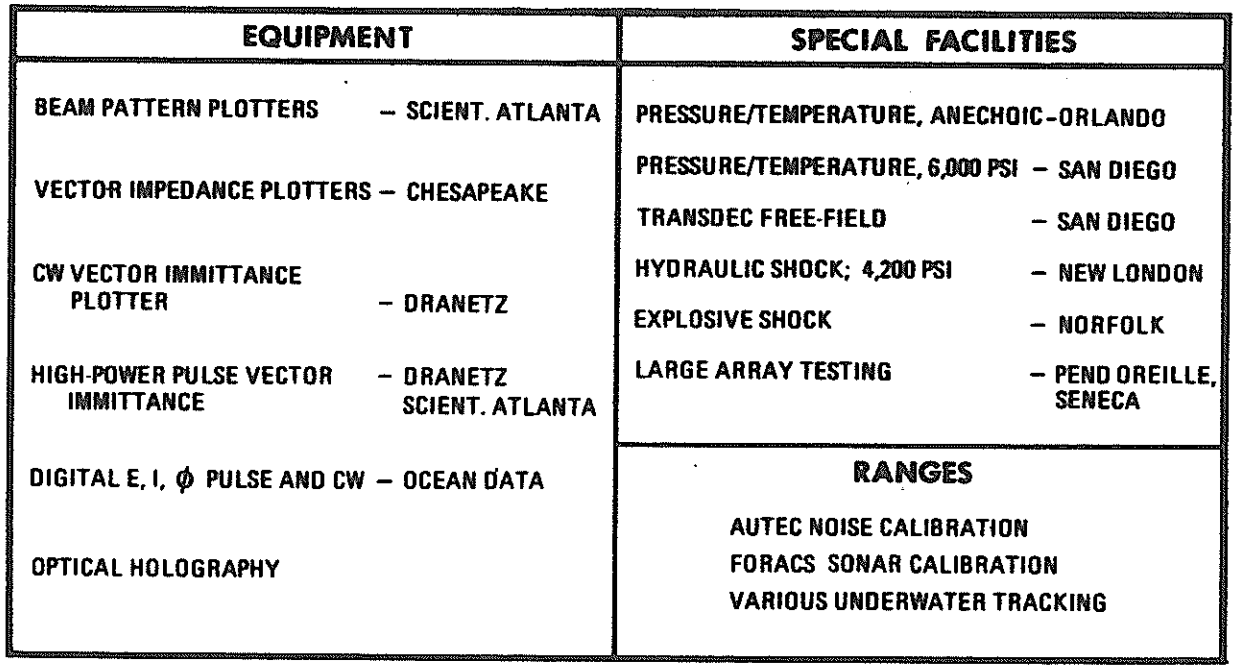

Figure 20. Advances in Acoustic Calibration

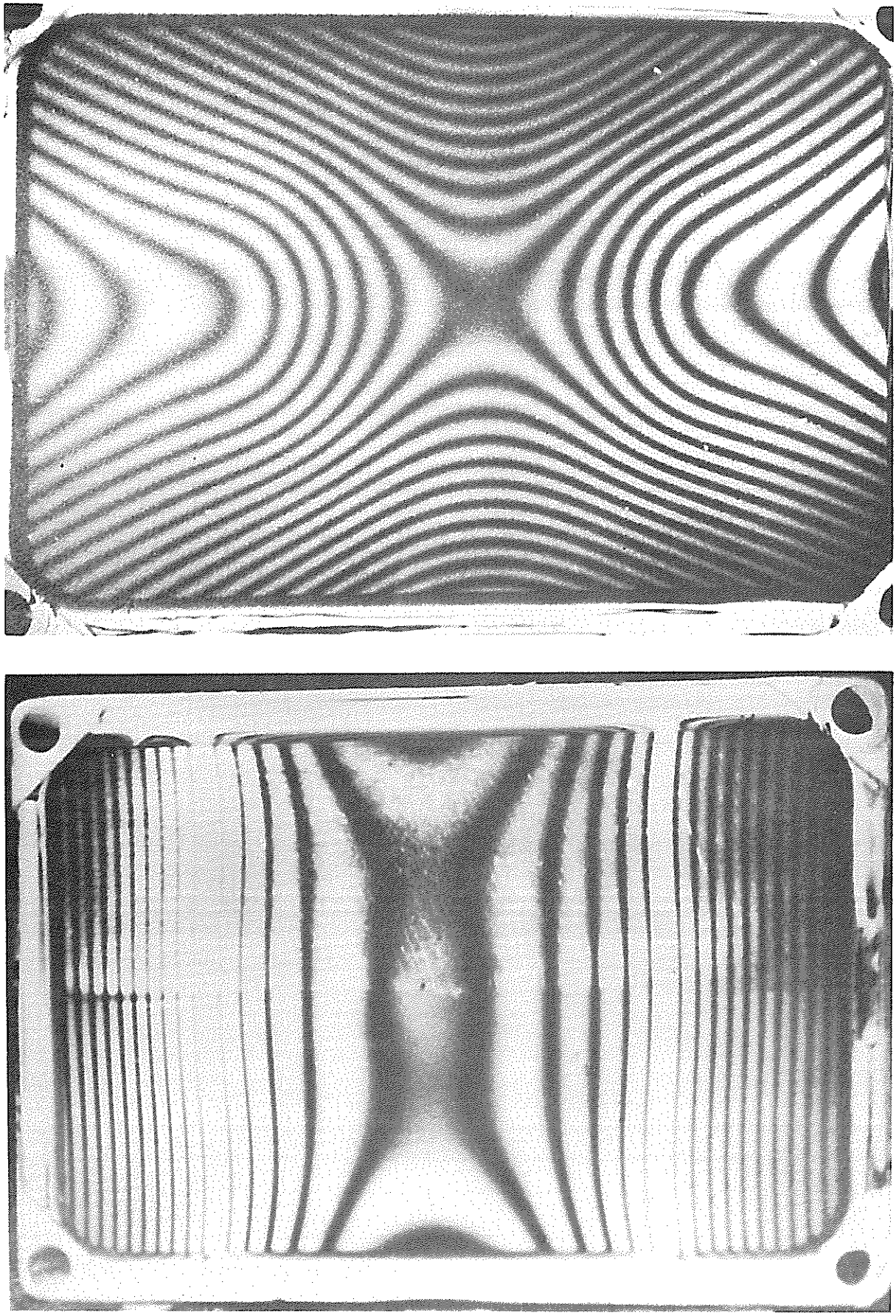

Figure 21. Holograms of Transducer Face at 10 Percent Δf (Raytheon)

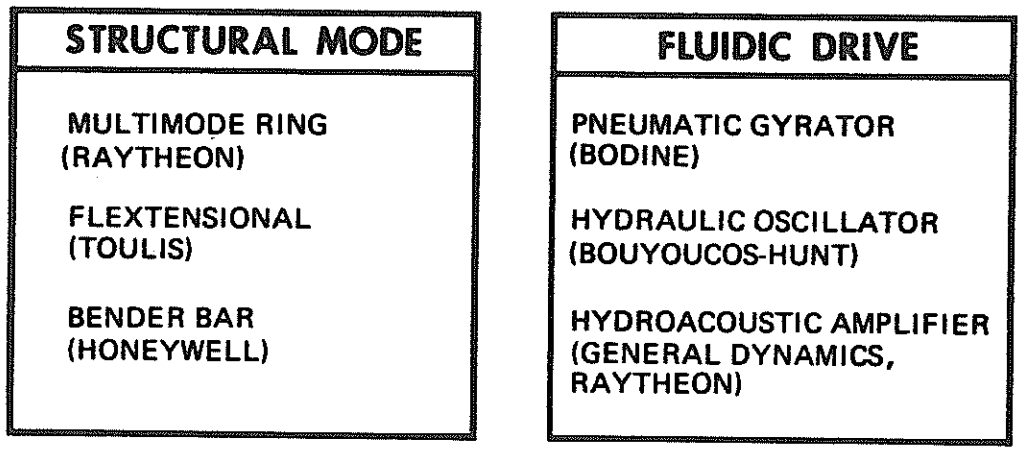

Figure 22. New Transduction Concepts

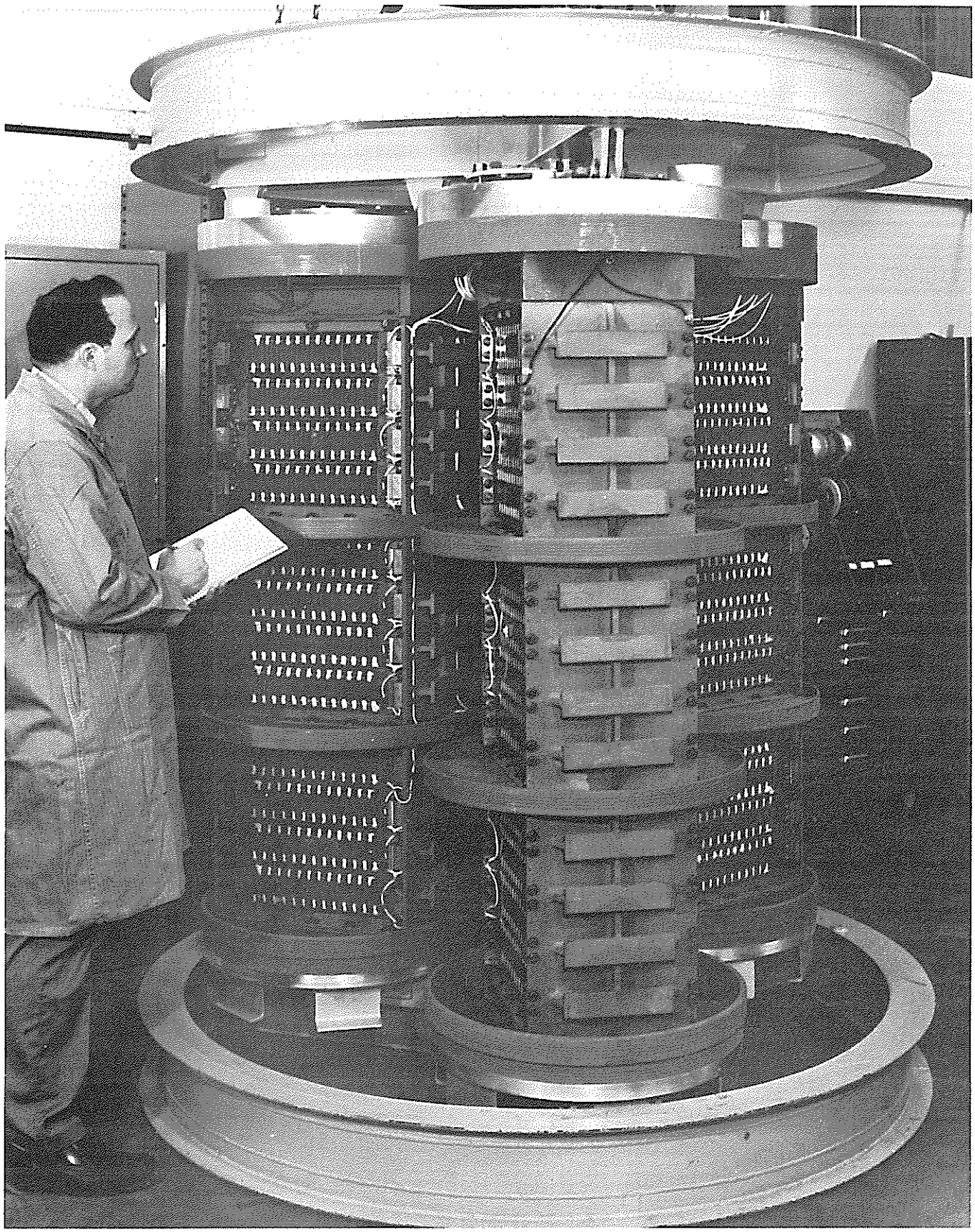

Figure 23. Bender Array (Honeywell)

Figure 24. Flex-Dimensional Element (North American Rockwell)

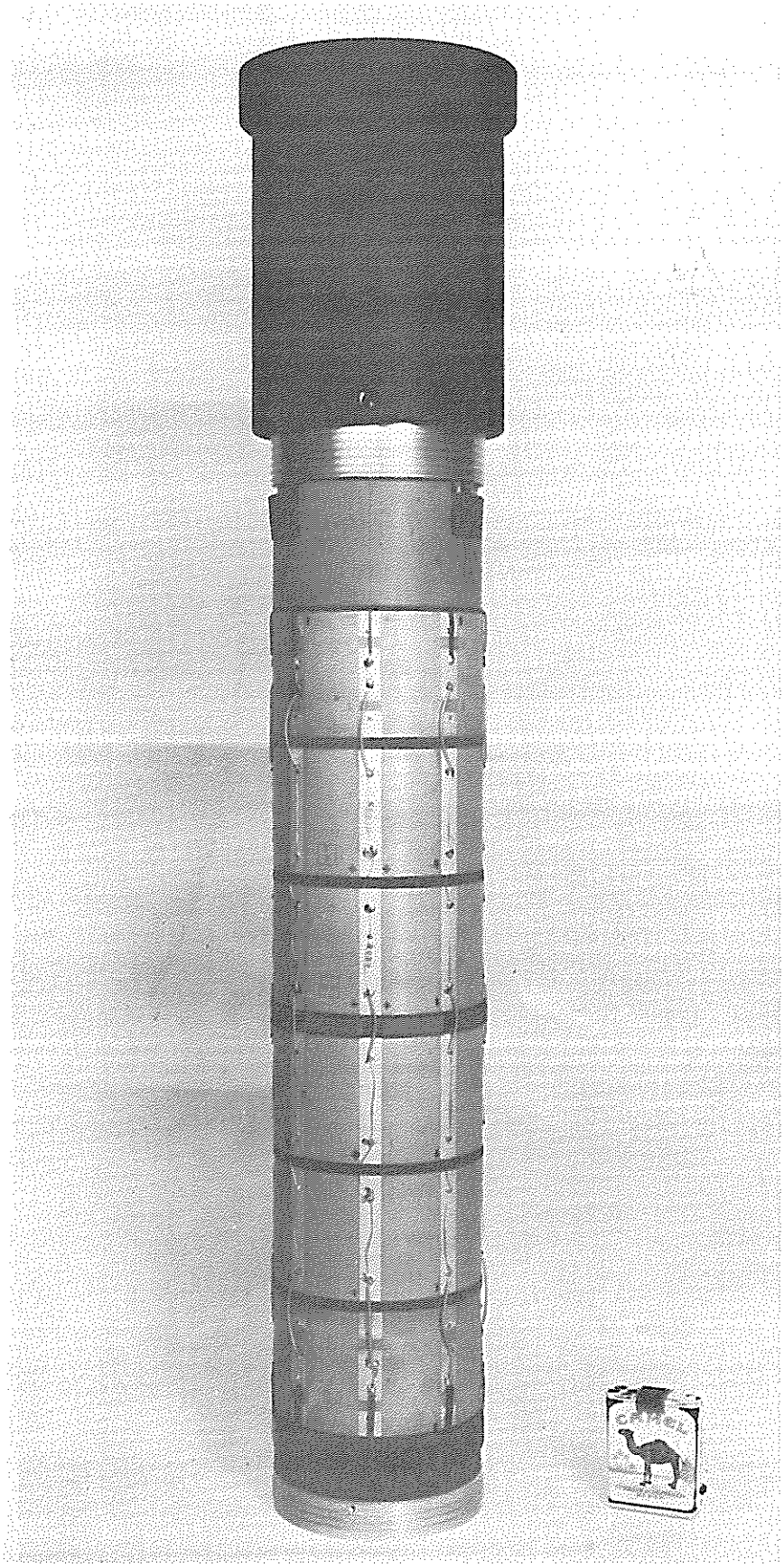

Figure 25. Multimode Transducer (Raytheon)

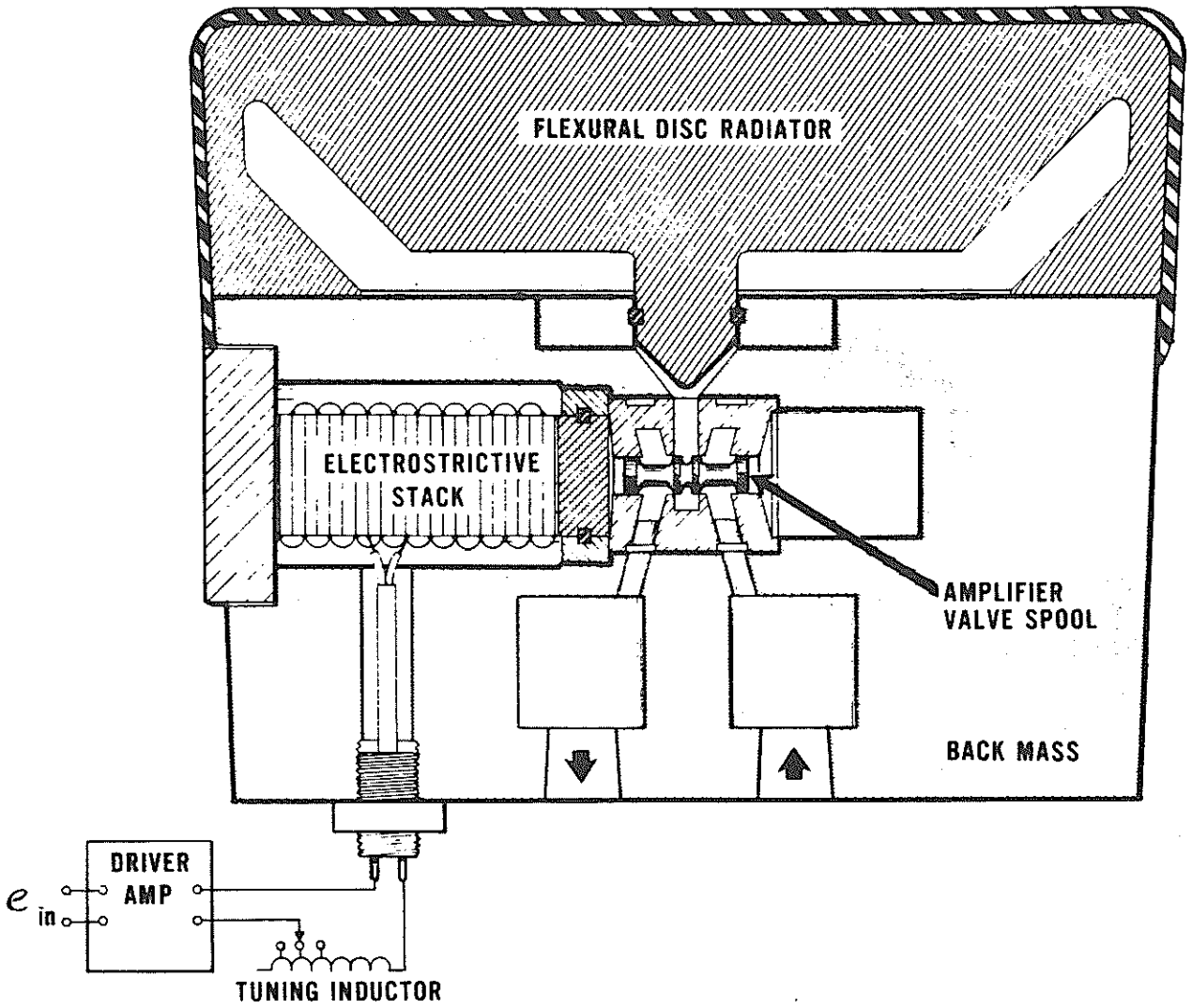

Figure 26. Amplifier/Transducer Module (General Dynamics)

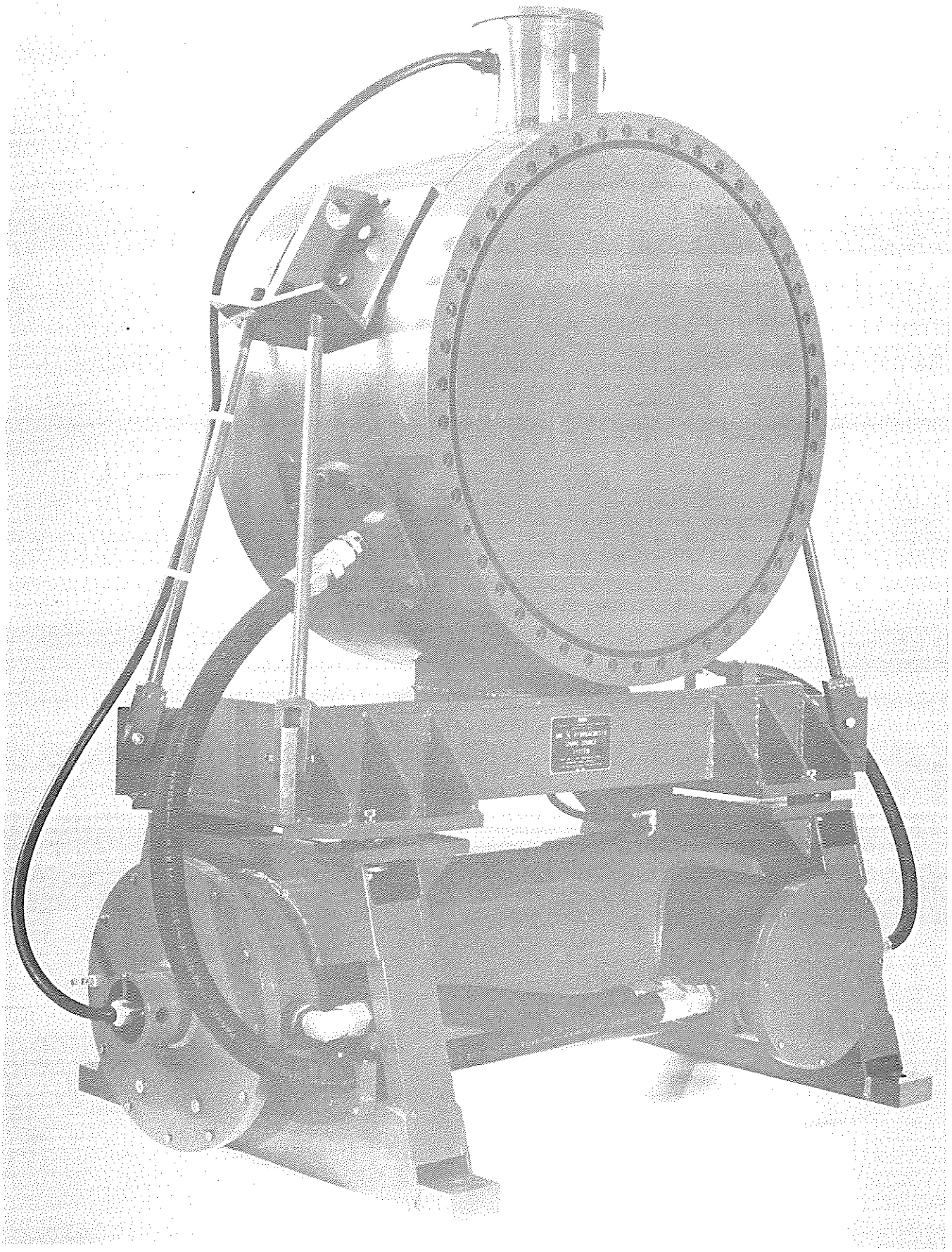

Figure 27. Hydroacoustic Source (GDE)

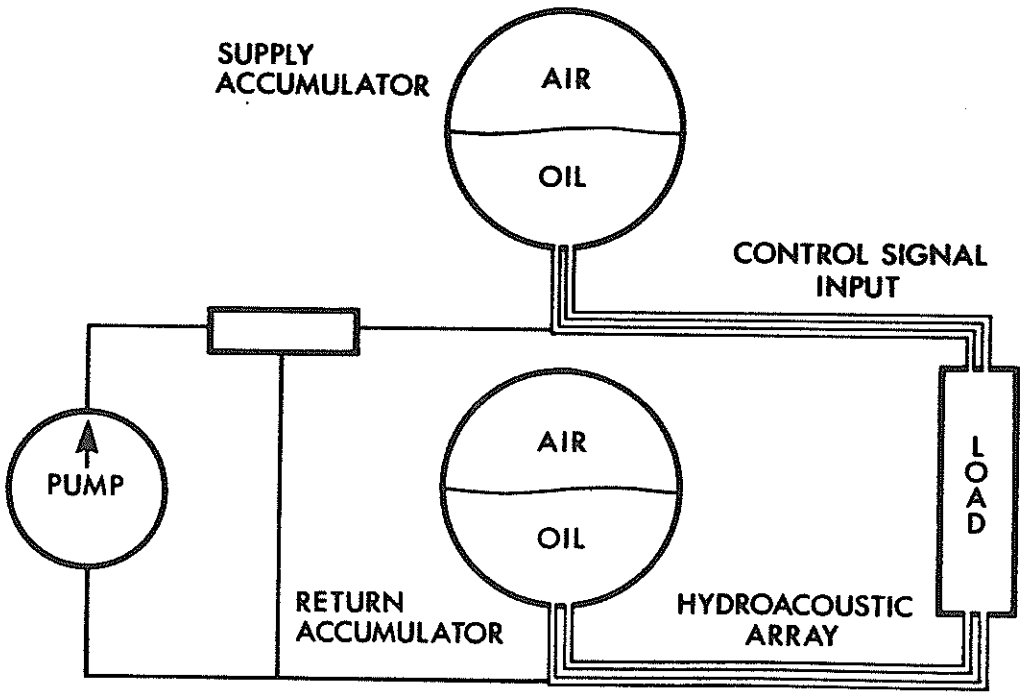

Figure 28. Hydraulic Energy Storage System (Bouyoucos, General Dynamics)

CIVIL USES OF UNDERWATER ACOUSTICS

Edwin B. Neitzel
Director of Engineering
Services Group
Texas Instruments Incorporated

I. INTRODUCTION

In discussing civil uses of underwater acoustics there are many ways of catagorizing the subject. A comprehensive introduction to this subject is presented by the National Academy of Science report entitled "Present and Future Civil Uses of Underwater Sound."

Almost all applications can be broken down into three general subjects: (1) the use of underwater acoustics for communication, (2) the use of underwater acoustics for location and delineation of objects, and (3) control of underwater equipment. These applications are shown in further detail in Table I.

It is of interest to note that the majority of the applications are associated with location. Doppler sonar systems are beginning to find extensive application for ship velocity determination. Systems are in operation for both submersible and surface vessels of all types. Accuracy of 0.25 percent in both the fore-aft and port-starboard direction have been obtained in water depths of more than 1000 feet.

The most universal application for underwater acoustics today and for the near future is water depth determination. Fathometers vary in complexity from the pleasure boat application systems costing a few hundred dollars to sophisticated phased-array narrow-beam applications costing hundreds of thousands of dollars.

Table I. Civil Uses by Application

Application	Use
Communication	Divers Commercial Submarines
Location	Vessel Location • Doppler Sonar • Sonabuoys • Beacons Object Location • Transponders • Side Looking Sonars • Fish Finders • Drill Head Locators • Holographic Image Forming Bottom and Subbottom Structure • Location and Delineation • Sonabuoy Refraction • Seismic Reflection • Fathometers
Control	Well Head Control Telemetry Bottom Instrumentation Control

Although it is not generally recognized in the literature, the use of seismic reflection data for subbottom delineation and deep structure mapping is finding increasing application. An illustration of the magnitude of the shipboard petroleum exploration market is that expenditure for free world marine seismic data collection is more than $10,000,000 per month.

In terms of the control application, extensive use is for the future. Improved encoding and fail-safe modulation systems have been developed within the last few years and are beginning to find application for petroleum well head and submerged valve control.

Any application involves system tradeoffs in regard to acoustic power, acoustic sensitivity of detection, and desired signal-to-noise ratio. With the very low frequency applications, we observe low attenuation and, therefore, long distance applications. For low frequency applications, equipment is normally costly to obtain for any directional sensing or control. This is obvious when one considers the basic physical phenomenon that an appreciable part of a wavelength is required for an antenna to obtain any reasonable directivity. With a wavelength of 500 feet at 10 Hz the complexity of the antenna structures are evident. Since we are involved in a tradeoff with hardware complexity at the low frequency and increasing attenuation at the high frequency, it is easy to observe the many applications that fall within the mid-band acoustic frequencies. These mid-band frequencies fall within the 1 to 100 kHz range. Civil uses catagorized by frequency band in one decade intervals are illustrated in Table II.

II. HIGH POWER TRANSMISSION AND HIGH SENSITIVITY RECEPTION

The theoretical tradeoffs associated with attenuation versus frequency have been treated many times in the literature. Let us, therefore, address a subject of increasing importance involving commercial applications. The subject is the extension of range of observation. Whether one considers an active or a passive system observation, we are concerned with signal-to-noise ratio. Therefore, the magnitude of acoustic noise and signal are of paramount interest in any extension of range.

Applications of extension in range can be for either horizontal control/observation or for vertical control/observation. The basic factors in the limitation of hardware design and physics of the ocean are the same.

Let us consider the acoustic power, the acoustic transmitting transducer power, the receiving sensitivity, and the noise for an illustrative high power system. This high power system is used in the seismic reflection method.

A commercially used seismic reflection or subbottom layering mapping system involves transmission and reception through the water column. Attenuation within the subbottom structures is much higher than that observed within the water layer. Uniqueness of this application is in dynamic range, harmonic distortion, and data processing. Dynamic range of 100 db with 0.2 percent harmonic distortion is commonly utilized.

Table II. Civil Uses Catagorized by Frequency Band

Frequency	Use
0 to 10 Hz	Deep penetration seismic reflections method Depth transducers
10 to 100 Hz	Seismic reflection method Hydrophone listening Sonar navigation and positioning
100 to 1000 Hz	High resolution subbottom profiling
1000 Hz to 10 kHz	Long distance sonar Bottom detail fathometers Sound velocimeter Underwater telephone Warning bells Long distance telemetry and control Fish finding
10 to 100 kHz	Fathometers Underwater telephone Marking pingers for range use Long distance telemetry Scanning sonar Transponders Pingers Fish finding Object locating beepers Low resolution scanning sonars
100 kHz to 1 MHz	Pleasure boat fathometers Doppler velocity sonar Short and medium range sonar Telemetry and control Scanning sonars

A. Transmitters

Table III is a comparison of current marine sources. To obtain very high acoustic energy in the water, the initial transducer was the detonation of an explosive charge. Energy density for the explosive charge is extremely high. A commonly used energy is 2300 Btu per pound of dynamite. Since the spectral content of the acoustic explosion or the acoustic impulse extends from dc to over 10 kHz, conversion efficiency for the seismic reflection system is low due to the fact that the bandpass of interest extends from approximately 5 to 100 Hz. As the repetition rate of data collection increased, the cost of the explosive source became prohibitive. Innovations resulted as a demand, and various mechanical and electromechanical transducers have evolved within the last five to ten years. Many systems are in the evaluation phase, but most prominently applied systems at the present time involve: (1) release of compressed air, (2) a vibratory type device, or (3) detonation of the explosive gas mixture of propane and oxygen.

Conversion efficiency within the seismic bandpass is noted from Table III to be relatively low. This is normally dictated by the practical physical size of the marine source that is towed at depth behind the ship. Although the water supports predominantly the compressional wave, energy transferred into the subbottom layers is partitioned further. For a seismic source on an elastic half space, this energy is normally partitioned as 7 percent compressional wave, 26 percent for shear wave, and 67 percent for Rayleigh waves. The additional 7 percent dilution of the compressional wave, which is normally used for the vertical incident seismic reflection pulse, further reduce the effective conversion efficiency of the source. Increasing the conversion efficiency of the source involves improved impedance matching techniques. For a given seismic source the highest possible power is often dictated by cavitation. Source Type B in Table III is for the controlled vibratory source which should find increasing marine applications with improved reliability and improved cost effectiveness.

B. Receivers

Figure 1 illustrates the noise of a long hydrophone streamer pulled through the water at different speeds. The most recently introduced innovation in oceanographic acoustics research and in commercial petroleum exploration

Table III. Comparison of Current Marine Sources

Type	Potential Energy/Source (ft-lb)	Equivalent Pounds Dynamite/Source	Energy Conversion Efficiency (%)	Frequency Spectrum (Hz)
A	9×10^5	0.66	6	5 to 100
B	4.8×10^5	0.35	10	10 to 60
C	3.6×10^5	0.26	3	20 to 100
D	7.1×10^5	0.52	6	5 to 50
E	1.5×10^6	1.00	<1	Wide
F	10^4	0.01	1	Wide

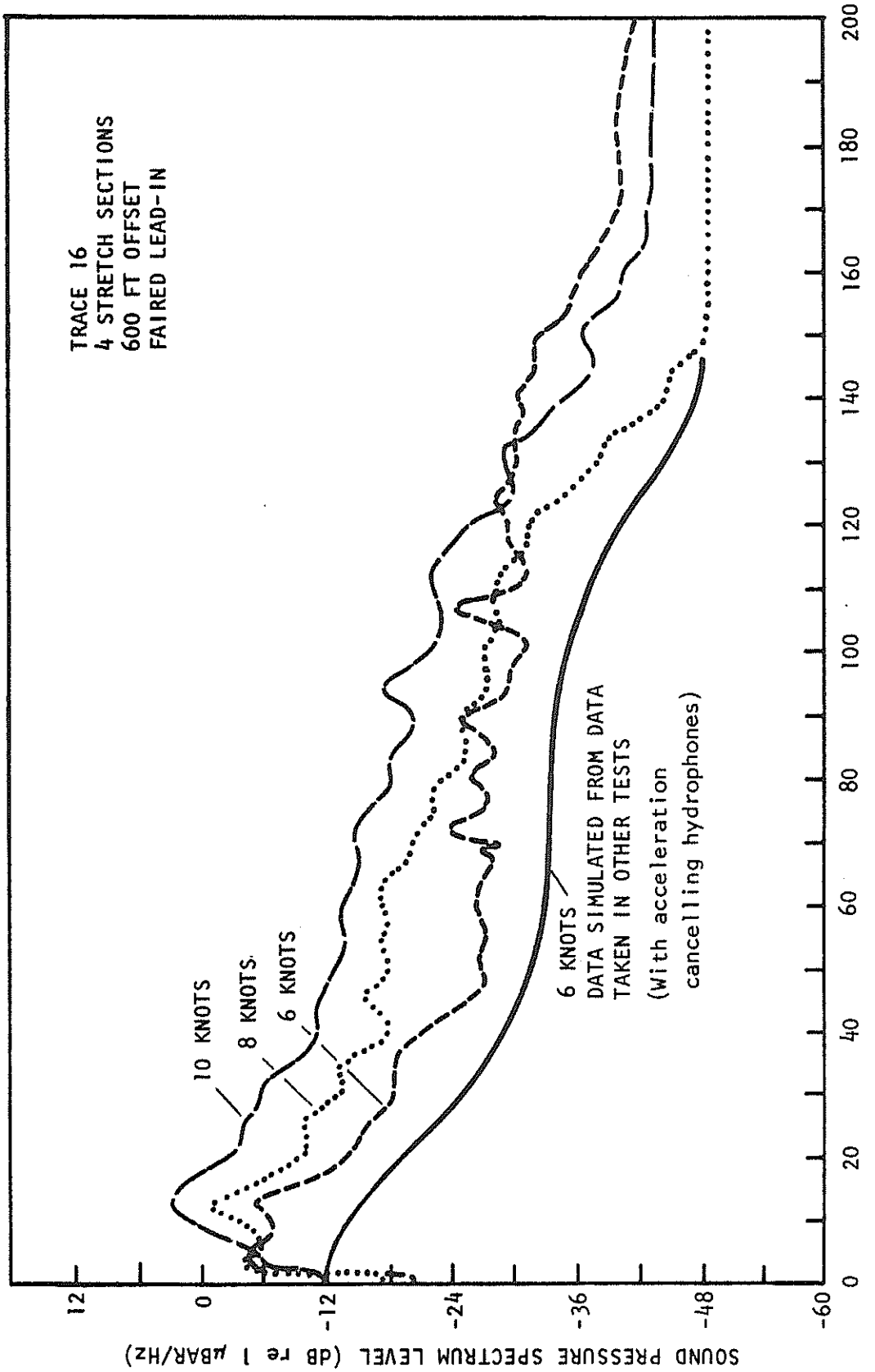

Figure 1. Streamer Noise Versus Frequency and Boat Speed

is the acceleration cancelling hydrophone which is noted to be 6 to 12 db improvement. Acceleration cancelling hydrophones attenuate streamer dynamics due to fluctuations of the cable from ship movement. An obvious additional extension of improved signal-to-noise ratio is obtained by the design of in-line acoustic antenna arrays with the pattern null in the ship direction.

C. Sonar Dopplers

Although the sonar doppler systems have been in development for over five years, extensive applications are just beginning to be realized. Applications for submersible vessel navigation, tanker docking maneuvers, and seismic vessel dead-reckoning navigation are finding extensive use. Figure 2 shows a typical integrated navigation system for seismic vessel navigation. With this system the digital computer is used for the statistical optimum estimate of the ship's position based on many input sensors. Some of these sensors are the satellite navigation receiver, high resolution sonar doppler, ship dynamics sensors, gyrocompass, and receivers for reception of shore based controlled carriers base stations. It is not unusual to provide 100-foot rms accuracy on a worldwide basis with systems of this type.

III. CONCLUSIONS

Although this paper incompasses a broad overview of civil uses of underwater acoustics, I prefer to draw three conclusions regarding commercial system innovations needs for the future. These include larger output transducers with improved conversion efficiency for the seismic reflection method, improved signal-to-noise ratio detection through quiet detector arrays at high boat speeds, and cost-effective long-range signal encoding modulation and carrier generation for control system applications. Innovations in these fields will find extensive application with the resultant economic rewards within the free world commercial market.

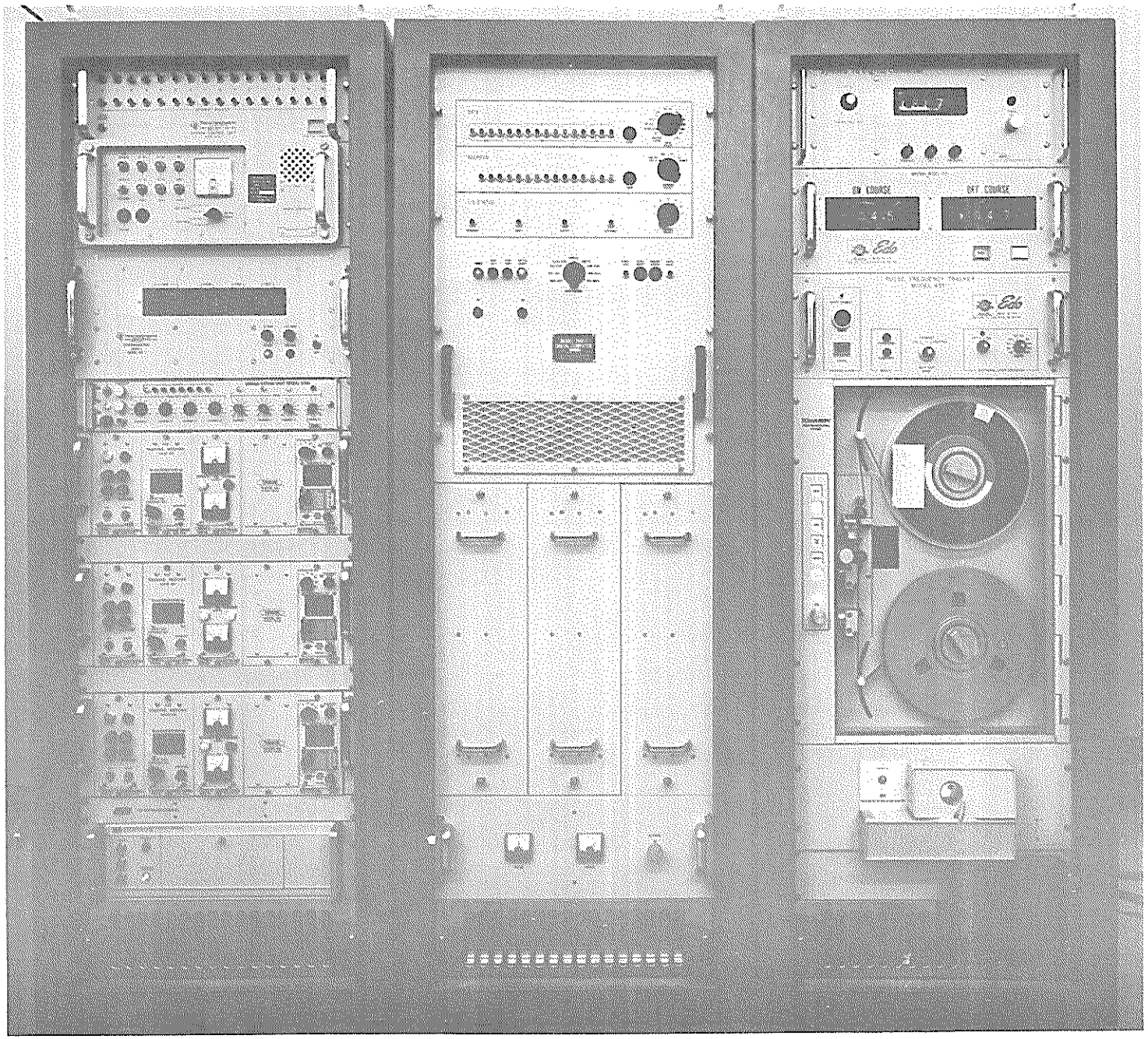

Figure 2. Integrated Shipboard Navigation System Utilizing Sonar Doppler Acoustics

ARRAYS AND SIGNAL PROCESSING

Anthony F. Gangi
Professor of Geophysics
Texas A&M University

INTRODUCTION

Arrays of receivers or transmitters are very useful in detecting and generating propagating waves of all types (acoustic, seismic, electromagnetic, etc.). The usefulness of these arrays lies in their ability to discriminate against unwanted signals and to enhance the desired signal (or signals). As such, arrays can be considered to be filters (actually, multi-dimensional or multi-channel filters) operating in the space-time domain. For example, a linear array can be considered a two-dimensional filter (one spatial dimension and the time "dimension") or it can be considered an N-channel filter if it has N sensors along the length of the array. In the same way, a planar array can be considered a three-dimensional filter or an N^2 channel filter if it is a square, equally-spaced planar array with N elements on a side.

In the following, we will consider only two-dimensional filters for simplicity (that is, linear arrays of sensors); the extension to higher dimensional filters follows directly from this analysis.

I. MULTI-DIMENSIONAL FILTERS

The output of a two-dimensional filter, $o(y,t)$, is related to the input, $i(x,\tau)$, for a linear, time invariant filter by the expression:

$$o(y,t) = \int_{-\infty}^{\infty} \int i(x,\tau)h(x,y,t-\tau)dxd\tau \qquad (1)$$

where $h(x,y,t)$ is the "impulse response" of the two-dimensional filter; that is, it is the output of the filter when the input is the function:

$$I(x,t) = \delta(x)\delta(t). \qquad (2)$$

The functions, $\delta(x)$ and $\delta(t)$, are Dirac delta functions defined by:

$$\int_{-\infty}^{\infty} g(z)\,\delta(x-z)\,dz \equiv g(x). \tag{3}$$

It should be noted that the choice of the origin time and the origin of the x-axis is arbitrary in equation (2).

Equation (1) describes a fairly general class of two-dimensional filters and it includes the case of (cylindrical) lenses used for optical data processing (see Cutrona, et. al.[1]), the case of steered or "beamed" linear arrays (or line sources[2]), and wavenumber-frequency (or convolutional[3]) filters. The type of filter represented by equation (1) depends upon the form of the kernel function, $h(x,y,t)$. For example, for the case of cylindrical lenses, the kernel function becomes:

$$h(x,y,t) = e^{ixy}\,\delta(t) \tag{4}$$

so that the output (in the focal plane of the lens) $o(y,t)$ will be the Fourier transform of the input (the intensity along the aperture of the lens[1]). For the case of a steered or "beamed" array, the kernel function has the form:

$$h(x,y,t) = g(x)\,\delta(t+xy) \tag{5}$$

while for a convolutional filter, the kernel function has the form[3,4]:

$$h(x,y,t) = h(x-y,t). \tag{6}$$

II. CONVOLUTIONAL FILTERS

The derivation of equation (1) is most readily seen by considering an array of sensors (located at the points $x_m = -M,-M+1,\ldots,-1,0,1,\ldots,M-1,M$) which are connected to $2M+1$ output points (located at $y_n = -M,-M+1,\ldots,-1,0,1,\ldots,M-1,M$) by means of $(2M+1)^2$ linear, time invariant filters which have impulse responses $h(x_m,y_n,t)$. Such an array is shown schematically (for $M=1$) in Figure 1 taken from Ref. 4. The output at a general output point, y_n, would then be given by:

$$o(y_n t) = \sum_{m=-M}^{M} \int_{-\infty}^{\infty} i(x_m,\tau)\,h(x_m,y_n,t-\tau)\,d\tau \tag{7}$$

since each output point is associated with a summing junction. If we allow M in equation (7) to go to infinity and at the same time decrease the spacing between the elements of both the input and output array, the summation will become an integration over x between the limits $\pm\infty$. Under these conditions, equation (7) becomes equation (1). Alternatively, equation (7) can be considered to be the space sampled representation of equation (1).

The case of an n-dimensional convolutional filter has been analyzed

by Burg[3]. He treats the case of a three-dimensional (two space dimensions and the time dimension) convolutional filter in detail. A convolutional n-dimensional filter has the property that the n-dimensional Fourier Transform of its output is just the product of the n-dimensional Fourier transforms of its input and its impulse response (analogous to the case of the linear, time invariant filter); that is (for example, for the three-dimensional case):

$$O(k_x,k_z,f) \equiv H(k_x,k_z,f)I(k_x,k_z,f) \tag{8}$$

where

$$O(k_x,k_z,f) = \int \int_{-\infty}^{\infty} \int o(x,z,t)e^{-i2\pi(ft-k_x x-k_z z)}dxdzdt \tag{9}$$

is the three dimensional Fourier Transform of the output and $H(k_x,k_z,f)$ and $I(k_x,k_z,f)$ are the three dimensional Fourier Transforms of the filter impulse response, $h(x,z,t)$, and the filter input, $i(x,z,t)$.

In the above expressions, the quantities k_x and k_z are called the slowness, the wavenumber and/or the spatial frequency (its units are cycles per unit length) in the x and z directions respectively. For a time harmonic wave of frequency f, traveling at a velocity c, incident upon the x-z plane at an angle $\pi/2-\theta$ and propagating at an angle ϕ with respect to the x axis (in the x-z plane), the spatial frequencies are given by:

$$k_x = 1/\lambda_x = (\cos\phi)/\lambda_H = (\cos\phi\cos\theta)/\lambda = (f/c)\cos\phi\cos\theta \tag{10a}$$

$$k_z = 1/\lambda_z = (\sin\phi)/\lambda_H = (\sin\phi\cos\theta)/\lambda = (f/c)\sin\phi\cos\theta \tag{10b}$$

where $\lambda = c/f$ is the wavelength of the time harmonic wave and λ_H is the horizontal wavelength of the wave ($\lambda_H = \lambda/\cos\theta$); that is, the wavelength in the horizontal x-z plane.

Burg[3] has extended the Wiener linear least-mean-square error theory from one-dimensional (time-domain) optimum filters to n-dimensional optimum (in the least-squares sense) filters. In particular, he shows how improvements in the signal-to-noise ratio can be achieved for a planar array of seismometers when the noise is coherent (i.e., propagating noise) and has a different frequency-wavenumber spectrum than the signal. He shows that in this case, improvements in signal-to-noise ratio greater than that obtained by simple beam pointing (or steering) are possible. However, Burg[3] points out (p. 709) that for the case of isotropic, completely incoherent noise, straight summation (or beam steering) and single channel (time) Wiener filtering would be the optimum processor.

III. THE WIDE-BAND VELOCITY FILTER

To gain some insight to the process of frequency-wavenumber filtering, let us consider an important example for linear arrays--namely, the wide-band velocity filter[5] (or "pie-slice" or "fan" filter[6]). This is a two-dimensional filter that has a response equal to 1 in the f-k (frequency - wavenumber) plane for $|f/k| < V_0$ and has a response equal to zero elsewhere (see Figure 2a). This says that all waves with a horizontal phase velocity v ($v=c/\cos\theta$) greater than V_0 will be passed with no attenuation while those with horizontal velocities less than V_0 will be attenuated. This is equivalent to saying that plane waves incident at angles greater than $\theta=\cos^{-1}(c/V_0)$ will be passed with no attenuation (c is the velocity of the plane wave in the medium and θ is the angle of incidence of the plane wave measured relative to the surface - see Figure 2b).

For this case, the impulse response of the system can be written (at $y=0$) as[4,5,6]:

$$h(x,t) = \left\{1/2\pi t\right\} * \left\{\left[\delta(t-x/V_0)-\delta(t+x/V_0)\right]/x\right\} \qquad (11)$$

where the asterisk denotes a time convolution. The results obtained from using such a filter are shown in Figure 3 which is taken from Embree, et. al.[5] The time domain operators[5] used to obtain this velocity filtering are shown in Figure 4. The results in Figure 3 show that there is no distortion or attenuation of the waveform for signals with velocities in the pass band. (Note, the horizontal velocities are the reciprocals of the dips and are given in traces/millisecond. These become usual velocities when the physical spacing between the sensors giving the traces is fixed; for example, if the sensors are separated by 3 meters, the velocity of ± 1 trace per millisecond corresponds to a ± 3 Km/sec horizontal velocity.)

The first processed trace of Figure 3c was obtained by passing input traces 1 through 12 through the time operators given in Figure 4; the second processed trace of Figure 3c was obtained by passing input traces 3 through 14 through the same time domain operators, etc. The processed traces of Figure 3b were obtained in a similar manner; however, in this case, a ± 1 trace/ms velocity filter was used. The ability of the velocity filters to attenuate the low velocity signals (i.e., high dip signals) in the input test record is readily apparent from the output traces (Figures 3b and 3c).

IV. STEERED ARRAYS

The above example shows what can be accomplished using multi-dimensional convolutional filters. Another important and common class of multi-dimensional filters is the steered array. The impulse response for a linear, steered array is given by equation (5) which, when substituted in equation (1), gives an input-output relationship:

$$\begin{aligned} o(y,t) &= \int_{-\infty}^{\infty}\int i(x,\tau)g(x)\delta(t-\tau+xy)\,dx\,d\tau \\ &= \int_{-\infty}^{\infty} i(x,t+xy)g(x)\,dx \end{aligned} \qquad (12)$$

In the above, g(x) is the aperture weighting function of the array. We note that if i(x,t) is a propagating plane wave which has the functional dependence:

$$i(x,t) = i(t-x/v), \tag{13}$$

that is, a plane wave propagating with horizontal velocity v, then

$$o(y,t) = \int_{-\infty}^{\infty} i[t+x(y-1/v)]g(x)dx. \tag{14}$$

For $y=1/v$, this becomes:

$$o(1/v,t) = i(t) \int_{-\infty}^{\infty} g(x)dx. \tag{15}$$

Therefore, we see that a steered array has an output that is proportional to the input if the input is a propagating wave which has the proper horizontal velocity. For values of $y \neq 1/v$, the output will be a smaller and distorted version of the input.

V. NARROW BAND STEERED ARRAYS

While steered or beamed arrays are and can be used for wideband signals, they are generally used with and analyzed for narrow-band signals. This is due to the fact that most sonar, radar and acoustic or electromagnetic communication signals tend to be narrow-banded. In this case, the analysis is greatly simplified since the input can be assumed to be a time harmonic plane wave of the form

$$i(x,t) = e^{i2\pi(ft-k_0x)} \tag{16}$$

for which equation (14) becomes:

$$\begin{aligned} o(y,t) &= e^{i2\pi ft} \int_{-\infty}^{\infty} g(x)e^{i2\pi f(y-y_0)x}dx \\ &= e^{i2\pi ft}G(y) \end{aligned} \tag{17}$$

where $y_0 = k_0/f = 1/v_0 = (\cos\theta_0)/c$ and G(y) is called the array pattern. In the above we see that the array pattern is just the Fourier Transform of the aperture weighting function g(x) when the array pattern is given in terms of fy. This property has been used to advantage to achieve different array patterns and is discussed in detail by Robinson[7], by Bracewell[8], by Elliot[2] and by Hansen[9].

In equation (17) we show the array pattern to be the output of the two-dimensional filter as y (or fy) is varied for a fixed input plane wave.

Ordinarily, the array pattern is expressed in terms of a fixed value of y (generally, for $y = 0$) and the input plane wave angle of incidence (or y_0) is varied. It can be seen from the form of the equation for the array pattern, namely (with $k = fy$)

$$G(k) = \int_{-\infty}^{\infty} g(x) e^{i2\pi(k-k_0)x} dx \tag{18}$$

that the array pattern will be the same in both cases.

For the case of an array of sensors, the array pattern can be written as:

$$G(k) = \sum_{n=-N}^{N} g(x_n) e^{i2\pi(k-k_0)x_n} \tag{19}$$

In the above, it is assumed that the weighting function $g(x)$ has the form:

$$g(x) = \sum_{n=-N}^{N} g(x_n)\delta(x-x_n) \equiv g(x) \sum_{n=-N}^{N} \delta(x-x_n) \tag{20}$$

for sensors located at the points x_n and for sensor gains (or weights) given by $g(x_n)$. From the above, it is apparent that it is not necessary to have uniform spacing for the array sensors.[10] From equation (20) it also can be seen that the weighting function for a space sampled linear array is just the product of the continuous weighting function - namely $g(x)$ - and the sampling function - namely the sum of the delta functions. Therefore, the sampled array pattern is just the convolution of the transform of the continuous weighting function $g(x)$ and the transform of the sum of the unit amplitude delta functions (i.e., the space sampling function). Here we have used the property that the transform of the product of two functions is the convolution of the transforms of each of the product functions (see, for example, reference 8, p. 110).

While general shapes for the array radiation pattern are useful in some applications, in most applications the primary concern is to obtain a narrow beam antenna pattern with low side-lobe levels. It is possible to design antenna patterns with low side-lobe levels, but generally at some sacrifice in the narrowness of the beam width (for a given length or aperture of the array). From equation (18) we see that a uniformly weighted array (i.e., one with $g(x) = 1$ for $-X \leq x \leq X$ would have a radiation pattern given by (for $k_0 = 0$)

$$G(k) = \int_{-X}^{X} e^{i2\pi kx} dx = X \left\{ \frac{\sin 2\pi kX}{2\pi kX} \right\} \tag{21}$$

The first side-lobe peaks of this array pattern occur near $kX = \pm 3/4$ and have a value of approximately $(2/3\pi)X$ or 13.5 db down from the main peak value (X) at $kX = 0$.

VI. THE BEAMWIDTH OF A STEERED ARRAY

The beamwidth of the array pattern may be determined from equation (21) and it is given by[2]:

$$\Theta = \theta_1 - \theta_2 = \cos^{-1}[\cos\theta_0 - 0.433\,\lambda/L] - \cos^{-1}[\cos\theta_0 + 0.433\,\lambda/L] \qquad (22)$$

$$\approx 50^\circ\,(\lambda/L)\csc\theta_0 \qquad \text{for } 20^\circ < \theta_0 \leq 90^\circ \qquad \text{and}$$

$$\approx 107^\circ\sqrt{\lambda/L} \qquad \text{for } \theta_0 = 0 \quad \text{(endfire)}.$$

where θ_1 and θ_2 are the angles at which the array pattern is 0.707 times its peak response, θ_0 is the direction of the peak response or main beam and L is the length of the array ($L = 2X = (2N+1)d$ for an array of $2N+1$ elements with uniform spacing d between elements).

From equation (22) it is seen that the beamwidth is a function of the scan angle θ_0. The variation of the beamwidth of a linear array with scan angle and array length is given in Figure 5 (from reference 2). The reason for the scan limit can be seen from Figure 6 (also from reference 2) where it is shown that as the scan angle varies from $\theta_0 = 90^\circ$ (broadside) toward $\theta_0 = 0^\circ$ (endfire) it is difficult to define a beamwidth when the array is scanned to within one-half beamwidth of endfire (Figure 6c).

The side-lobe levels of the array pattern can be decreased by using different weighting functions on the array aperture. However, this generally results in an increase in the array beamwidth. Figure 7 from Southworth[11] shows the effect on the array pattern due to different "cosine-on-a-pedestal" weightings; that is, for a weighting similar to:

$$g(x) = a + (1-a)\cos(\pi x/L); \qquad -L/2 \leq x \leq L/2$$

We see that as a is decreased, the side-lobes decrease but the beamwidth increases. This aperture weighting is closely related to the Taylor distribution (see refs. 2,9) and is commonly used in array design. Another aperture weighting that is commonly used gives an array pattern expressible in terms of Chebyshev polynomials.[2,12,13] This is called the Dolph-Chebyshev distribution and it has the property that all the side-lobes of the array pattern have the same amplitude.

The change in beamwidth for the cosine-on-a-pedestal weighting and for the Chebyshev distribution is given in Figure 8 taken from Elliot.[2] The array beamwidth increases much more rapidly for the cosine-on-a-pedestal distribution since the side-lobe level is for the nearest side-lobe only (all other side-lobe levels are smaller - see Figure 7) while the Chebyshev response has a constant side-lobe level. For either case, side-lobe levels 30 db down from the main beam are readily achieved without a large increase in the beamwidth. However, for side-lobe levels 40 db

down from the main beam or lobe level, the Chebyshev array has the advantage of only increasing the beamwidth slightly as compared to the cosine-on-a-pedestal aperture weighting.

VII. THE DIRECTIVITY OF A STEERED ARRAY

Another important property of arrays is their directivity. The directivity gives a measure of the power or signal gathering capability of the array. The array directivity is sometimes called the array gain since it usually represents the increase in signal achieved by an array compared to a single sensor or element of the array. The directivity is determined from the array pattern if the element pattern is isotropic. The directivity is defined as the ratio of the power density in the direction of the main beam maximum to the average power density from the array. That is, (for linear arrays):

$$D = \frac{2G(\theta_0)G^*(\theta_0)}{\int_0^{\pi} G(\theta)G^*(\theta) \sin\theta \, d\theta} \tag{23}$$

where $G^*(\theta)$ is the complex conjugate of the array pattern $G(\theta)$.

For a uniform spacing, $d/\lambda = 0.5$, between the $2N+1$ sensors of a linear array, the directivity reduces to[2]:

$$D = \left[\sum_{-N}^{N} g(x_n)\right]^2 \Big/ \sum_{-N}^{N} g^2(x_n) \tag{24}$$

Note, the directivity is independent of scan angle. For the case of a uniform weighting, $g(x_n) = 1$, we have[2]:

$$D = 2L/\lambda \quad ; \quad L = (2N+1)d \tag{25}$$

while for a cosine-on-a-pedestal distribution:

$$g(nd) = 1 + 2a \cos(2\pi nd/L)$$

we have[2]:

$$D = 2L/\lambda \, (1+2a^2).$$

The directivity, D, can be related to the beamwidth Θ of the array. It is found that for the usual weighting functions, the relationship can be given (to within about 10% accuracy) by the rule of thumb[2]:

$$D \approx 100^{\circ}/\Theta \tag{26}$$

It is theoretically possible to achieve higher directivities than those given by equation (25). In this case we speak of arrays having superdirectivity or supergain. However, it is found that to achieve these superdirectivities it is necessary to have a very narrow bandwidth for the array or, equivalently, a very high Q for the array. In actual practice it is found that the directivity given by equation (25) is very close to the practical limit that can be obtained. Supergain antennas are very sensitive to small errors in their spacing or their weighting. A very detailed review of the supergain or superdirectivity phenomenon is given by Hansen[9] (p. 82f).

REFERENCES

[1]L. J. Cutrona, E. N. Leith, C. J. Palermo and L. J. Porcello, "Optical Data Processing and Filtering Systems," IRE Trans. on Information Theory IT-6, 386-400 (1960).

[2]R. S. Elliot, "Beamwidth and Directivity of Large Scanning Arrays," (in two parts), Microwave Journal 6, 53-60 (1963) and 7, 74-82 (1964). See also R. S. Elliot, "The Theory of Antenna Arrays," in Microwave Scanning Antennas, vol. 2, Ed. by R. C. Hansen (Academic Press, New York, N. Y., 1966) Chapt. 1.

[3]J. P. Burg, "Three Dimensional Filtering with an Array of Seismometers," Geophysics 29, 693-713 (1964).

[4]A. F. Gangi and D. Disher, "A Space-Time Filter for Seismic Models," Geophysics 33, 88-104 (1968).

[5]P. Embree, J. Burg and M. Backus, "Wide-band Velocity Filtering -- The Pie-Slice Process," Geophysics 28, 948-974 (1963).

[6]M. Fail and G. Grau, "Les Filtres en Eventail," Geophysical Prospecting 11, 9-163 (1963).

[7]E. A. Robinson, Statistical Communication and Detection, (Charles Griffin and Co. Ltd., London, 1967) Chapt. 3.

[8]R. Bracewell, The Fourier Transform and its Applications, (McGraw-Hill Book Co., New York, N. Y., 1965) Chapt. 13.

[9]R. C. Hansen, "Aperture Theory" in Microwave Scanning Antennas, vol. 1, Ed. by R. C. Hansen (Academic Press, New York, N. Y., 1964) Chapt. 1.

[10]H. Unz, "Linear Arrays with Arbitrarily Distributed Elements," I.R.E. Trans. Ant. and Prop. AP-8, 222-223 (1960).

[11]G. C. Southworth, "Arrays of Linear Elements" in Antenna Engineering Handbook, Ed. by H. Jasik (McGraw-Hill Book Co., Inc., New York, N.Y., 1961) Chapt. 5.

[12]C. Dolph, "A Current Distribution for Broadside Arrays...," Proc. I.R.E. 34, 335-348 (1946).

[13]M. Holzman, "Chebyshev Optimized Geophone Arrays," Geophysics 28, 145-155 (1963).

GENERAL REFERENCES

C. W. Horton, Sr., Signals Processing of Underwater Acoustic Waves, (United States Government Printing Office, Washington, D. C., 1969). Chapters 9, 10, 11, 12.

J. W. Horton, Fundamentals of Sonar, (United States Naval Institute, Annapolis, Md., 1959) Chapt. 5.

E. C. Jordon, Electromagnetic Waves and Radiating Systems (Prentice-Hall, Englewood Cliffs, N. J., 1950) Chapt. 12.

J. D. Kraus, Antennas, (McGraw-Hill Book Co., Inc., New York, N. Y., 1950).

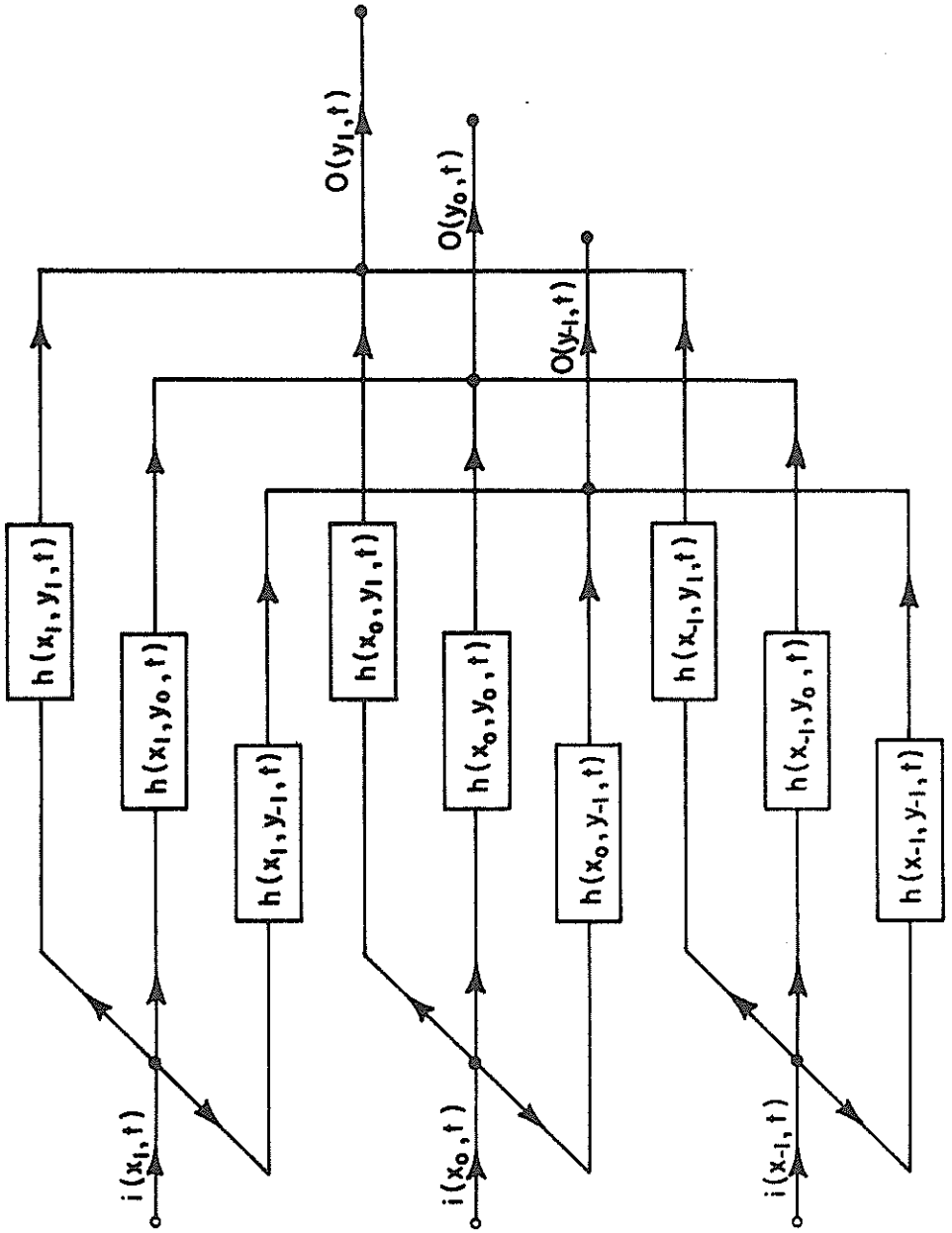

Figure 1. A Linear, Time Invariant, Two-Dimensional Filter. (Space-sampled Linear Array).

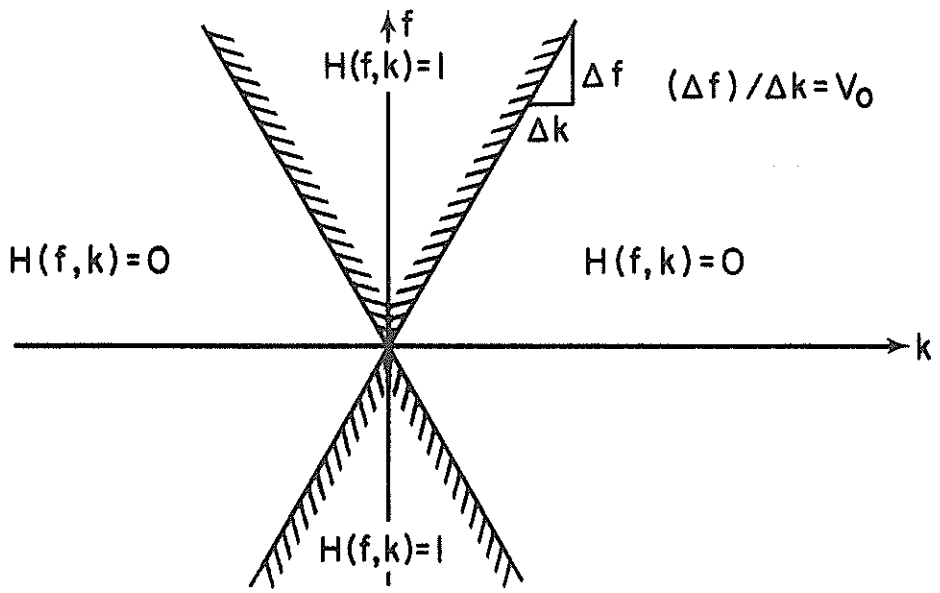

a) Velocity filter response in the f-k plane

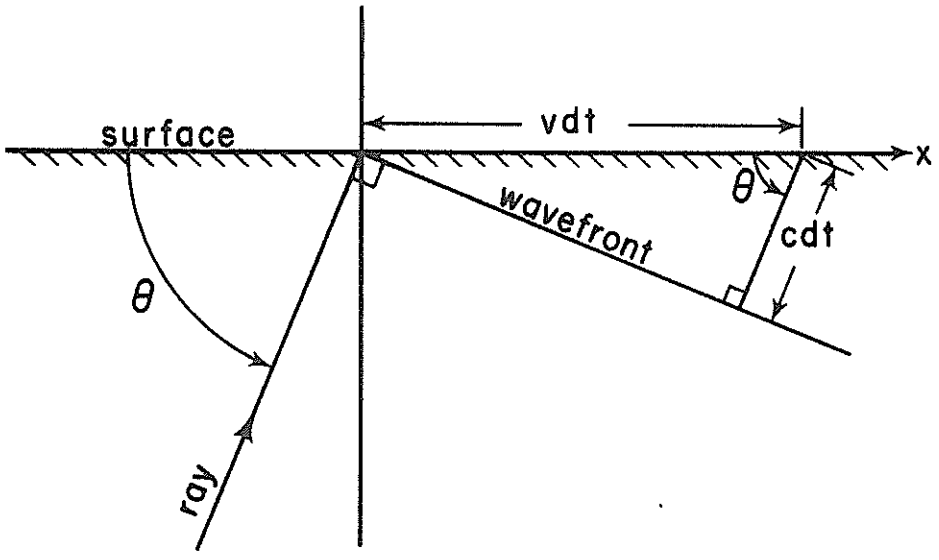

b) Plane wave incident on a linear array on a surface

FIGURE 2. VELOCITY FILTERING AND INCIDENT WAVES

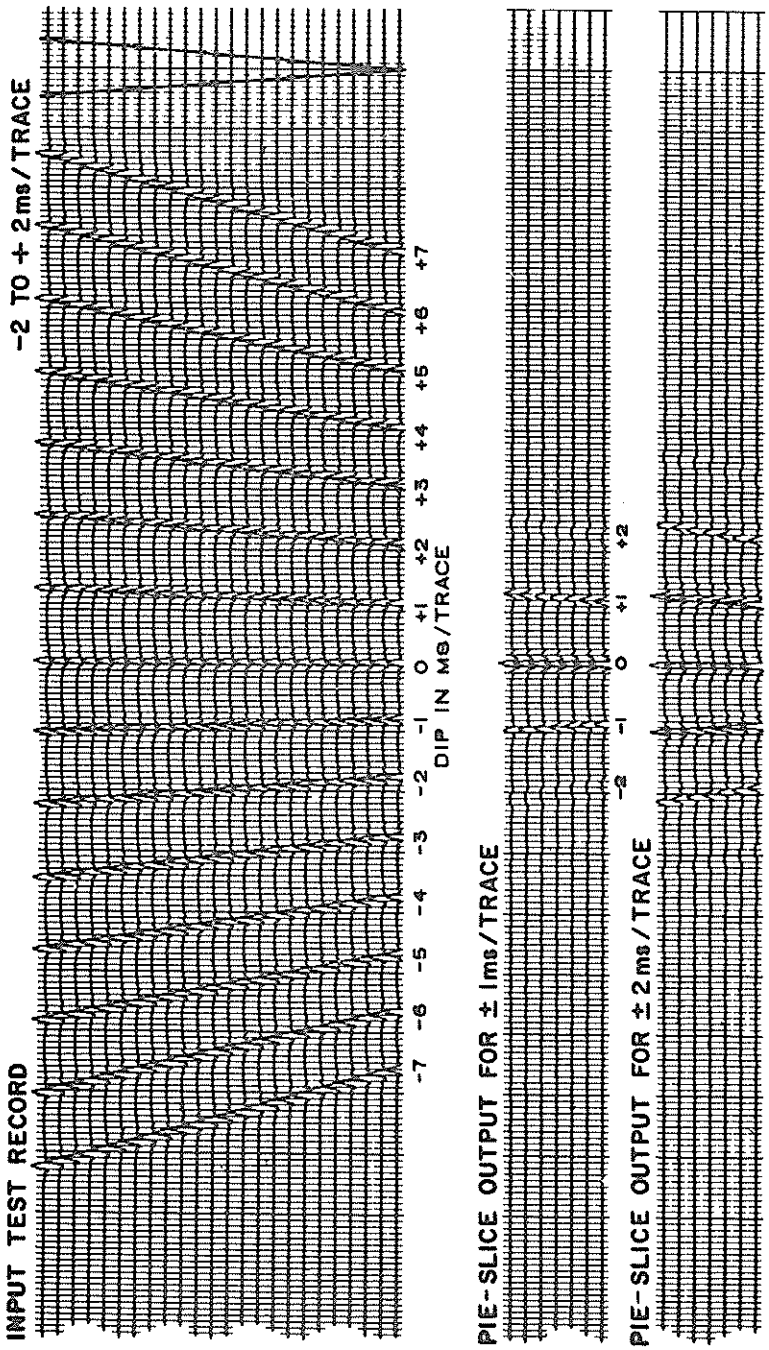

Figure 3. Results from a ±1 Trace/ms and a ±0.5 Trace/ms Wideband Velocity Filter. (From Embree, et.al.[5])

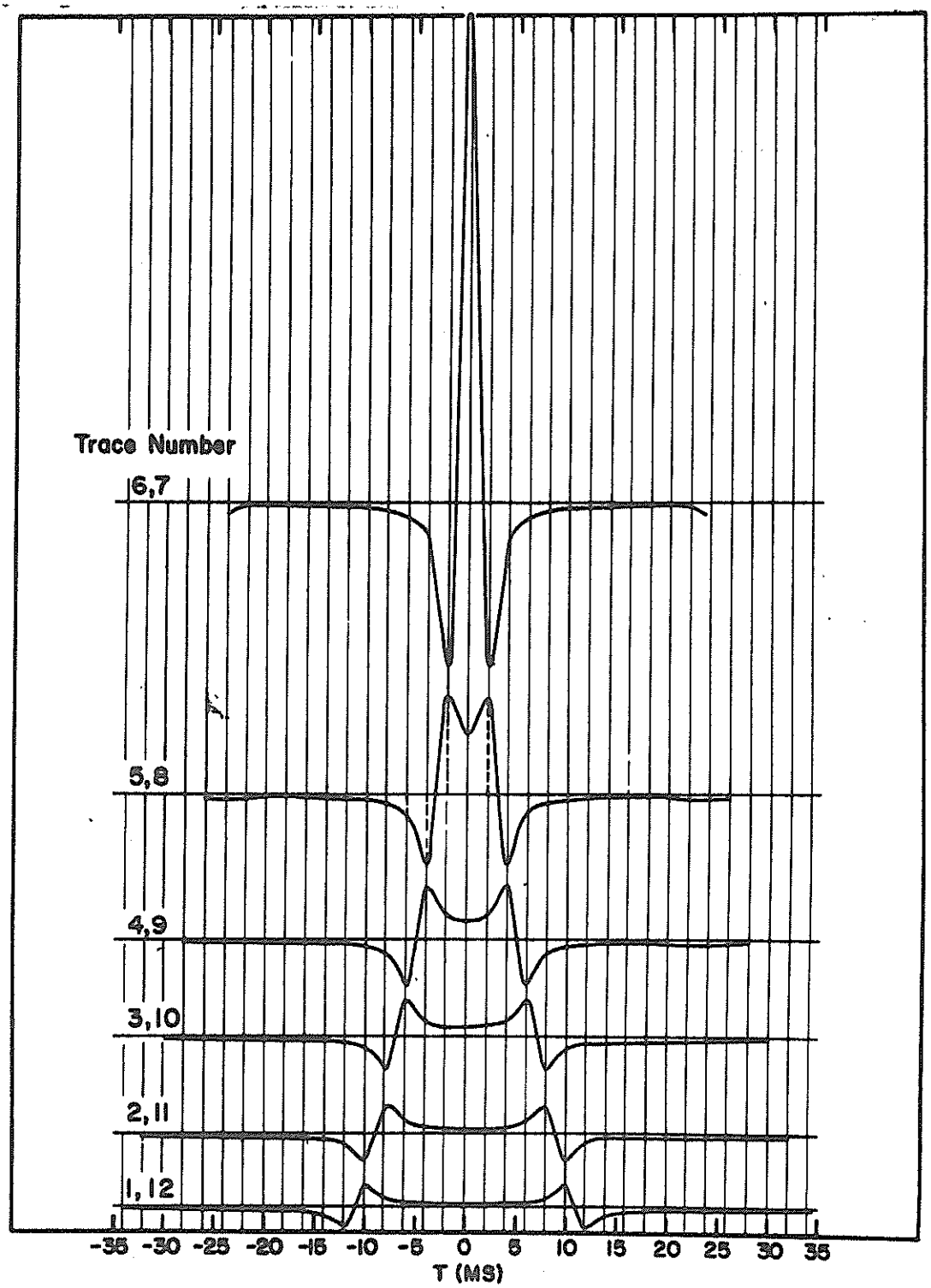

Figure 4. Impulse Response at y=0 for a 12 Trace, ±0.5 Trace/ms Wideband Velocity Filter. (From Embree, et.al.[5])

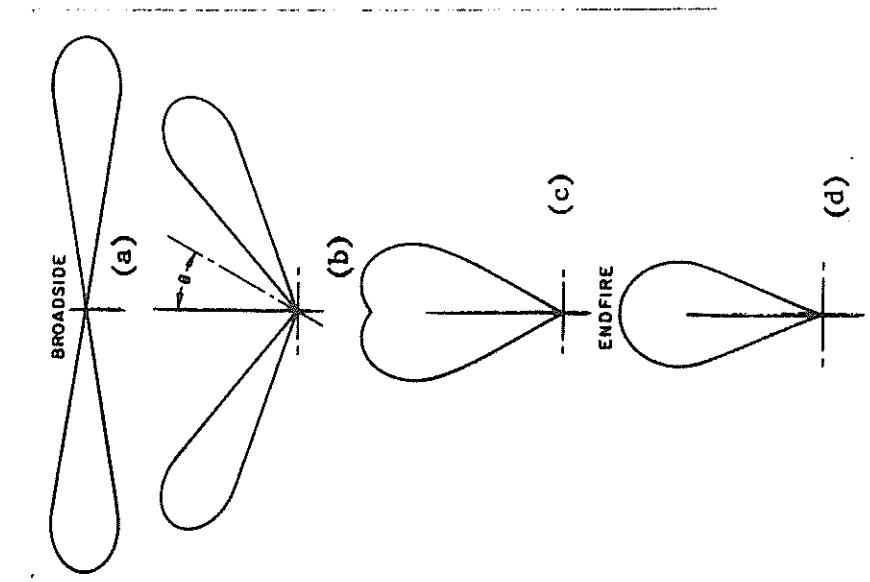

Figure 6. Scanned Array Beam Patterns. (From Elliot[2])

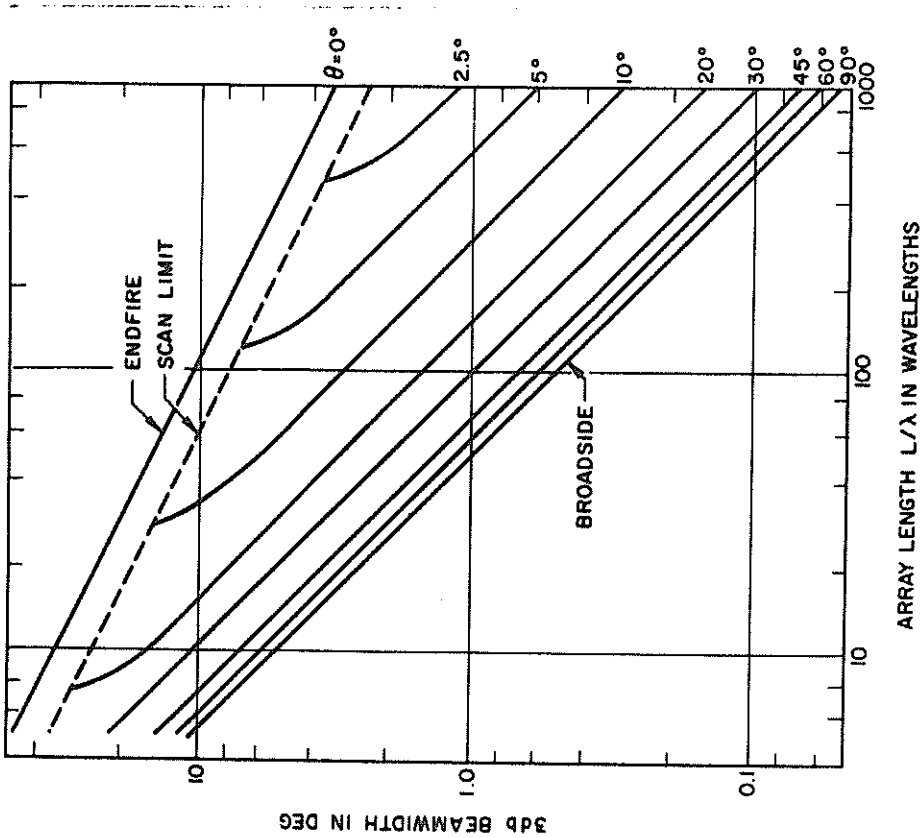

Figure 5. Beamwidth Versus Array Length and Scan Angle, (From Elliot[2]).

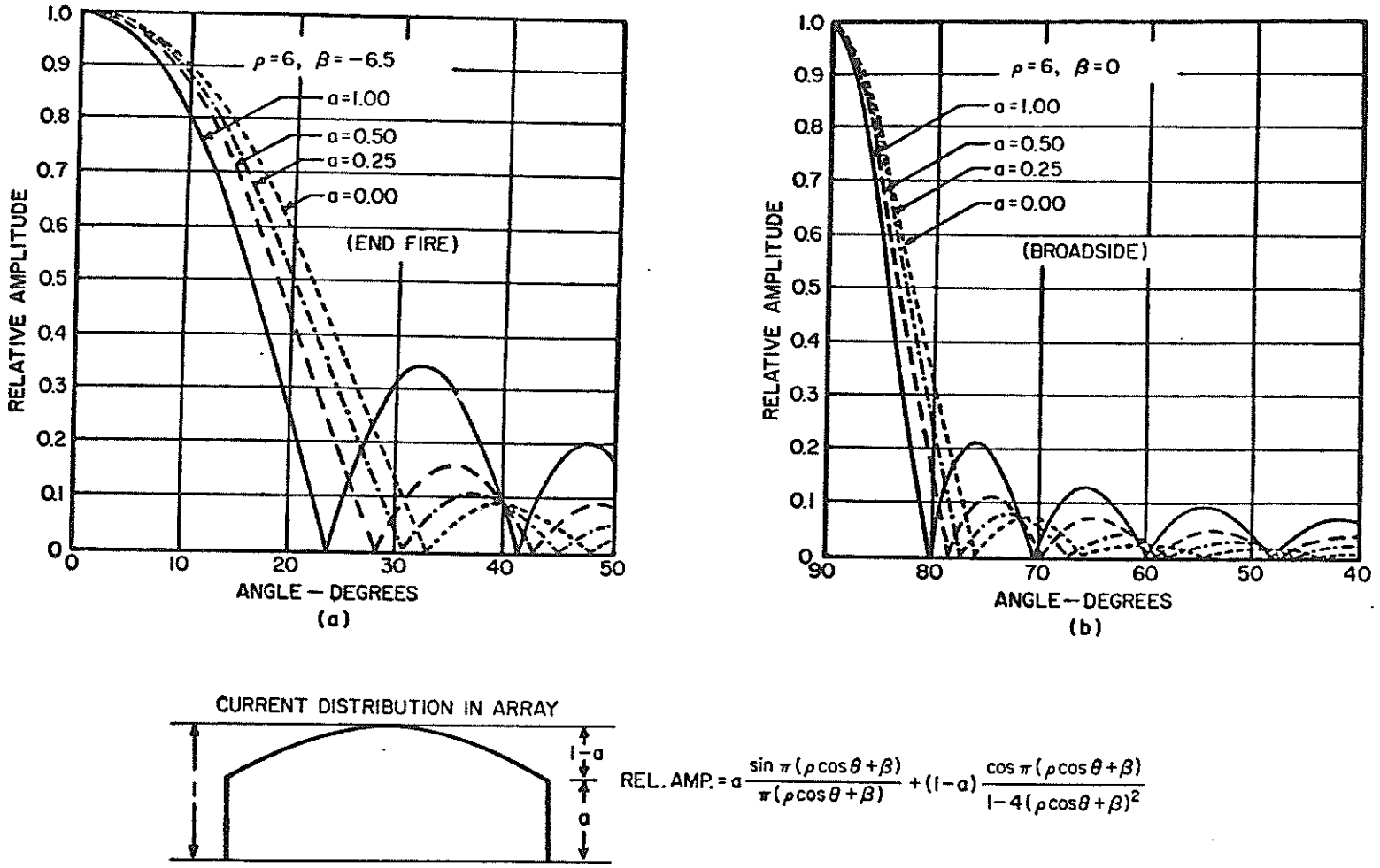

Figure 7. Variations in Array Patterns due to Aperture Weightings. (From Southworth[11]).

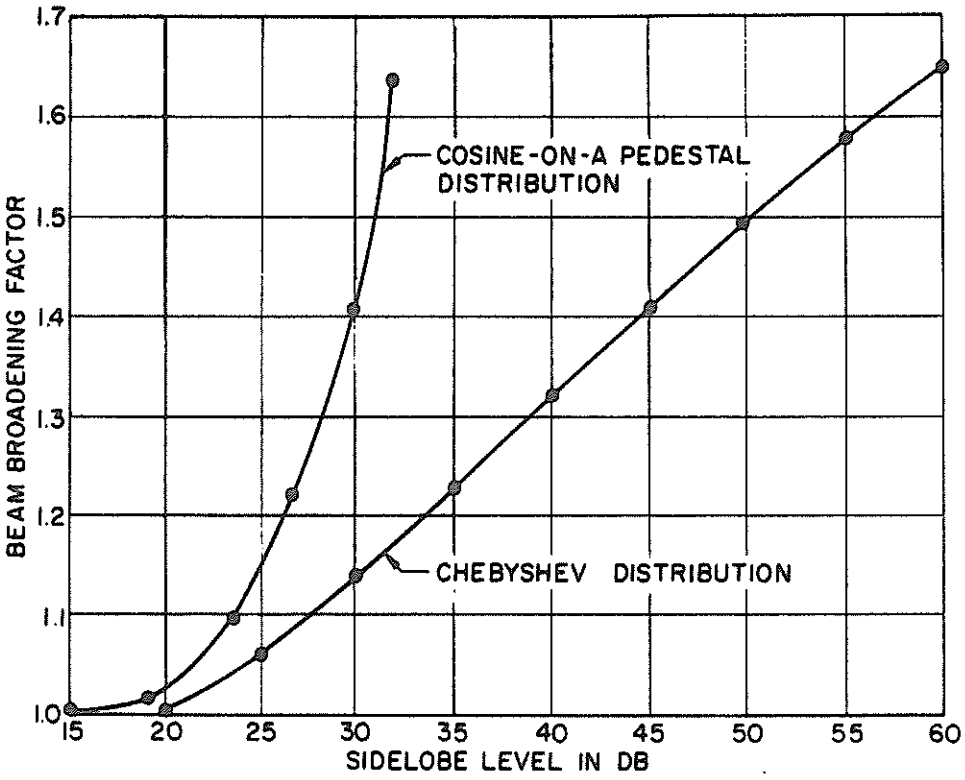

Figure 8. Beam Broadening Factor Versus Side-Lobe Level. (From Elliot[2]).

USES OF SOUND IN THE OCEAN

Dr. Ira Dyer
Professor of Ocean Engineering
Massachusetts Institute
of Technology

The high absorption in water of electromagnetic (EM) waves, including those of optical wavelengths, imposes upon sound waves many of the observational and control tasks we assign to EM in air. The concepts of radar-based piloting systems, for example, can only be used underwater provided we replace EM with sound. Even so, most system concepts need major revision since the EM wave speed is of the order of 10^5 greater than that of sound in water. Thus, information rates in underwater acoustic systems are very much smaller than in their EM counterparts. As a result, we are more often presented with displays of temporally evolving events in underwater sound systems rather than with instantaneously composed spatial pictures as in EM systems. While such displays are sometimes difficult to interpret, sound wave systems do possess considerable utility and are put to an amazing range of tasks in the ocean.

About 50 years ago, apparatus that used sound to determine the depth of water was demonstrated. The introduction of the depth sounder, can be said to be the beginning of an age that has seen widespread acceptance of acoustic systems for various underwater tasks. Figure 1 shows schematically the operating principle of a depth sounder: 1) a relatively short acoustic tone burst is emitted in the downward direction, 2) the tone burst reflects from the ocean bottom, and 3) upon reception, the round trip time is measured and displayed as water column depth.

The depth sounder is often designed to display a continuous record of depth corresponding to the track of the vessel. Such records, an example of which is given in Fig. 2, are the basis of most topographic or contour charts of bottom depth, often called bathymetric charts. Such a chart plus a depth sounder, either discrete or continuous in display, is a valuable tool in navigation.

High resolution depth sounders have very narrow beamwidths. The beamwidth of a standard depth sounder is about 60° so that the depth it records is in reality a minimum or an average depth over a quite large area on the ocean bottom. While this is adequate for surface navigation, some applications (e.g., emplantment of rigs or deployment of deep platforms) often require more detailed information such as bottom slope or roughness. To meet these requirements, depth sounders with beamwidths as small as about 3° have recently been developed. Even so, 3° corresponds to a rather large area for deep water; for continental shelves on the other hand considerable bottom detail can be obtained.

Measurement of the change in frequency of a sound wave, after it has reflected from the ocean bottom, enables measurement of the ship's speed over the bottom. While acoustic speedometers are not as common as depth sounders, having been introduced commercially only recently, there is good reason to believe that they will become generally accepted, especially for near shore piloting and docking of large cargo carriers and tankers. Incorporation of a time base and integrater in the speedometer yields a log, i.e. total distance travelled. The use of acoustic odometry, like speedometry, is now not widespread, but may very well become popular in the future.

With pulses of greater power and lower frequency than used in a depth sounder, geologists and geophysicists learn a great deal about bottom sediments and structures. Figure 3 illustrates this application, termed sub-bottom profiling which is now a standard and often used geophysical tool. With a sub-bottom profiler, acoustic energy penetrates the bottom and is reflected back from each layer or horizon. As in a depth sounder, the round trip time to each horizon is

measured and converted to depth. Continuous records corresponding to the ship's track are always used to aid in data analysis.

Sub-bottom profilers use impulsive sources (explosives, combustion expansions, pneumatic expansions, sparks, etc.) to obtain the power needed at low frequencies. While necessary for bottom penetration, the low frequencies limit the ability of the profilers to resolve thin laminae. High resolution sub-bottom profilers are available to meet this need; they operate at much higher frequencies by generating briefer impulses or through the use of tone bursts. Such profilers can resolve thin structures in the upper 50 to 200 ft. of the bottom, and have considerable potential in uncovering near-surface faults and in detailing soil conditions for rig implantment. An example of such a record is given in Fig. 4.

All of the foregoing applications concern sound reflected from horizontal or nearly horizontal interfaces. Sound is also used to determine the location of three-dimensional objects within the water column itself. When so used, the sound is directed to some mid-water position as shown in Fig. 5. A reflection or echo from the object is then received. Systems to accomplish this usually have higher angular resolution than a depth sounder, so that the object's azimuth and depression angle can be determined. The round trip time once again is used to gauge the distance to the object, thus locating it. Such a device is called an echo locator. (Echo locators are also known as sonars from Sound Navigation And Ranging, and more particularly as active sonars to distinguish them as devices which emit sound waves under control of the observer. Systems capable only of receiving sound waves are known as passive sonars.) Echo locators are widely used by military forces (to locate submarines), as commercial fish finders, and in underwater collision avoidance systems.

With high enough resolution, an echo locator can be used for image formation. Actually images produced by the best systems available today are quite crude. In many cases, nevertheless, we need to identify an object we have located. (For example, an object on the ocean floor may be a hulk, a rock out-cropping, or

the sunken rig we are seeking.) While some excellent acoustic identification aids exists, such as side scan sonars (see Fig. 6), the practitioner often must resort to diving or manned submersibles for direct identification, or to photographic probes for visual clues.

Many acoustic devices are used underwater as terminals in an information system. Underwater telephones consist of transmitting and receiving units, with the water acting as a "softwire" connection. In the same manner, data may be telemetered from a data acquisition buoy to a ship, as sketched in Fig. 7. The data may have been stored in the buoy for some time, and transmitted to the ship upon receipt of a command signal from the ship. Or the ship may opt to recover the buoy by triggering a release mechanism with a command signal. All such applications are favored today by a wide selection of available devices, specifically designed and tested for these tasks. A typical telemetry system is shown in Fig. 8. In this case data are encoded by timing the signals emitted by the pinger, and are read digitally with the meter shown. Since the information received is basically a sequence of time intervals, the data may also be recorded on a precision graphic recorder such as used in profiling.

All who ply coastal waters in surface craft are aware of the vast array of navigational aids usually available; cans, nuns, whistles, gongs, bells, lights, horns, radio beacons, etc. Comparable underwater navigational aids based on sound are possible but are far from being deployed on a massive scale. On the other hand, specialized acoustic markers, beacons, and other underwater signalling aids are commercially available and are becoming more widely used. With an acoustic beacon, as shown in Fig. 9, a manned submersible can return to a particular area for further work, much as a surface craft may home on a radio beacon in fog. In many such applications, the beacon only operates (transponds) upon receipt of a keying signal from the search craft; this conserves power and provides security. It is not farfetched to imagine that shipping lanes near busy harbors could be marked and controlled by underwater acoustic beacons (perhaps using the ships' depth sounders as receiving systems) but shipping practices change slowly and such a system may be well off in the future.

Instead of multiple beacons and one receiver, much can be done with the reverse, i.e., one source and multiple receivers. There are commercially available station-keeping systems whose principle of operation is sketched in Fig. 10. A single bottom mounted beacon is used. Three hydrophones are mounted on the ship; the phase difference among these hydrophones forms an error signal for correction of the ship's position with respect to the beacon.

In a somewhat similar fashion, underwater floats or vehicles can be tracked. The float or vehicle in this application is fitted with a pinger and observed with an array of hydrophones, usually bottom-mounted. The difference in time of sound arrival among the hydrophones is then related to the source position. Tracking systems are commonly used in vehicle test ranges, and have also been used to measure deep ocean currents through the drift of floats. Perhaps the simplest application of tracking and quite possibly the most useful, is illustrated in Fig. 11. Here a pinger is attached to an instrument package being lowered overboard. The package's position with respect to the bottom can be readily monitored on a depth sounder recorder by observing the time difference between the direct and the bottom-reflected waves.

Various fundamental properties of the ocean can be measured with sound; sediment thickness and current have already been mentioned. Surface wave height, current microstructure, and turbidity are a few more examples. A research worker, however, is less apt to make use of a standard device, for his requirements generally dictate highly specialized performance and often unique construction.

Although the samples contained herein are not all-encompassing, the diversity of underwater sound applications has no doubt been noticed by the reader. Actually, the physical principles upon which these applications are based are reasonably few; and once understood, reasonably powerful. This being the case it might be expected that technological efforts at sea

would always be surrounded by sound systems of various kinds. Actually such systems are all too often engineered and produced on a custom basis, thus driving their prices beyond the reach of many. I look forward to the day when all such systems can be produced, like depth sounders for example, on an off-the-shelf basis, so that they can more readily be placed in the ocean engineer's tool kit.

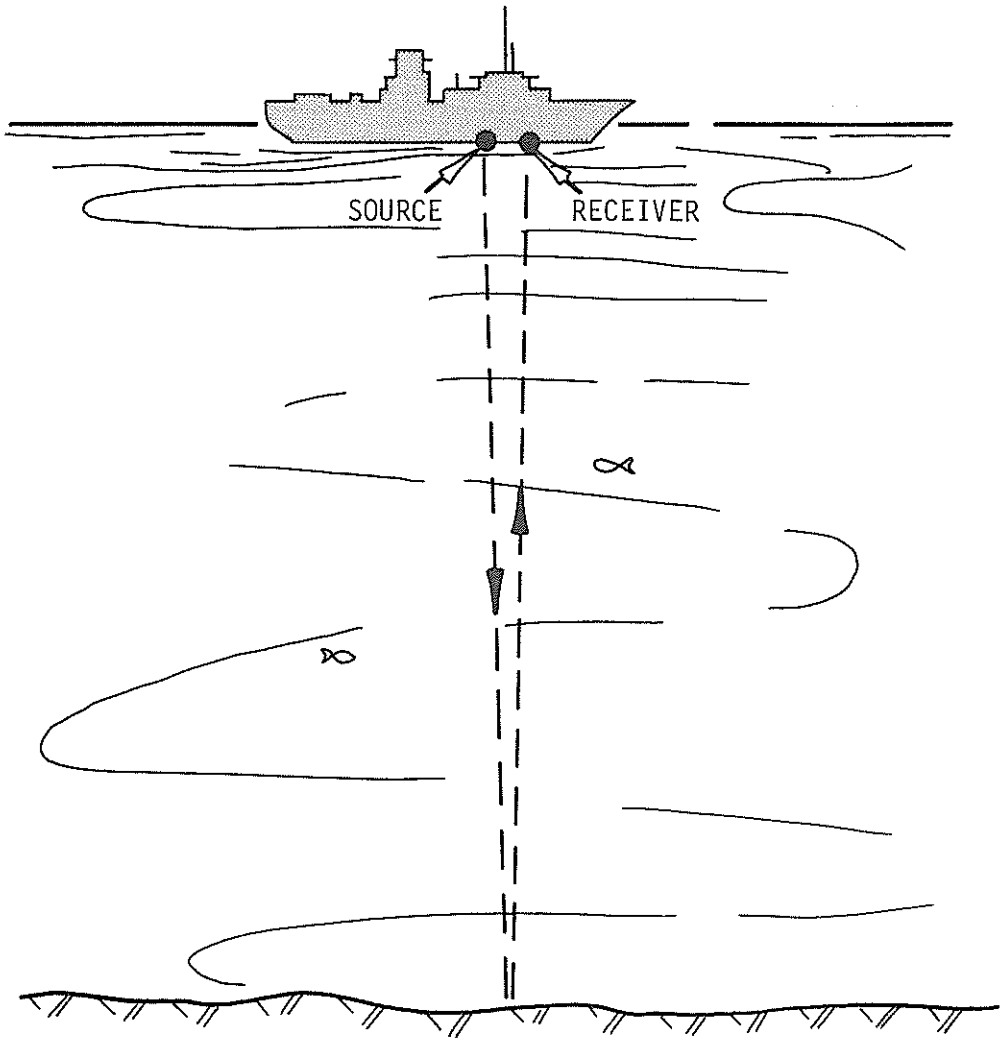

FIGURE 1. Depth Sounder

(Source and Receiver Shown Separated for Schematic Clarity)

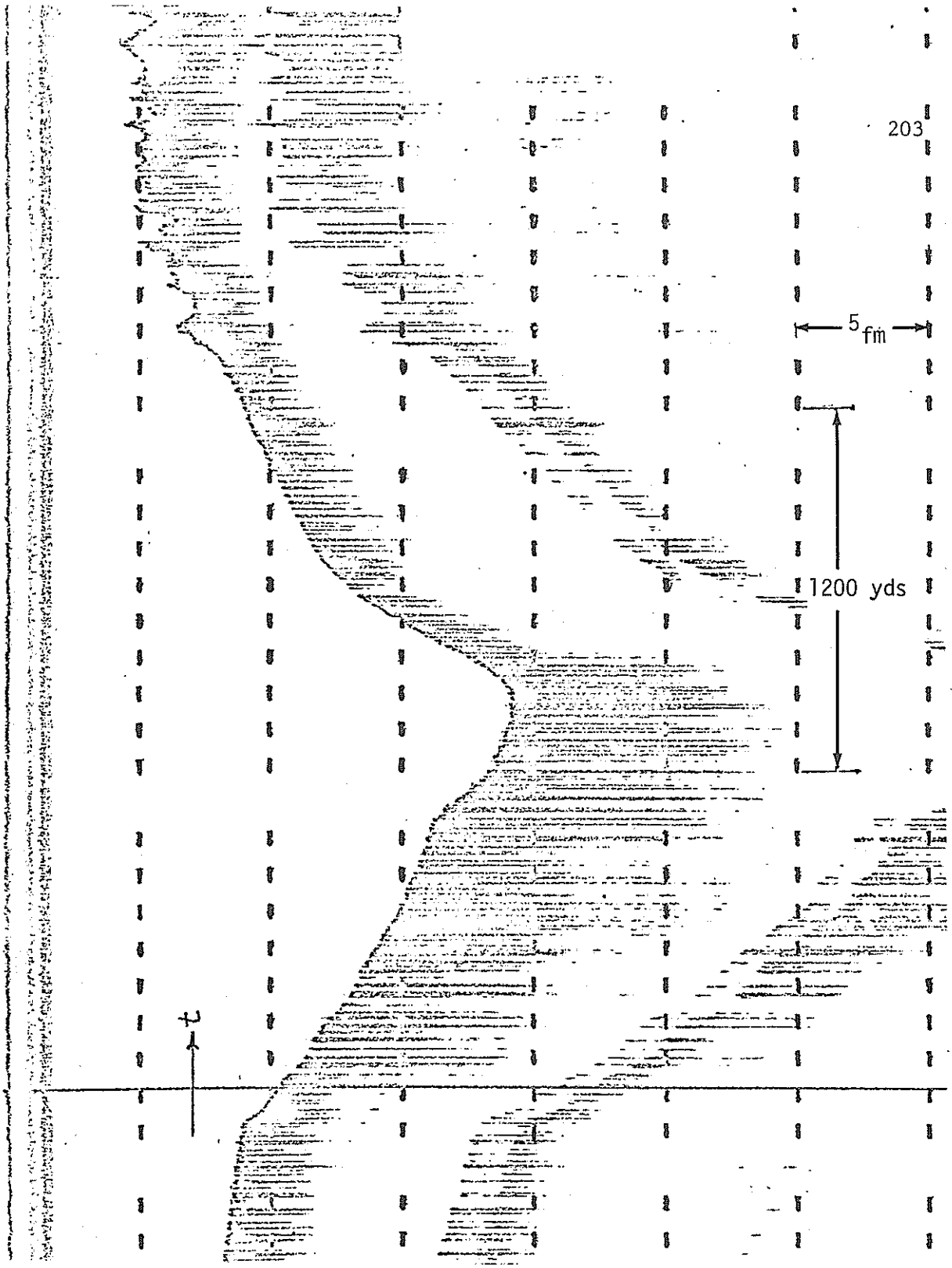

FIGURE 2. A typical depth record. This was taken in shallow water (Quicks Hole/Lone Rock, in Buzzards Bay, Mass.) with an EDO UQN-1 sounder. Its frequency is 12 kHz and its beamwidth about 55°. In shallow water the standard depth sounder can provide considerable bottom detail, but for this case (very sharp slopes) significant uncertainties remain. (Courtesy of W. C. Pfingstag.)

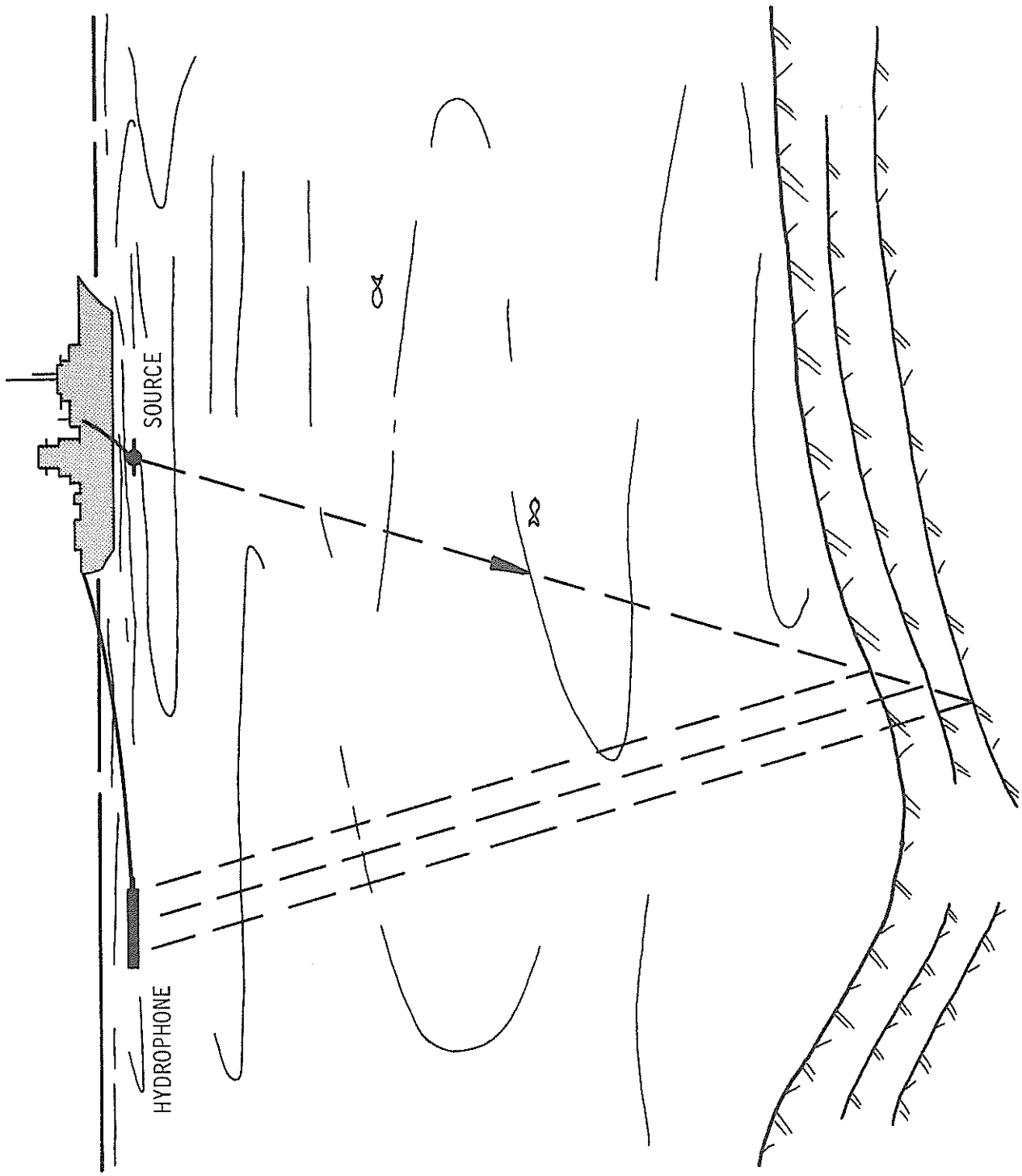

FIGURE 3. Sub-Bottom (Seismic) Profiling System

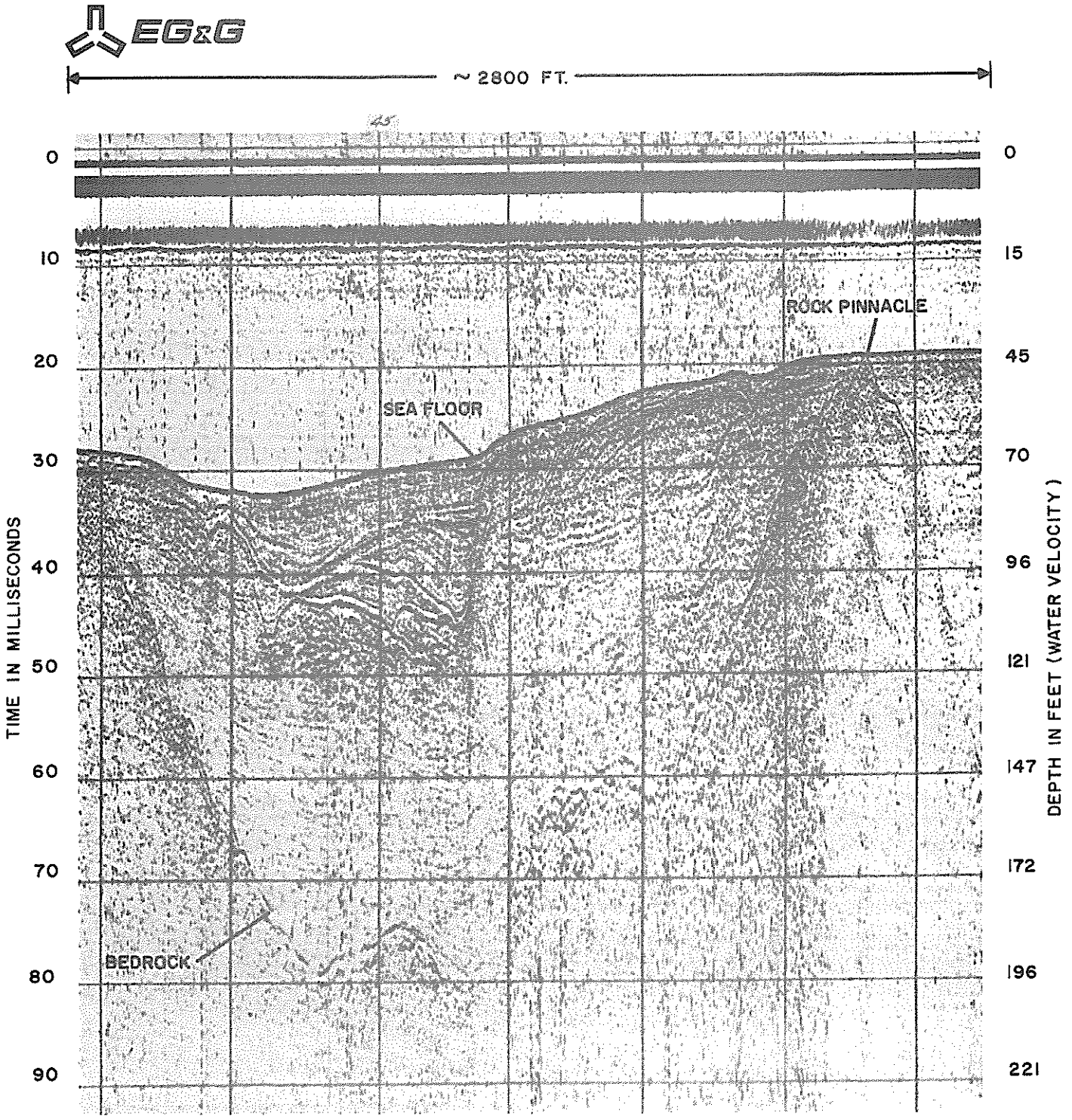

FIGURE 4. A high resolution sub-bottom profile. (Courtesy EG&G, Inc.)

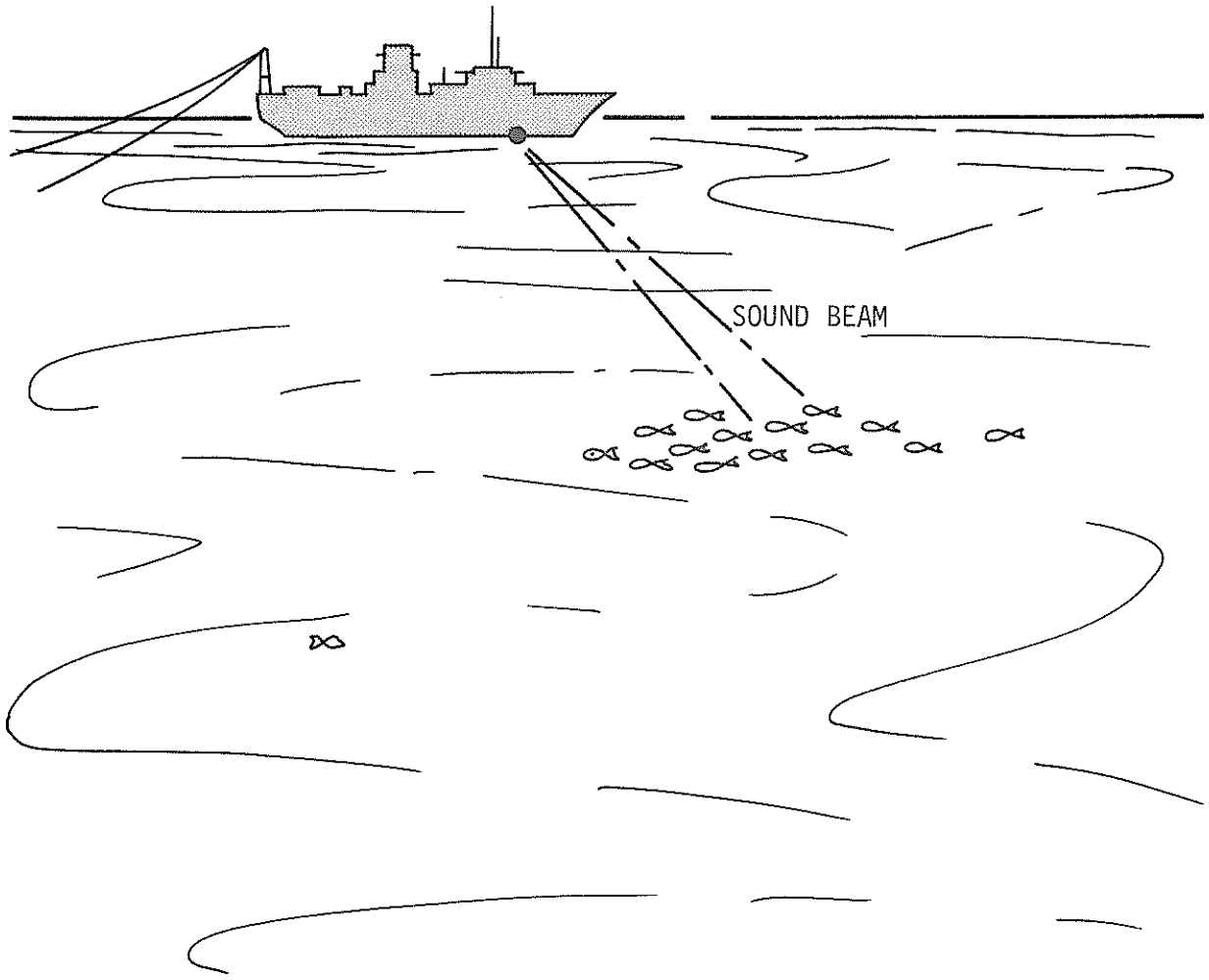

FIGURE 5. Echo Locator (Scanning Active Sonar)

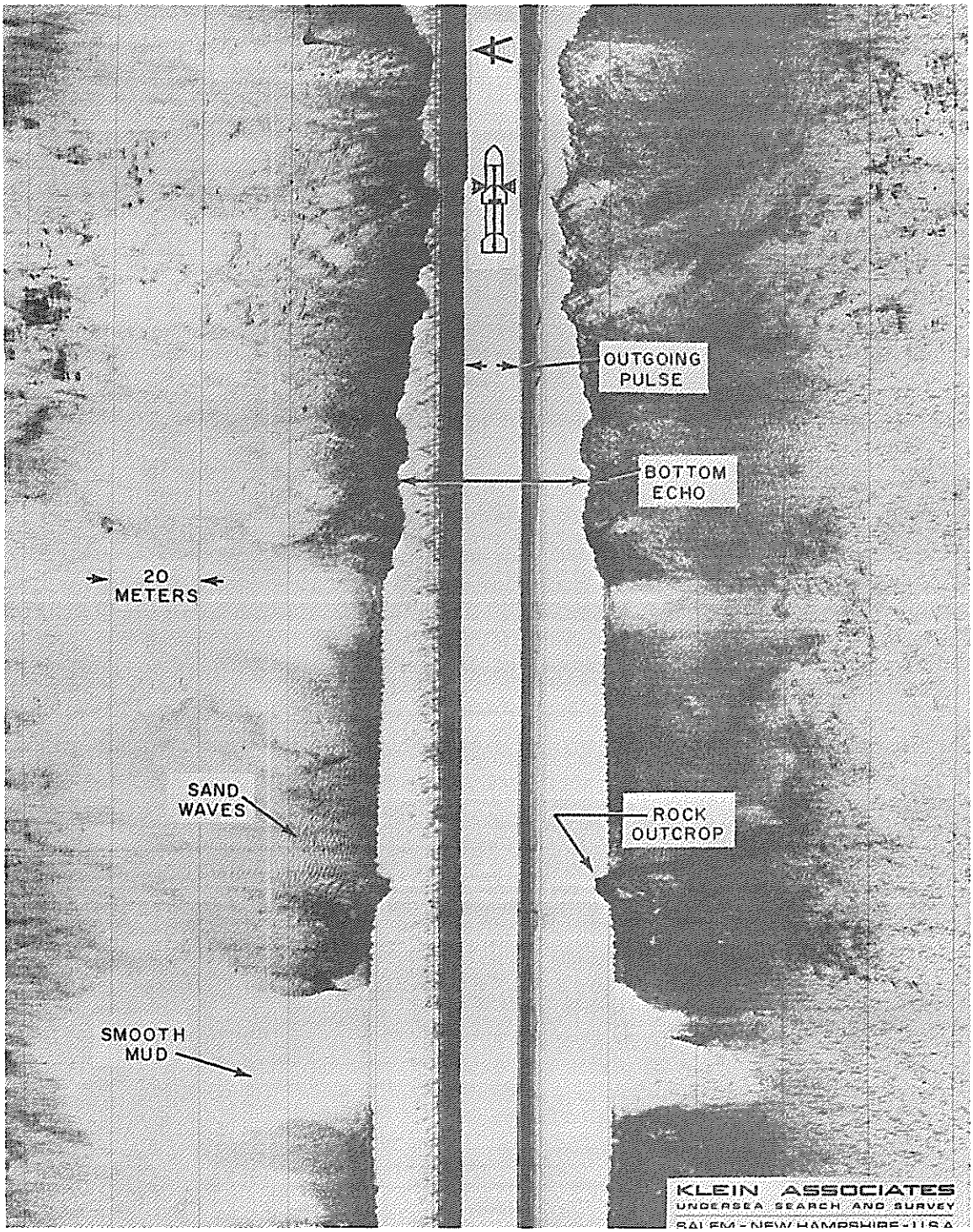

FIGURE 6. A double side scan record, showing various features of a continental shelf bottom. (Courtesy Klein Associates, Inc.)

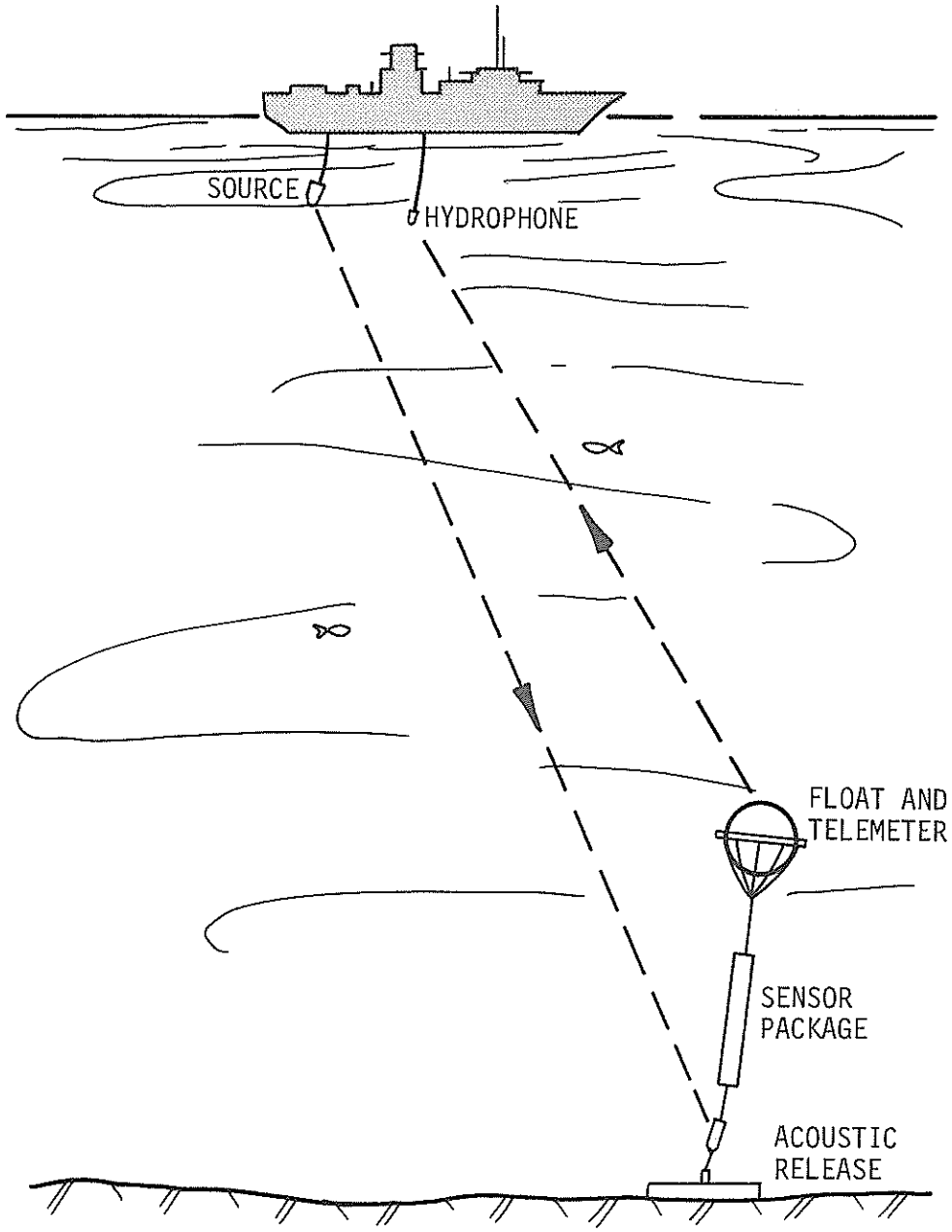

FIGURE 7. Telemetry, Command, and Release Operations

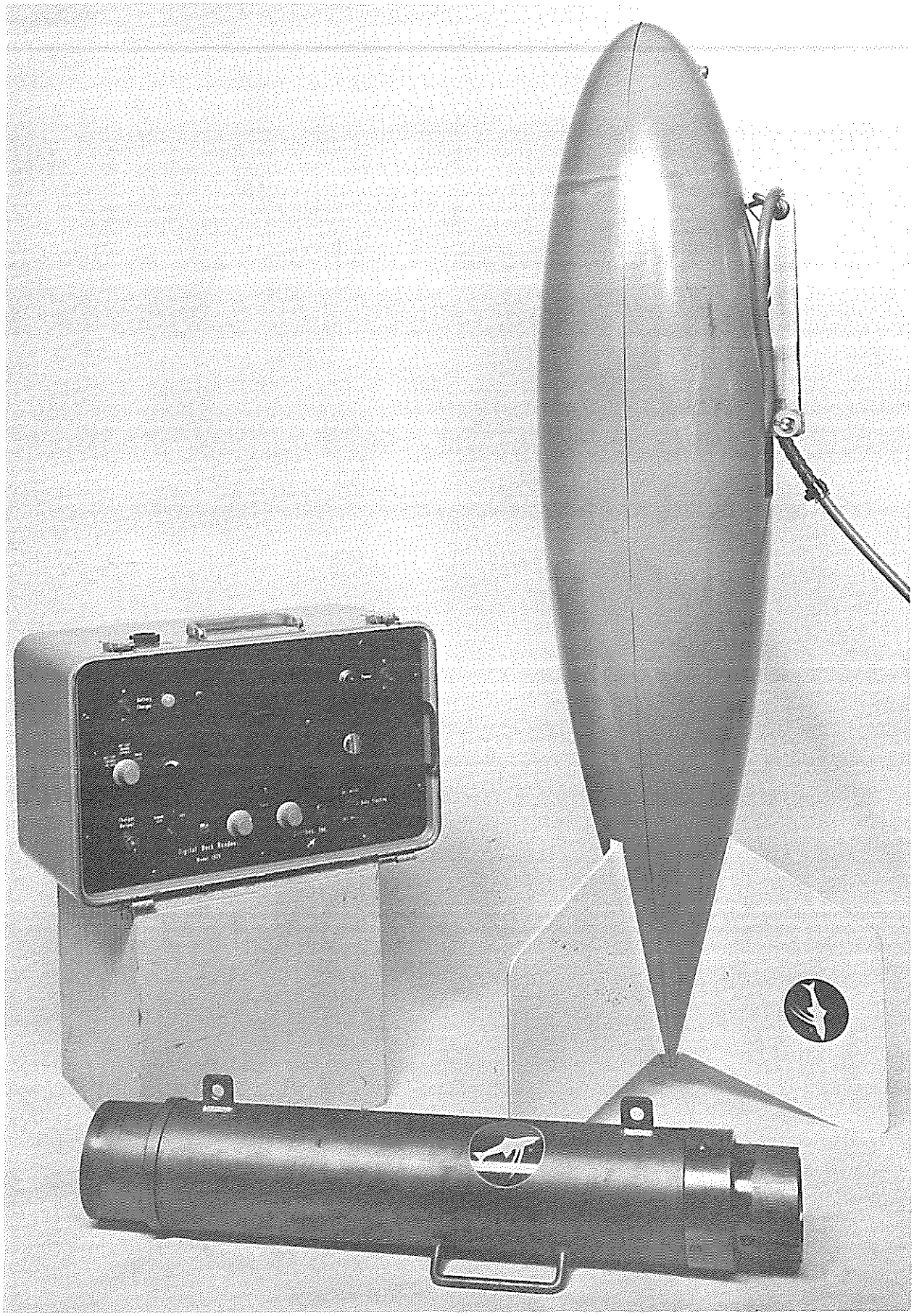

FIGURE 8. Major units of a telemetry system. Data are radiated by the pinger (cylindrical in shape), received by a hydrophone in the faired body (to facilitate towing), and displayed digitally. (Courtesy of Benthos, Inc.)

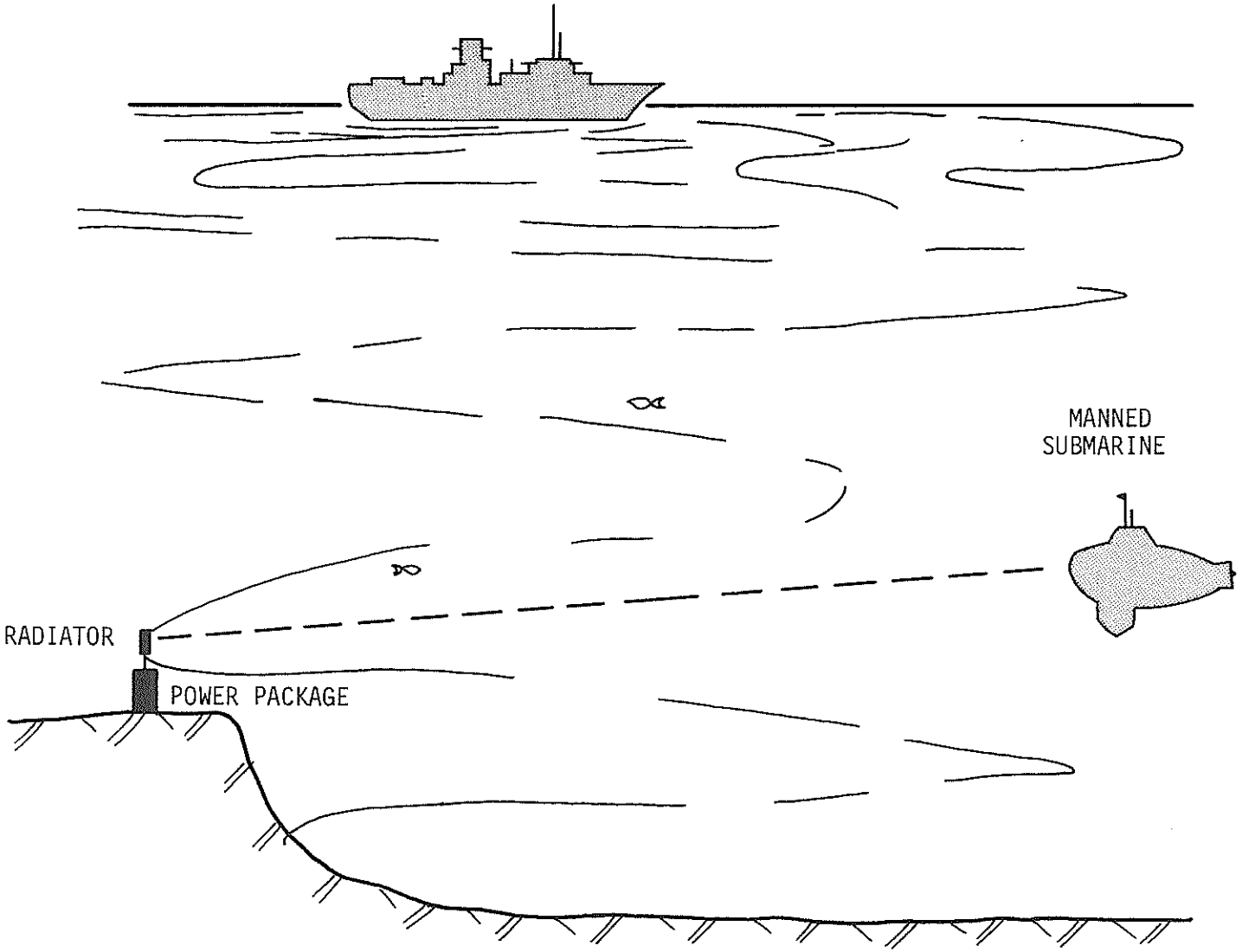

FIGURE 9. Submersible Homing on an Acoustic Beacon

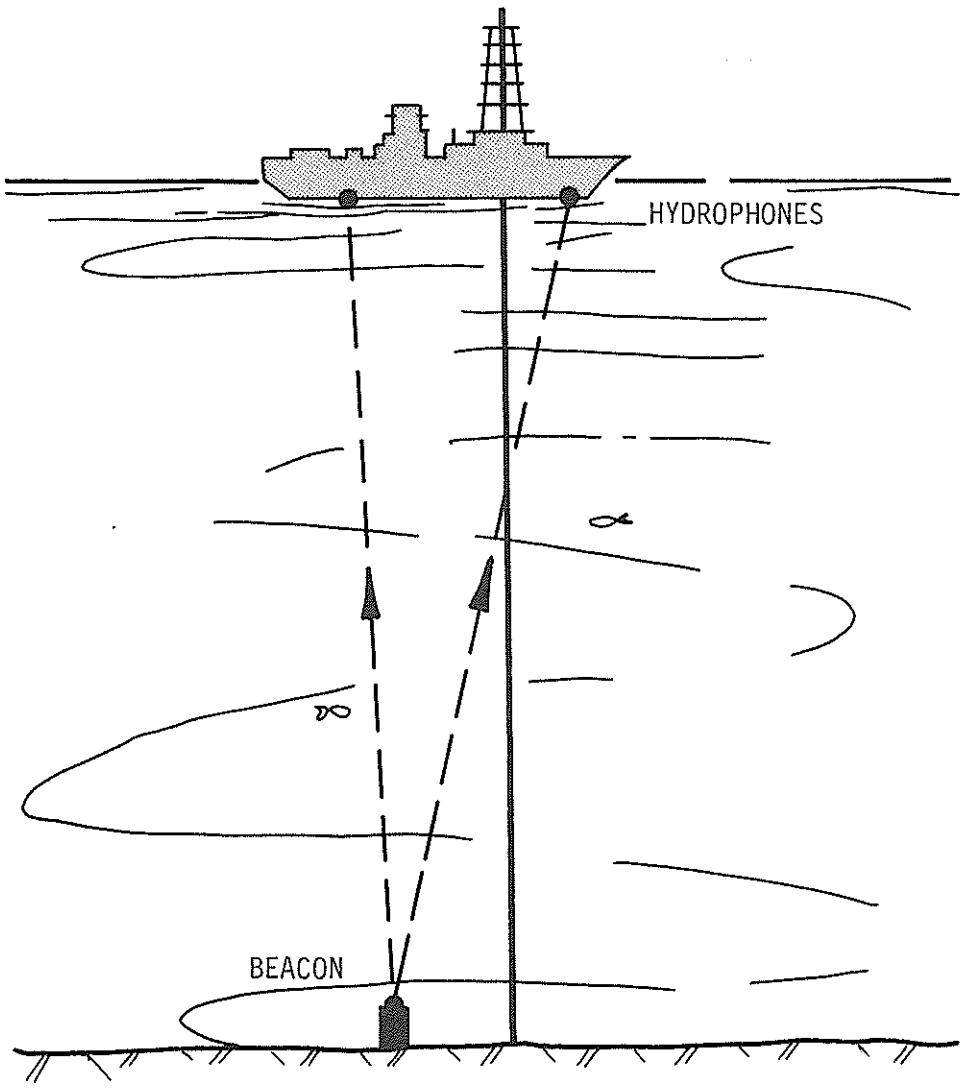

FIGURE 10. Station-Keeping With One Beacon and Multiple Hydrophones

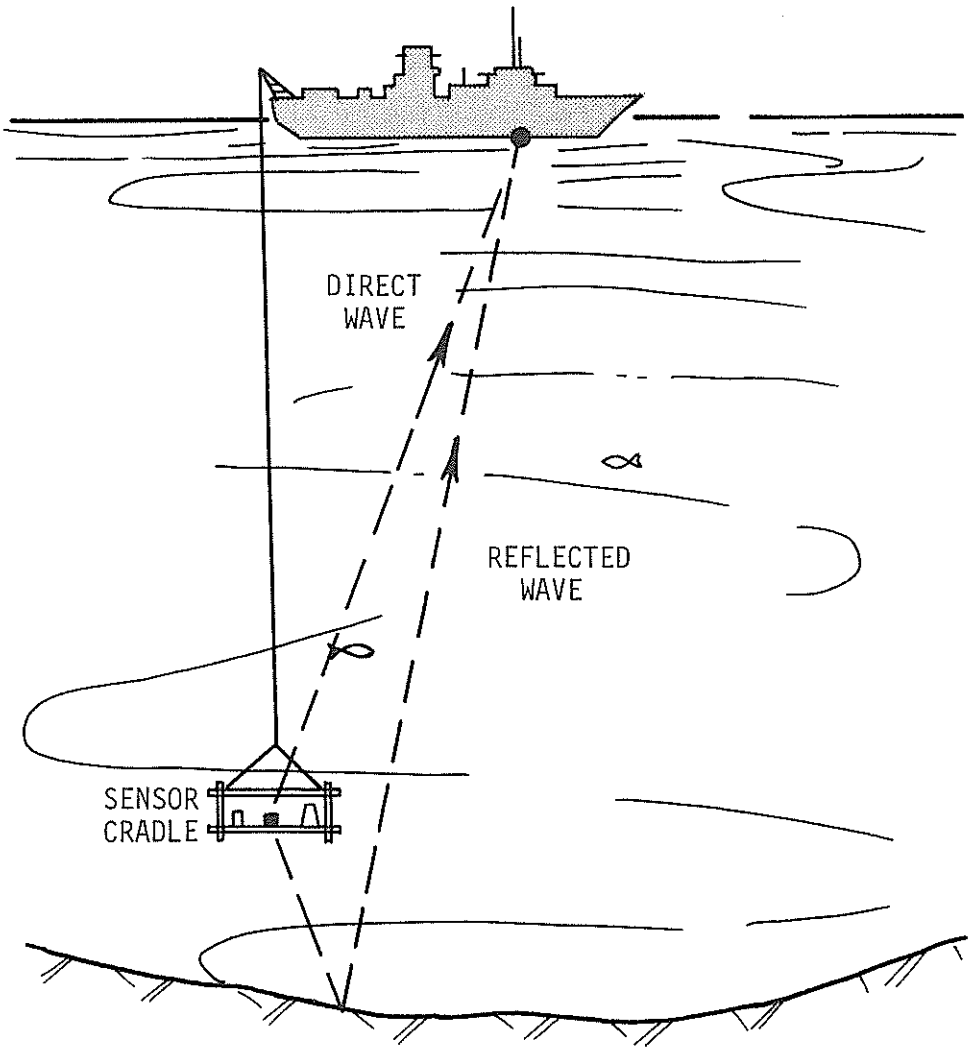

FIGURE 11. Tracking An Instrument Package Lowered to the Botton With a Pinger

CREDITS

The paper "Twenty Years in Underwater Acoustics: Generation and Reception" was presented at the Eightieth Meeting of the Acoustical Society of America and will be published in an Acoustical Society publication TWENTY YEARS IN UNDERWATER ACOUSTICS. A modified form of the paper "Scattering and Reverbration" was also presented at the meeting and will be published in the publication.